Estimation of Non-linear Seismic Site Effects for Deep Deposits of the Mississippi Embayment

Duhee Park, Ph.D.
Post Doctoral Researcher
Department of Civil & Environmental Engineering
University of Illinois at Urbana Champaign
Room 2216 NCEL 205 N. Mathews Avenue
e-mail: dpark1@uiuc.edu

Youssef M.A. Hashash, Ph.D., PE
Associate Professor
Department of Civil & Environmental Engineering
University of Illinois at Urbana Champaign
Room 2230C NCEL 205 N. Mathews Avenue
e-mail: hashash@uiuc.edu

National Science Foundation
Mid America Earthquake Center

October 2004

ABSTRACT

This report describes the development of a new one-dimensional nonlinear site response model and application of the model in probabilistic hazard analysis of the Mississippi embayment (ME) for estimation of depth dependent site coefficients.

The first part of the report describes the development of a new one-dimensional nonlinear site response model, DEESPOIL, to simulate seismic wave propagation through deep deposits. DEEPSOIL incorporates several enhancements over currently available non-linear models. A confining pressure dependent non-linear constitutive soil model is developed. Full and extended Rayleigh viscous damping formulations have been incorporated in the site response analysis code to increase the accuracy of the solution. Current formulations of non-linear site response analysis contain a frequency dependent viscous damping term that often artificially filters out high frequency components of ground motion. The proposed formulations preserve most of these components.

The second part of the report describes the probabilistic seismic hazard analysis with non-linear site effect performed in the ME to develop site coefficients. Current site coefficients, proposed in National Earthquake Hazard Reduction Program (NEHRP), are used with USGS hazard maps to develop site specific recommended response spectrum. The coefficients are developed for 30 m thick soil profile and do not account for the depth of the soil column. A suite of ground motion time histories are developed that in sum result in the same hazard level as USGS hazard maps. The generated motions are propagated through the generic profiles of the ME using DEEPSOIL. The results of the analyses are presented in the form of site coefficient as functions of a) depth of the soil profile and b) level of shaking (spectral accelerations at 0.2 and 1.0 sec, both at B/C boundary). The site coefficients are comparable to NEHRP coefficients for 30 m thick profiles, but they show significant depth dependence for thicker soil profiles. A wide range of depth dependent site coefficients is developed for the ME.

ACKNOWLEDGEMENTS

This project was funded by the Mid America Earthquake Center under grant EEC-9701785.

The authors would like to acknowledge Dr. David M. Boore for his helpful advice, as well as the SMSIM code. Dr. Mitchell M. Withers for providing the earthquake data. Dr. Chiun-Lin Wu for his code. Dr. Glen Rix, Dr. Shahram Pezeshk, and Dr. Roy Van Arsdale for their data.

The authors would also like to thank Dr. Chris Cramer, Dr. Robert B. Herrmann, Dr. James H. Long, Dr. Gholamreza Mesri, Dr. Timothy D. Stark, and Dr. Yi-Kwei Wen for their valuable comments.

TABLE OF CONTENTS

LIST OF TABLES

LIST OF FIGURES

LIST OF SYMBOLS

a	=	material constant of extended modified hyperbolic equation
a'	=	coefficient of recurrence relationship
a_0	=	coefficient of Rayleigh damping formulation
a_1	=	coefficient of Rayleigh damping formulation
a_b	=	coefficient of extended Rayleigh damping formulation
a_{RO}	=	material constant in Ramsberg-Osgood model
$A(f)$	=	soil amplification function at a given frequency f
A_m	=	amplitude of waves traveling upwards
b	=	material constant of extended modified hyperbolic equation
b_e	=	coefficient of extended Rayleigh damping formulation
b'	=	coefficient of recurrence relationship
c	=	material constant of extended modified hyperbolic equation
d	=	material constant of extended modified hyperbolic equation
B_m	=	amplitude of waves traveling downwards
$[C]$	=	viscous damping matrix
ΔE	=	total area of the hysteresis loop
E_D	=	energy dissipated in a single cycle
E_S	=	kinetic energy
f	=	frequency
f_{max}	=	maximum frequency that can be propagated through the soil layer
f_n	=	natural frequency of nth mode of the soil column
F_a	=	site coefficient at short period (0.2 sec)
F_v	=	site coefficient at long period (1.0 sec)
F_{bb}	=	backbone curve
F_{ij}	=	transfer function that relates displacement amplitude at layer i to that at layer j

G	=	shear modulus
G_{mo}	=	initial shear modulus
G_{max}	=	maximum shear modulus
h_m	=	thickness of soil layer
H	=	total thickness of soil column
$\{I\}$	=	unit vector
k	=	stiffness of soil layer
$[K]$	=	stiffness matrix
M (m)	=	earthquake moment magnitude
m_0	=	lower threshold magnitude
m_{max}	=	maximum magnitude that can occur at the source
$[M]$	=	mass matrix
n	=	mode number
n_k	=	number of simulated earthquakes within the selected grid
$P(f)$	=	soil attenuation function at a given frequency f
Q	=	quality factor
r	=	material constant in Ramsberg-Osgood model
R	=	earthquake epicentral distance
s	=	material constant of modified hyperbolic equation
S_a	=	spectral acceleration in NEHRP design response spectrum
S_S	=	USGS mapped (2% in 50 years) spectral acceleration at 0.2 sec
S_1	=	USGS mapped (2% in 50 years) spectral acceleration at 1.0 sec
S_{MS}	=	maximum considered earthquake spectral response acceleration for short period (0.2 sec)
S_{M1}	=	maximum considered earthquake spectral response acceleration for long period (1.0 sec)
t	=	time
t_{10}	=	10-year period

T	=	period
T_0	=	period that defines the low end of the constant spectral acceleration section of NEHRP design response spectrum
T_s	=	period that defines the upper end of the constant spectral acceleration section of NEHRP design response spectrum
$tt_z(f)$	=	travel time to a depth of a quarter wavelength at a given frequency f
u	=	nodal relative displacement
u_k	=	random variable with a uniform distribution between 0 and 1
$\{u\}$	=	vector of nodal relative displacement
$\{\dot{u}\}$	=	vector of nodal relative velocity
$\{\ddot{u}\}$	=	vector of nodal relative acceleration
V_s	=	shear wave velocity
$\bar{V}_s^s(f)$	=	average shear wave velocity from the surface to a depth of a quarter wavelength for the given f
z	=	depth below ground surface
α'	=	coefficient of recurrence relationship (in exponential term)
β	=	material constant of modified hyperbolic equation
β'	=	coefficient of recurrence relationship (in exponential term)
V_s^0	=	source shear velocity
γ	=	shear strain
$\dot{\gamma}$	=	shear strain rate
γ_c	=	cyclic shear strain amplitude
γ_r	=	reference strain
γ_{rev}	=	reversal shear strain
γ_0	=	harmonic shear strain amplitude
η	=	viscosity
λ_m	=	mean annual rate of exceedance of earthquake magnitude m

κ	=	a measure of damping
ν	=	mean annual rate of exceedance of lower threshold magnitude m_0
ρ	=	density of soil
ρ_0	=	density at source of the earthquake
$\overline{\rho}_s(f)$	=	average density from the surface to a depth of a quarter wavelength for the given f
τ	=	shear stress
τ_{mo}	=	shear strength
τ_{rev}	=	reversal shear stress
τ_y	=	material constant of Ramsberg-Osgood model
ω	=	circular frequency
ω_n	=	natural circular frequency of the soil column
ξ	=	equivalent damping ratio

LIST OF ABBREVIATIONS

1D	=	one-dimensional
2D	=	two-dimensional
3D	=	three-dimensional
ATC	=	Applied Technological Council
CRF	=	conventional Rayleigh damping formulation
CDF	=	cumulative density function
CEUS	=	central and eastern United States
DSHA	=	deterministic seismic hazard analysis
ERF	=	extended Rayleigh damping formulation
FD	=	frequency domain
FEMA	=	Federal Emergency Management Agency
ME	=	Mississippi embayment
NEHRP	=	National Earthquake Hazard Reduction Program
NLPD	=	nonlinear pressure dependent
NLPI	=	nonlinear pressure independent
NMSZ	=	New Madrid Seismic Zone
PDF	=	probability density function
PE_{annual}	=	annual probability of exceedance
PE_t	=	probability of exceedance in *t* years
PGA	=	peak ground acceleration
PSHA	=	probabilistic seismic hazard analysis
QWM	=	quarter wavelength method
RF	=	Rayleigh damping formulation
RFS	=	ratio of surface Fourier spectrum to input Fourier spectrum
RRS	=	ratio of surface response spectrum to input response spectrum
R-TS	=	recorded ground motion time series
RUS	=	ratio of surface uniform hazard response spectrum to input uniform hazard response spectrum

S-TS	=	synthetic ground motion time series
TD	=	time domain
TS	=	time series
UHRS	=	Uniform hazard response spectrum
USGS	=	United States Geological Survey

CHAPTER 1 INTRODUCTION

Estimation of earthquake generated ground motion at a given site is essential for quantifying potential consequences of an earthquake including ground deformation and failure as well as damage to structures.

Figure 1-1 is a schematic of ground motion propagation from source to a site of interest. The rupture at the fault initiates stress waves that propagate through the earth to the bedrock beneath the soil layers, and finally through soil layers to reach the ground surface. The rupture mechanism and wave passage effects up to the bedrock are simulated separately in a seismic hazard analysis (e.g. U.S. Geological Survey hazard maps, Frankel et al., 2002), which provide ground motion parameters up to top of bedrock. Site response deals with the ground motion propagation through the soil profile. Local site effects, which heavily influence the characteristics of ground motions, are quantified through empirical correlations or numerical simulations.

The presence of a deep soil deposit adds significant uncertainty to estimating seismic hazard and surface ground motions. In the central United States, deep deposits of the Mississippi embayment, Figure 1-2, which are up to 1 km thick near Memphis, overlie New Madrid Seismic Zone, considered to be the most seismically active zone in the central and eastern United States. The region has experienced three consecutive earthquakes of magnitudes higher than 7 during 1811-1812. U.S. Geological Survey (USGS) hazard maps with NEHRP (FEMA, 1997) site coefficients are commonly used to estimate ground motions in the embayment. USGS hazard maps are developed through probabilistic seismic hazard analysis. In contrast site coefficients are developed for a uniform 30 m thick soil profile (FEMA, 1997) and are deterministically derived from compilations of empirical earthquake data and numerical simulations. The coefficients do not account for the special character of the deposits of the embayment.

This study develops new techniques and procedures to assess the effect of the deep deposits of the Mississippi embayment on seismic ground motion propagation. The study is divided into 3 main sections: 1) development of a new nonlinear site response analysis

model to simulate strong ground motion propagation through very deep deposits; 2) development of dynamic soil properties for Mississippi embayment deposits to be used in site response analysis; and 3) development of probabilistic seismic hazard analysis with nonlinear site effects to generate site coefficients for the embayment.

1.1 Non-linear site response analysis model

CHAPTER 2 presents a literature review on local site effects. Empirical procedures to account for the site effects are introduced. Numerical analysis procedures used for the simulation of one-dimensional site response analysis are also described. These include equivalent linear frequency domain, and non-linear time domain analysis procedures. Available procedures are not designed to simulate strong ground motion propagation for very deep deposits.

CHAPTER 3 describes the development of a new one-dimensional nonlinear site response analysis program for deep and shallow deposits called DEEPSOIL. The model's new features include a) confining pressure dependent soil model, b) new viscous damping formulation to better simulate wave propagation through thick deposits, and c) increased numerical accuracy. The performance of the developed model is evaluated through comparisons with other non-linear site response analysis models, equivalent linear site response analysis models and field recordings from the Loma Prieta Earthquake.

1.2 Dynamic soil properties for Mississippi embayment

CHAPTER 4 reviews efforts to characterize dynamic properties of the Mississippi embayment soils and develops properties for use in DEEPSOIL. Results from cyclic laboratory tests performed by Laird and Stokoe (1993) at confining pressures up to 3 MPa are used to characterize the pressure dependent behavior of soils due to the lack of data specific to the Mississippi embayment. The estimated dynamic properties are further constrained using laboratory test results of shallow embayment soils. Viscous damping soil properties are constrained using weak motion recordings from a recent earthquake near the embayment.

1.3 Probabilistic seismic hazard analysis for the Mississippi embayment with nonlinear site effects

CHAPTER 3 presents a review of published procedures for seismic hazard analysis and estimation of site coefficients in the Mississippi embayment. U.S. Geological Survey (USGS) hazard maps, developed using the conventional probabilistic seismic hazard analysis (PSHA), are widely used to determine the seismic hazard. USGS maps show four ground motion parameters for a reference rock condition. The USGS hazard maps are used with site coefficients proposed in 1997 NEHRP Provisions to account for site effects. The coefficients are based on site classifications that do not account for the existence of deep deposits such as those in the Mississippi embayment.

An alternative procedure for performing the PSHA was developed by Wen and Wu (2001). The procedure allows for generation of seismic motions that as a sum result in the hazard level estimated by PSHA. Embayment site effects are modeled using the quarter wavelength model, a linear attenuation model that does not account for non-linear soil response during large earthquake.

CHAPTER 6 presents a new PSHA analysis procedure combined with non-linear site response analysis (DEEPSOIL) to develop site coefficients within the Mississippi embayment. An extension of the PSHA procedure proposed by Wen and Wu (2001) is developed to generate a suite of ground motions at the rock. The ground motions are propagated using embayment specific soil profiles and the surface motions are compiled to develop the uniform hazard response spectrum. The uniform hazard response spectrum is compared to the 1997 NEHRP response spectrum and depth dependent site coefficients are proposed. The generated surface motions can be used as input motions in performance design of structures.

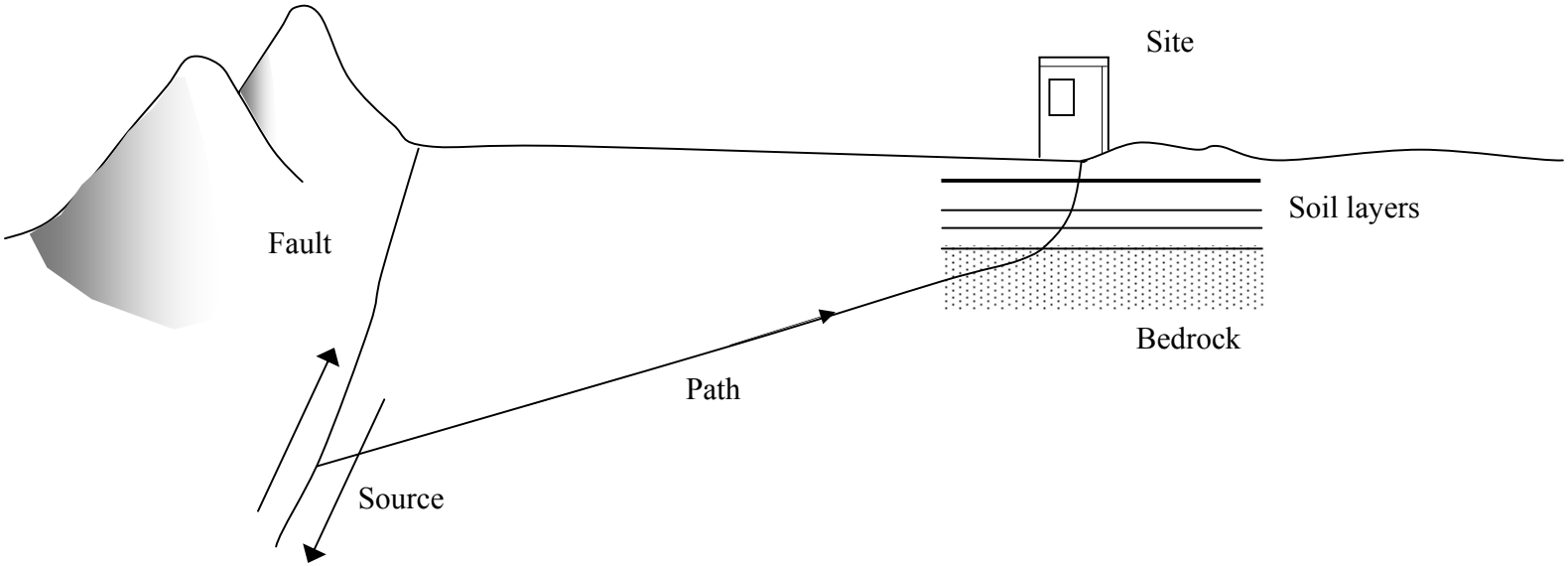

Figure 1-1 Schematic ground motion propagation from source to site (after Kramer, 1996)

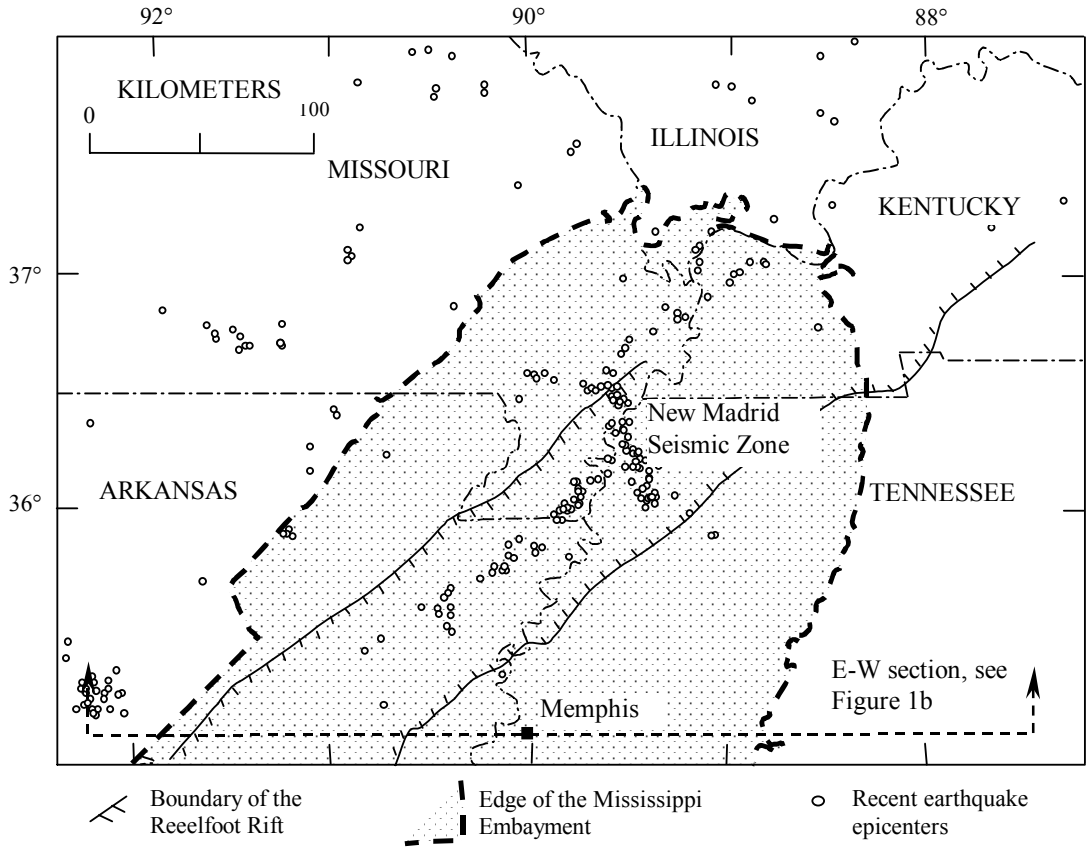

a. Plan view of the Mississippi embayment.

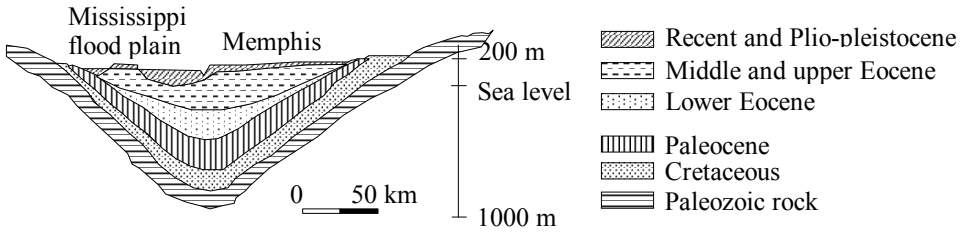

b. E-W section through Memphis (after Ng et al., 1989). Note: Vertical dimension is highly exaggerated, and the embayment trough has a shallow slope of less than 1/150.

Figure 1-2 The Mississippi embayment.

CHAPTER 2 ONE DIMENSIONAL SITE RESPONSE ANALYSIS

2.1 Evidence of local site effects

The influence of local site effects on ground motion characteristics are well demonstrated through several recent earthquakes. A good example of site effects is the recorded motions at six stations along a 4 mile section in San Francisco during a nearby M (moment magnitude) ≈ 5.3 earthquake in 1957 (Idriss, 1968). Even though the stations are located relatively close to each other, significant variation in ground motion content related to thickness of the underlying soil column is illustrated in Figure 2-1.

Three recordings made at the rock outcrop show similar response, both in terms of peak ground acceleration (PGA) and response spectra. Three recordings made at the soil profiles, however, show dramatic changes in frequency content, as can be observed from the response spectra. The PGA is lower at two soil sites (Alexander and Southern Pacific Co. Building), but there is amplification at longer periods compared to the rock outcrop motions. At State Building, another recording at a soil site shows similar PGA compared to rock outcrop PGA but with higher amplification around 0.5 sec.

Another example displaying the significance of local site effects is the recorded motions during the Loma Prieta Earthquake (M = 7.1, 1989). Recordings were made during the earthquake at Yerba Buena Island, a weak rock outcrop, and Treasure Island, which is a man made hydraulic fill underlain by loose sandy soil and soft San Francisco Bay Mud. Even though the two recording stations are at the almost same distance from the source, the recorded motions exhibit pronounced differences, as shown in Figure 2-2. The peak ground acceleration has been amplified from 0.06g at Yerba Buena Island to 0.16g at Treasure Island. The response spectra show the high amplification at all periods, demonstrating the significant influence of the soft soil profile on ground motion amplification.

During 1994 Northridge earthquake (M = 6.7, epicentral distance = 6 km), exceptionally high ground motions (PGA of 1.82g) were recorded at the Tarzana Station (Vahdani and Wikstrom, 2002). The PGA at a depth of 100 m (shear wave velocity = 1 km/sec), on the other hand, was estimated as 0.46g (Silva, 2000). The response spectra of recorded surface motions and estimated rock motion are shown in Figure 2-3. 1994 Northridge earthquake provided abundant ground motion recordings in addition to the Tarzana Station recordings. ROSRINE, a

collaborative research project ultimately focusing on improving engineering models for estimation of earthquake ground motions, was initiated to primarily focus on the collection, synthesis, and dissemination of high quality subsurface data obtained from instrument sites that recorded strong shaking during the 1994 Northridge earthquake (ROSRINE, 2003). Project activities include ground motion modeling, estimation of site and source effects and laboratory tests.

The examples presented clearly demonstrate the importance of accounting for local site effects, including ground motion amplification and frequency content shift.

2.2 Empirical procedures for characterizing site effects

There have been efforts to compile empirical data on site effects and to quantify the site effects by developing correlations between a rock outcrop motion and motion at soil sites. Based on the statistical study of 147 recordings from western U.S. earthquakes of about magnitude 6.5, Seed et al. (1976) developed peak acceleration attenuation relationships for different site conditions, as shown in Figure 2-4. Peak accelerations at soil sites are greater than on rock up to 0.1g and smaller at higher acceleration levels. The influence of different site conditions is also recognized, since different correlations are proposed for stiff soils and deep cohesionless soils.

Idriss (1990) developed an empirical correlation between the peak acceleration at rock outcrop and soft soil, as shown in Figure 2-5. The relationship is based on recordings from Mexico City (1985) and the San Francisco Bay area (Loma Prieta earthquake, 1989) and site response analyses. The amplification at soil sites is high at low accelerations and decreases with increase in amplitude of the input motion. For very strong ground motions (higher than 0.4g at rock sites), the peak acceleration at soft soil sites are lower than at rock sites. The developed relationship is to be used independent of earthquake magnitude.

Soil sites do not only influence peak ground motion parameters, but also frequency content of the ground motion. Seed et al. (1976) compiled response spectra recorded for 4 different site conditions; a) rock sites, b) stiff soil sites (less than 200 m deep), c) deep cohesionless soil sites (greater than 76 m deep), and d) sites underlain by soft to medium-stiff clay deposits, as shown in Figure 2-6. 107 earthquake records from western U.S., Japan, and Turkey are compiled. The response spectra are normalized to peak ground acceleration to allow comparison of the overall shapes of the spectra. The effect of local site condition on frequency

content of the ground motion and thus the shape of the response spectra is significant. Deep and soft sites strongly amplify long period motions even though the peak spectral accelerations are lower than at stiff soils. These findings have eventually influenced the development of site-specific design codes, discussed in detail in section 5.6.1.1.

2.3 Simulation of local site effects

While empirical procedures are important and useful, the limited availability of recordings and the range of applicable site conditions make it impossible to apply the empirical relations to all situations encountered during seismic design. Numerical simulations need to be performed to cover the range of input ground motions and site effects at which no recordings are available.

Site response analysis is commonly used to account for local site effects and to estimate the surface ground motion (Idriss, 1968; Roesset, 1977; Idriss, 1990; Kramer, 1996; Borja et al., 2002). A complete site response analysis would model the rupture mechanisms at the source of an earthquake, propagation of stress waves to the top of bedrock beneath a particular site, and finally compute ground motion propagation through the soil column, which lies above the bedrock. In reality, a seismic hazard analysis is performed to predict motion characteristics up to bedrock. The site response is solely used to determine the response of the soil deposit to the motion of the bedrock immediately beneath it (Kramer, 1996).

The procedure for site response analysis consists of the following steps (Kramer, 1996):

1. Define the soil profile and the boundary between the bottom of the soil profile and underlying rock/stiff layer: The soil properties, such as density and shear wave velocity, are defined. The bottom boundary is defined as the boundary between the soil profile and underlying bedrock or a stiff soil layer.
2. Define the input ground motion in the rock or a stiff layer: It is difficult to estimate input ground motion due to the inherent uncertainty of future seismic events. Seismic hazard analysis is commonly performed to quantify the seismic hazard and define input ground motion parameters. Seismic hazard analysis is described in 0. The input ground motion is imposed at the boundary of soil / rock or a stiff layer within the soil profile.
3. Define cyclic soil & pore water pressure response (stiffness and damping). The cyclic behavior of in-situ soil is determined from laboratory tests. Parameters that influence dynamic/cyclic soil behavior are introduced in section 2.4. Soil response is represented as

either linear, equivalent linear or non-linear. Soil constitutive models developed to represent nonlinear cyclic behavior of soils are presented in section 2.5.

4. Compute the ground motion through the layer and at the ground surface by solving analytically the governing differential equation of wave propagation and dynamic equilibrium. The numerical formulations of available site response analysis methods and how the cyclic behavior is accounted for in each of the analysis methods is presented in sections 2.6 through 2.8.

Site response analysis is commonly performed assuming one-dimensional (1D) wave propagation. The one-dimensional ground response analysis approach is based on the assumption that all soil layers are horizontal and that the response of a soil deposit is predominantly caused by SH-wave propagating vertically from the underlying bedrock. One-dimensional ground response analysis cannot model sloping or irregular ground surface, deep basins, and embedded structures. In such cases, two-dimensional (2D) and three-dimensional (3D) site response analyses have been used (Kramer, 1996).

2D and 3D analyses are employed to model basin effects. The curvature of a basin in which softer alluvial soils have been deposited can trap body waves and cause some incident body waves to propagate through the alluvium as surface waves. These waves can produce stronger shaking and longer durations than would be predicted by 1D analysis that considers only vertically propagating S-waves. Various 2D and 3D analysis methods, such as finite element, finite difference, and thin-layer methods, have been developed and used to assess the effect of topography and basin structure on wave propagation (Bielak et al., 1999; Law and Lam, 1999; Sakai and Sawad, 1996; Takemiya and Adam, 1998).

It is, however, not feasible to perform 2D or 3D analysis in a large geologic structure such as the Mississippi embayment at this time. The embayment is approximately 200 km in width and longer than 300 km in length. The size of the embayment limits the mesh element size, thereby filtering out high frequency components of the ground motion. In addition, the dip of Mississippi Embayment edges is very small. Therefore, 1D approximation of wave propagation is acceptable.

2.4 Cyclic soil behavior

Soil behavior is nonlinear when shear strains exceed about 10^{-5} (Hardin and Drnevich, 1972b; Ishihara, 1996). The nonlinear behavior of soils is the most important factor in ground motion propagation and should be accounted for when soil shearing strains are expected to exceed the linear threshold strain.

In site response analysis, soil properties including shear modulus and cyclic soil behavior are required. Shear modulus is estimated using field tests such as seismic down-hole or cross-hole tests. Cyclic soil behavior is characterized using laboratory tests such as resonant column, cyclic triaxial, or simple shear tests (Kramer, 1996).

Typical response of a soil sample tested under cyclic loading is shown in Figure 2-7a. An idealized hysteresis loop of soil under cyclic loading is shown in Figure 2-7b. The maximum shear modulus is defined as G_{max} and corresponds to the initial shear modulus. The slope of stress-strain curve at a particular strain is the tangent shear modulus (G_{tan}). The secant shear modulus (G_{sec}) is the average shear modulus for a given load cycle. The secant shear modulus decreases with increase in cyclic shear strain, as can be observed from Figure 2-7.

Instead of defining the actual hysteresis loop, the cyclic soil behavior is often represented as shear modulus degradation and damping ratio curves, as shown in Figure 2-8. The shear modulus degradation curve relates secant shear modulus to cyclic shear strain, whereby shear modulus is normalized by the maximum or initial shear modulus. The damping curve relates the energy dissipated in one cycle of loading to the cyclic shear strain and is determined from the hysteresis loop in Figure 2-7. The energy dissipated in one cycle of loading, E_D, is given by the area inside the hysteresis loop. The strain energy stored in the system is given by E_S, and calculated as:

$$E_S = \frac{1}{2} G_{\sec} \gamma_c^{\,2} \tag{2-1}$$

The damping ratio is calculated as:

$$\xi = \frac{E_D}{4\pi E_S} \tag{2-2}$$

Damping ratio increases with cyclic shear strain as the soil response becomes more nonlinear.

Use of shear modulus and damping curves allows representation of the nonlinear behavior in sufficient detail for many practical purposes. Modulus degradation and damping

curves for a wide range of soils have been developed by several researchers including Seed et al. (1986) and Vucetic and Dobry (1991).

2.4.1 Factors affecting cyclic soil behavior

A range of environmental and loading factors influence cyclic soil behavior and are summarized by Hardin and Drnevich (1972a), Hardin and Drnevich (1972b), Dobry and Vucetic (1987), and in Table 2-1. Hardin and co-workers identify the following primary and secondary factors that influence shear modulus degradation and damping ratio:

- Strain amplitude
- Void ratio
- Degree of saturation for cohesive soils
- Effective mean principle stress
- Number of cycles of loading

Secondary factors include:

- Octahedral shear stress
- OCR
- Effective strength parameters, c' and ϕ'
- Time effects (thixotropy)

For deep soil deposits the influence of confining pressure (or effective mean principle stress) on cyclic behavior of soils is very important but has been generally neglected in most site response analysis studies. The influence of confining pressure is discussed in greater detail in the following section.

2.4.2 Influence of confining pressure on cyclic soil behavior

The effect of confining pressure on dynamic properties has been recognized by Iwasaki et al. (1978), Kokusho (1980), and Hardin et al. (1994). Ishibashi and Zhang (1993) published relations relating modulus reduction to confining pressure and soil plasticity index. Hardin et al. (1994) presented high pressure (up to 3.5 MPa) test data on sand and concluded "damping ratios at conventional pressures are approximately equivalent to those at pressures up to 3.5 MPa."

Hardin et al. (1994) suggested that additional research is necessary to further understand cyclic soil response at very high pressures.

Laird and Stokoe (1993) performed resonant column and torsional shear tests at strain levels up to 10^{-3} and confining pressures up to 3.5 MPa using remolded sand specimens, as well as undisturbed specimens of sand, silty sand, silt, lean clay, and fat clay. Low and high amplitude cyclic torsional shear and resonant column tests were used to determine the effect of strain amplitude and confinement on shear modulus and damping curves. In this study, only results from remolded sand specimens (washed mortar sand) are used. Laboratory testing was part of the ROSRINE project (ROSRINE, 2003) examining local site response in the Los Angeles Basin. Figure 2-9 shows shear modulus and damping values obtained from these tests. Measurements show that increase in confining pressure results in lesser shear modulus degradation at a given cyclic shear strain. Confining pressure increase also influences soil damping. Both small strain and hysteretic damping decrease with increase in confining pressure.

Figure 2-9 includes data from Laird and Stokoe (1993), the measured range of sand properties from Seed and Idriss (1970) and curves obtained from the model proposed by Ishibashi and Zhang (1993) for cohesionless soils. The specific effect of confining pressure is not available in the curves proposed by Seed and Idriss (1970). The data from Laird and Stokoe (1993) show significantly less degradation of shear modulus compared with the modulus degradation range presented by Seed and Idriss (1970). Even at a moderate confining pressure (221 kPa), the test data exceed the boundaries of the Seed and Idriss curves. Damping falls below the proposed range at a confining pressure of 55kPa or larger. Modulus degradation curves by Ishibashi and Zhang (1993) give a much stiffer response of sand compared to the measured values from Laird and Stokoe (1993). Similarly, the Ishibashi and Zhang (1993) damping curves do not capture measured behavior. The data from Laird and Stokoe (1993) is considered more reliable since it is derived from experiments designed to account for the influence of confining pressure.

2.5 Material constitutive model representation of cyclic soil behavior

The significant increase in development and application of modern computer based analysis techniques, such as finite element, finite difference, and boundary integral methods, has greatly facilitated the numerical solution of complex boundary value problems. The numerical

solution is only valid, however, if the material behavior that makes up the system is realistically simulated. A material constitutive model, relating stress to strain, is used to represent the material behavior.

Development of a constitutive model for soil has proven to be a difficult task, since it requires simulation of complex phenomena such as nonlinearity, hardening and softening, anisotropy, residual or initial stress, volume change during shear, stress history and stress paths, three dimensional states of stress and strain, and fluid in pores.

Often, a simplification of the soil behavior is necessary in site response analysis. It is often not possible to perform quality laboratory tests on in-situ soil samples and therefore the complex soil behavior cannot be accurately estimated. In addition, the variation of soil properties within the site is large and cannot be represented using the results of selected soil samples. The aforementioned difficulties in estimating and characterizing the soil behavior lead to simplification of the soil behavior and use of simple shear soil models or linear viscoelastic soil models in site response analysis.

2.5.1 Linear viscoelastic model

The simplest form of constitutive law used in modeling dynamic response of geologic materials is the linear viscoelastic model. The stress-strain relationship is linear, but the energy dissipating characteristics of soils are taken into account. The linear viscoelastic model is valid only for limited applications such as propagation of weak ground motions through soil, or propagation of motions through very stiff material such as rock whereby the induced strain amplitude is small. Three different types of the linear viscoelastic models are introduced in the following.

2.5.1.1 Kelvin-Voigt model

Kelvin-Voigt model consists of a spring and dashpot connected in parallel. The shear stress is calculated as:

$$\tau = G\gamma + \eta\dot{\gamma} \tag{2-3}$$

where G is the shear modulus of the spring and η is the viscosity of the dashpot. For a harmonic shear strain of the form

$$\gamma = \gamma_0 \sin \omega t \tag{2-4}$$

the energy dissipated in a single cycle is:

$$E_D = \int_{t_0}^{t_0+2\pi/\omega} \tau d\gamma = \int_{t_0}^{t_0+2\pi/\omega} \tau \frac{\partial \gamma}{\partial t} dt = \pi \eta \omega \gamma_0^{\ 2} \tag{2-5}$$

Equation (2-5) indicates that the dissipated energy is a function of the frequency of the loading. The frequency dependent nature of the viscous damping in the Kelvin-Voigt model cannot simulate the damping of the soils, which are known to be nearly constant over the frequency range of interest in engineering applications (Kramer, 1996; EPRI, 1993). Analytical solution using the Kelvin-Voigt model is presented in Appendix A.1.

2.5.1.2 Hysteretic model

Hysteretic model incorporates rate-independent dashpot to eliminate the frequency dependence of damping. The viscosity is expressed in terms of equivalent, damping ratio ξ, which is defined as:

$$\xi = \frac{E_D}{4\pi E_S} = \frac{\eta \omega}{2G} \tag{2-6}$$

where $E_S = 1/2G\gamma_0^2$. Equation (2-6) is similar to Equation (A-5), but assumes that the equivalent damping ratio is independent of the forcing frequency, or $\omega / \omega_n = 1$.

Rearranging Equation (2-6) to eliminate frequency dependence results in

$$\eta = \frac{2G}{\omega} \xi \tag{2-7}$$

Substituting Equation (2-7) into Equation (2-3), shear stress is written as

$$\tau = G^* \gamma \tag{2-8}$$

where G^* is the complex shear modulus defined as:

$$G^* = G(1 + i2\xi) \tag{2-9}$$

Assuming that the damping is small, an approximation of the complex shear modulus is commonly adopted which is defined as:

$$G^* = G(1 - \xi^2 + i2\xi) \tag{2-10}$$

which is based on the approximate complex shear modulus (Kramer, 1996):

$$v_s^{\ *} = \sqrt{\frac{G^*}{\rho}} = \sqrt{\frac{G(1+i2\xi)}{\rho}} \approx \sqrt{\frac{G}{\rho}}(1+i\xi) = v_s(1+i\xi) \tag{2-11}$$

Introduction of imaginary term is necessary to represent the phase lag and hence the damping property of soils. Using the Equations (2-9) or (2-10), the shear stress becomes independent of frequency. The solution of the hysteretic model subjected to a harmonic loading is presented in Appendix A.2.

2.5.1.3 Udaka model (1975)

Udaka developed a complex modulus that results in identical response amplitude as the Kelvin-Voigt model (Udaka, 1975). The complex shear modulus is written as:

$$G^* = G\left(1 - 2\xi^2 + 2i\xi\sqrt{1-\xi^2}\right) \tag{2-12}$$

The complex shear modulus has been derived through back-calculation to obtain an identical match with the Kelvin-Voigt model in response amplitude. However, the calculated phase angle does not match the Kelvin-Voigt model. The solution to harmonic loading using the Udaka model is presented in Appendix A.3.

Udaka model is an approximate solution developed to better simulate the Kelvin-Voigt model but at the same time preserve the convenience of the use of the complex shear modulus. Therefore, the model has the same limitation as the Kelvin-Voigt model, which results in frequency dependent damping.

2.5.2 Non-linear simple-shear model

It is possible to represent the nonlinear, path dependent soil behavior using a nonlinear soil model, which ranges from a very simple shear model to the state-of-the-art bounding surface models.

Simple shear models, while not realistic in many geotechnical applications such as simulation of deep excavations, are an acceptable approximation in 1D site response analysis where horizontal shear waves propagate vertically. The cyclic simple shear model relates the horizontal shear stress to the horizontal shear strain. A nonlinear simple-shear model is characterized by a) backbone curve and 2) rules to characterize unloading and reloading behavior. The backbone curve is the stress-stress relationship for initial loading and is described in the following sections. The Masing criteria (Masing, 1926) and extended Masing criteria (Pyke, 1979; Vucetic, 1990) define unloading-reloading criteria and behavior under general cyclic loading conditions as shown in Figure 2-10.

The Masing criteria and extended Masing criteria are the following:

1. For initial loading, the stress-strain curve follows the backbone curve.
2. The unloading and reloading curve can be defined using the backbone curve as follows:

$$\frac{\tau - \tau_{rev}}{2} = F_{bb}(\frac{\gamma - \gamma_{rev}}{2}) \tag{2-13}$$

   where τ_{rev} is the stress and γ_{rev} is the strain at a reversal point, and F_{bb} is the backbone curve.
3. If the unloading and reloading curve exceeds the past maximum past strain and intersects the backbone curve, it follows the backbone curve until the next stress reversal.
4. If an unloading or reloading curve crosses an unloading or reloading curve from the previous cycle, the stress-strain curve follows that of the previous cycle.

Criteria 1 and 2 describe the Masing criteria. Models that follow the four criteria are called extended Masing models.

2.5.2.1 Non-linear simple-shear hyperbolic model

The hyperbolic model was developed by Konder and Zelasko (1963) to model the stress-strain behavior of soils subjected to constant rate of loading. The hyperbolic equation, illustrated in Figure 2-11, is defined as:

$$\tau = \frac{G_{mo}\gamma}{1 + \left(\frac{G_{mo}}{\tau_{mo}}\gamma\right)} = \frac{G_{mo}\gamma}{1 + \left(\frac{\gamma}{\gamma_r}\right)} \tag{2-14}$$

where τ = shear stress; γ = shear strain; G_{mo} = initial shear modulus; τ_{mo} = shear strength; and $\gamma_r = \tau_{mo} / G_{mo}$ is the reference shear strain. The reference strain is a strain at which failure would occur if a soil were to behave elastically. It has been considered a material constant by Hardin and Drnevich (1972a). The reference strain can also be represented as a function of initial tangent modulus and undrained shear strength in clays (Mesri et al., 1981).

The hyperbolic model has been implemented in many site response analysis codes, such as DESRA (Lee and Finn, 1978).

2.5.2.2 Non-linear simple-shear modified hyperbolic model

The modified hyperbolic model is an extension of the hyperbolic model proposed by Matasovic and Vucetic (1995) to allow more flexibility in modeling nonlinear behavior. The backbone curve formulation of the modified hyperbolic models is defined as:

$$\tau = \frac{G_{mo}\gamma}{1+\beta\left(\frac{G_{mo}}{\tau_{mo}}\gamma\right)^{s}} = \frac{G_{mo}\gamma}{1+\beta\left(\frac{\gamma}{\gamma_{r}}\right)^{s}} \tag{2-15}$$

Two parameters β and s are added to the hyperbolic equation to adjust the shape of the backbone curve to represent a wider range of measured soil behavior.

2.5.2.3 Non-linear simple shear Ramsberg-Osgood model

The backbone curve of the Ramsberg-Osgood (RO) model is given by:

$$\frac{\gamma}{\gamma_{r}} = \frac{\tau}{\tau_{y}}\left(1+a_{RO}\left|\frac{\tau}{\tau_{y}}\right|^{r-1}\right) \tag{2-16}$$

where τ_y and γ_y are shear stress and shear strain to be appropriately chosen, and a_{RO} and r are material constants. It is a common practice to specify τ_y and γ_y as τ_{mo} and γ_r, respectively. In such case, Equation (2-16) becomes to

$$\tau = \frac{G_{mo}\gamma}{\left(1+a\left|\frac{\tau}{\tau_{mo}}\right|^{r-1}\right)} = \frac{G_{mo}\gamma}{\left(1+a\left|\frac{\tau}{G_{mo}\gamma_{r}}\right|^{r-1}\right)} \tag{2-17}$$

The main limitation of the Ramsberg-Osgood model is that the stress increases infinitely with increase in strain, which contradicts the actual soil behavior.

2.5.3 Plasticity based models

The complex behavior of soils, such as nonlinearity, hardening and softening, and anisotropy, cannot be accurately simulated using a simple equation relating shear stress to shear strain. Advanced models based on the concepts of plasticity have been developed to capture such behaviors. Plasticity models require definition of a) yield surface (represents the stress condition beyond which the material behaves plastically), b) hardening rule (describe the changes in the size and shape of the yield surface), and c) flow rule (relates increments of plastic strain to increments of stress). The earliest plasticity soil models include Cam-Clay (Roscoe and Schofield, 1963) and modified Cam-Clay models (Roscoe and Burland, 1968), widely used in geotechnical engineering to represent clay behavior. More complex plasticity models, including nested plasticity models (Mroz, 1967; Prevost, 1977) and bounding surface models (Dafalias and Popov, 1979; Dafalias, 1980) have been introduced. Whittle (1987) developed a bounding surface model, referred to as MIT-E3, that captures important aspects of soil behavior such as

nonlinearity at small strains, stress-strain-strength anisotropy and irrecoverable strains regardless of the position of the state of stress with respect to the yield surface. MIT-E3 has been successfully incorporated in a finite element code to simulate the deep excavations in clays (Hashash, 1992). Pestana-Nascimento (1994) developed an effective stress model, referred to as MIT-S1, which describes the rate independent behavior of freshly deposited and overconsolidated soils. MIT-S1 has been used to develop confining pressure dependent shear modulus degradation and damping ratio curves to be used in an equivalent linear site response analysis model (Assimaki et al., 2000).

Various plasticity models have been developed to model cyclic soil behavior. Prevost introduced effective stress nested yield surface plasticity model to simulate sand dilation during liquefaction (Prevost, 1985; Prevost, 1998). Borja and Amies (1994) and Borja et al. (1999) introduced a total stress bounding surface model to simulate 3D cyclic soil behavior that has been incorporated in a 3D site response code. A 3D effective stress model based on a multi-yield surface stress-space model by Prevost (1985) has been developed to model liquefaction (Parra, 1996). The model has been successfully used to simulate liquefaction-induced shear deformation and lateral spreading (Elgamal et al., 1999; Elgamal and Yang, 2000).

Although the use of plasticity models allows better representation of the nonlinear behavior of soils, they require a plethora of parameters. Plasticity models are useful in performing site specific analysis if the material properties are well defined through extensive laboratory testing. Such site specific information on dynamic soil properties is often not available. Therefore, plasticity models are infrequently used in a site response analysis.

2.6 Numerical formulation for one-dimensional site response analysis

The 1D equation of motion for vertically propagating shear waves through unbounded medium can be written as:

$$\rho \frac{\partial^2 u}{\partial z^2} = \frac{\partial \tau}{\partial z} \tag{2-18}$$

where ρ = density of medium, τ = shear stress, u = horizontal displacement and z = depth below ground surface. Equation (2-20) can be solved in frequency domain or in time domain.

Soil behavior is commonly approximated as a Kelvin-Voigt solid. The shear stress-shear strain relationship is expressed as:

$$\tau = G\gamma + \eta \frac{\partial \gamma}{\partial t} \tag{2-19}$$

where G = shear modulus, γ = shear strain and η = viscosity.

Substituting Equation (2-19) into (2-18) results in:

$$\rho \frac{\partial^2 u}{\partial t^2} = G \frac{\partial^2 u}{\partial z^2} + \eta \frac{\partial^3 u}{\partial z^2 \partial t} \tag{2-20}$$

Equation (2-20) can be solved in frequency domain or in time domain.

2.7 Frequency domain solution for one-dimensional site response analysis

Equation (2-20) can be solved for a harmonic wave propagating through a multi-layered soil column (Schnabel et al., 1972), as shown in Figure 2-12a. Introducing a local coordinate Z for each layer and solving the wave equation, the displacement at the top and bottom of a layer m becomes:

$$\begin{aligned} u(Z_m = 0, t) &= u_m = \left(A_m + B_m\right) e^{i\omega t} \\ u(Z_m = h_m, t) &= u_{m+1} = \left(A_m e^{ik^*_m h_m} + B_m e^{-ik^*_m h_m}\right) e^{i\omega t} \end{aligned} \tag{2-21}$$

where u = displacement, A_m and B_m = amplitudes of waves traveling upwards (-z) and downwards (z) at layer m, and h_m = thickness of layer m. k^*_m is defined as (Kramer, 1996):

$$k^*_m = \frac{\omega}{\left(v_s^*\right)_m \left(1 + i\xi_m\right)} \tag{2-22}$$

where $\left(v_s^*\right)_m$ is the complex shear velocity and ξ_m is the damping ratio at layer m. $\left(v_s^*\right)_m$ is defined as:

$$\left(v_s^*\right)_m = \sqrt{\frac{G^*}{\rho}} \tag{2-23}$$

where G^* is complex shear modulus, defined in Equations (2-9), (2-10), and (2-12).

Applying the boundary conditions and compatibility requirements will result in the recursive formulae for successive layers.

$$\begin{aligned} A_{m+1} &= \frac{1}{2} A_m (1 + \alpha^*_m) e^{ik^*_m h_m} + \frac{1}{2} B_m (1 - \alpha^*_m) e^{-ik^*_m h_m} \\ B_{m+1} &= \frac{1}{2} A_m (1 - \alpha^*_m) e^{ik^*_m h_m} + \frac{1}{2} B_m (1 + \alpha^*_m) e^{-ik^*_m h_m} \end{aligned} \tag{2-24}$$

where $\alpha^*_{m+1} = \dfrac{\rho_m (v_s)_m (1 + i\xi_m)}{\rho_{m+1} (v_s)_{m+1} (1 + i\xi_{m+1})}$ and ρ_m is the density of layer m. The motion at any layer can be easily computed from motion in any other layer (e.g. input motion imposed at the bottom of

the soil column) using the transfer function, F_{ij}, that relates displacement amplitude at layer *i* to that at layer *j*:

$$F_{ij}(\omega) = \frac{|u_i|}{|u_j|} = \frac{A_i(\omega) + B_i(\omega)}{A_j(\omega) + B_j(\omega)} \tag{2-25}$$

$|\ddot{u}| = \omega|\dot{u}| = \omega^2|u|$ for harmonic motions and the transfer function can be used to compute accelerations and velocities. When substituting Equation (2-7) into (2-20), the wave equation becomes independent of frequency for a harmonic loading with circular frequency of ω.

Since the solution for an arbitrary loading is performed by transforming the motion into a finite sum of harmonic motions using Fourier transform, the damping of the system becomes independent of the frequency of the input motion if the hysteretic model is used due to the frequency independent viscosity shown in Equation (2-7). On the other hand, the frequency domain solution becomes frequency dependent if the Udaka model is used.

The frequency domain solution is not unique and depends on the type of the linear viscoelastic model, or complex shear modulus, incorporated. The important influence of the complex shear modulus on the frequency domain solution is discussed in detail in section 3.5.4.

2.7.1 Equivalent linear analysis for one-dimensional site response analysis

The frequency domain solution is predicated on the assumption that modulus and damping properties are constant and independent of the strain level. The equivalent linear approximation method was developed to capture non-linear cyclic response of soil within the framework of the frequency domain solution (Schnabel et al., 1972). The nonlinear hysteretic stress-strain behavior is approximated by the modulus degradation and damping curves.

The schematic drawing of the equivalent linear method is shown in Figure 2-13. For a given ground motion time history, the propagated ground motion is calculated using an initial estimate of modulus and damping values. The computation is performed in the frequency domain. Then, the strain time histories for each layer, from which the maximum strain values are obtained, are calculated. An effective shear strain (equal to about 65% of peak strain) is computed for a given soil layer and corresponding estimates of shear modulus and damping is obtained from the shear modulus reduction and damping curves. This process is repeated until a converged solution is reached. This approach has provided results that compare well with field recordings and is widely used in engineering practice (Seed and Idriss, 1983; Dobry et al., 1994).

The main limitation of the equivalent linear analysis is that constant shear modulus and damping is used throughout the analysis. It represents soil as a linear viscoelastic material. When propagating a strong ground motion, for which the effective strain would be large, using constant values of shear modulus and damping throughout the ground motion record doesn't account for the variations of soil properties with change in strain levels experienced by soils. The constant linear modulus and damping would filter out important high frequency components and overestimate the stiffness at large strain levels.

This limitation has been recognized by Sugito et al. (1994) and Assimaki et al. (2000), and the use of frequency dependent modulus degradation and damping in equivalent linear analysis has been proposed. The high frequency components are associated with small loops and associated modulus degradation and hysteretic damping are small. On the other hand, the low frequency loops result in larger cyclic loops and corresponding degradation and hysteretic damping is high. Assimaki et al. (2000) proposes use of the smoothed strain Fourier spectrum to estimate the frequency dependent modulus and damping. The strain Fourier spectrum of each layer is calculated, normalized to peak strain, and then smoothed. The frequency dependent strain level is obtained and corresponding shear modulus and damping is selected. The actual relationship between frequency and shear modulus and damping is not constant at a given frequency and therefore smoothed spectrum is only an approximation of the actual behavior. It is a phenomenological model developed as a mathematical convenience, but does not reflect a real soil behavior.

2.7.2 Quarter wavelength method

Quarter wavelength method (QWM) is a simple frequency domain analysis procedure assuming soil profile as an elastic medium. In QWM, the soil amplification is modeled as:

$$Amp(f) = A(f)P(f) \tag{2-26}$$

where *A(f)* is the amplification function and *P(f)* is the attenuation function.

The amplification function is defined as:

$$A(f) = \sqrt{\frac{\rho^0 \cdot V_s^0}{\overline{\rho}^s(f) \cdot \overline{V}_s^s(f)}} \tag{2-27}$$

where ρ is density (g/cm^3) and V_S is shear velocity (m/sec); superscript ^{0} denotes the source and ^{s} the site; f is frequency (Hz). $\overline{\rho}^s(f)$ and $\overline{V}_s^s(f)$ are explained next.

The frequency-dependent effective velocity $\overline{V}_s^s(f)$ is defined as the average shear wave velocity from the surface to a depth of a quarter wavelength for the given frequency *f*. The travel time to the depth of a quarter wavelength can be calculated as:

$$tt_z(f)=\frac{1}{4f} \tag{2-28}$$

The depth of the quarter wavelength *z* can be calculated as

$$tt_z(f)=\sum_{i=1}^{m}\frac{h^{(i)}}{V_s^{(i)}} \qquad z=\sum_{i=1}^{m}h^{(i)} \tag{2-29}$$

where $h^{(i)}$ is the thickness of the i^{th} layer, $V_s^{(i)}$ is the shear velocity of i^{th} layer. The effective velocity at a given frequency f is determined by

$$\overline{\beta}_s(f)=\frac{z}{tt_z(f)} \tag{2-30}$$

$\overline{\rho}_s(f)$ is defined as:

$$\overline{\rho}_s(f)=\frac{1}{tt_z(f)}\left[\sum_{i=1}^{m}\frac{h^{(i)}}{V_s^{(i)}}\cdot\rho_s^{(i)}\right] \tag{2-31}$$

The soil attenuation is modeled using the attenuation function *P(f)*, which is defined as:

$$P(f)=e^{-\pi\cdot\kappa\cdot f} \tag{2-32}$$

where κ is a parameter that accounts for shear velocity and damping over the soil column and defined as:

$$\kappa=\sum_{i=1}^{N}\left[\int_0^{h^{(i)}}\frac{dz}{V_s^{(i)}\cdot Q(h)}\right] \tag{2-33}$$

where *N* is the number of soil layers, *h* is the depth measured from the ground surface, and *Q* is the quality factor. *Q* is a parameter that describes the energy dissipation and defined as:

$$Q=\frac{1}{2\xi}\quad for\ Q^{-1}<<1 \tag{2-34}$$

where ξ is the damping ratio.

In summary, the QWM is a simplified form of the frequency domain solution whereby the average properties up to a quarter wavelength are considered.

2.8 Time domain solution

Frequency domain solution only enables linear viscoelastic representation of the true nonlinear soil behavior. When propagating strong ground motion, the strain variation during the course of loading is significant and cannot be approximated by a representative strain throughout the duration of the shaking. The actual nonlinear behavior can only be simulated via a time domain analysis using step-by-step integration scheme.

In 1-D time domain analysis, the unbounded medium, shown in Figure 2-12a, is idealized as discrete lumped mass system, as shown in Figure 2-12b. The wave propagation equation, Equation (2-20), is written as:

$$[M]\{\ddot{u}\}+[C]\{\dot{u}\}+[K]\{u\}=-[M]\{I\}\ddot{u}_g \tag{2-35}$$

where [M] = mass matrix; [C] = viscous damping matrix; [K] = stiffness matrix; $\{\ddot{u}\}$ = vector of nodal relative acceleration; $\{\dot{u}\}$ = vector of nodal relative velocities; and $\{u\}$ = vector of nodal relative displacements. $\ddot{u}_g$ is the acceleration at the base of the soil column and {I} is the unit vector. Equation (2-35) is solved numerically at each time step. There are several numerical schemes available to solve the dynamic equation, including a) central difference, b) Newmark β, and c) Wilson θ methods. Details of the numerical integration methods are summarized in Appendix B. Note that in time domain analysis, the motion is not decomposed into upwards and downwards components, as in frequency domain analysis. Instead, the calculated motions at the layers, $\{\ddot{u}\}$, and input motion at the base of the soil column, $\ddot{u}_g$, are the sum of both components.

In 1D analysis, each individual layer *i* is represented by a corresponding mass, a spring, and a dashpot for viscous damping. Lumping half the mass of each of two consecutive layers at their common boundary forms the mass matrix. Since 1D model only considers vertical propagation of horizontal shear waves, a simple shear model is used. The stiffness matrix is defined as:

$$k_i=\frac{G_i}{h_i} \tag{2-36}$$

where G_i is the shear modulus and h_i is the thickness of layer *i*. For a linear-elastic material, G_i is constant. When using a nonlinear soil model, k_i is the tangent stiffness of the shear model and updated at each time step.

Viscous damping is added, in the form of damping matrix [C], to represent damping at very small strains. It is not possible to make the viscous damping frequency independent since in time domain analysis, an arbitrary motion is not decomposed into a finite sum of harmonic components. This can cause artificial damping which originates from uncontrolled frequency dependence of damping. This issue is discussed in detail in section 3.2.

2.9 Summary

The effect of local geology on ground motion propagation is significant and cannot be ignored in seismic design. Empirical procedures have been developed to estimate site effects but are limited in their applicability. Site response analysis is commonly performed to estimate and characterize site effects by solving the dynamic equations of motion through an idealized soil column. Simulation of complex cyclic soil behavior is an important part of performing site response analysis. Soil models have been developed that range from simple equivalent linear models represented by shear modulus degradation and damping ratio curves to complex bounding surface plasticity based soil models. `

There are two main numerical methods for solving the dynamic equation of motion used in site response analysis; a) equivalent linear analysis method solved in frequency domain and b) nonlinear analysis performed in time domain. Although the equivalent linear analysis is widely used in engineering practice due to its simplicity, it is essentially a linear method that does not account for the change in soil properties throughout the duration of the ground motion. Nonlinear analysis, on the other hand, uses a step-by-step integration scheme and more accurately simulates the true nonlinear behavior of soils.

Factors	*G/G_{max}*	*Damping ratio*
Effective confining pressure, σ'_m	Increases with σ'_m; effect decreases with increasing PI	Decreases with σ'_m; effect decreases with increasing PI
Void ratio, e	Increases with e	Decreases with e
Geologic age, t_g	May increase with t_g	Decreases with t_g
Cementation, c	May increase with c	May decrease with c
Overconsolidation ratio, OCR	Not affected	Not affected
Plasticity index, PI	Increases with PI	Decreases with PI
Cyclic strain, γ_c	Decreases with γ_c	Increases with γ_c
Strain rate, $\dot{\gamma}$	G increases with $\dot{\gamma}$, but G/G_{max} probably not affected if G and G_{max} are measured at same $\dot{\gamma}$.	Stays constant or may increase with $\dot{\gamma}$
Number of loading cycles, N	Decreases after N cycles of large γ_c (G_{max} measured before N cycles) for clays; for sands, can increase (under drained conditions) or decrease under undrained conditions	Not significant for moderate γ_c and N

Table 2-1 Various environmental and loading conditions influencing cyclic soil behavior of normally consolidated and moderately consolidated soils (after Dobry and Vucetic, 1987).

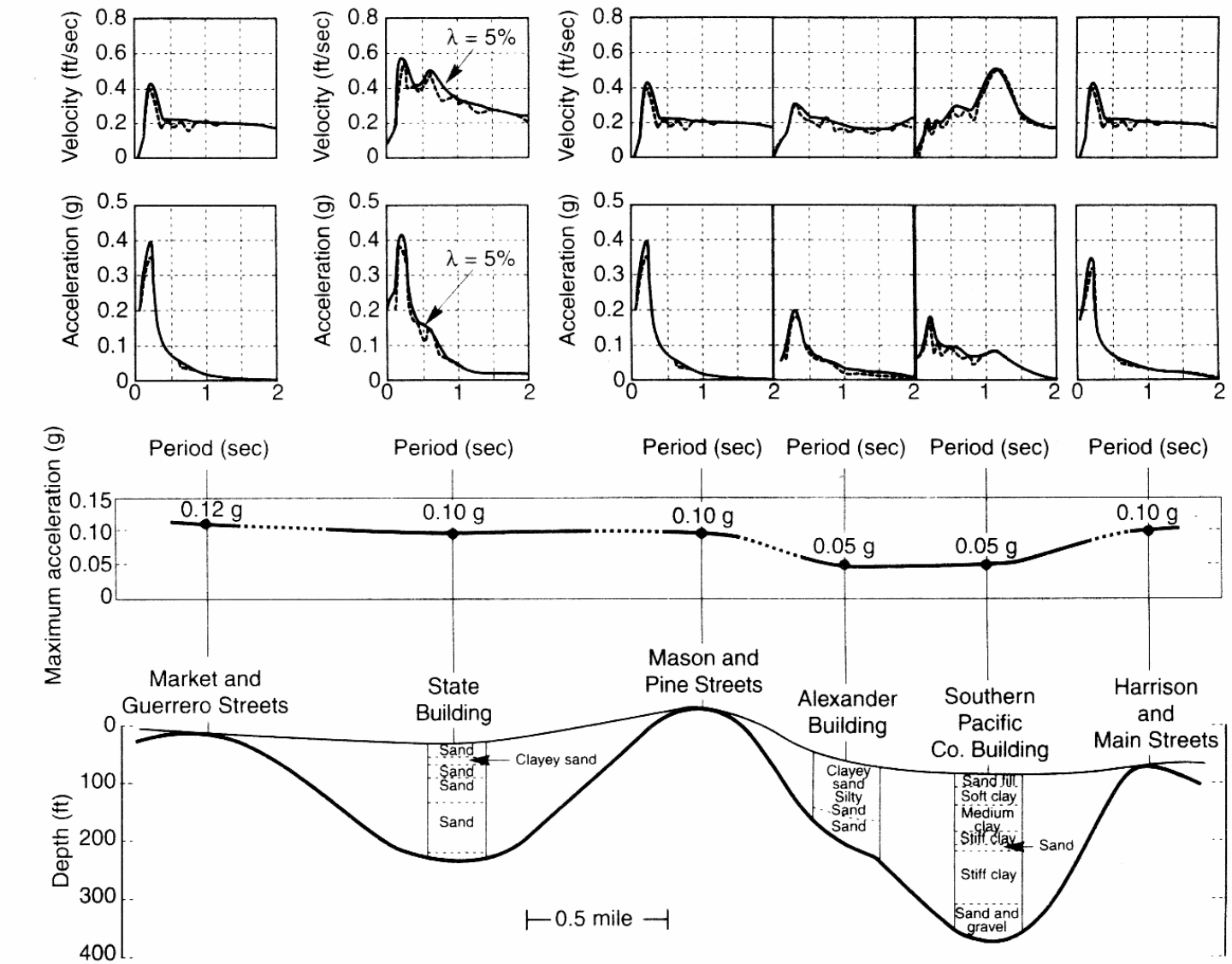

Figure 2-1 Variation of peak ground acceleration and spectral acceleration along a 4-mile section in San Francisco recorded during 1957 San Francisco earthquake (Idriss, 1968).

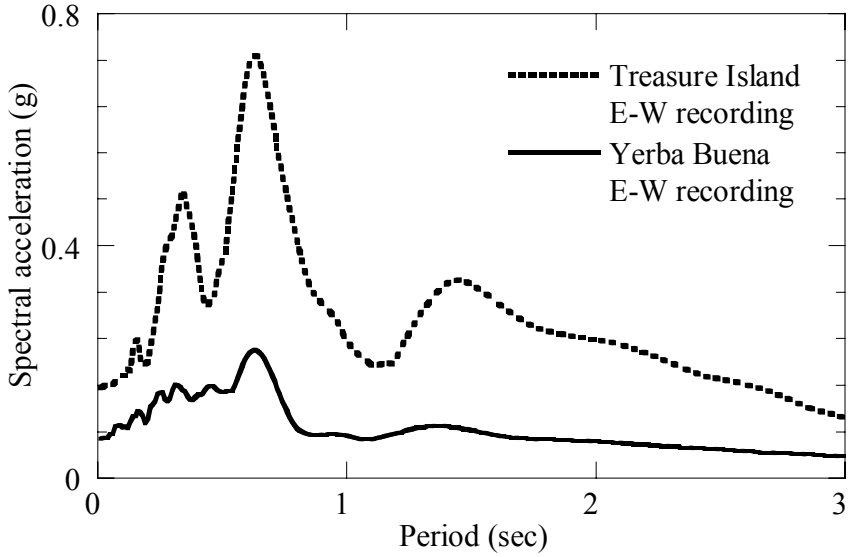

Figure 2-2 Comparison of E-W recorded motions at Yerba Buena Island and Treasure Island during 1989 Loma Prieta earthquake.

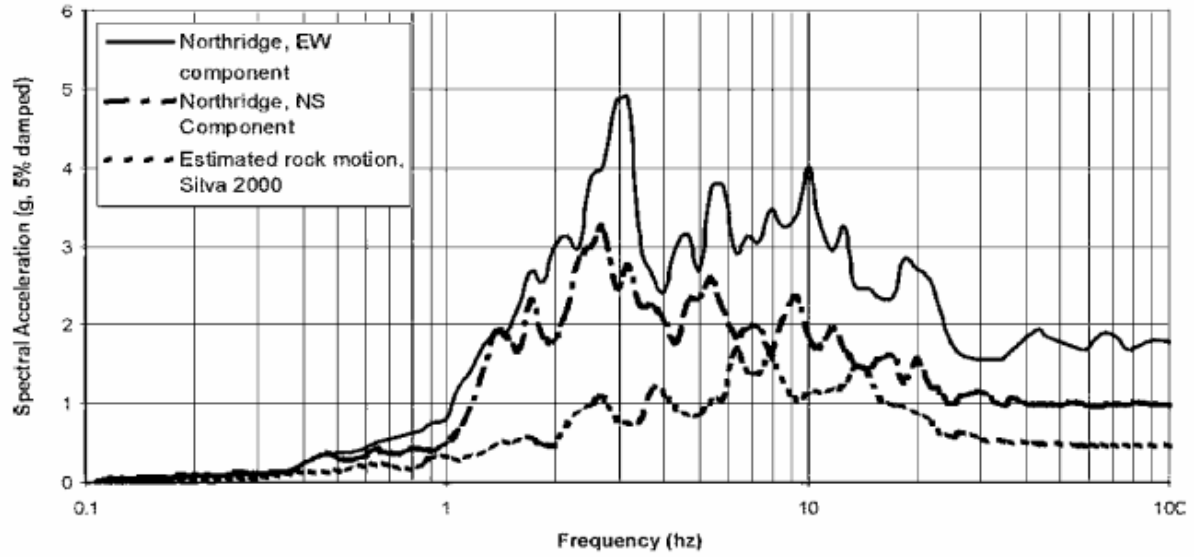

Figure 2-3 Recorded motions at the surface and estimated rock motion at Tarzana station during 1994 Northridge earthquake (Vahdani and Wikstrom, 2002).

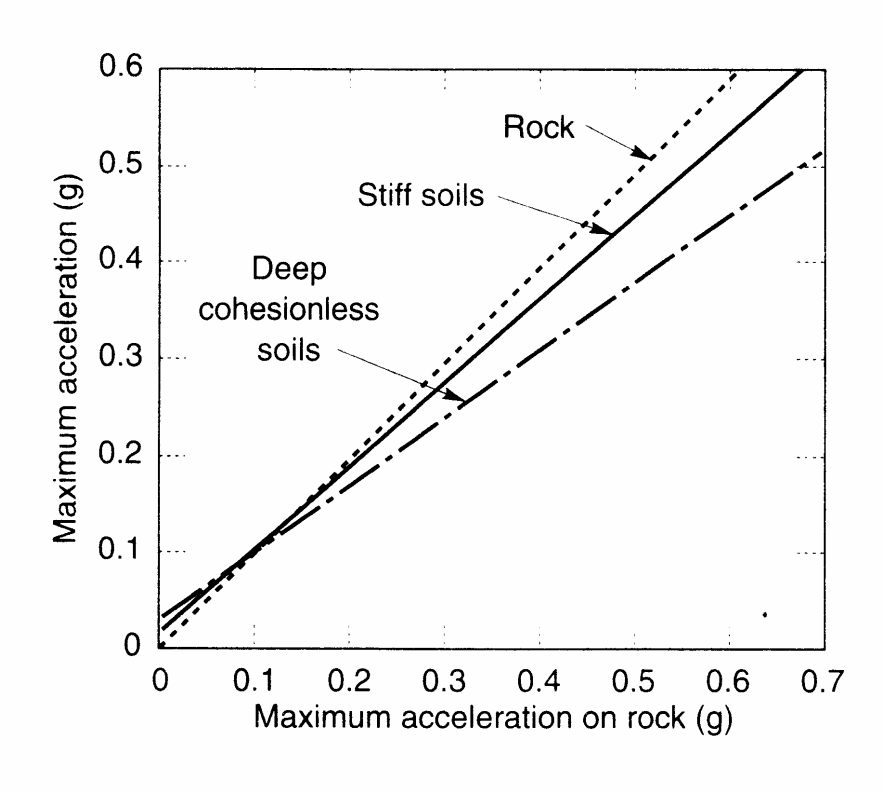

Figure 2-4 Approximate relationship between peak accelerations at rock outcrop and soil sites (Seed et al., 1976).

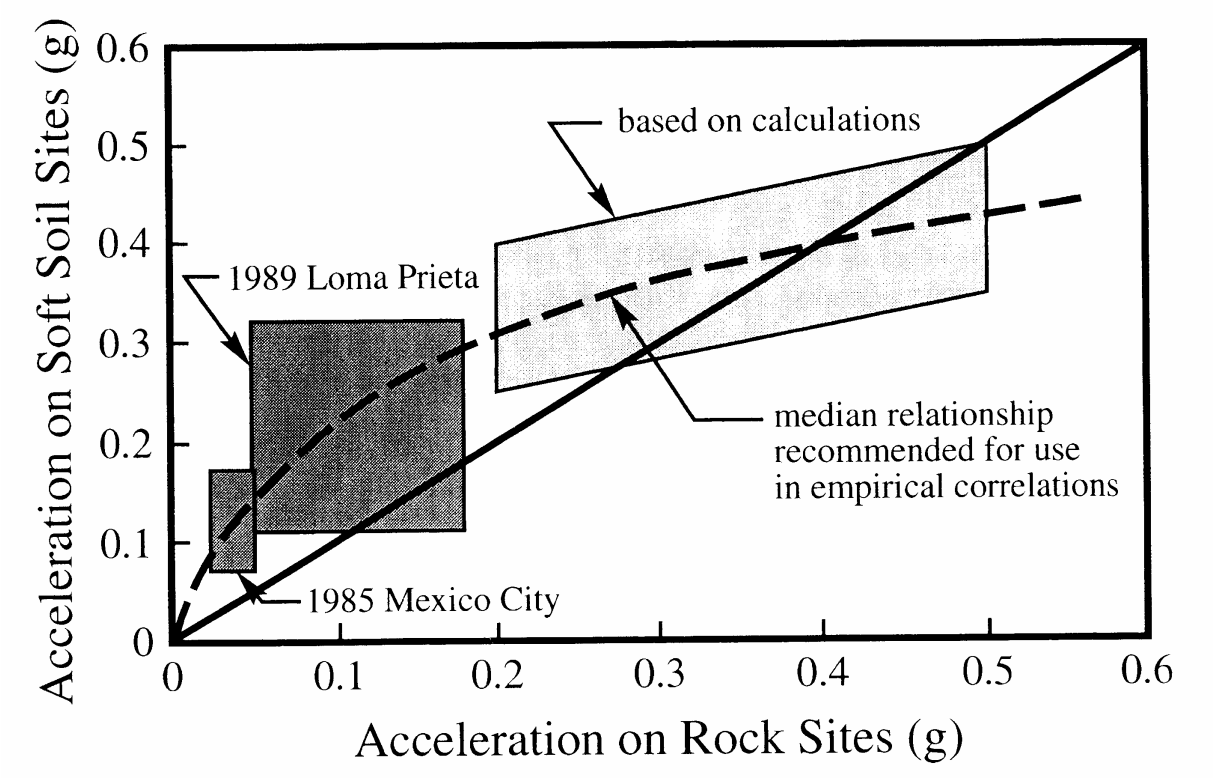

Figure 2-5 Relationship between peak acceleration on rock and soft soil sites (Idriss, 1990).

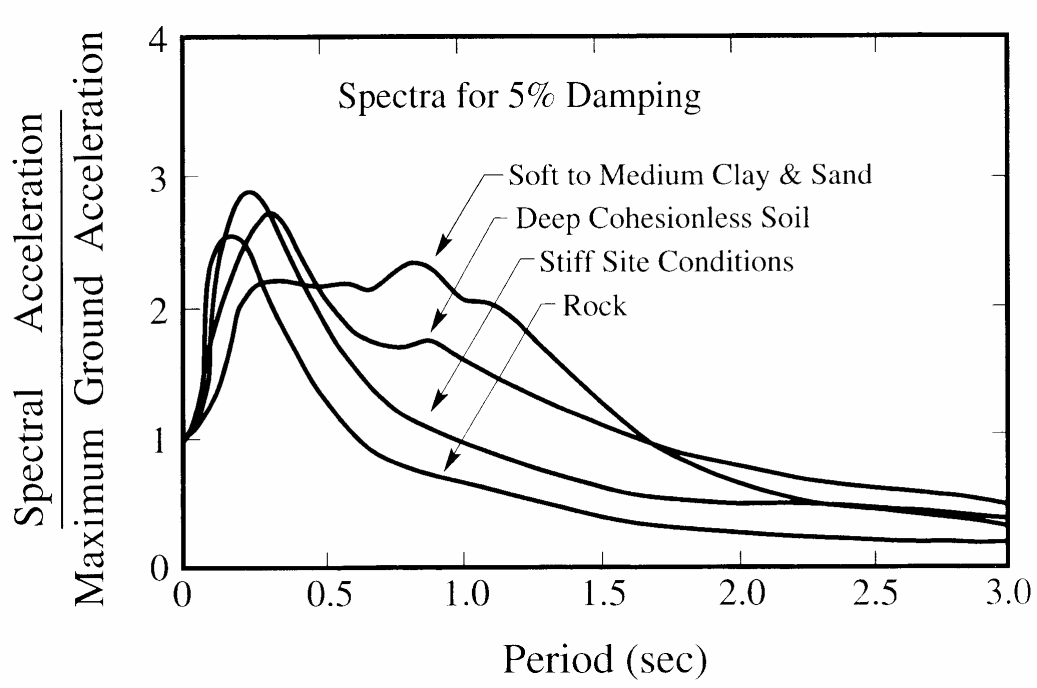

Figure 2-6 Average normalized response spectra (5% damping) for different local site conditions (Seed et al., 1976).

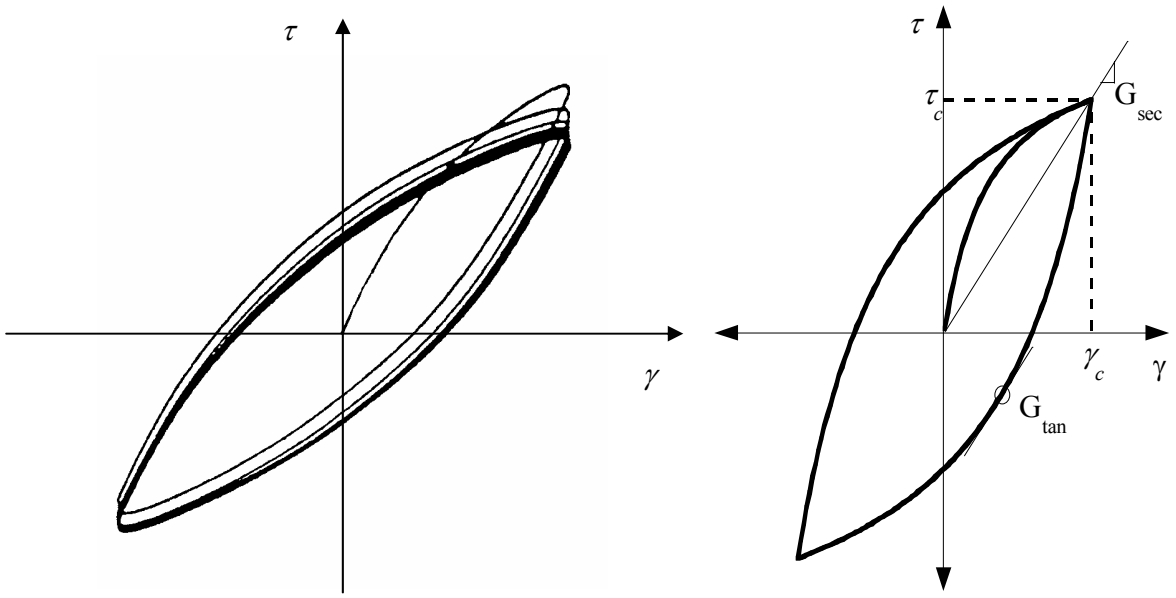

(a) (b)

Figure 2-7 a) Measured hysteretic stress-strain loops for a typical clay (EPRI, 1993) and b) idealized hysteresis loop.

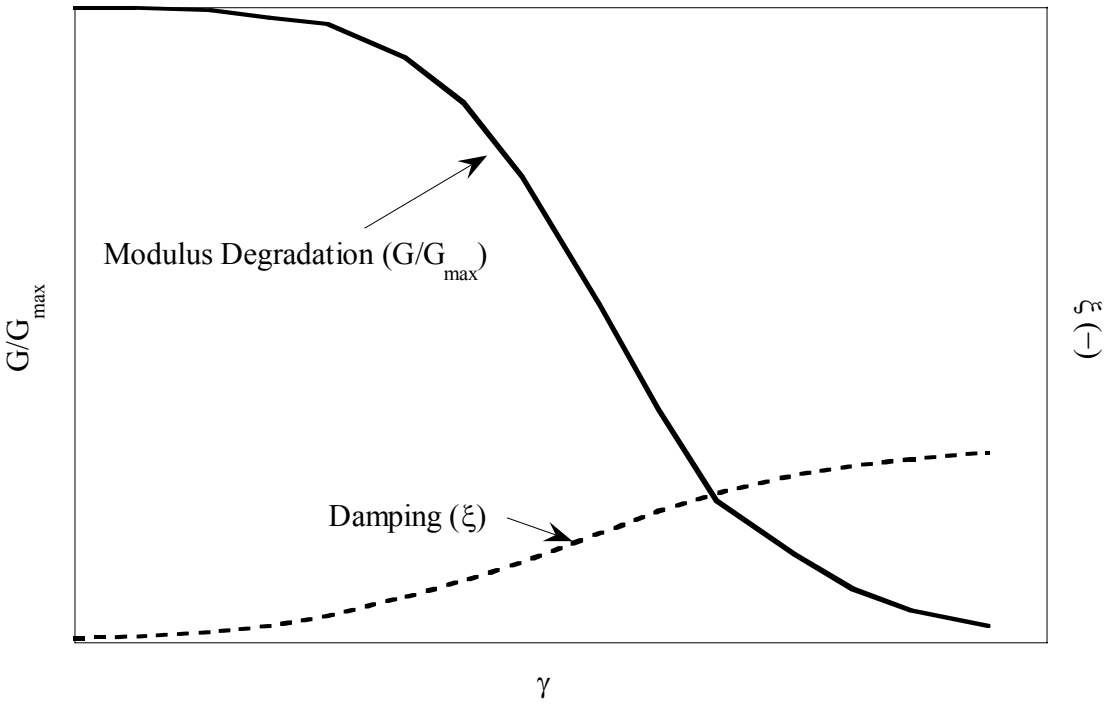

Figure 2-8 Shear modulus degradation and damping ratio curves.

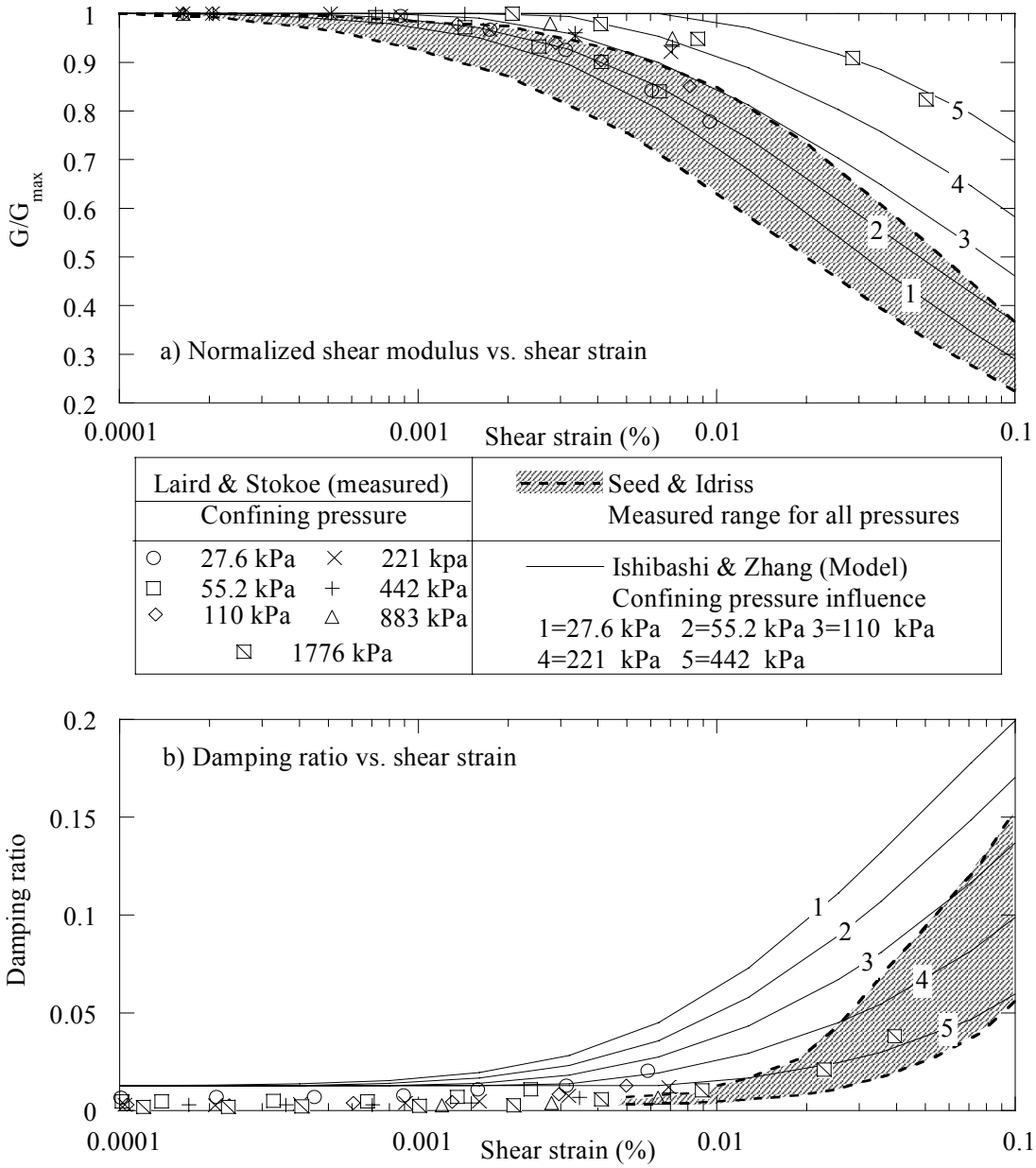

Figure 2-9 Influence of confining pressure on modulus degradation and damping ratio of soil. Data points and curves are developed from laboratory measurements and proposed models published in the literature.

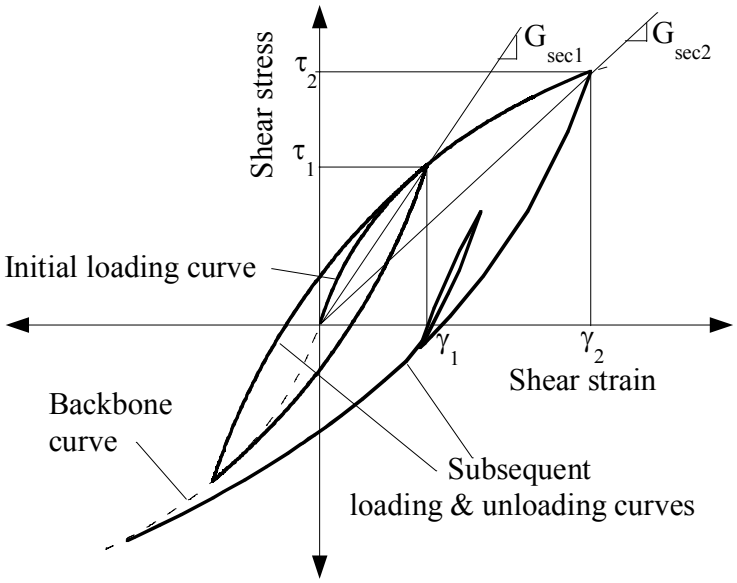

Figure 2-10 Hyperbolic, non-linear soil model with extended Masing rule to define loading and unloading behavior.

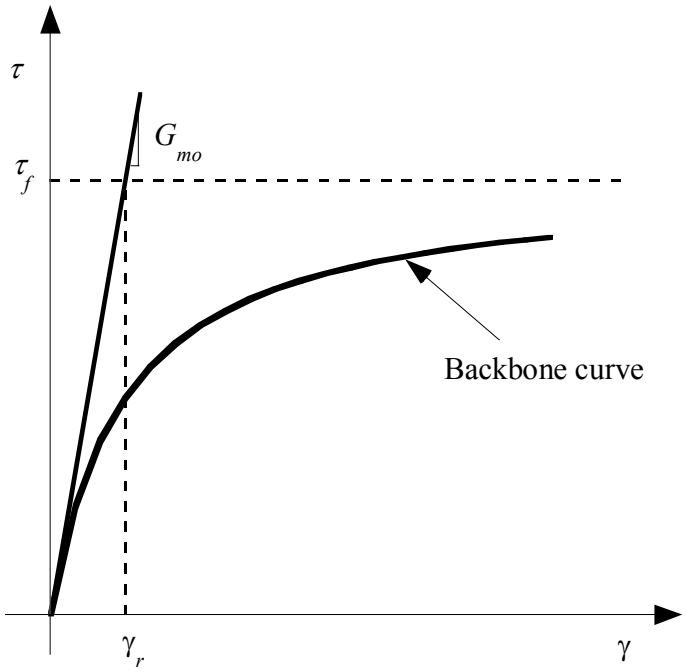

Figure 2-11 Hyperbolic stress-strain relationship and definition of reference strain.

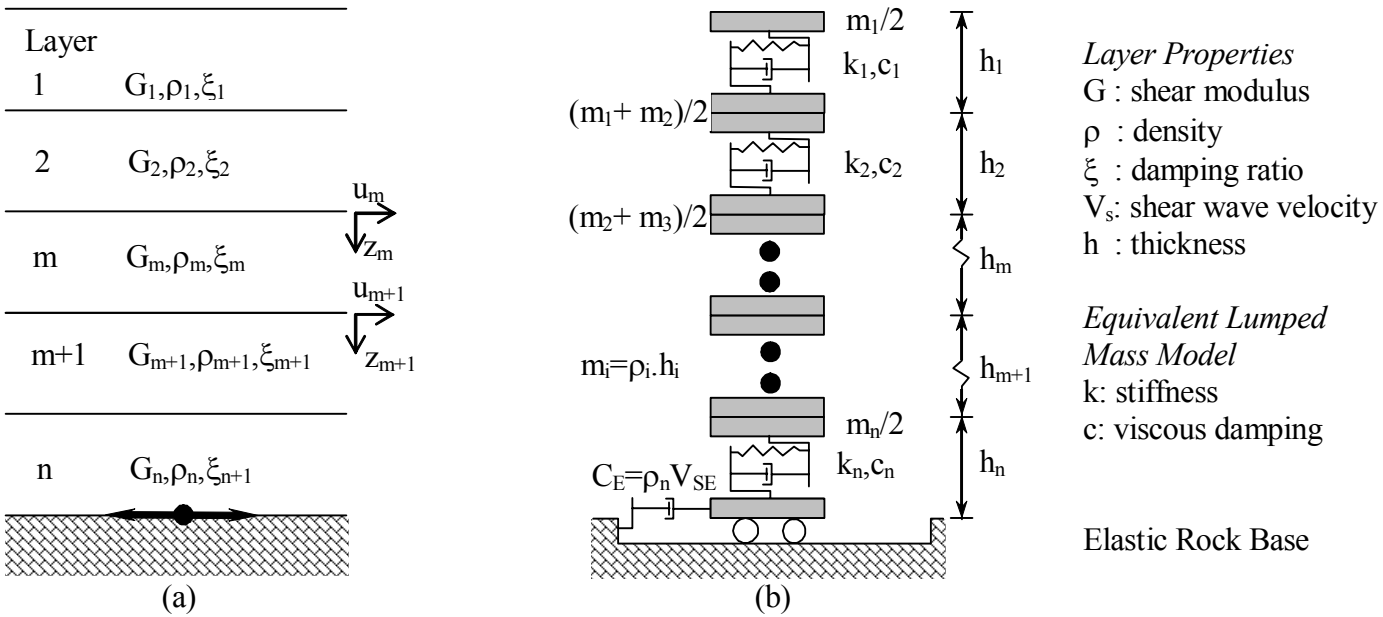

Figure 2-12 Idealized soil stratigraphy (a) Layered soil column (used for frequency domain solution) and (b) multi-degree-of-freedom lumped parameter idealization (used for time domain solution).

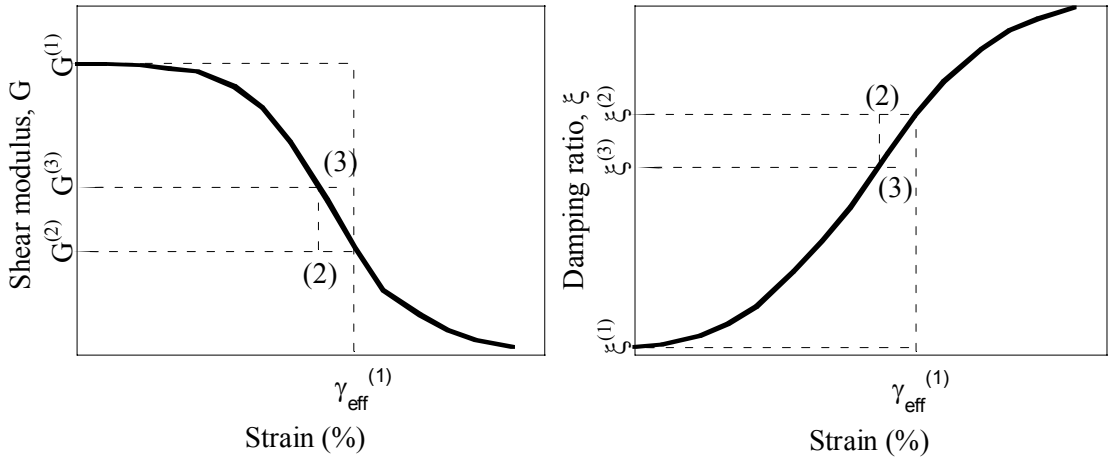

Figure 2-13 Schematic representation of the iterative scheme used in equivalent linear analysis

CHAPTER 3 ONE DIMENSIONAL SITE RESPONSE ANALYSIS MODEL DEVELOPMENT

3.1 Introduction

This chapter describes the development of a new one-dimensional (1D) non-linear time domain and equivalent linear site response analysis model (DEEPSOIL) to accurately simulate wave propagation through very deep deposits. The non-linear model incorporates several improvements over conventional 1D models published in the literature. Section 3.2 describes development of a new viscous damping formulation to reduce the artificial damping introduced numerically through uncontrolled frequency dependent viscous damping. Guidelines on correct use of the viscous damping term in a time domain analysis are presented. Section 3.3 describes the development of a confining pressure dependent nonlinear soil model. The model parameters are constrained using laboratory test data. Section 3.4 describes the scheme implemented to increase numerical accuracy and efficiency of the integration scheme of the equilibrium equations and the nonlinear soil model.

The significance of the proposed model on wave propagation analysis through a deep soil deposit is presented in section 3.5. The non-linear model is verified using a well-known case study in section 3.6.

3.2 Viscous damping formulation

In a non-linear soil model, soil damping is captured through hysteretic loading-unloading cycles. Hysteretic damping of the soil model defined by Matasovic (1993), section 2.5.2.2, as well other models (e.g. Finn et al., 1977), can capture damping at strains larger than 10^{-6} to 10^{-4}, depending on the values of material properties. The use of the damping matrix [C] in the equation of motion, Equation (2-35), is still necessary to include damping at very small strains where the response of many constitutive models is nearly linear elastic, and hence, to avoid unrealistic resonance during wave propagation.

3.2.1 Simplified Rayleigh damping formulation

The viscous damping matrix is frequency dependent in a time domain analysis. The type of the damping formulation determines the degree of frequency dependence of damping. In the

original damping formulation proposed by Rayleigh and Lindsay (1945), the [C] matrix is assumed to be proportional to the mass and stiffness matrices:

$$[C] = a_0[M] + a_1[K] \tag{3-1}$$

The viscous damping matrix is dependent on stiffness, mass and the natural modes of the soil column. The natural modes and the soil column stiffness are derived from the shear wave velocity profile of the soil column.

The damping matrix is assumed in many current site response analysis programs to be only stiffness proportional since the value of a_0[M] is small compared to a_1[K] (e.g. Finn et al., 1977; Matasovic, 1993; Borja et al., 1999). Small strain viscous damping effects are assumed proportional only to the stiffness of the soil layers. The viscous damping matrix is further simplified to:

$$[C] = a_1[K] \tag{3-2}$$

where $a_1 = 2\xi / \omega_1$ and ω_1 = frequency of the first natural mode of the soil column.

The viscous damping matrix for a multi-layered soil is expressed as:

$$[C] = \frac{2}{\omega}[\xi_i K_i] = \frac{2}{\omega}\begin{bmatrix} \xi_1 K_1 & -\xi_1 K_1 & \\ -\xi_1 K_1 & \xi_1 K_1 + \xi_2 K_2 & -\xi_2 K_2 \\ & -\xi_2 K_2 & \ldots\ldots \end{bmatrix} \tag{3-3}$$

where ω is natural circular frequency of the first natural mode and ξ_i is the equivalent damping ratio for layer i at small strains. The viscous damping matrix is dependent on the first natural mode of the soil column and the soil column stiffness, which are derived from the shear wave velocity profile of the soil column. [C] is commonly taken as independent of strain level and the effect of hysteretic damping induced by nonlinear soil behavior can be separated from (but added to) viscous damping.

The value of the equivalent damping ratio ξ is obtained from the damping ratio curves at small strains. A constant small strain viscous damping is used in some non-linear models with a recommended upper bound value of 1.5 – 4 % for most soils, independent of confining pressure (Matasovic, 1993; Lanzo and Vucetic, 1999).

In order to assess the accuracy of the simplified viscous damping formulation, a series of linear site response analyses are conducted using four idealized soil columns 50m, 100 m, 500 m and 1000 m thick with constant stiffness (V_s = 450 m/sec) and constant viscous damping ratio of

1.8%, as shown in Figure 3-1. The analyses compare linear time domain (TD) wave propagation analysis with linear frequency domain wave propagation analysis. The frequency domain (FD) analysis represents the correct analysis for linear elastic material with frequency independent damping property as the solution of the wave equations can be derived in closed form (e.g. Kramer, 1996). Figure 3-2 shows the computed surface response for a harmonic input motion with soil thickness up to 500m. TD analyses provide identical results to FD analysis for the analyses using zero viscous damping.

TD analysis with viscous damping ratio of 1.8% gives results similar to FD analysis for the 50 m soil column. However, for 100 m and 500 m soil columns the TD analysis gives a response lower than FD analysis. The accuracy of the computed response deteriorates with increasing soil column thickness. The approximation of the viscous damping matrix in TD analysis maybe acceptable for soil columns less than about 50 m thick and when the contribution of the viscous damping is very small.

The simplified damping formulation in Equation (3-3) introduces excessive damping in the time domain analysis that increases with increasing column thickness. The contribution of higher modes is small for relatively short soil columns but may become important for deeper soil columns and when propagating high frequency motion. The simplified damping formulation depends only on the first mode of the deposit and is proportional to the stiffness matrix. If only stiffness proportional damping is used, then the damping ratio being used for higher modes is (Clough and Penzien, 1993; Chopra, 1995):

$$\xi_n = \frac{\beta_R \omega_n}{2} = \xi \frac{\omega_n}{\omega_1} \tag{3-4}$$

Equation (3-4) results in frequency dependent damping ratio, continuously increasing with increase in frequency, as shown in Figure 3-3. The frequency dependent damping ratio will be referred to as effective damping ratio in this study. This implies that the effective damping ratio is increasing at higher natural modes and explains the underestimate of surface ground motion for time domain analysis shown in Figure 3-2. An improved formulation is needed to reduce the overestimation of effective damping ratio at higher natural modes.

3.2.2 Full Rayleigh damping formulation

Full Rayleigh formulation can be implemented in site response analysis. If the damping ratio is constant throughout the soil profile, scalar values of a_0 and a_1 can be computed using two significant natural modes m and n using the following equation (Chopra, 1995):

$$\begin{bmatrix} \xi_m \\ \xi_n \end{bmatrix} = \frac{1}{4\pi} \begin{bmatrix} 1/f_m & f_m \\ 1/f_n & f_n \end{bmatrix} \begin{Bmatrix} a_0 \\ a_1 \end{Bmatrix} \tag{3-5}$$

This matrix can be solved for a_0 and a_1:

$$a_0 = 2\omega_{(m)}\omega_{(n)} \left(\frac{\omega_{(m)}\xi_{(n)} - \omega_{(n)}\xi_{(m)}}{\omega_{(m)}^2 - \omega_{(n)}^2} \right) \& \; a_1 = 2 \left(\frac{\omega_{(m)}\xi_{(m)} - \omega_{(n)}\xi_{(n)}}{\omega_{(m)}^2 - \omega_{(n)}^2} \right) \tag{3-6}$$

If the damping ratio ξ is frequency independent then:

$$\alpha_R = 2\xi \left(\frac{\omega_{(m)}\omega_{(n)}}{\omega_{(m)} + \omega_{(n)}} \right) \& \; \beta_R = 2\xi \left(\frac{1}{\omega_{(m)} + \omega_{(n)}} \right) \tag{3-7}$$

When choosing a higher mode, the mass matrix component will counter-balance part of the contribution of the stiffness matrix component. As higher modes are used, a_0 increases and a_1 decreases.

The Rayleigh damping formulation using two significant modes has been incorporated for example in the two-dimensional finite element program QUAD4M by Hudson et al. (1994). For a multi-layered soil with frequency independent damping ratio, Equation (3-1) can be expanded as follows:

$$\begin{aligned} [C] = {} & 2 \left(\frac{\omega_{(m)}\omega_{(n)}}{\omega_{(m)} + \omega_{(n)}} \right) \begin{bmatrix} \xi_1 M_1 & & \\ & \xi_2 M_2 & \\ & & \ldots\ldots \end{bmatrix} \\ & + 2 \left(\frac{1}{\omega_{(m)} + \omega_{(n)}} \right) \begin{bmatrix} \xi_1 K_1 & -\xi_1 K_1 & \\ -\xi_1 K_1 & \xi_1 K_1 + \xi_2 K_2 & -\xi_2 K_2 \\ & -\xi_2 K_2 & \ldots\ldots \end{bmatrix} \end{aligned} \tag{3-8}$$

With frequency dependent damping ratio, Equation (3-8) can be expanded as follows:

$$[C]=\left(\frac{2\omega_{(m)}\omega_{(n)}}{\omega_{(m)}^2-\omega_{(n)}^2}\right)\begin{bmatrix}\left(\omega_{(m)}\xi_{1(n)}-\omega_{(n)}\xi_{1(m)}\right)M_1 & & \\ & \left(\omega_{(m)}\xi_{2(n)}-\omega_{(n)}\xi_{2(m)}\right)M_2 & \\ & & .....\end{bmatrix}+$$

$$2\left(\frac{}{\omega_{(m)}^2-\omega_{(n)}^2}\right)\begin{bmatrix}\left(\omega_{(m)}\xi_{1(m)}-\omega_{(n)}\xi_{1(n)}\right)K_1 & -\left(\omega_{(m)}\xi_{1(m)}-\omega_{(n)}\xi_{1(n)}\right)K_1 & \\ -\left(\omega_{(m)}\xi_{1(m)}-\omega_{(n)}\xi_{1(n)}\right)K_1 & \left\langle\left(\omega_{(m)}\xi_{1(m)}-\omega_{(n)}\xi_{1(n)}\right)K_1+\right. & -\left(\omega_{(m)}\xi_{2(m)}-\omega_{(n)}\xi_{2(n)}\right)K_2 \\ & \left.\left(\omega_{(m)}\xi_{2(m)}-\omega_{(n)}\xi_{2(n)}\right)K_2\right\rangle & \\ & -\left(\omega_{(m)}\xi_{2(m)}-\omega_{(n)}\xi_{2(n)}\right)K_2 & .....\end{bmatrix}$$

(3-9)

In site response analysis the natural frequency of the selected mode is commonly calculated as (Kramer, 1996):

$$f_n=\frac{V_s}{4H}(2n-1) \tag{3-10}$$

where n is the mode number and f_n is the natural frequency of the corresponding mode. It is common practice to choose frequencies that correspond to the first mode of the soil column and a higher mode that corresponds to the predominant frequency of the input motion (Hudson, 1994; Rathje and Bray, 2001; Borja et al., 2002). Equal values of modal damping ratios are specified for the two modes since the damping ratios are known to be frequency independent in the frequency range of interest (Kramer, 1996; EPRI, 1993).

Equation (3-5) results in frequency dependent damping ratio even if the specified damping ratio at the two selected modes is equal, as shown in Figure 3-3. However, the frequency dependence of damping ratio is significantly reduced compared to the simplified Rayleigh damping formulation.

3.2.3 Extended Rayleigh viscous damping formulation

Equation (3-1) can be extended so that more than 2 frequencies/modes are specified, and is referred to as extended Rayleigh formulation. Using the orthogonality conditions of the mass and stiffness matrices, the damping matrix can consist of any combination of mass and stiffness matrices (Clough and Penzien, 1993), as follows:

$$[C] = [M] \sum_{b_e=0}^{N-1} a_b \left[[M]^{-1} [K] \right]^{b_e} \tag{3-11}$$

where N is the number of frequencies/modes incorporated. The coefficient a_b is a scalar value assuming constant damping ratio throughout the profile and is defined as follows:

$$\xi_n = \frac{1}{4\pi f} \sum_{b_e=0}^{N-1} a_b \left(2\pi f_n\right)^{2b_e} \tag{3-12}$$

Equation (3-11) implies that the damping matrix can be extended to incorporate any number of frequencies/modes. The formulation reduces to full Rayleigh damping formulation, Equation (3-1), when b_e = 0 to 1. The matrix resulting from Equation (3-12) is numerically ill-conditioned since coefficients f_n^{-1}, f_n, f_n^3, f_n^5 … can differ by orders of magnitude. Having more than 4 frequencies/modes can result in a singular matrix depending on f_n and in such case, a_b cannot be calculated.

Addition of a frequency/mode is accompanied by an increase in the number of diagonal bands of the viscous damping matrix, resulting in a significant increase in the numerical cost of the solution. Incorporating odd number of modes is also problematic since it will result in negative damping at certain frequencies (Clough and Penzien, 1993). Only 4 modes are used in this study. The coefficients a_b is calculated from Equation (3-12) for b = 0 to 3:

$$\begin{bmatrix} \xi_m \\ \xi_n \\ \xi_o \\ \xi_p \end{bmatrix} = \frac{1}{4\pi} \begin{bmatrix} 1/f_m & f_m & f_m^3 & f_m^5 \\ 1/f_n & f_n & f_n^3 & f_n^5 \\ 1/f_o & f_o & f_o^3 & f_o^5 \\ 1/f_p & f_p & f_p^3 & f_p^5 \end{bmatrix} \begin{Bmatrix} a_0 \\ a_1 \\ a_2 \\ a_3 \end{Bmatrix} \tag{3-13}$$

where f_m, f_n, f_o, and f_p are selected frequencies and ξ_m, ξ_n, ξ_o, and ξ_p are the damping ratios at these frequencies.

The effective damping resulting from Equation (3-13) is illustrated in Figure 3-3 assuming the damping ratios are equal at the selected frequencies/modes. The damping ratio remains close to the target damping ratio over a wider range of frequencies than the Rayleigh damping formulation and is exact at the four specified frequencies.

For b_e = 0 to 3, Equation (3-11) can be expanded to model varying damping ratio in the different soil layers:

$$
\begin{aligned}
[C] &= [a_0][M] + a_1[K] + [a_2]\left\{[K][M]^{-1}[K]\right\} + [a_3]\left\{[K][M]^{-1}[K][M]^{-1}[K]\right\} \\
&= \begin{bmatrix} a_{01}M_1 & 0 & 0 \\ 0 & a_{02}M_2 & 0 \\ 0 & 0 & ..... \end{bmatrix} + \begin{bmatrix} a_{11}K_1 & a_{11}K_{12} & 0 \\ a_{12}K_{21} & a_{12}K_{22} & a_{12}K_{23} \\ 0 & a_{13}K_{32} & ..... \end{bmatrix} + \\
&\begin{bmatrix} a_{21} & 0 & 0 \\ 0 & a_{22} & 0 \\ 0 & 0 & ... \end{bmatrix} \begin{bmatrix} \frac{K_{11}^{\ 2}}{M_1} + \frac{K_{12}K_{21}}{M_2} & \frac{K_{21}K_{11}}{M_1} + \frac{K_{22}K_{21}}{M_2} & \frac{K_{12}K_{23}}{M_2} \\ \frac{K_{21}K_{11}}{M_1} + \frac{K_{22}K_{21}}{M_2} & \frac{K_{21}K_{12}}{M_1} + \frac{K_{22}^{\ 2}}{M_2} & \frac{K_{22}K_{23}}{M_2} + \frac{K_{23}K_{33}}{M_3} \\ \frac{K_{32}K_{21}}{M_2} & \frac{K_{32}K_{22}}{M_2} + \frac{K_{33}K_{32}}{M_3} & ..... \end{bmatrix} + \\
&\begin{bmatrix} a_{31} & 0 & 0 \\ 0 & a_{32} & 0 \\ 0 & 0 & ... \end{bmatrix} \left\{[K][M]^{-1}[K][M]^{-1}[K]\right\}
\end{aligned}
\tag{3-14}
$$

where a_{bi} represents coefficient of layer i and calculated using Equation (3-13).

The extended Rayleigh damping formulation is incorporated in a site response analysis code for the first time in this study and its effectiveness is evaluated.

3.2.4 Selection of frequencies/modes for the Rayleigh damping formulations

The frequency dependent nature of the Rayleigh damping formulations implies that the accuracy of the time domain solution depends on the frequencies/modes selected to define the damping function. In this section, a series of analyses are presented to examine the influence of the selected frequencies/modes of Rayleigh damping formulations on site response analysis and to illustrate how to choose the optimum frequencies/modes. Linear wave propagation analysis is used in the selection process since viscous damping is independent of, but additive to, hysteretic damping resulting from a non-linear material model. The optimum frequencies/modes are selected such that the linear time domain solution (with frequency dependent damping), compares well with the linear frequency domain solution (with frequency independent damping and therefore using the hysteretic model) that represents the correct solution. The selection process using linear analysis is a required step prior to performing a nonlinear site response analysis. In other words, the significant frequencies/modes should be selected through a linear analysis and the chosen frequencies/modes can then be employed in the nonlinear analysis.

Both the frequency and time domain solutions are solved using the newly developed site response program DEEPSOIL using the complex shear modulus defined in Equation (2-10). More details of DEEPSOIL will be presented in section 3.4

Three soil columns, 100 m, 500 m and 1000 m, representative of the profiles in the Mississippi embayment, are used (shear wave velocity profile (2) in Figure 3-1). The corresponding natural frequencies are 1.1 Hz (0.9 sec), 0.35 Hz (2.9 sec), and 0.2 Hz (5.18 sec) for the 100 m, 500 m, and 1000 m columns respectively. In time domain analysis, the thickness of the layer controls the maximum frequency that can be propagated:

$$f_{\max} = \frac{(V_s)_i}{4h_i} \tag{3-15}$$

where f_{max} = maximum frequency that layer i can propagate, $(V_s)_i$ = shear velocity, h_i = thickness of each layer. The layer thickness has been chosen so that f_{max} is equal to 50 Hz through all layers within the soil column. The 100 m column has 49 layers whereas the 1000 m column has 277 layers.

Two viscous damping profiles are used (Figure 3-1). The viscous damping profile (1) has a constant damping ratio of 1.8 % and the viscous damping profile (2) has a vertical variation of damping ratio, decreasing with depth. The viscous damping profile (2) represents the confining pressure dependent small strain damping from the design soil curves developed by EPRI (1993).

Four input motions, two synthetic (referred to as S-TS) and two recorded time series (R-TS) at rock outcrops, are used (Figure 3-4 and Figure 3-5). The main characteristics of the motions are summarized in Table 3-2.

The synthetic ground motions are generated by SMSIM version 2.2 (Boore, 2002) using M (moment magnitude) =5 – R (epicentral distance) =20 km (S-TS1) and M=8 - R=32 km (S-TS2), as shown in Figure 3-4. Synthetic ground motions are routinely used in areas such as the Mississippi embayment due to the absence of strong motion records. SMSIM has been used in development of the USGS seismic hazard maps in the central and eastern United States (Frankel, 1996). For S-TS1, (M=5 - R =20 km), the ground motion content is concentrated in a limited frequency range of 2–15 Hz, whereas the content is evenly distributed over the frequency range of 1-50 Hz in S-TS2 (M=8, R=32 km motion).

R-TS1 is the recorded motion during the 1985 Nahanni earthquake (M=6.9, R=16 km), in the Northwest Territories of Canada, as shown in Figure 3-5. The predominant frequency of the

motion is about 16 Hz and has limited content below 1 Hz. R-TS2 is E-W recording at Yerba Buena Island during the 1989 Loma Prieta earthquake (M = 6.9, R = 80.6 km), in northern California, Figure 3-5. Contrary to other motions, the highest concentration of the ground motion content is at low frequencies, from 0.1 to 1 Hz.

Linear wave propagation analyses are performed using selected combinations of the four motions and the three soil columns. The purpose of the analyses is to 1) investigate how to choose the significant frequencies/modes in RF and ERF, 2) compare the accuracy of RF and ERF, and 3) demonstrate the effect of the depth of the soil profile on accuracy of the time domain solution.

S-TS1, 100m soil column

Analyses are performed using M=5 - R=20 km synthetic motion, 100 m, 500 m, and 1000 m soil columns, and viscous damping profile (1). Three analyses are performed for each profile, two using RF and one using ERF, and the results are compared to the frequency domain solution. The first RF analysis follows the conventional guideline for selecting frequencies. The 1st frequency corresponds to the first mode/natural frequency of the soil column, calculated using Equation (3-5), and the 2nd frequency corresponds to the predominant frequency of the input motion (Hudson, 1994; Rathje and Bray, 2001; Borja et al., 2002) or a higher mode. Such solution will be referred to as CRF in this study. In the second RF analysis and the ERF analysis, significant frequencies are chosen independent of soil column modes with the aim of obtaining the best match with the frequency domain solution.

The results for the 100 m profile are shown in Figure 3-6. Figure 3-6a shows the Fourier spectrum ratio of the computed surface motion to the input motion. Figure 3-6b plots the effective damping ratio for the CRF, RF and ERF analyses. Figure 3-6c plots the 5% damped elastic response spectrum of the computed surface motion.

The CRF effective damping ratio underestimates the target damping ratio between 1.1 and 4 Hz (corresponding to 1st and 2nd modes of the soil column) and overestimates the target damping ratio at other frequencies, as shown in Figure 3-6b. The Fourier spectrum ratio, Figure 3-6a, and response spectrum, Figure 3-6c, show that CRF underestimates the surface motion at frequencies greater than 4 Hz. CRF analysis results in significant filtering of ground motion within a frequency range relevant to engineering applications.

The performance of the RF analysis can be improved by a different selection of the two significant frequencies. The frequencies should be selected in part to cover the range of significant frequencies in the input motion. For S-TS1, the optimal range chosen is 2 – 10 Hz through a trial and error process to obtain a good match with the Fourier and response spectra of the frequency domain solution. Although RF does not capture the full range of frequency amplification, as shown in Figure 3-6a, the response spectrum agrees well with the frequency domain solution, Figure 3-6c.

High frequency components of the surface motion can be preserved with the ERF solution. The first two frequencies chosen are identical to the ones used in RF. For 3rd and 4th frequencies, 35 and 45 Hz are selected respectively. ERF solution captures the high frequency components much better than RF, Figure 3-6a, since effective damping ratio does not increase linearly at frequencies high than the selected 2nd frequency (10 Hz in this analysis). However, the 5% damped response spectrum is very similar for both RF and ERF.

S-TS1, 500m soil column

Increase in depth of the soil column is accompanied by decrease in the natural frequency of the soil column and increase in the number of resonant modes as illustrated by the frequency domain solution in Figure 3-7a. Using CRF, the frequencies selected are 0.35 and 4 Hz. At 10 Hz, the effective damping ratio for 100 m profile is 3.7% whereas it is 4.2% for the 500 m profile. Therefore, CRF for 500 m column introduces higher damping compared to the 100 m column at frequencies higher than 4 Hz.

Using 2 and 10 Hz in the RF, the match with the frequency domain solution is significantly improved at higher frequencies , as shown in Figure 3-7a. The lower estimate at low frequencies (the first two modes) is not as important due to low input motion content up to 2 Hz. Comparison of the 5% damped elastic response spectra shows the good match with the frequency domain solution. The ERF solution, using frequencies of 2, 10, 35, 45 Hz, results in a slightly better match with the frequency domain solution.

S-TS1, 1000m soil column

The 1000 m column is most sensitive to overestimation or underestimation of effective damping ratio due to significant increase in number of resonant modes. Decrease in natural frequency of the soil column (0.2 Hz) is accompanied by further widening of the effective

damping ratio curve for CRF, as shown in Figure 3-8b. CRF solution highly underestimates the high frequency motion. RF solution using frequencies of 2 and 7 Hz shows a better match with the frequency domain solution at higher frequencies (Figure 3-8a), however the mismatch at lower frequencies increases. Overall the solution improves significantly when the elastic response spectra are compared in Figure 3-8c. The 2nd frequency has been reduced from 10 to 7 Hz since the frequency range where the motion is amplified (Fourier spectrum ratio > 1) has decreased (Figure 3-8a). The use of ERF results in some but limited improvement of the results.

R-TS1 100m and 1000m columns

The predominant frequency of the R-TS1 input motion is 16 Hz. For 100m profile, CRF (1.1 and 16 Hz) slightly overestimates the response but overall provides a reasonable match with the frequency domain solution, as shown in Figure 3-9a, c. The match is improved when using RF with 3 and 16 Hz. ERF (3, 16, 35, 45 Hz), provides a better match for Fourier spectrum ratio at high frequencies, but again the difference is small when comparing the 5% damped elastic response spectra.

For 1000 m profile, Figure 3-10, CRF significantly overestimates the response due to underestimation of the effective damping ratio (0.2 to 16 Hz). RF solution using 1.5 and 6.5 Hz and ERF using 1.5, 6.5, 35 and 45 Hz compare well with the frequency domain solution when the elastic response spectra are compared.

S-TS2 & R-TS2 1000 m column

Figure 3-11 shows comparison of the surface elastic response spectra for the 1000m column using input motions R-TS2 and S-TS2. Both analyses show that the use of the CRF results in significant underestimation of the surface response. The RF and ERF solution whereby the significant frequencies are chosen through an iterative procedure to match the frequency domain solution provide a significantly improved response.

Effect of variable damping profile

Figure 3-12 presents analysis results for 1000m column using S-TS2 and damping profile (2) to investigate the effect of varying viscous damping ratio throughout the profile and the validity of Equation (3-14). Profile (2) has a much lower damping, in comparison to viscous damping profile (1), and it accounts for effect of confining pressure on small strain damping.

The CRF solution significantly underestimates the surface response. RF (1.0 and 6.4 Hz) and ERF (1.0, 6.4, 35, 45 Hz) provide a better match with the frequency domain solution especially when the elastic response spectra are compared. Nevertheless, the match is not exact because the RF and ERF solution still result in frequency dependent damping.

The linear analyses presented show that:

- CRF may underestimate or overestimate the ground motion response at high frequencies. The accuracy of the solution deteriorates with increase in depth of the soil column.
- ERF provides the best match with the frequency domain solution, but is computationally expensive (An ERF analysis can be 1.3 to 10 times slower than RF analysis, depending on the profile and input motion).
- The 5% damped surface elastic response spectra computed with the RF and ERF using the proposed iterative procedure for selecting the significant frequencies compare well with the frequency domain solution.
- For all ERF analyses performed in this study, constant 3rd and 4th frequencies of 35 and 45 Hz respectively are appropriate.

3.2.5 Update of the viscous damping matrix

In current applications, [C] is taken as strain independent and has a constant value throughout an analysis. The natural modes and the soil column stiffness are derived from the shear wave velocity profile of the soil column. In a non-linear analysis, the mass matrix remains constant but the stiffness matrix is related to the strain level in the soil column. The natural periods or frequencies vary with the stiffness variation of the soil column. In the Newmark β method, Equation (2-35) is integrated or linearized over a given time increment. All matrix quantities including the [C] matrix should correspond to soil properties at that given time increment and strain level. The [C] matrix has to be updated to accurately represent the viscous

damping ratio properties, ξ, of the soil layers. Therefore, the [C] matrix is strain dependent and its strain dependent components including frequencies of natural modes and stiffness matrix are updated at each time increment.

3.3 Confining pressure dependent constitutive model

For deep deposits, confining pressure is the most important parameter which influences the cyclic soil behavior. A new soil model is developed in DEEPSOIL to account for the effect of confining pressure. The nonlinear constitutive model is based on the modified hyperbolic model developed by Matasovic and Vucetic (1995):

$$\tau = \frac{G_{mo}\gamma}{1 + \beta\left(\frac{G_{mo}}{\tau_{mo}}\gamma\right)^{s}} = \frac{G_{mo}\gamma}{1 + \beta\left(\frac{\gamma}{\gamma_{r}}\right)^{s}} \tag{3-16}$$

where τ = shear stress; γ = shear strain; G_{mo} = initial shear modulus; τ_{mo} = shear stress at approximately 1% shear strain; and $\gamma_r = \tau_{mo} / G_{mo}$ is the reference shear strain (Hardin and Drnevich, 1972) and is considered a material constant. The reference strain can also be represented as a function of initial tangent modulus and undrained shear strength in clays (Mesri et al., 1981). The model is a modification of the hyperbolic model by Konder and Zelasko (1963). Two parameters β and s are added to adjust the shape of the backbone curve to represent a wider range of measured soil behavior. The Masing criteria (Masing, 1926) and extended Masing criteria (Pyke, 1979; Vucetic, 1990) define unloading-reloading criteria and behavior under general cyclic loading conditions as shown in Figure 2-10.

To allow coupling between the confining pressure and the shear stress, the following pressure-dependent reference strain is newly proposed:

$$\gamma_r = a \left(\frac{\sigma_{vo}'}{\sigma_{ref}}\right)^{b} \tag{3-17}$$

where a and b are curve fitting parameters, σ_{vo}' is effective vertical stress, and σ_{ref} is a reference confining pressure. Note that σ_{ref} is the pressure at which $a = \tau_{mo} / G_{mo}$. Figure 3-13 shows that using the proposed equation, the model can capture the variation in shear modulus and hysteretic damping measured in the laboratory experiment. Figure 3-13 plots the extrapolated modulus degradation and damping curve to an effective stress of 10000 kPa (equivalent to a depth of 1000 m, with the water table at ground surface).

Laird and Stokoe (1993) data also show a dependency of very small strain soil damping on confining pressure. A new equation is proposed to describe the dependency of small strain equivalent damping ratio on confining pressure:

$$\xi = \frac{c}{(\sigma_{vo}')^d} \tag{3-18}$$

where c and d are material parameters and σ_{vo}' is the effective vertical stress.

Figure 3-13b shows a comparison between the small strain damping from Laird and Stokoe (1993) data. Figure 3-13b includes plots of the total damping ratio equal to hysteretic plus small strain damping. The proposed equation captures measured damping at very small strains, as shown in the inset. Total damping curves fall within range of measured data but do not provide an exact fit.

3.4 Numerical implementation of non-linear site response analysis model: DEEPSOIL

A new site response analysis model, DEEPSOIL, is developed. The program incorporates several enhancements over conventional site response models including new viscous damping formulation described in section 3.2 and confining pressure dependent soil model described in section 3.3. A graphical user interface is developed, as illustrated by the start window shown in Figure 3-14.

3.4.1 Numerical integration

The dynamic equation of motion, Equation (2-35), is solved using Newmark β average acceleration method (Newmark, 1959). The scheme is an implicit integration method that is unconditionally stable. In addition, it does not introduce any arithmetic damping. Details of the Newmark β integration method are summarized in Appendix B.

3.4.2 Viscous damping formulation

Three types of the viscous damping formulations, discussed in section 3.2, are implemented in the non-linear time domain solution in DEEPSOIL. The user can choose the modes or frequencies of the soil column for the viscous damping formulations. In addition, the user can choose a constant [C] or a variable [C] matrix formulation, discussed in section 3.2.5.

3.4.3 Flexible incrementation scheme

The input acceleration time series is given as acceleration (increment) values at constant time intervals. Corresponding strain and stress values are computed throughout the soil column. It is important to subdivide acceleration increments to accurately compute the non-linear stress-strain response of soil. Flexible and fixed sub-incrementation schemes are implemented in the nonlinear time domain solution in DEEPSOIL. In a fixed sub-incrementation scheme, each time-step is divided into equal user-defined N sub-increments throughout the time series. In a flexible sub-incrementation scheme, a time increment is subdivided only if computed strain increment in the soil exceeds a user-defined maximum strain increment (γ_{max}).

Figure 3-15 presents a comparison of the computed 5% damped surface response spectra using the fixed and the flexible sub-incrementation schemes. Four analyses are performed to compare the accuracy and effectiveness of the computation. Except for the $N = 1$ fixed scheme, all of the schemes give similar results. The flexible sub-incrementation scheme with $\gamma_{max} = 0.05$ % has been used throughout this study since it gives accurate results at a minimal computational cost.

3.4.4 Implementation of equivalent linear frequency domain analysis

In addition to the new nonlinear wave propagation model, the equivalent linear analysis model is also implemented in DEEPSOIL. The equivalent linear solution scheme implemented in DEEPSOIL is similar to that in SHAKE (Schnabel et al., 1972), without the limitation on number of layers and material properties. Another important difference is the definition of the complex shear modulus. In addition, the limitation on the number of FFT data points (4096 in SHAKE91, Idriss and Sun, 1992) has been removed by dynamically allocating the array size.

DEEPSOIL allows choosing three types of complex shear modulus, described in section 2.5.1 and defined in Equations (2-9), (2-10), and (2-12). SHAKE only incorporates the Udaka model which uses the complex shear modulus defined in Equation (2-12). The significance of the complex shear modulus on the equivalent linear solution is described in detail in section 3.5.4.

3.4.5 User interface

A graphical user-friendly interface, Figure 3-14, is developed to enhance accessibility and understanding of the developed site response code DEEPSOIL. Running DEEPSOIL is done in a step-to-step procedure. Nonlinear analysis consists of the following 7 steps:

- *Step 1*: Open profile or make a new profile.
- *Step 2*: Choose soil profile properties: shear wave velocity or G_{max}, unit weight, small strain damping ratio, and location of water table.
- *Step 3*: Define nonlinear parameters. This step is discussed further in section 3.4.5.1.
- *Step 4*: Choose step control (flexible of fixed sub-incrementation scheme).
- *Step 5*: Choose input motion from the motion library. Choose layers for output. (If desired, deconvolution can be performed on the input ground motion).
- *Step 6*: Choose frequencies / modes of the Rayleighd damping formulation. This step will be discussed further in the following section. This step is discussed further in section 3.4.5.2.
- *Step 7*: Run the analysis.

Equivalent linear analysis consists of the following 6 steps:

- *Step 1*: Open profile or make a new profile (identical to Step 1 of nonlinear analysis).
- *Step 2*: Choose soil profile properties (identical to Step 1 of nonlinear analysis).
- *Step 3*: Choose material properties. The shear modulus degradation and damping ratio curve can be defined by discrete points (as in SHAKE), or using modified hyperbolic equation.
- *Step 4*: Choose iteration number and Fourier transfer type (DFT or FFT).
- *Step 5*: Choose input motion (identical to Step 5 of nonlinear analysis).
- *Step 6*: Run the analysis.

3.4.5.1 Visual procedure for selecting non-linear model properties

Seven parameters are needed to fully define the extended modified hyperbolic model, described by Equations (3-17) to (3-19), three for the modified hyperbolic model and additional three to define the extended pressure dependent model.

A visual procedure for selecting the nonlinear material model parameters is implemented in the user interface of DEEPSOIL and shown in Figure 3-16 (Step 3 of the nonlinear analysis). After choosing the material parameters, the nonlinear hysteretic soil model is represented in the form of the shear modulus degradation and damping ratio curve. This graphical feature enables comparison with the library of the previously defined curves if it is desired to obtain sets of parameters to represent those curves.

In selecting the parameters, three parameters that define the modified hyperbolic model (β, s, a) at a reference confining pressure should be initially chosen. Note that a is defined as reference strain in the user interface. Then, the confining pressure dependent soil parameters for the extended modified hyperbolic model (σ_{ref}, b, d) should be chosen to account for pressure dependency. The pressure dependent reference strain, Equation (3-18), and damping ratio, Equation (3-19), are automatically adjusted using the current effective vertical stress of the layer.

3.4.5.2 Visual procedure for choosing modes/frequencies for Rayleigh damping

Section 3.2 demonstrated the importance and difficulties of selecting optimum frequencies/modes for Rayleigh damping formulation. The user interface provides a quick method to check the appropriateness of the selected frequencies/modes. The window for this procedure is shown in Figure 3-17 (Step 6 in the nonlinear analysis). The surface Fourier amplitude spectrum and response spectrum of the linear time domain analysis using the selected frequencies/modes can be directly compared to the solution of linear frequency domain analysis. The effective damping ratio is plotted below the response spectrum to allow determination of zones of overdamping and underdamping. The set of frequencies/modes that provides the best match with the frequency domain solution can be visually chosen. The selected frequencies/modes are used to run the nonlinear analysis.

3.4.6 Guidelines for performing a nonlinear analysis with viscous damping

A guideline is proposed for performing a nonlinear analysis with viscous damping:

1. *Layer thickness:* use Equation (3-15) to determine the maximum layer thickness and thus avoid filtering of relevant frequencies.
2. *Viscous Damping formulation:* select the appropriate frequencies for RF or ERF formulation. The selection is performed through an iterative procedure and by comparing the results of a linear time domain analysis with linear frequency domain solution. RF formulation is adequate if the elastic response spectrum is needed. ERF may be necessary if the Fourier spectral content is desired. The ERF is computationally expensive compared to RF. For many engineering applications, RF will provide acceptable results. Care should be exercised when selecting frequencies to avoid negative damping in the resulting frequency dependent damping.

3. *Simplified Rayleigh damping formulation:* The simplified damping formulation should not be used for any analysis, except for very short soil columns (less than 50 m).
4. *Rayleigh damping formulation:* The conventional guideline of using the first and a higher mode of the soil column or the predominant period of the input motion will not always result in a good match with the linear frequency domain solution especially for deep soil columns. The two significant frequencies can be chosen in part to cover the range of frequencies where there is significant input motion content. A new set of frequencies will have to be selected if a different input motion is selected.
5. *Extended Rayleigh damping formulation:* Four significant frequencies are used. The first two are usually identical to the two frequencies chosen for RF. The spacing between 3rd and 4th frequencies should be approximately 10 Hz. If higher spacing is used, it can result in negative damping ratio. In this paper acceptable results for all ground motions and soil profiles are obtained when 3rd and 4th frequencies are equal to 35 Hz and 45 Hz respectively. ERF improves the Fourier spectrum match by preserving frequencies higher than the 2nd frequency. However, such improvement over RF has negligible influence when calculating the 5 % damped elastic response spectrum.
6. *Non-linear analysis:* Once the appropriate frequencies for the viscous damping formulation are chosen based on the linear analysis, a full non-linear analysis can be performed.

This selection process will have to be repeated if a different input motion or soil column properties is used.

3.5 Evaluation of DEEPSOIL

3.5.1 Significance of Rayleigh damping formulation

The development of RF and ERF and corresponding significant frequencies/modes selection procedure is introduced to enhance the accuracy of the time domain non-linear site response solution. Nonlinear site response analyses are presented using S-TS2 and 1000 m soil column. The RF and ERF frequencies used are those selected in the linear analysis shown in Figure 3-11b and Figure 3-12.

Non-linear soil model: The confining pressure dependent modified hyperbolic model, introduced in section 3.3 is used. Model properties are chosen such that the resulting modulus

degradation and damping curves approximate the laboratory test data of Laird and Stokoe (1993) and shown in Figure 3-18.

Small strain damping: Figure 3-18b shows that the hysteretic damping from the hyperbolic model is negligible at small strains and underestimates damping values obtained from laboratory measurements. Note that Figure 3-18b differs from Figure 3-13b in that the former only shows hysteretic damping, whereas the latter displays both hysteretic and smalls train damping from the laboratory tests. Instead of using small strain damping properties measured from laboratory tests, the small strain damping profiles (1) and (2) are used to represent the small strain damping and are added to the hysteric damping quantities, Figure 3-18b, in the following analyses. Figure 3-19 shows the combined damping curves represented in the site response analysis that result from the addition of small strain damping to the hysteretic damping.

Figure 3-20 shows the response spectra of the nonlinear analyses performed. CRF solution results in pronounced underestimation of high frequency components up to 0.7 sec. RF and ERF solutions are almost identical, except at short periods for viscous damping profile (2), where ERF shows slightly higher response than RF. ERF also shows higher response at periods greater than 4 sec for both viscous damping profiles.

The nonlinear response analysis results are compared to the equivalent linear solution. Identical modulus degradation and damping are used. Equivalent linear analysis is often used to approximate non-linear soil response. Equivalent linear analysis uses constant linear shear modulus and damping throughout the duration of the motion selected at a representative level of strain. For both profiles, equivalent linear solution underestimates the response at periods less than 0.3 sec. The equivalent linear analysis filters these higher frequency components. Nonlinear analysis is able to preserve such high frequency components. The equivalent linear analysis also underestimates the response at longer periods. If equivalent linear analysis is compared to the nonlinear analysis with CRF, it can lead to a misleading conclusion that the equivalent linear solution is comparable or provides larger estimates than the nonlinear solution at most period ranges.

The analyses demonstrate the importance of accurately selecting the viscous damping formulation in a nonlinear site response analysis.

3.5.2 Significance of variable [C] matrix

In the proposed damping formulation, Equation (2-35), the [C] matrix can be updated at every time step. This implementation is in contrast to the common implementation where [C] is constant and based on the initial soil properties. The results using the updated and constant form of [C] dependent on the initial soil properties only are compared Figure 3-21. S-ST2 is used as input motion. The variable [C] analyses gave a slightly higher response than the constant [C] analyses. The main difference is in the high frequency range of the ground motion and is best seen in plots of the Fourier amplitude of computed surface ground motion in Figure 3-21. This difference is a result of the significant non-linear effects and reduction in stiffness experienced by the soil.

3.5.3 Significance of confining pressure dependent soil model

The influence of confining pressure on 1-D site response is demonstrated through comparisons of analyses using non-linear, confining pressure-dependent (NLPD) and independent (NLPI) soil models. Figure 3-22 and Figure 3-23 present such comparisons using ground motion R-TS2 and all three soil columns. Figure 3-22 compares computed time series at the ground surface using the two soil models. For the 1000 m column, the NLPD model gives a response with a larger a_{max} and greater number of high frequency peaks than the NLPI model. The 500 m column shows a similar response. For the 100 m column, the NLPI and NLPD time series are quite similar, though the NLPD model shows greater amplitude of high frequency components early in the time series (t=0-8 sec).

The difference between the two models can be observed better by examining the surface response spectra shown in Figure 3-23. For a soil thickness of 1000 m, the influence of the confining pressure is very pronounced. Short period spectral accelerations are much larger for the NLPD model compared to the NLPI model. For both models, motion amplification is computed at a period of about T=5.0 seconds which corresponds to the theoretical characteristic site period for the 1000 m soil column. Similar observations can be made for the 500 m column. For the 100 m column, response spectra are also similar for T>0.9 sec. However, for shorter periods the NLPD model spectral acceleration is larger than that of the NLPI model. The influence of pressure-dependent behavior is still observable for the 100 m thick column.

Figure 3-24 shows a comparison of the soil model effect on surface response spectra using time series S-TS2 for the 1000 m. Observations similar to those made for analyses using input time series R-TS2 can be made. The NLPD model gives a significantly larger spectral response for periods less than 1 sec compared to NLPI. For periods larger than 1 sec, the NLPD model also gives larger or equal spectral response compared to the NLPI model. The effect of the pressure dependent model is more pronounced than when propagating R-TS2, due to more high frequency contents of the input motion of the S-TS2.

The higher response computed using the NLPD model compared to the NLPI model is a result of stiffer soil modulus degradation curves and lower damping in the soil column in the NLPD model. A measure of cumulative damping in the column is the quantity kappa:

$$\kappa = \int \frac{2\xi}{V_s} dz \tag{3-19}$$

Figure 3-25 plots values of κ versus strain level for NLPD and NLPI model and the three soil columns used in the analyses. The values of the damping ratio ξ and V_s are obtained from damping ratio and modulus degradation curves, as shown in Figure 3-19b and Figure 3-19a. The NLPD model has consistently lower κ than that for the NLPI model.

The pressure dependent model, NLPD, shows that there is significantly less damping of ground motion even for very deep soil columns. The analyses show that ignoring pressure dependent cyclic soil behavior may lead to significant underestimates of propagated ground motion. The analyses suggest that a larger portion of the seismic input motion (or energy) reaches the surface of very deep deposits than would be obtained from conventional analyses.

3.5.4 Significance of complex modulus

Three types of the complex shear modulus introduced in section 2.5.1 are incorporated in DEEPSOIL equivalent linear model. All three types of the complex modulus are used in the equivalent linear analyses to demonstrate the influence of the complex shear modulus on wave propagation solution. The input motions used in the analyses are shown in Figure 3-26. Motion-1 has a PGA of 0.76g, whereas motion-2 has a PGA of 1.0g. The shear velocity of the soil column and the dynamic soil curves used in the analyses are shown in Figure 3-27.

Using motion-1, the effect of the complex shear modulus is not significant and all of the solutions are similar, as shown in Figure 3-28a. However, when propagating a very strong ground motion, motion-2, the effect of the complex shear modulus is significant, as shown in

Figure 3-28b. The surface response is much lower using the Udaka model than using the hysteretic model.

The reason for the discrepancy can be best explained by observing the maximum strains calculated in the soil column. Figure 3-29 shows the maximum strain calculated at depths 6.25 m and 7.2 m at various iteration steps. Maximum strain increases with iteration number using Udaka model at depth of 6.25 m, whereas the hysteretic models converge quickly. Udaka's model does not fully converge even after 50 iterations at depth of 7.2 m, and strain continues to increase. The excessive strain level developed results in unrealistic soft behavior at the surface. The analyses clearly demonstrate the importance of complex shear modulus and the inappropriateness of the Udaka's model to converge when propagating a strong ground motion.

3.6 Evaluation of DEEPSOIL using recordings at Treasure Island

During the 1989 Loma Prieta Earthquake in Northern California ground motion recordings were obtained on fill material underlain by sediments at Treasure Island and on rock at adjacent Yerba Buena Island. Several site response studies using these recordings were made using the equivalent linear analysis (Seed et al., 1990, Hryciw et al., 1991) and the non-linear analysis (Finn et al., 1993; Matasovic, 1993) methods. In these studies, the computed surface response spectra were in general agreement with measured spectra. However, the nonlinear analyses had some difficulty in capturing the recorded response in the short period/high frequency range.

A similar site response analysis using the Yerba Buena-Treasure Islands recordings is made using the non-linear site response analysis program DEEPSOIL. The analysis is presented to further illustrate the significance of viscous damping formulation on computed site response. The soil shear wave velocity profile used, Figure 3-30, is based on data from Gibbs et al. (1992) and Pass (1994). Shear wave velocity of the rock is taken as 2700m/sec. Non-linear hyperbolic model parameters were obtained from modulus degradation and damping curves published in Hwang and Stokoe (1993). Figure 3-30 shows the modulus degradation and damping curves obtained from the calibrated modified hyperbolic model. The recording at Yerba Buena Island is used as the input motion at the base of the column. The site response analysis is conducted by first obtaining a best estimate of soil parameters using available data without any attempt to match model results to recorded motions. Figure 3-31 shows plots of the computed and recorded

response spectra of the E-W and N-S components. For both motion components the analysis results using the first mode (simplified) viscous damping formulation significantly underestimates ground motion response at periods less than 0.5 sec.

For the E-W motion component using the pressure dependent soil model and 1st and 2nd modes viscous damping formulation (RF) significantly improves ground motion response at periods below 0.5 sec and captures the high frequency (low period) peaks in the response spectra. The use of the new formulation also improves the response at the highest peak of the response spectrum. Use of higher modes (1st and 8th natural modes) does not result in significant improvement of the results and is indicative of the convergence of the solution at higher modes.

For the N-S motion component the proposed modifications results in a dramatic improvement of computed ground motion response at periods below 0.5 sec compared to conventional viscous damping formulation. The results nearly match computed ground response and capture the peaks in this low period/high frequency range. At longer periods, the computed results underestimate recorded motion. This result is also reported in other studies and is attributed by Finn et al. (1993) to ground motion incoherency between the Yerba Buena Island and Treasure Island recordings.

The case history shows that the new damping formulation significantly improves computed ground motion response, especially at short periods, for a soil column less than 100 m thick. The effect of the incorporation of pressure dependent model has less influence on the response, but can still be observed. The analysis results show that the developed model provides better estimate of actual recorded motions at high frequencies compared to a conventional nonlinear analysis.

3.7 Summary

This chapter outlines the developments of a new one-dimensional nonlinear site response analysis program DEEPSOIL. The program is also capable of performing equivalent linear analysis. Major enhancements have been made over a conventional nonlinear code, which include:

1) New viscous damping formulation to reduce artificial damping
2) Confining pressure dependent non-linear hyperbolic soil model
3) Enhanced numerical accuracy through flexible sub-incrementation scheme

The significance of the developments is demonstrated through theoretical comparisons of the different formulation, site response analyses using various soil profiles and wide range of input ground motions, and Treasure Island case study. Three papers have been published as a result of the work described in this chapter: Hashash and Park (2001), Hashash and Park (2002), and Park and Hashash (2003).

Table 3-1. Material properties used in the proposed extended hyperbolic model.

Symbol	Description	Source	Value selected to match Laird and Stokoe (1993) curves
G_{mo}	Initial shear modulus.	Basic soil property	ρV_s^2
β	Dimensionless coefficient used to modify the classical hyperbolic model.	(Matasovic, 1993)	1.4
s	Dimensionless coefficient used to modify the classical hyperbolic model.	(Matasovic, 1993)	0.8
σ_{ref}	Reference stress.	New: proposed in this study	0.18 MPa
a[1]	Dimensionless constant used in the computation of reference strain variation with confining pressure.	New: proposed in this study	0.163
b[3]	Dimensionless constant used in the computation of reference strain variation with confining pressure.	New: proposed in this study	0.63
c[2]	Dimensionless constant used in the computation of small strain variation with confining pressure.	New: proposed in this study	1.5
d[3]	Dimensionless constant used in the computation of small strain variation with confining pressure.	New: proposed in this study	0.3

[1] Equivalent to γ_r if b is zero.
[2] Equivalent to small strain damping ratio at reference stress.
[3] Set to zero for pressure independent behavior.

Table 3-2 Summary of ground motions used in response analyses.

Ground motion number	Location and event	PGA (g)	Dominant frequency (range) (Hz)	Linear frequency and time domain analyses			Equivalent linear/non-linear analysis
				Soil column thickness (m)			
				100 m	500 m	1000 m	1000 m
Synthetic ground motion (S-TS) generated using SMSIM							
S-TS 1	M = 5, R = 20 km	0.059	4 (2-15)	x	x	x	
S-TS 2	M = 7, R = 32 km	0.653	1* (1–50)			x	x
Recorded ground motion (R-TS) from rock sites							
R-TS 1	Station 6099, Nahanni Earthquake (1985)	0.148	16 (10-20)	x		x	
R-TS 2	Yerba Buena Island, Loma Prieta Earthquake (1989)	0.067	0.7 (0.1–1)			x	

TS: Time series also referred to as time history.

- It is not meaningful to define a predominant frequency as the motion content is evenly distributed over a wide frequency range.

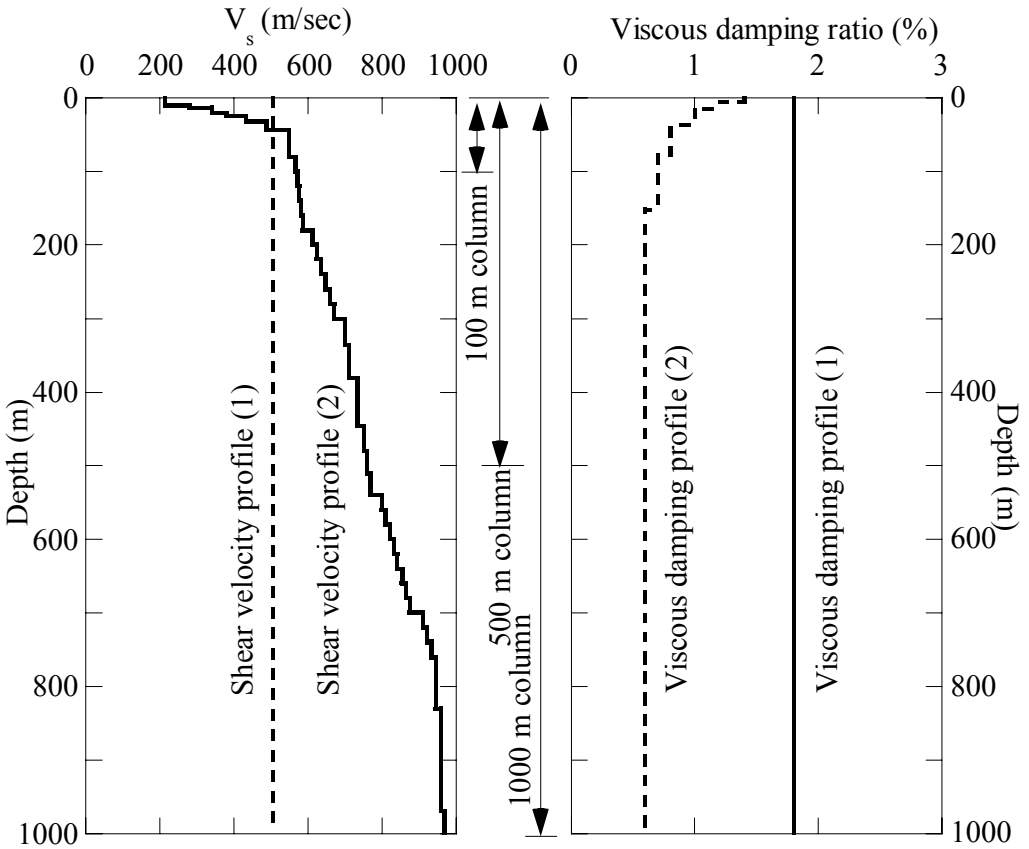

Figure 3-1 Shear wave velocity and viscous damping profiles used in analyses. The profile properties are representative of conditions encountered in the Mississippi embayment. Central U.S. Bedrock shear wave velocity is 3000 m/sec. Shear wave velocity profile is the generic profile of the Mississippi embayment developed by Romero and Rix (2001).

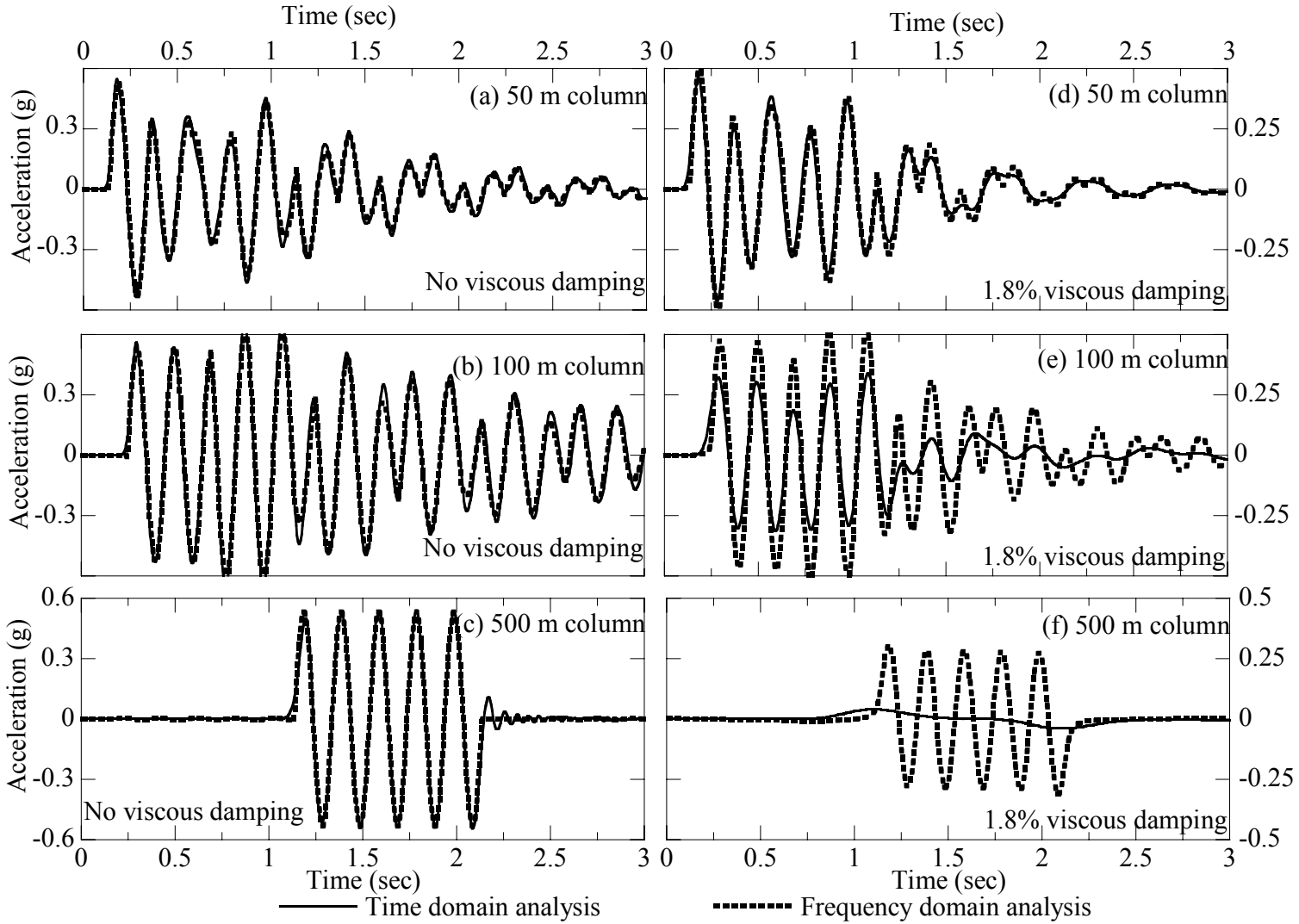

Figure 3-2 Computed surface ground motion, linear frequency and time domain site response, V_s profile (1). Linear time domain analysis uses first natural mode approximation only of viscous damping formulation. Harmonic input motion, amplitude=0.3g, period=0.2 sec, duration=1 sec.

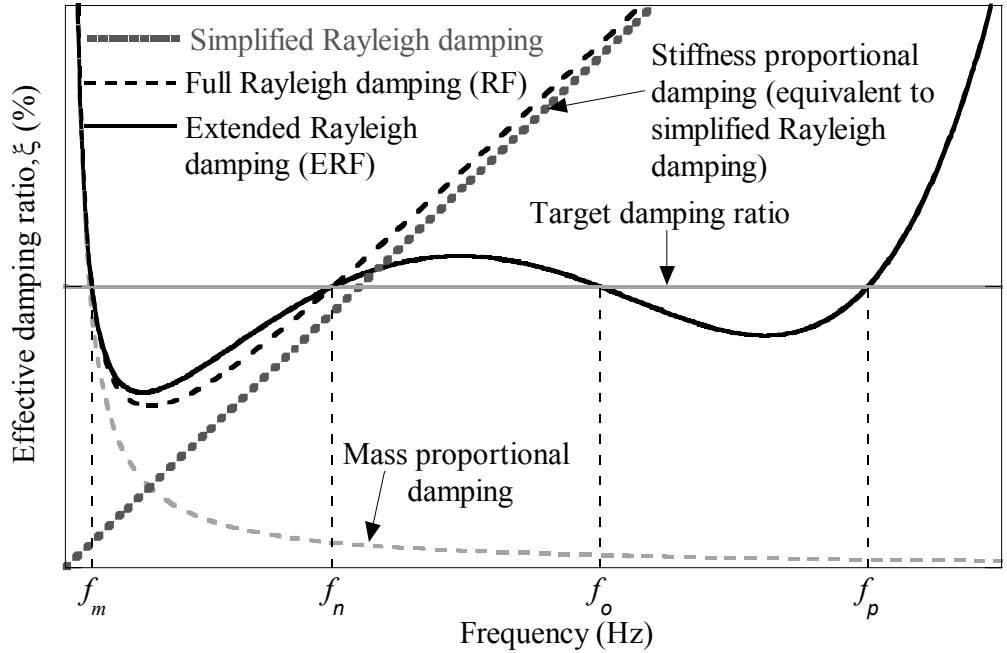

Figure 3-3 Effective (frequency dependent) damping using a) simplified, b) full (RF) and c) extended Rayleigh damping formulations (ERF). RF results in exact target damping ratio at 2 frequencies/modes, whereas ERF at 4 frequencies/modes.

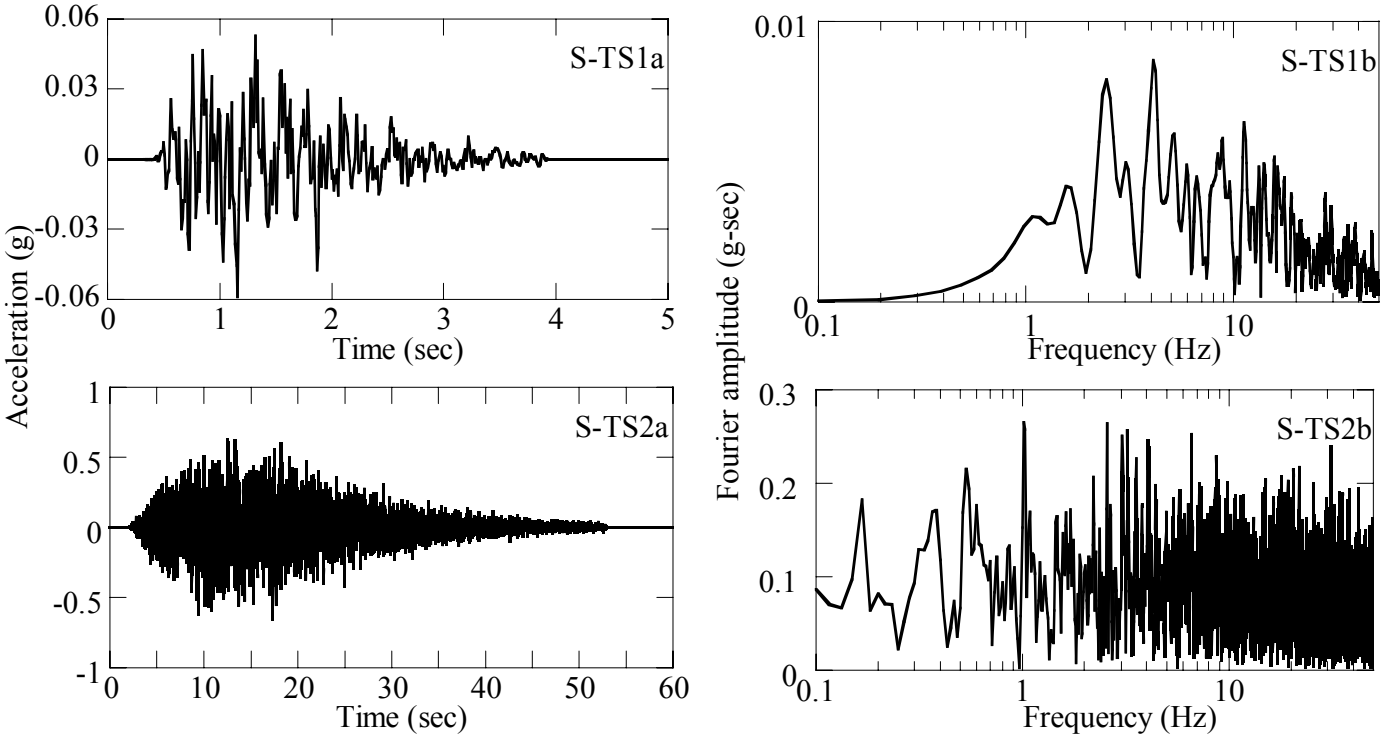

Figure 3-4 Synthetic motions generated using SMSIM (Boore, 2002): a) Time history and b) Fourier amplitude. S-TS1: M = 5, R = 20 km, S-TS2: M = 8, R = 32 km.

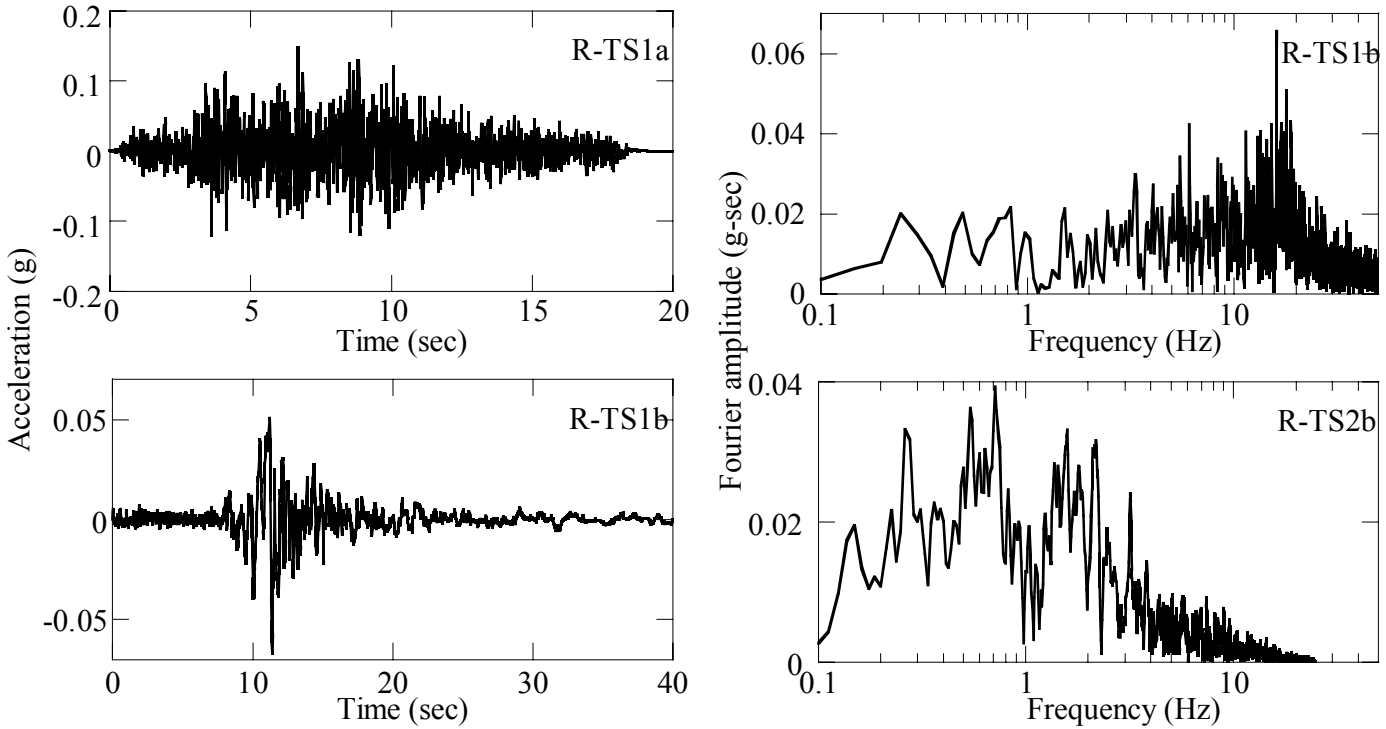

Figure 3-5 Recorded ground motions from rock sites: a) Time history and b) Fourier amplitude.

R-TS1: recording at station 6099 during Nahanni Earthquake (1985), and R-TS 2: E-W recording at Yerba Buena Island during Loma Prieta Earthquake (1989).

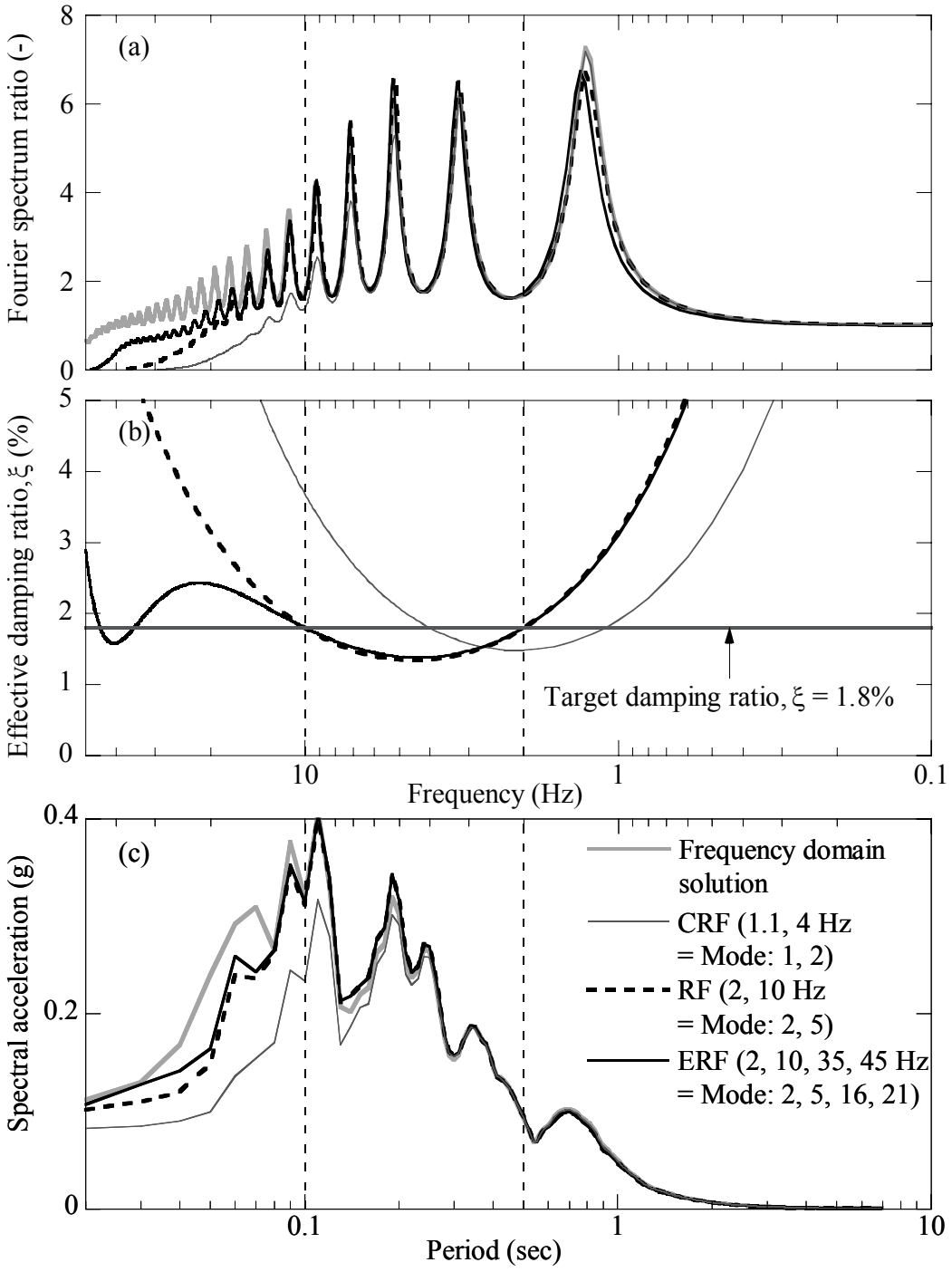

Figure 3-6 Linear frequency and time domain analyses for 100 m soil column, damping profile (1), Input motion S-TS1, a) Fourier spectrum ratio, b) effective damping ratio, and c) 5% damped elastic response spectra.

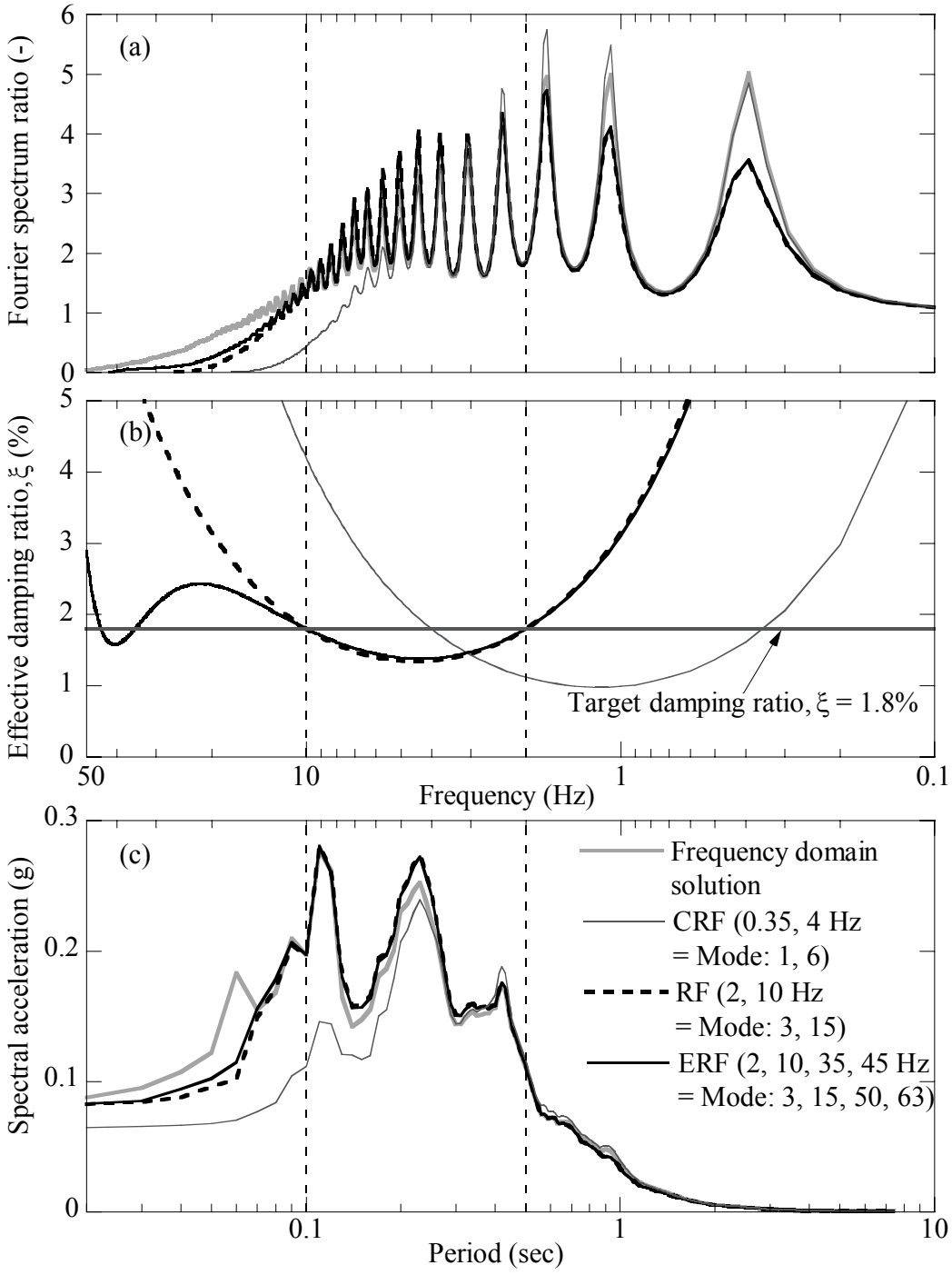

Figure 3-7 Linear frequency and time domain analyses for 500 m soil column, damping profile (1), Input motion S-TS1, a) Fourier spectrum ratio, b) effective damping ratio, and c) 5% damped elastic response spectra.

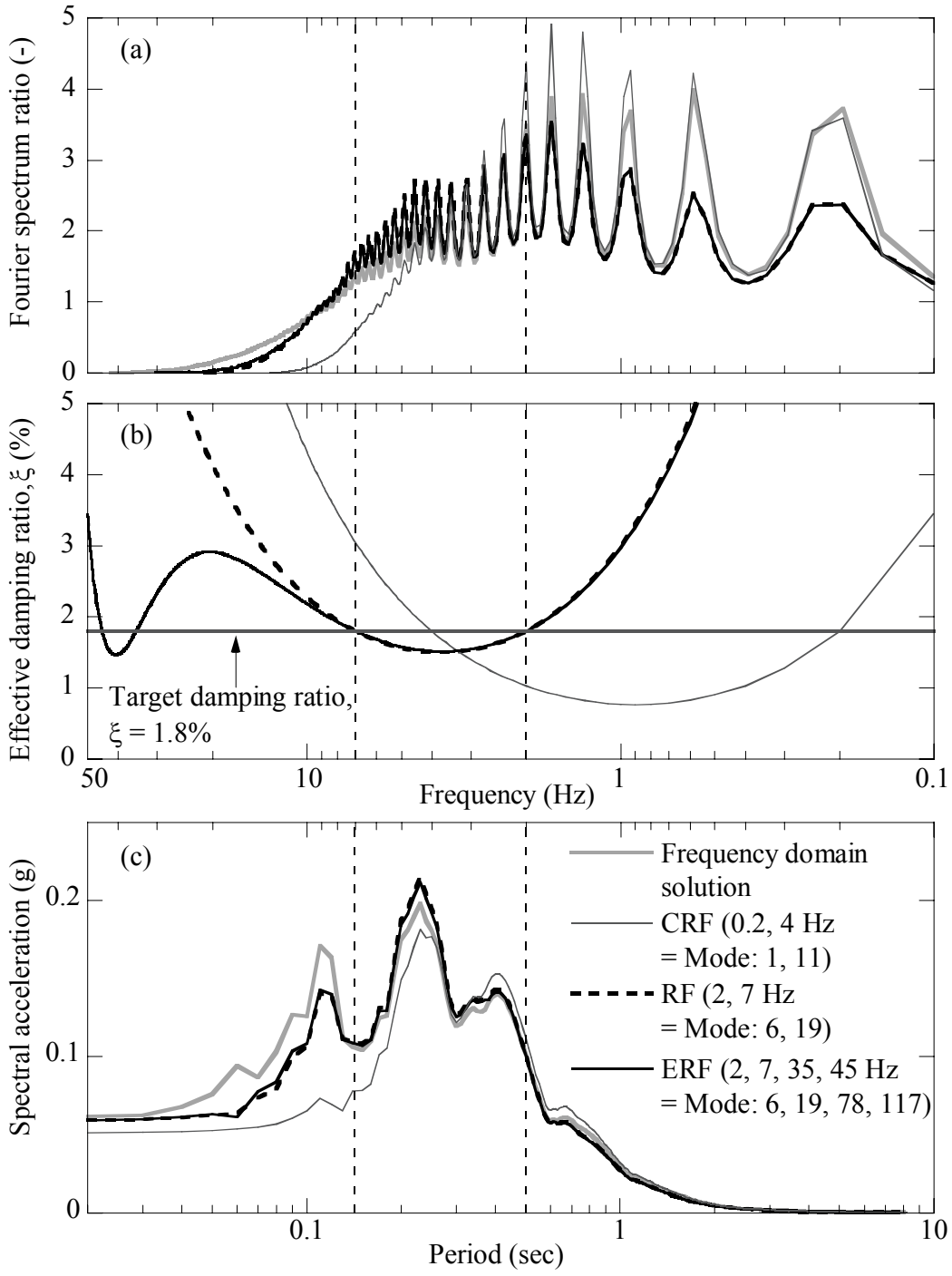

Figure 3-8 Linear frequency and time domain analyses for 1000 m soil column, damping profile (1), Input motion S-TS1, a) Fourier spectrum ratio, b) effective damping ratio, and c) 5% damped elastic response spectra.

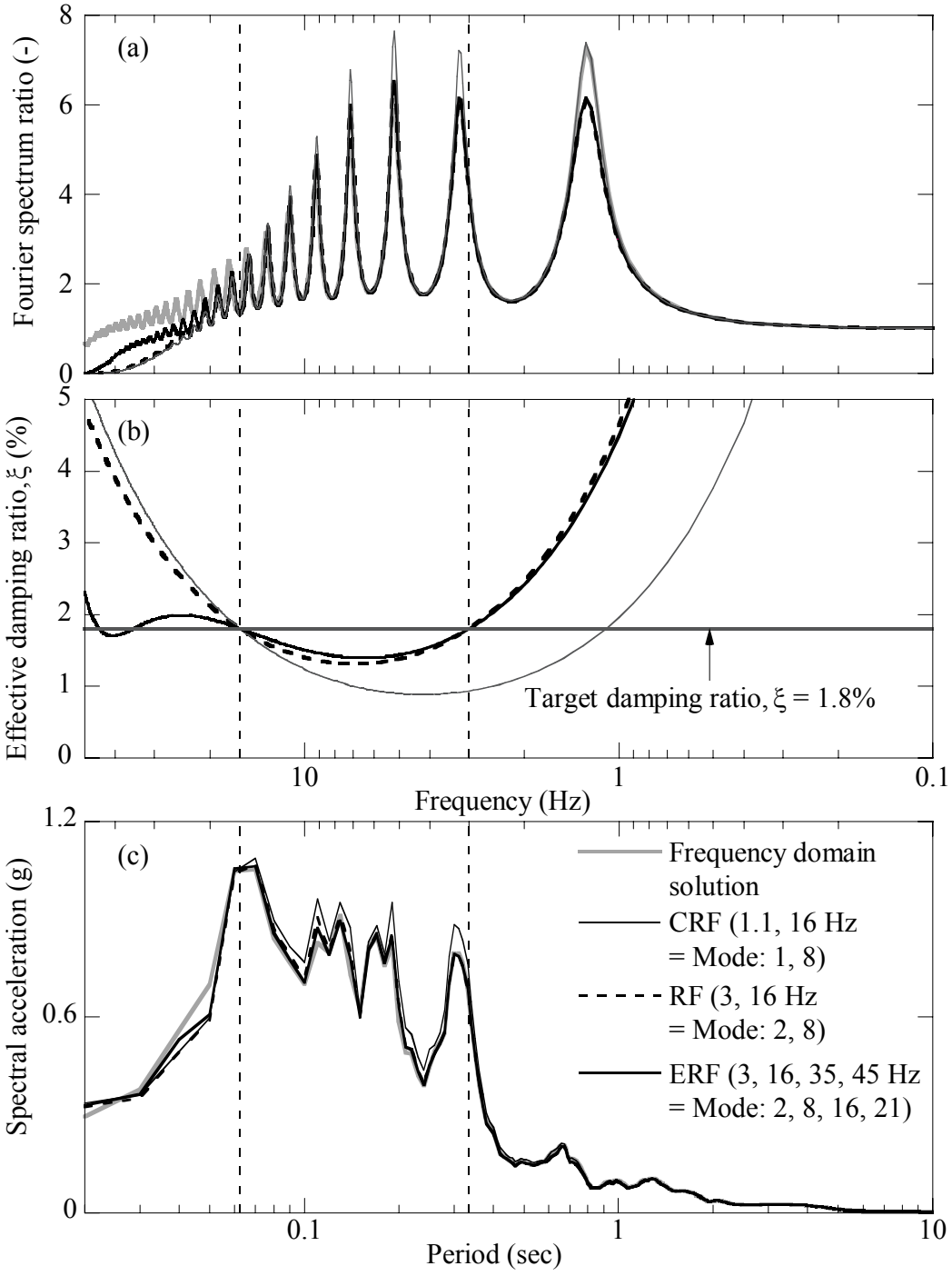

Figure 3-9 Linear frequency and time domain analyses for 100 m soil column, damping profile (1), Input motion R-TS1, a) Fourier spectrum ratio, b) effective damping ratio, and c) 5% damped elastic response spectra.

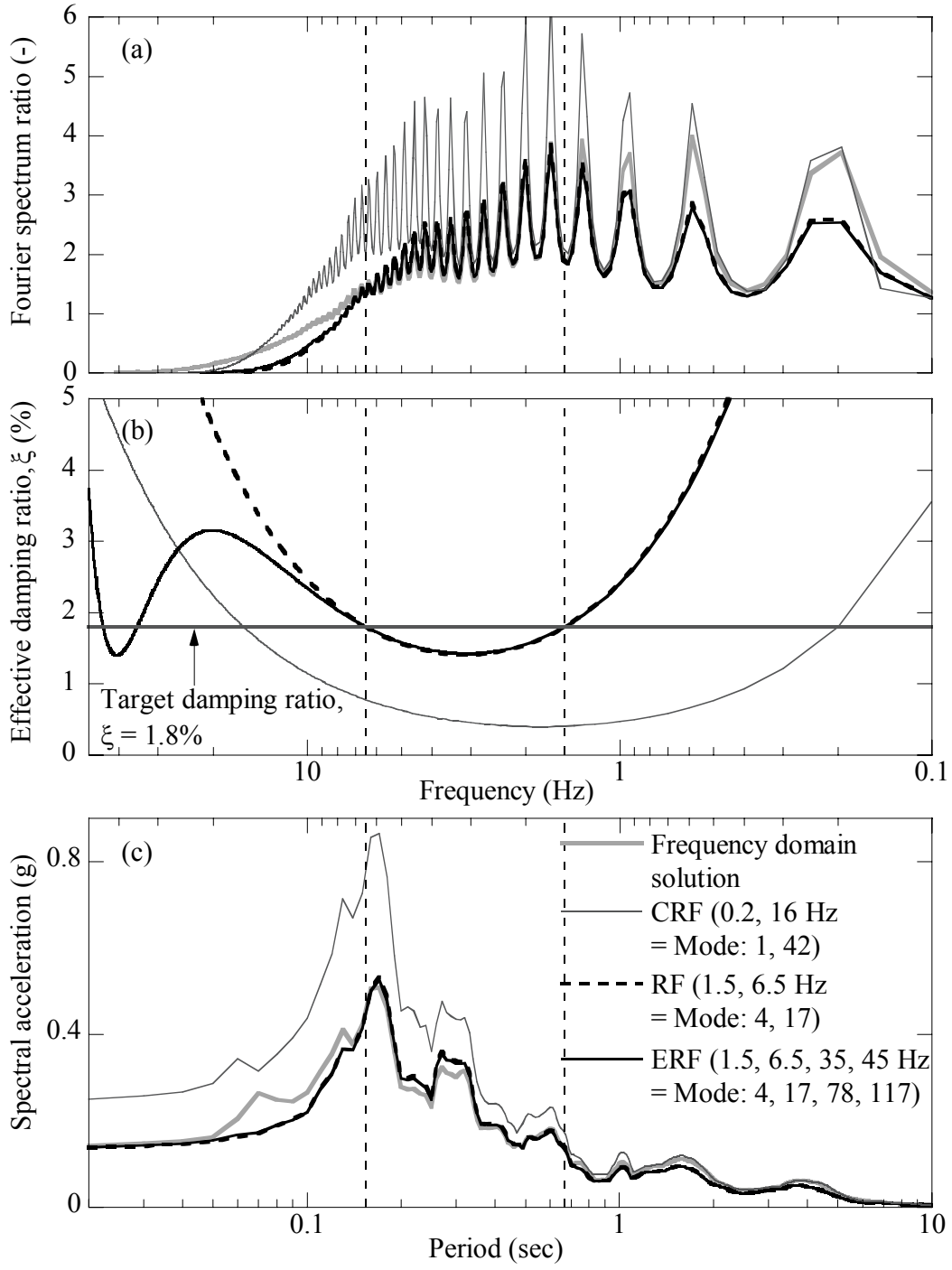

Figure 3-10 Linear frequency and time domain analyses for 1000 m soil column, damping profile (1), Input motion R-TS1, a) Fourier spectrum ratio, b) effective damping ratio, and c) 5% damped elastic response spectra.

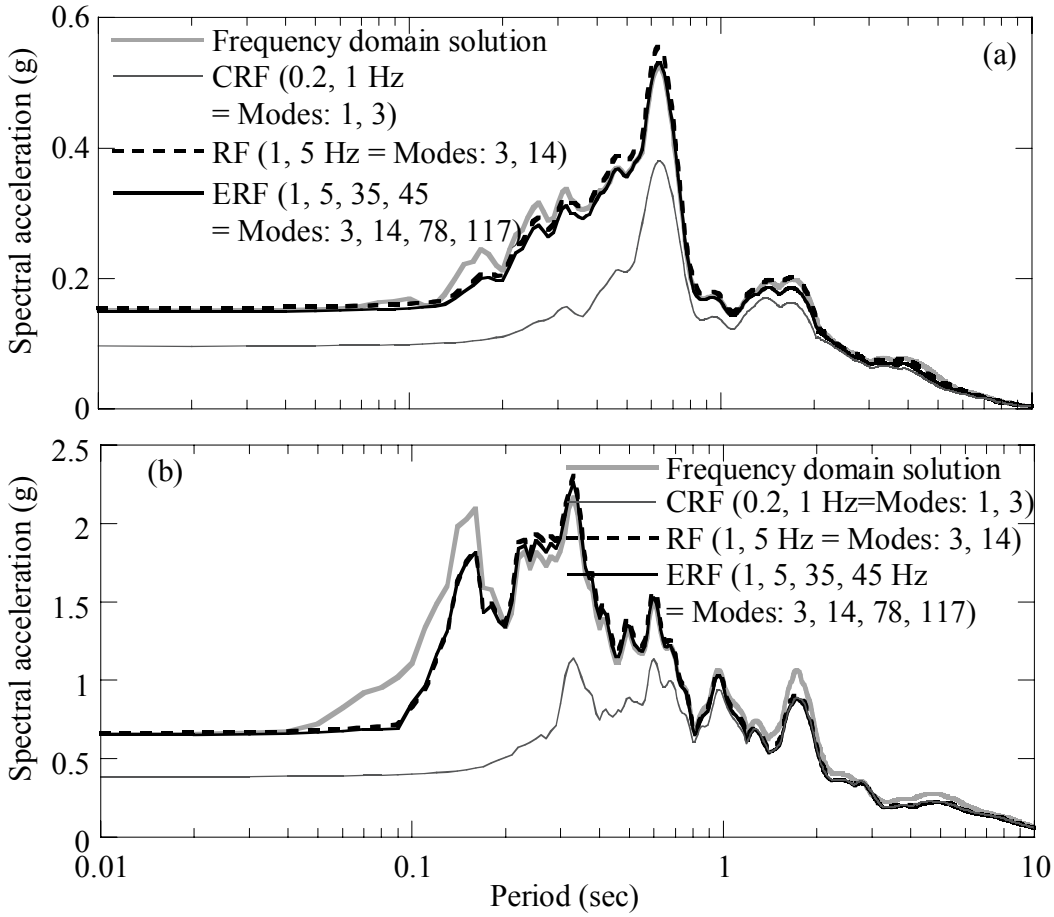

Figure 3-11 The 5% damped elastic response spectra from linear frequency and time domain analyses for 1000 m soil column, damping profile (1), a) Input motion R-TS2, and b) Input motion S-TS2.

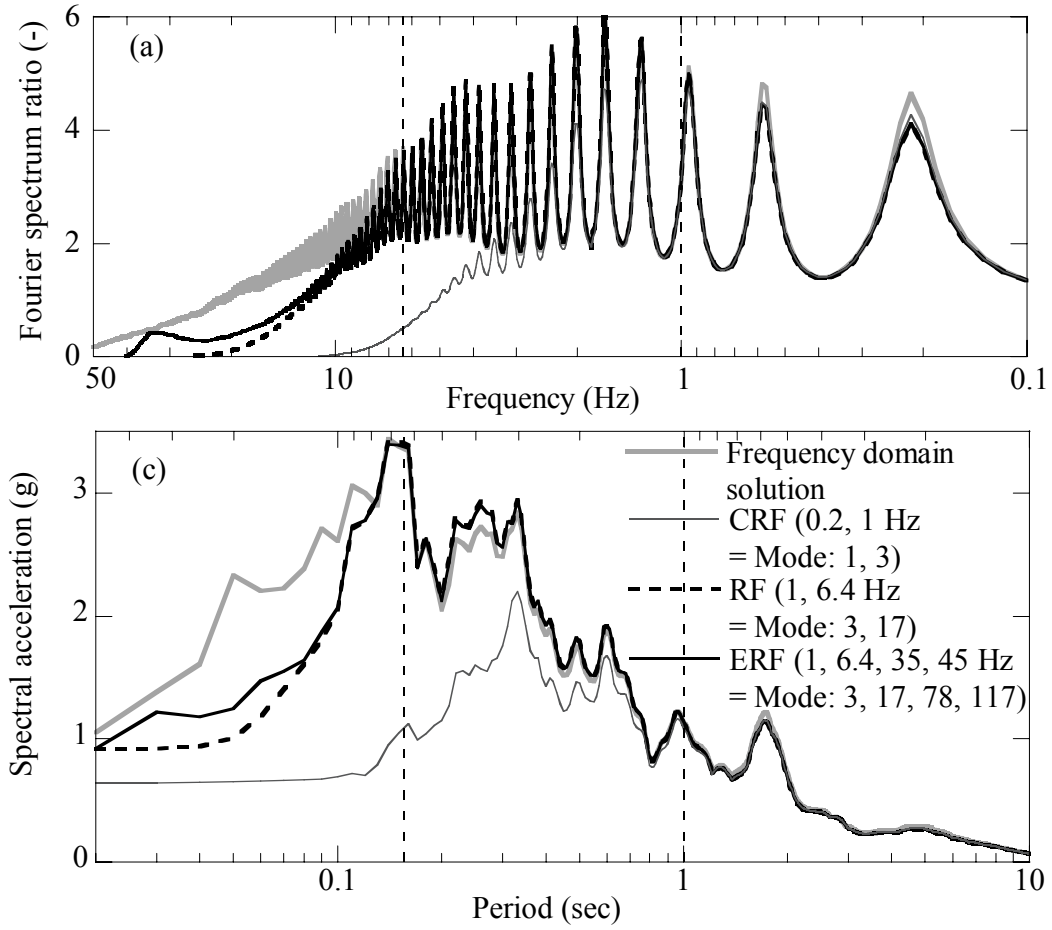

Figure 3-12 Linear frequency and time domain analyses for 1000 m soil column, damping profile (2), Input motion S-TS2, a) Fourier spectrum ratio, b) 5% damped elastic response spectra.

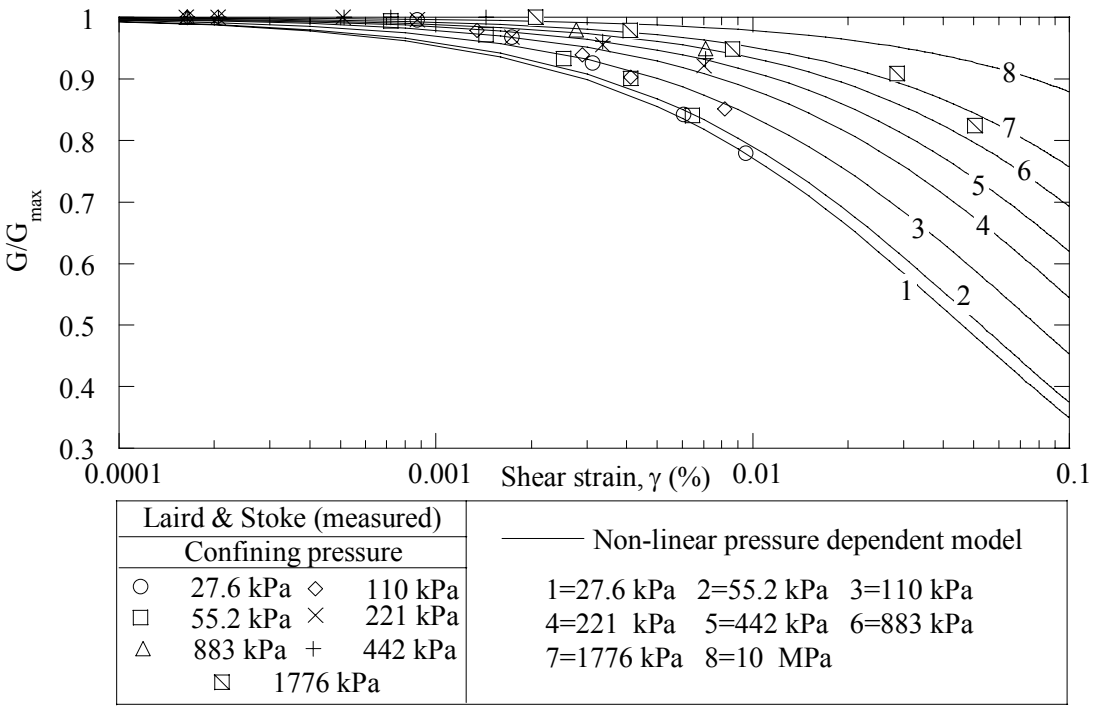

(a) Modulus degradation curves

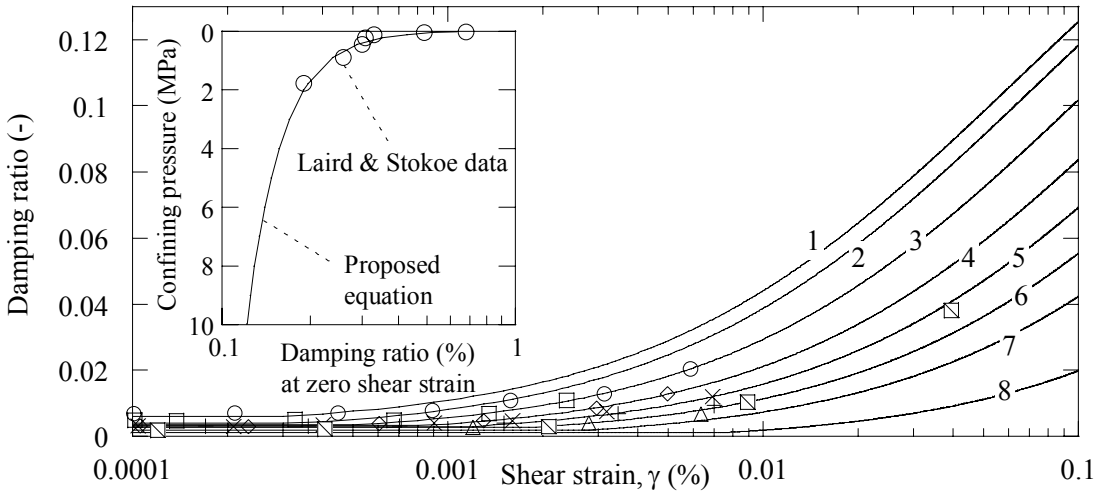

(b) Damping ratio curves

Figure 3-13 Influence of confining pressure on modulus degradation and damping ratio curves in DEEPSOIL nonlinear model used for modeling of site response in the Mississippi embayment. Data from Laird and Stokoe (1993) shown for comparison.

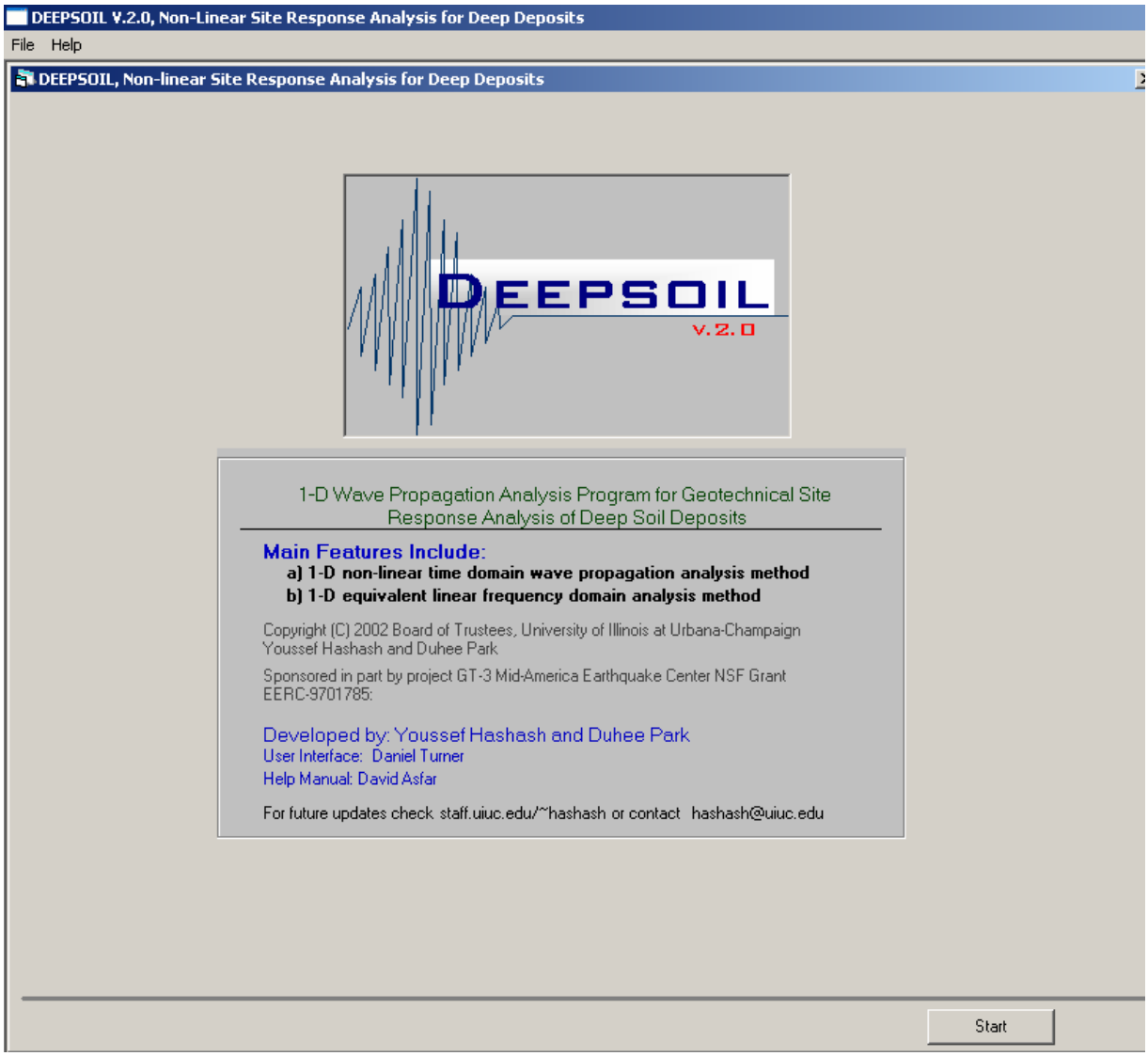

Figure 3-14 Start window of the user interface for DEEPSOIL.

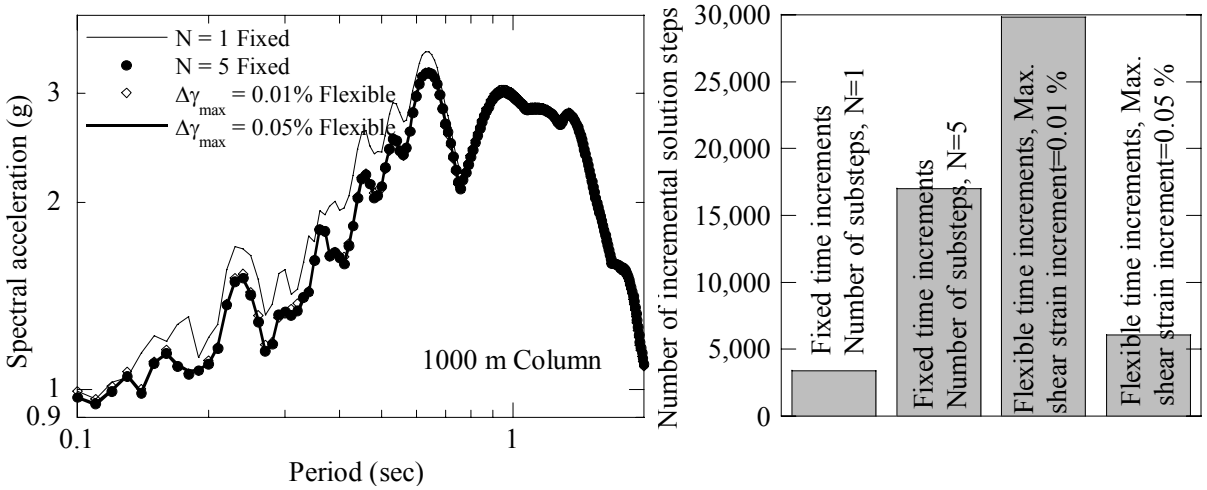

a) Computed surface response spectra b) Number of global computation steps

Figure 3-15 Numerical accuracy of computed surface response using fixed and flexible incrementation solution schemes, dynamic properties listed in Table 3-1, input time history: recorded motion during Kobe earthquake at station JMS (N-S component), time interval 0.02 sec, 3400 points.

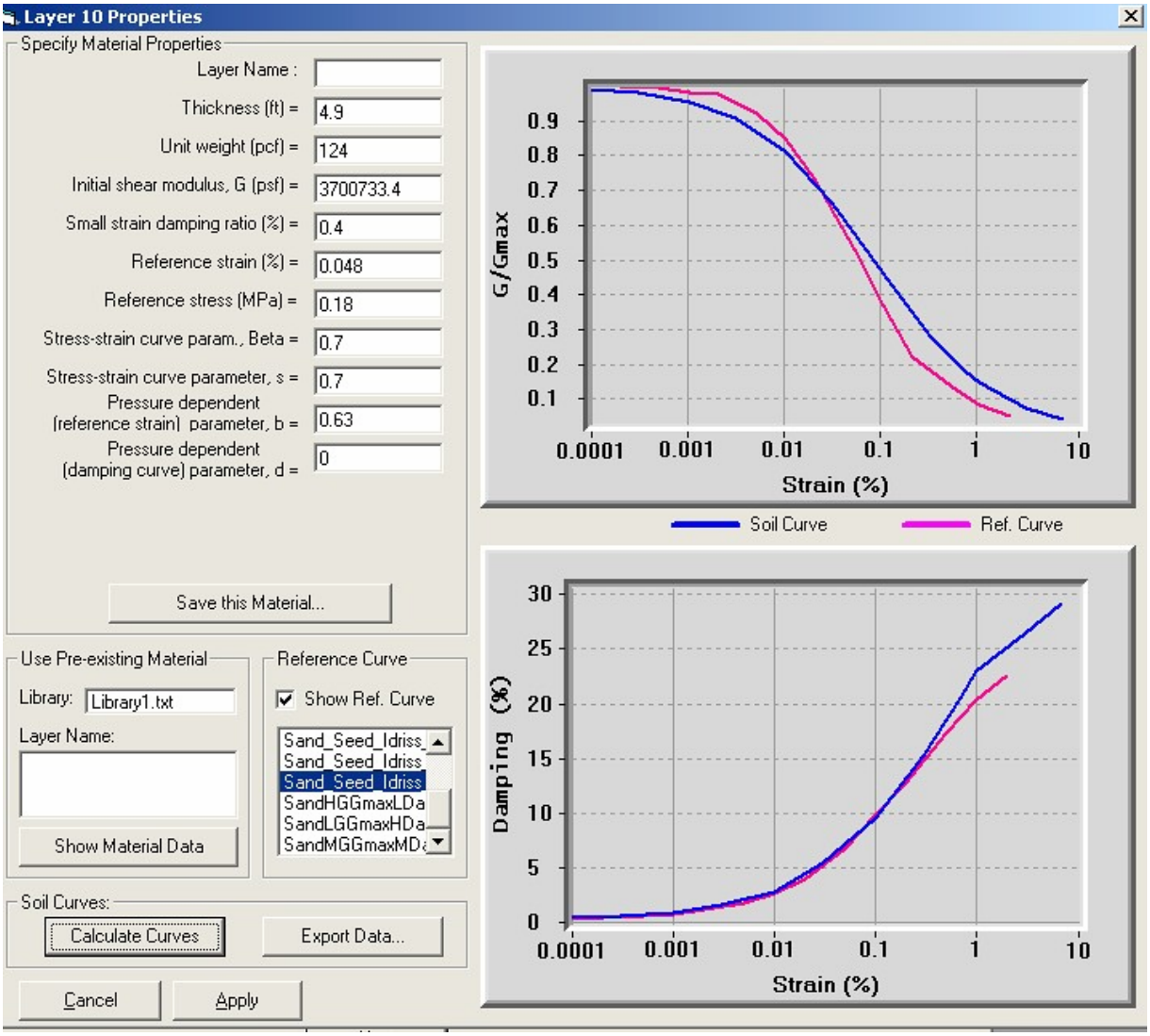

Figure 3-16 Visual procedure for selecting non-linear soil model properties (from User interface of DEEPSOIL).

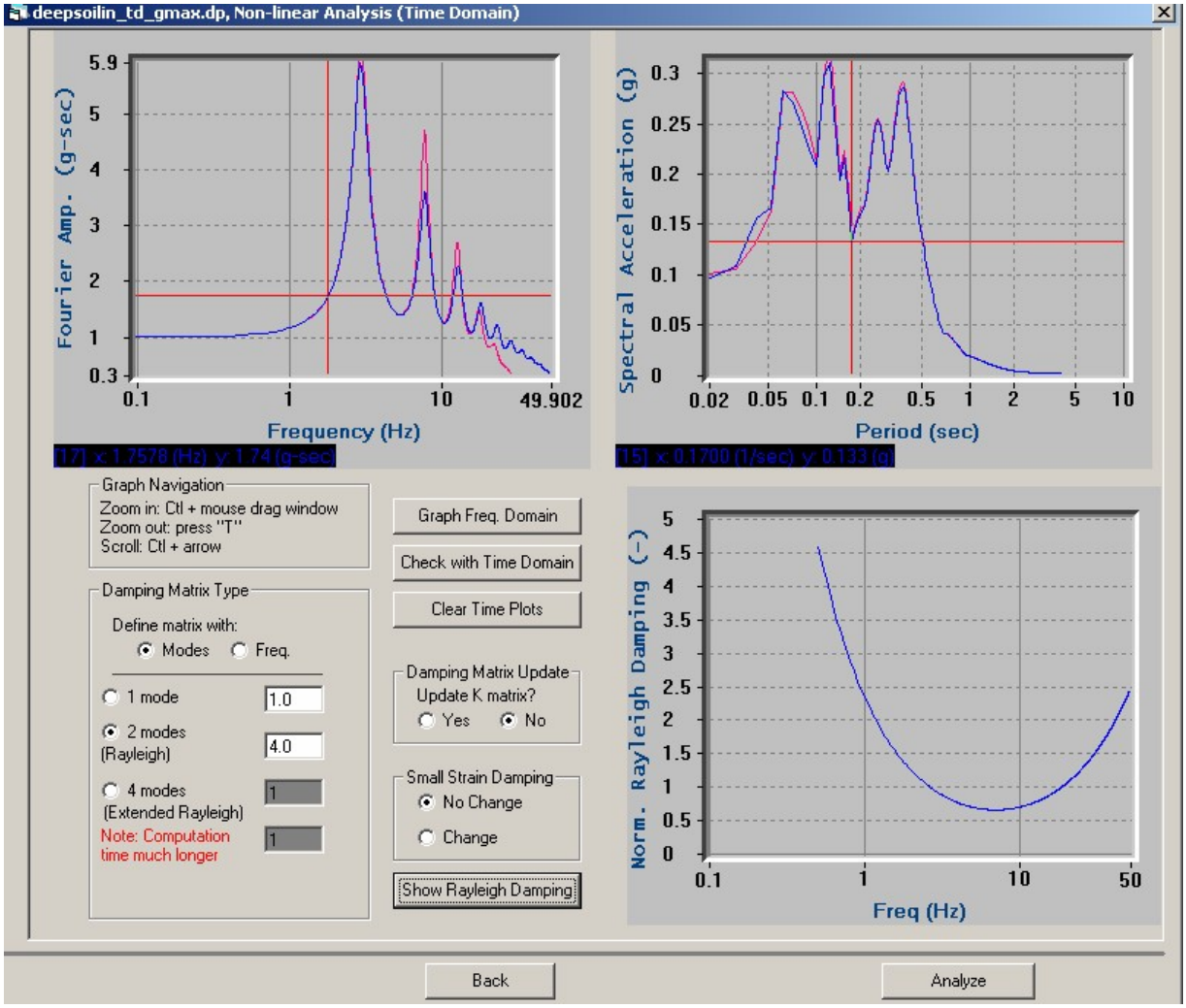

Figure 3-17 Visual procedure for choosing modes/frequencies for Rayleigh damping (from User interface of DEEPSOIL).

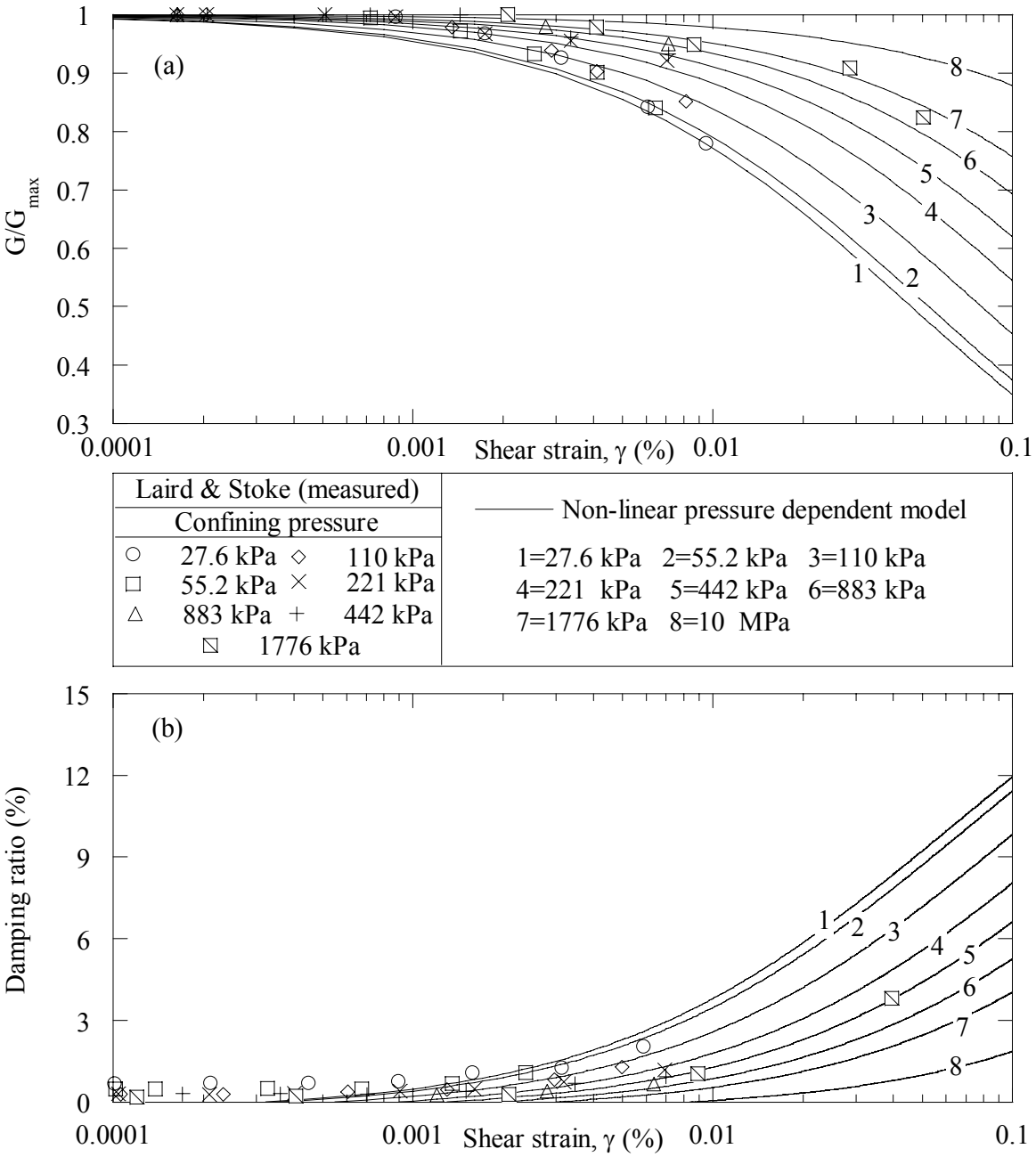

Figure 3-18 Influence of confining pressure on a) shear modulus degradation and b) damping ratio curves in DEEPSOIL nonlinear model used for site response analyses in the Mississippi embayment. Data from Laird and Stokoe [1993] shown for comparison.

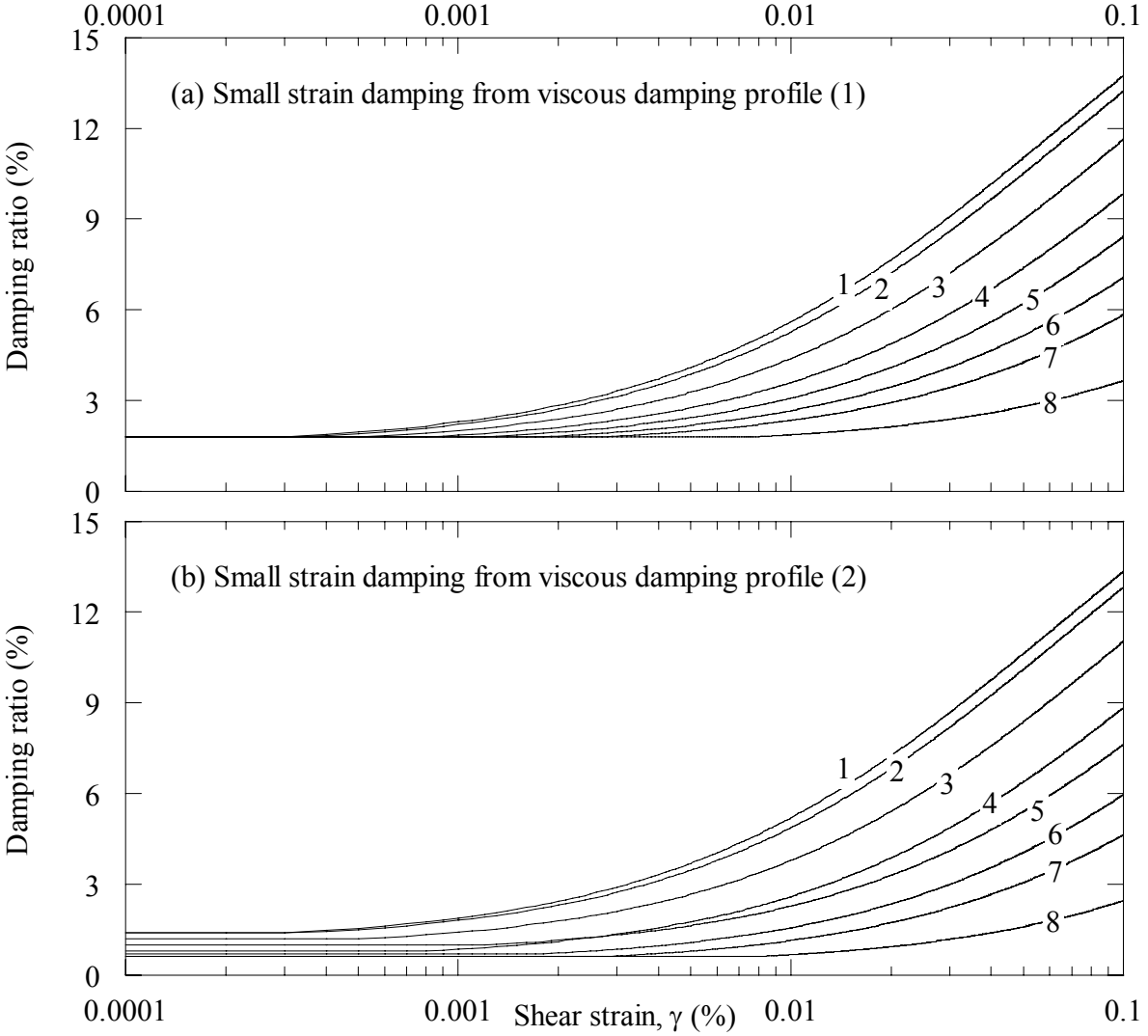

Figure 3-19 Cumulative damping of hysteretic damping from modified hyperbolic model constrained to data from Laird and Stokoe (1993) and (a) viscous damping profile (1), and (b) viscous damping profile (2).

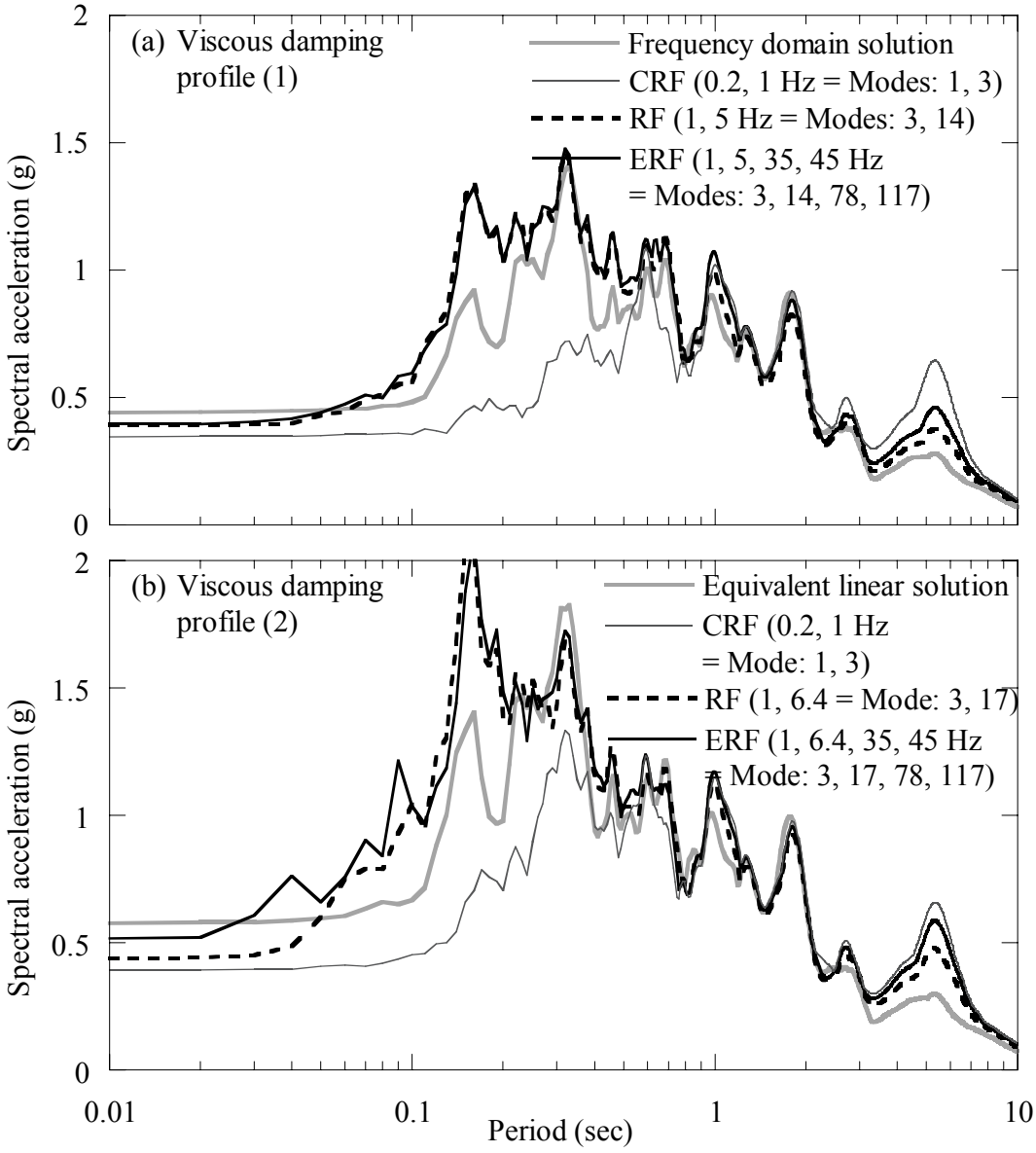

Figure 3-20 The 5% damped response spectra of equivalent linear and nonlinear analyses for 1000 m soil column, input motion S-TS2 (a) using damping profile (1) and (b) damping profile (2).

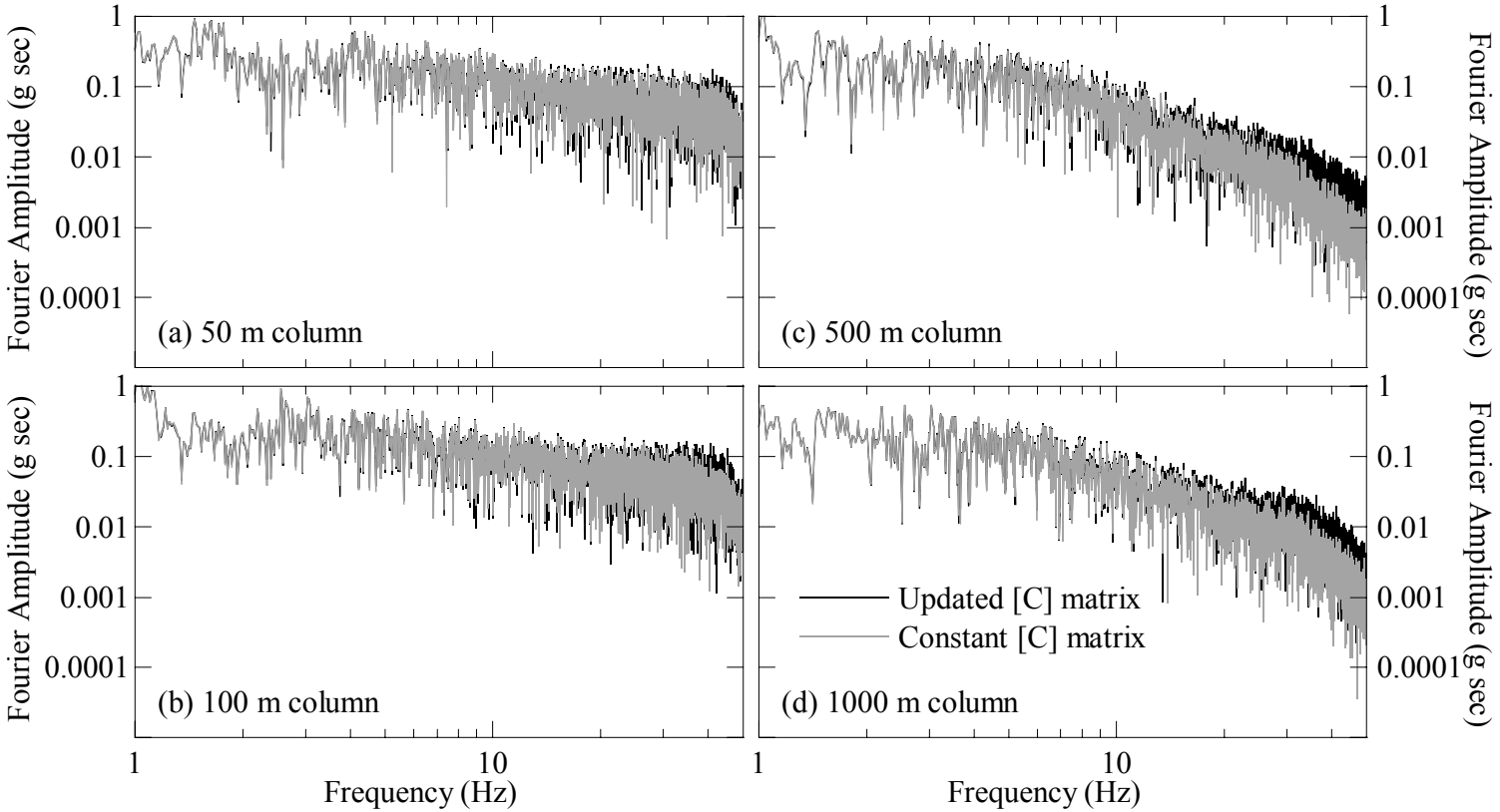

Figure 3-21 Computed surface Fourier spectra, nonlinear time domain site response, V_s and viscous damping profiles (2), non-linear soil properties. Non-linear time domain analysis uses full Rayleigh viscous damping formulation with and without the update of the [C] matrix. Input motion: STS-2.

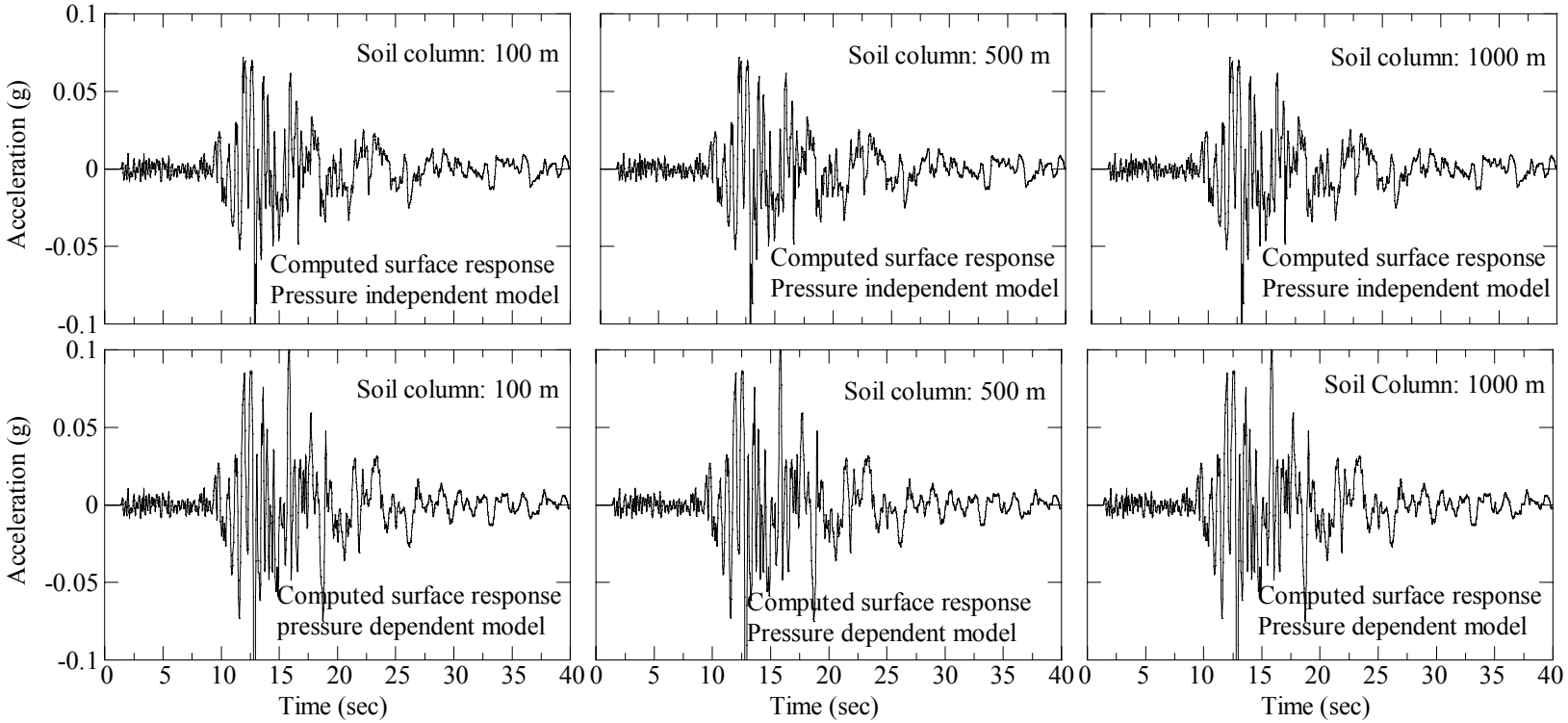

Figure 3-22 Comparison of computed surface acceleration time series from site response analyses using pressure independent and pressure dependent soil models. Input time series R-TS2 (Yerba Buena, Loma Prieta). The pressure dependent model (lower row) shows higher amplitude and greater high frequency content compared to the pressure independent model (upper row).

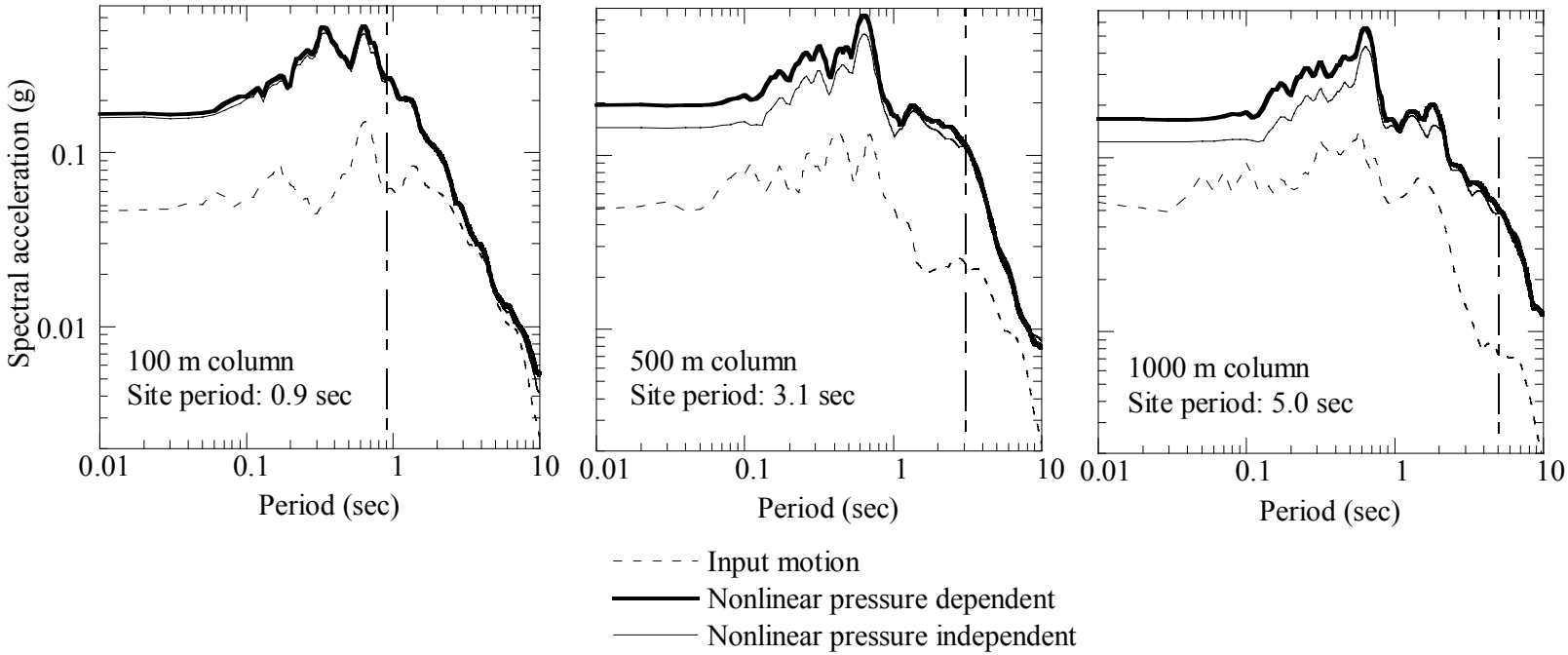

Figure 3-23 Surface response spectra, with 5% damping, from same analyses presented in Figure 3-22. Note the overall higher spectral acceleration in the pressure dependent model analyses (dark solid lines) compared to pressure independent analyses (light solid lines).

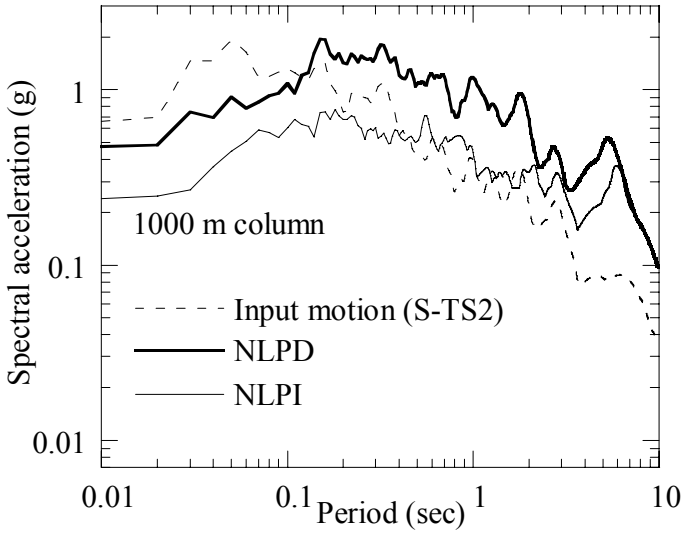

Figure 3-24 Comparison of computed surface response spectra with 5% damping from site response analyses using pressure independent and pressure dependent soil models. Input time series, S-TS2. Note the overall higher spectral acceleration using the pressure dependent model compared to the pressure independent model.

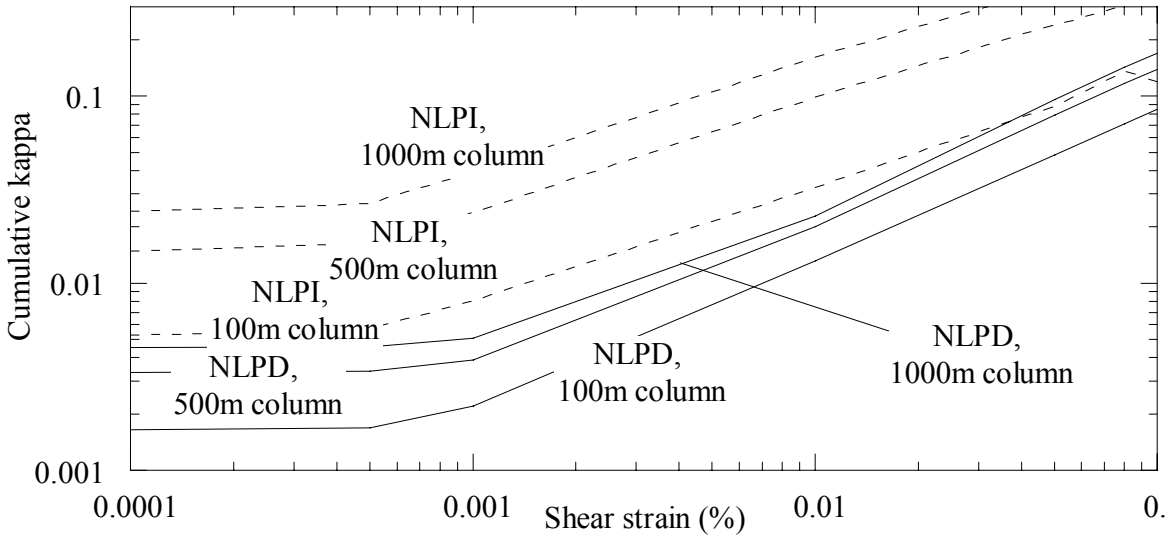

Figure 3-25 Cumulative damping factor kappa in soil columns for pressure dependent and presure independent soil models. Kappa increases with increasing strain level and is consistently smaller for the pressure dependent model compared to the pressure independent model. The lower kappa explains the higher response computed using the pressure dependent mode.

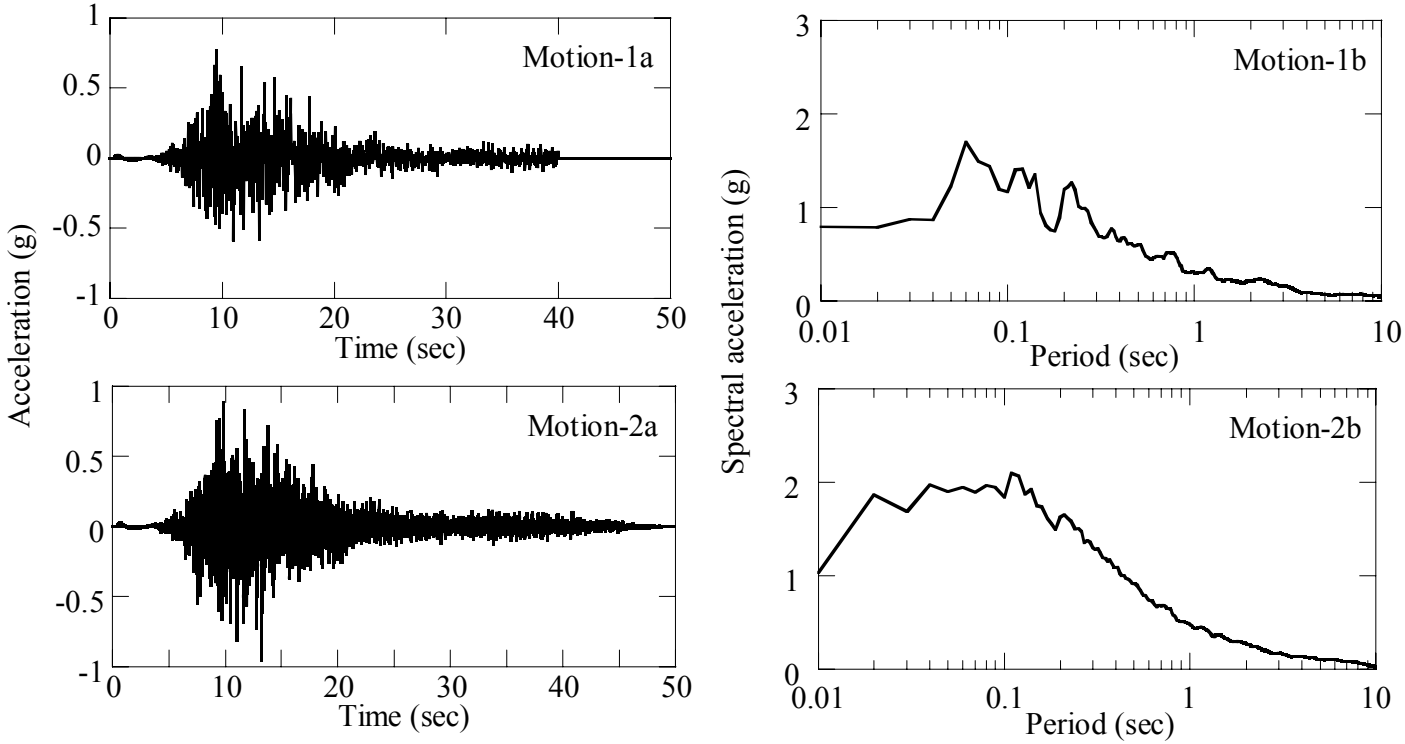

Figure 3-26 Input motions used to demonstrate the effect of the complex shear modulus on equivalent linear solution: a) Time history and b) Fourier amplitude.

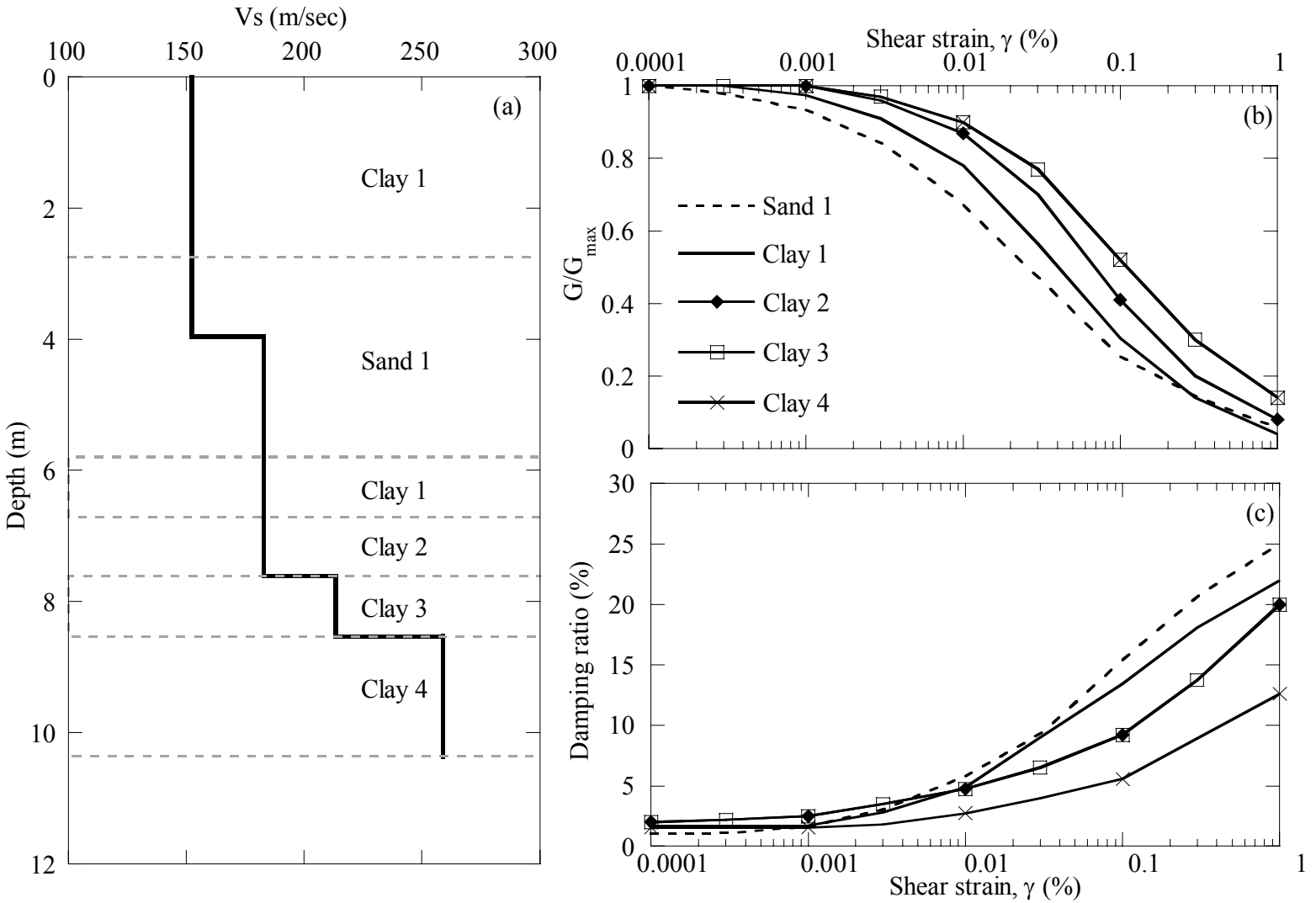

Figure 3-27 Soil profile and soil properties used to observe the effect of complex shear modulus on equivalent linear analysis.

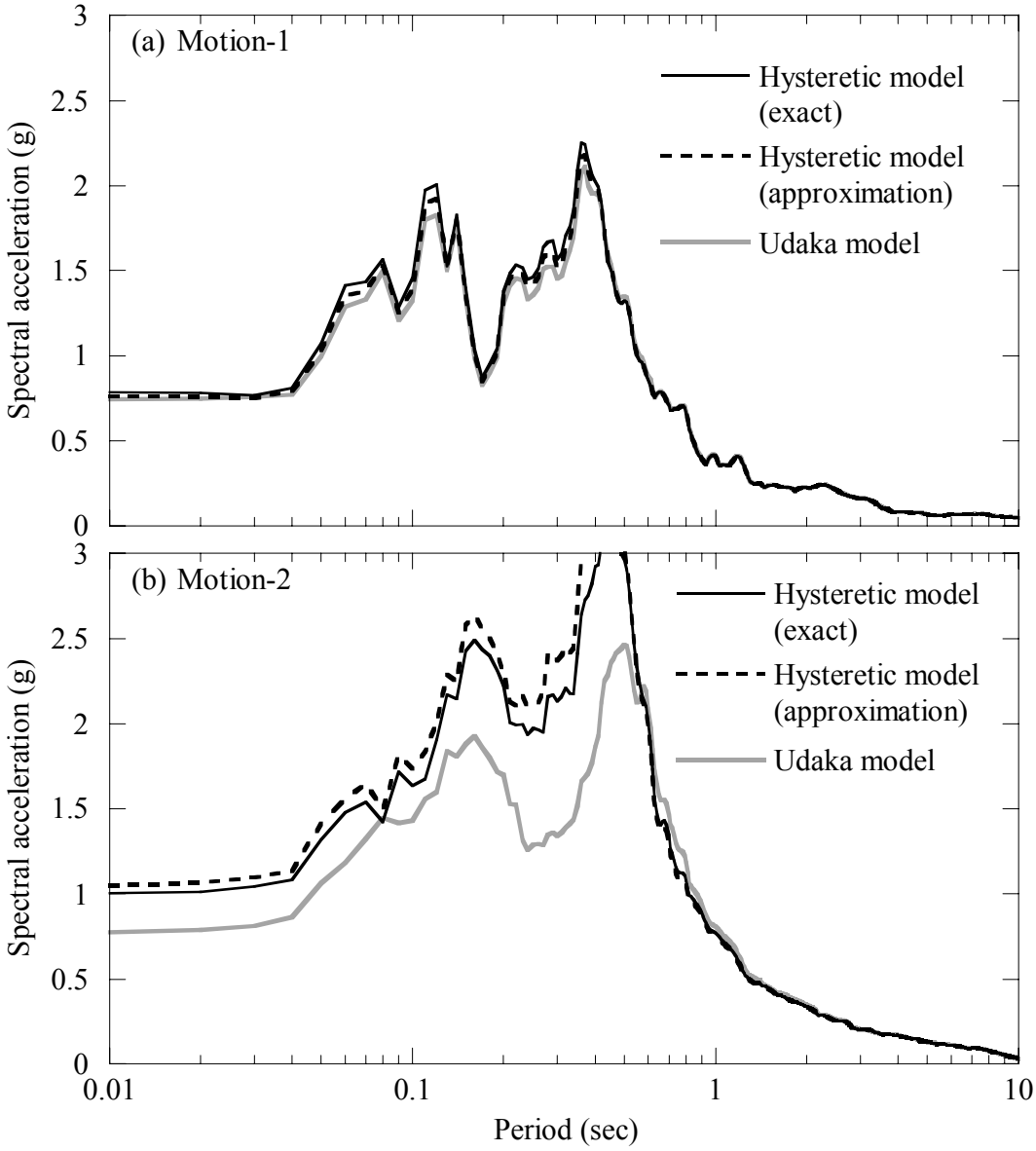

Figure 3-28 Comparison of surface response spectra using three types of the complex shear moduli.

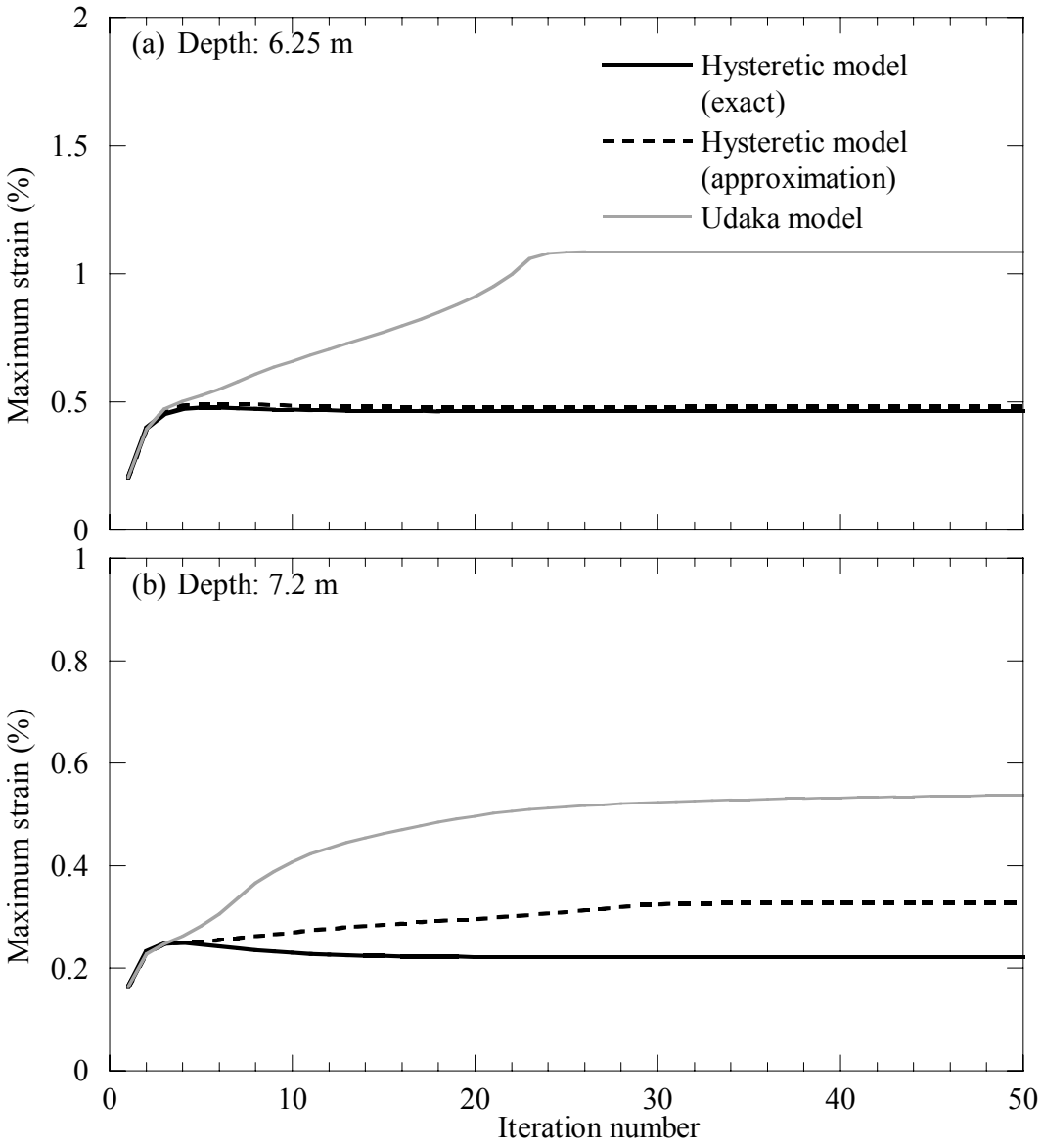

Figure 3-29 Maximum strain calculated at depths 6.3 m and 7.2 m using three types of complex shear modulus.

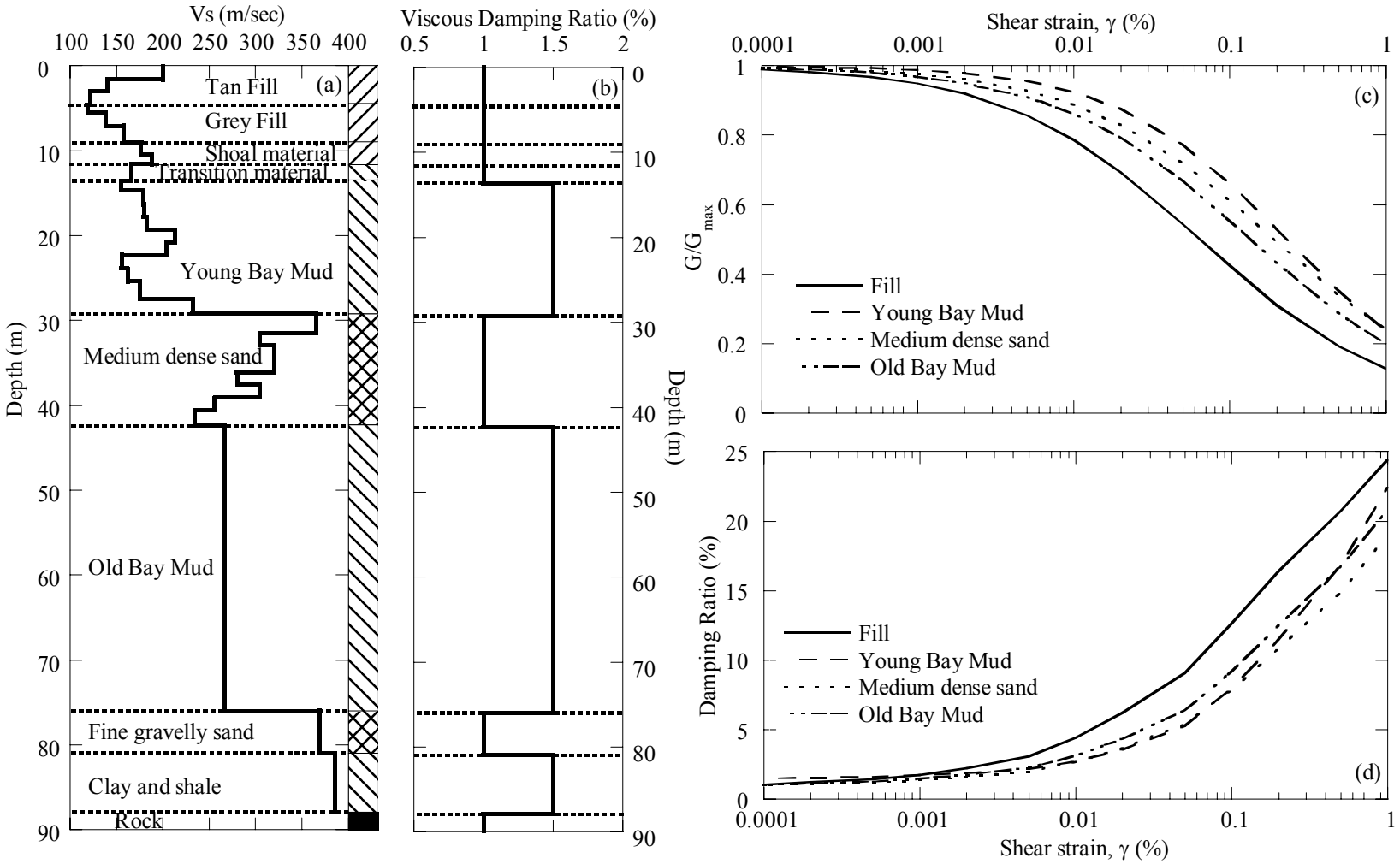

Figure 3-30 Soil profile and soil properties used in the non-linear analysis of the Treasure Island case history.

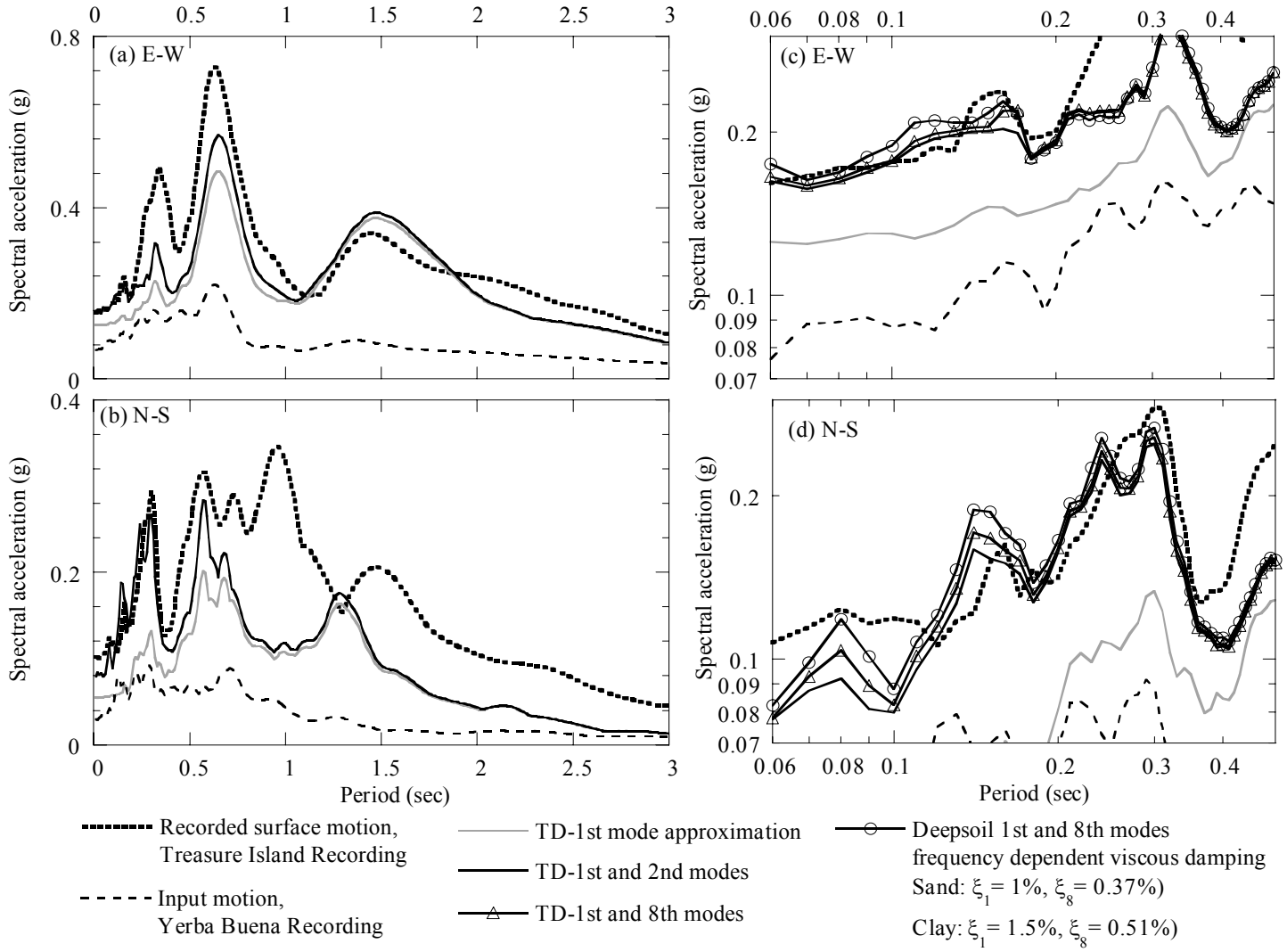

Figure 3-31 Comparison of recorded motions with computed response spectra (E-W and N-S components). DEEPSOIL represents pressure dependent model / full viscous damping formulation.

CHAPTER 4 ESTIMATION OF DYNAMIC PROPERTIES OF THE MISSISSIPPI EMBAYMENT

4.1 Introduction

Deep deposits of the Mississippi embayment, overlying the New Madrid Seismic Zone, present unique challenges for the estimation of local site effects on propagated ground motion. Limited information is available on the dynamic properties of these deposits. This chapter develops generalized depth dependent modulus degradation and damping curves specific to the embayment deposits. Depth dependent small strain damping is estimated using weak motion recordings during the Enola earthquake, 2001. Modulus degradation and damping curves are further constrained using limited laboratory test data of embayment soils at low confining pressure. At high confining pressures embayment specific data is unavailable and test data from outside the embayment is used in developing the dynamic properties. The representative modulus degradation and damping curves are used in a large-scale probabilistic seismic hazard analysis study in the Mississippi embayment, CHAPTER 6, that integrates nonlinear site effects.

4.2 Geology and seismicity in the Mississippi embayment

The Mississippi embayment, which overlies the New Madrid Seismic Zone (Figure 4-1a), is a syncline or a trough-like depression that plunges southward along an axis that approximates the course of the Mississippi River. The embayment, beginning near the Gulf of Mexico and extending north to the confluence of the Ohio and Mississippi Rivers as shown in Figure 4-1a, is surrounded by the Illinois Basin to the north, the Nashville dome and southern Appalachian Plateau to the east, and the Ouachita and Ozark uplifts to the west (Shedlock and Johnston, 1994). The Paleozoic rock forms the bedrock floor of the Mississippi embayment and is located about 1000 m below Memphis and Shelby County, which is near the central part of the Mississippi embayment, as shown in Figure 4-1b (Ng et al., 1989). The embayment is filled with sediments of clay, silt, sand, gravel, chalk and lignite ranging in age from Cretaceous to recent Holocene. There is no well-consolidated rock above the Paleozoic rock, except some local beds of ferruginous and calcareous sandstone and limestone (Parks and Lounsbury, 1976).

The geologic column of the embayment is shown in Figure 4-2 . The details of the geology of the embayment are summarized by Van Arsdale and TenBrink (2000) as follows:

"*Upper Cretaceous sediments unconformably overlie lower Paleozoic strata as old as Cambrian Knox Group in the embayment (Cox and Van Arsdale, 1997). The Coffee Formation is a well-sorted, loose-to-friable sand that is interbedded with thin carbonaceous clays. Overlying the Coffee Formation is the southern part of the Demopolis Formation, which is a calcareous marine clay. Overlying the Demopolis Formation is the McNairy Sand, which is calcareous marine sand.*

An unconformity separates the Late Cretaceous McNairy Sand and overlying Paleocene Midway Group. This unconformity marks the Late Cretaceous regression, subaerial exposure of the Late Cretaceous sediments, and Paleocene transgression of the Mississippi embayment sea. The Midway Group is a marine clay that is 100 m to 160 m thick. Unconformably overlying the Midway Group is the Paleocene to Eocene Wilcox Group. The Wilcox is subdivided into the Old Breastworks Formation (clayey silt), the Fort Pillow Sand (marine sand), and the Flour Island Formation (alternating beds of silt, clay, and sand). An unconformity marks the top of the Wilcox Group. The overlying middle Eocene Claiborne Group is subdivided into Memphis sand (110 to 223 m thick and is a fluvial/deltaic sand), the Cook Mountain Formation (clay and silt fluvial/deltaic unit with minor sand lenses and lignite beds) and Cockfield Formation (fluvial/deltaic silt and clay interbedded with sand and lignite beds). The Eocene to Oligocene Jackson Formation is a fluvial / deltaic silty sand interbedded with clayey silt and lignite.

The surface and near-surface stratigraphy is different east and west of the Mississippi River, as shown in Figure 4-3. West of the Mississippi Valley bluff line, the surface stratigraphy consists of Mississippi River Pleistocene (terraces) and Holocene alluvium. East of the bluff line the near-surface stratigraphy consists of Lafayette Formation (Upland Gravel) and the overlying Pleistocene loess. The Mississippi River sediments, which are approximately 50 m thick, consist of a basal sandy gravel overlain by sands and capped by silts and clays. These flood plain sediments are below the Lafayette Formation and inset 64 m into the Jackson Formation."

The New Madrid Seismic Zone (Figure 4-1a) is a clustered pattern of earthquake epicenters between 5 and 15 km deep and lies mostly within the Reelfoot rift. The New Madrid Seismic Zone (NMSZ) is regarded as the most seismically active zone in the eastern United States. The NMSZ was the source of three major earthquakes with estimated body wave magnitudes greater than 7.0 in the winter of 1811 –1812 (Otto, 1973). In addition, paleoliquefaction studies identified several pre-historic earthquakes in this region with similar

magnitudes. Recent research indicate that the probability of occurrence of an earthquake larger than M_b = 6.6 in the next fifty years is approximately 20 – 30% and has a return period of approximately 400 – 1100 years (Schweig and Van Arsdale, 1996). The fault system is estimated to be less than 200 km long, and recent geodetic observations show the lack of relative motion measure across the system.

Although large-magnitude earthquakes such as the events of the 1811-1812 are infrequent, the area continues to be seismically active. Hays (1980) found that at least one earthquake with a body-wave magnitude (M_b) greater than 4.75 occurs in the Eastern US every two years. Johnston (1996) have associated each of the three 1811 –1812 earthquakes with a specific fault by using historical accounts and geological evidence. Their interpretation is consistent with the spatial distribution and source characterization of contemporary seismicity in the NMSZ (Figure 4-1a).

Another concern of the NMSZ is the low attenuation of the area. The attenuation in the geologic materials in the Central United States is significantly lower than in the Western United States (McKeown, 1982). Nuttli (1973) estimated that attenuation of short-period surface waves in the central and eastern United States was an order of magnitude less than attenuation in the Western United States. The large felt area (one million square miles) of the 1811-1812 events is attributed to the lower attenuation that results in propagation of the seismic wave energy to longer distance. The large extent of possible damage by an earthquake in the NMSZ is attributed to lower attenuation.

4.3 Shear wave velocity profiles

Romero et al. (2001) classified the embayment into two categories based on geologic age. Holocene-age deposits (called Lowlands) are found along the floodplains of the Mississippi River and its tributaries whereas Pleistocene-age deposits (called Uplands) are located in the interfluve, terrace regions (Figure 4-3).

Various shear wave velocity profiles, Figure 4-3, were aggregated and synthesized by Romero et al. (2001) to develop regional generic profiles for ME and site specific profiles for the Memphis Metropolitan Area.

Generic profiles developed for the two geologic categories of the Mississippi embayment are shown in Figure 4-4b, up to a depth of 70 m. The Lowlands profile shows lower shear

velocity compared to the Uplands profile due to loose Holocene-age deposits found in the alluvial plains. The profiles are extended to the maximum depth of the embayment near Memphis, which is approximately 1000 m. Several profiles are available for the deep Mississippi embayment deposits based on travel time, Mini-Sosie test, and boring logs (Romero et al., 2001). A composite profile is obtained by calculating the arithmetic mean of the profiles, as shown in Figure 4-4a.

4.4 Available dynamic soil properties for deep deposits

In a deep soil deposit such as the Mississippi embayment, the soil behavior is significantly influenced by the confining pressure. Soil will experience stiffer response with depth due to high overburden pressure. In the Mississippi embayment, there is a lack of laboratory test data on in-situ soil samples at high confining pressure.

EPRI (1993) develops a set of dynamic curves to represent six different ranges of depths, down to a depth of 305 m only as shown in Figure 4-5. Resonant column, torsional shear and large-scale triaxial chamber laboratory test results on samples obtained from Gilroy (California), Treasure Island (San Francisco Bay Area), and Lotung (Taiwan) as well as literature review of available dynamic curves were used to develop the curves.

These curves are not specific to the ME and have not been verified or constrained with embayment specific laboratory or field tests. The curves have been used in modeling of embayment site response effects by Romero and Rix (2001) and Toro and Silva (2001). The studies assume that the soil behaves as a linear viscoelastic material at depths greater than 150 m.

These curves are used as one possible set of dynamic properties. Model constants for the nonlinear constitutive model in DEEPSOIL, described in CHAPTER 3, are selected to match the EPRI soil curves. The constants are listed in Table 4-1. The resulting modulus degradation and damping curves are compared to EPRI curves in Figure 4-5. The curves are calculated at confining pressures corresponding to the median depth of the respective EPRI depth range. The unit weight of the soil is assumed to be 19.5 kN/m^3 and the water table is taken at the surface. Figure 4-5 shows that a good, though not identical, match with the EPRI curves is obtained. The definition of the confining pressure dependent parameters for the non-linear constitutive model allows extrapolation of material properties to higher depths/confining pressures. Dashed line 7 provides the estimated curves at a depth of 1000 m.

4.5 Estimation of small strain damping properties

During the Enola earthquake (May 4th 2001, epicenter = 35.24 N/92.25 W, moment magnitude = 4.5), recordings were made at 8 stations within the embayment (Withers, 2000), as shown in Figure 4-6. Table 4-2 lists the locations, geologic age, depth of the soil columns, and distances from the epicenter. Three stations are located on Uplands, and five are located on Lowlands. Thickness of the soil columns, ranging from 250 m to 760 m, are estimated using the structural geologic contour map by Van Arsdale and TenBrink (2000).

The weak motion recordings induce very small deformations in the embayment soils and are used to back calculate generic small strain soil damping profile in the ME by performing linear site response analysis. SMSIM has been used in development of attenuation relationships for 1996 and 2002 USGS hazard maps (Frankel, 1996; Frankel et al., 2002)

1. *Input motion*: Vertical array recordings or a nearby rock outcrop recording is routinely used as input motions for simulating field recordings and evaluating site effects. No such recordings are available in the embayment for the Enola earthquake, and hence, synthetically generated motions are used to represent the bedrock motion. The synthetic motions are generated using the point source stochastic model SMSIM (Boore, 2002) and input parameters for the central and eastern U.S (Frankel et al., 2002). SMSIM has been used in development of attenuation relationships for 1996 and 2002 USGS hazard maps (Frankel, 1996; Frankel et al., 2002). Twenty motions are generated for each site to account for variability in the ground motion.
2. *1-D site response analysis:* The generated input ground motions are propagated through the soil profiles, ranging in thickness from 250 m to 760 m. Linear site response analyses are performed since the propagated motions for the Enola Earthquake are very small, with peak ground acceleration (PGA) at less than 0.003 g. Generic shear wave velocity profiles, Figure 4-4, are used in the analyses.

The EPRI small strain damping properties (Figure 4-5 and Figure 4-7) are initially used to represent the damping profile. The computed surface response significantly overestimates the field recording. The damping profile is then increased, Figure 4-7, until a reasonable match is obtained between the computed and recorded surface motions. The variation of embayment

depths across the recording stations permits the evaluation of the variation of damping with depth.

Figure 4-8 compares the response spectra of the recorded motions with the propagated motions at selected stations. The response spectra of the computed motions represent averages of twenty motions propagated at each site. Even though a single small strain damping profile is used, Figure 4-7, the calculated surface responses compare well with the recorded motions. The damping ratio is 3.5% near the surface and 0.4% below 650m. The estimated damping values are much higher than EPRI (1993) at depths lower than 650 m, but slightly lower at greater depths.

A measure of cumulative damping in the column is the quantity kappa, defined as:

$$\kappa = \int \frac{2\xi}{V_s} dz \tag{4-1}$$

The overall kappa of the back-calculated small strain damping profile, at 0.0054, is close to the kappa of 0.0048, previously estimated damping for the 1000 m profile in the embayment (Herrman et al., 1986).

4.6 High confining pressure dependent dynamic properties of the ME

This study proposes use of the laboratory test data of Laird and Stokoe (1993) in characterizing the high confining pressure dependent dynamic properties, as shown in Figure 4-9. The main reason for using the Laird and Stokoe's test data is because of the similarity with laboratory test data of shallow soils from the ME, as shown next. Note that the original small strain damping properties are removed and replaced by the back-calculated small strain damping properties, Figure 4-7. The back-calculated small strain damping properties are much higher than Laird and Stokoe's test data, but also compare well match well with test data of shallow soils from the ME, as shown in the next section. The non-linear soil model is used to extrapolate the pressure dependent properties to full depth of the ME deposits. Selected material constants for the non-linear soil model of the ME are compared to those selected for EPRI in Table 4-1.

4.7 Laboratory tests of shallow embayment soils

Chang et al. (1989) collected 35 soil samples in the northern ME region (Arkansas and Tennessee) and resonant column tests are performed to determine the dynamic properties of the collected soil samples. The soil groups include alluvial sands, sands and gravels, silty to sandy

clays, and loess, and are summarized in Table 4-2 Summary of recording stations during Enola Earthquake, 2000.

Station Name	Longitude	Latitude	Geologic age	Distance from epicenter (km)	Depth of soil column (m)
GLAT	36.27	-89.29	Uplands	291	610
HICK	36.54	-89.23	Uplands	307	500
HALT	35.91	-89.34	Uplands	274	660
GNAR	35.965	-90.02	Lowlands	217	700
LPAR	35.60	-90.30	Lowlands	233	760
HBAR	35.56	-90.66	Lowlands	149	660
PEBM	36.11	-89.75	Lowlands	237	720
PENM	36.45	-89.63	Lowlands	272	500
HENM	36.72	-89.47	Lowlands	299	320
PARM	36.67	-89.75	Lowlands	276	250

Table 4-3. The soil samples are tested under confining pressures of 34.5, 137.9, 379.2, and 413.7 kPa. For each of the soil groups, upper, mean, and lower bound curves are developed.

Figure 4-10 to Figure 4-12 compare the developed dynamic curves of the ME with the laboratory test data of selected soil groups (soil groups A2, A3, and B2). Both the developed G/G_{max} and damping curves are within the bounds of the laboratory test data.

4.8 Comparison with interpreted dynamic properties

Figure 4-13 compares modulus degradation and damping curves developed based on ME specific data and generic EPRI curves. Both sets of curves are derived from calibrated extended modified hyperbolic models, shown in Figure 4-5 and Figure 4-9. The material constants for the nonlinear soil model are listed in Table 4-1. Shear modulus reduction curves are similar at low confining pressures, but the effect of confining pressure is more pronounced in the ME curves. The ME curves become stiffer than the EPRI curves with increase in confining pressure. The small strain damping ratio of EPRI curves are consistently lower than those of the ME curves. The damping ratios of the ME curves at strains higher than 0.1% are higher than the EPRI curves at low confining pressures (up to 20 m), but lower at higher confining pressures This is due to the lower hysteretic damping associated with the stiffer response at high confining pressures of the ME curves compared to the EPRI curves.

While the ME curves are constrained by embayment specific data, there remains considerable uncertainty in the embayment material properties. The developed properties are generic properties of the ME and not site specific. In order to account for uncertainty in dynamic properties, both ME and EPRI curves are used in a large scale study to characterize site effects of the ME in the companion paper.

4.9 Site response analysis using the proposed (ME) and EPRI dynamic properties

Equivalent and nonlinear site response analyses are performed using two sets of dynamic properties to evaluate and illustrate the influence of the dynamic properties on propagation of ground motion in the Mississippi Embayment.

The shear wave velocity profile used in the analyses is the Uplands profile and the depth of the profile is 1000 m. Three motions of different intensities are used as input motions, as shown in Figure 4-14.Motion 1 represents a weak ground motion (M = 7.7, R = 168 km, PGA = 0.1 g), whereas Motion 2 (M = 7.7, R = 26 km, PGA = 0.62 g) and Motion 3 (M =8.0, R = 32 km, PGA = 0.65g) represent strong motions. The PGA of Motion 3 is similar to Motion 2, but Motion 3 has longer duration and richer high frequency contents. All motions are generated using SMSIM (Boore, 2002).

Figure 4-15compares the responses using Motion 1. For the weak motion, the effect of the small strain damping is pronounced due to very low hysteretic damping. Therefore, the response using the proposed ME properties is much lower than when using the EPRI curves. The results of the nonlinear and equivalent linear analysis are very similar when propagating the weak motion.

Figure 4-16 compares the results using Motion 2. When propagating a strong motion, output is influenced not only by small strain damping, but by overall dynamic behavior of soils. Except at very long periods, the response spectrum is larger using the ME properties. This is due to the higher confining pressure dependency of the ME properties compared to EPRI properties, and thus stiffer behavior. At very long periods (higher than 5 seconds), the response when using EPRI curves is higher due to softer behavior of soils. The influence of the material properties is more subtle when propagating a strong ground motion.

The difference between the equivalent linear and nonlinear analysis is evident when propagating the strong ground motion (Motion 2), in which equivalent linear analyses show

lower response at periods 0.1 to 0.4 sec than the nonlinear analyses. This is because constant stiffness and damping is used throughout the analysis, resulting in filtering of high frequency components of the ground motion. The response at long period is lower than nonlinear analysis due to stiffer behavior at high strains.

The discrepancy between the two analysis methods increases with the intensity of the input ground motion, as shown in Figure 4-17. Significant portions of the high frequency components are filtered out using the equivalent linear analysis. The influence is especially dramatic when using the EPRI properties, in which the low small strain damping results in less filtering out of the high frequency components. Equivalent linear analysis underestimates amplification at high frequency / short period. The examples demonstrate the need for nonlinear analysis when propagating strong ground motions in the ME.

4.10 Summary

Estimation of dynamic properties in the Mississippi embayment is difficult due to the lack of laboratory test data of in-situ soil samples at high confining pressures. Laboratory tests performed up to 3.5 MPa are used to characterize the pressure dependency of the dynamic soil behavior. The soil properties are extrapolated to a depth of 1000 m. The small strain damping properties of the laboratory test data have been constrained using weak motion recordings in the embayment during the Enola earthquake, 2001. The back-calculated small strain damping is much higher than the estimated damping from laboratory tests. The back-calculated small strain damping is combined with hysteretic damping from the laboratory tests to develop representative properties of the Mississippi embayment. The proposed curves are compared to the limited in-situ soil laboratory tests. The proposed curves fall within the bounds of embayment in-situ test results, including the small strain damping properties. The proposed curves are also compared to the generic confining pressure dependent properties. The proposed curves show higher pressure dependency and higher small strain damping ratio. Both the proposed and generic soil properties are used to characterize the dynamic soil behavior in site response analyses presented in CHAPTER 6.

Table 4-1. Material constants used in the proposed extended hyperbolic model to match ME and EPRI dynamic curves.

Symbol	Description	ME	EPRI
β	Dimensionless coefficient used to modify the classical hyperbolic model.	1.4	0.7
s	Dimensionless coefficient used to modify the classical hyperbolic model.	0.8	0.8
σ_{ref}	Reference stress.	0.18 MPa	0.18 MPa
a	Dimensionless constant used in the computation of reference strain variation with confining pressure.	0.163 %	0.05 %
b	Dimensionless constant used in the computation of reference strain variation with confining pressure.	0.63	0.4
c	Dimensionless constant used in the computation of small strain variation with confining pressure.	Chosen to match back-calculated small strain damping	Chosen to match small strain damping of EPRI curves
d	Dimensionless constant used in the computation of small strain variation with confining pressure.	0.0	0.0

Table 4-2 Summary of recording stations during Enola Earthquake, 2000.

Station Name	Longitude	Latitude	Geologic age	Distance from epicenter (km)	Depth of soil column (m)
GLAT	36.27	-89.29	Uplands	291	610
HICK	36.54	-89.23	Uplands	307	500
HALT	35.91	-89.34	Uplands	274	660
GNAR	35.965	-90.02	Lowlands	217	700
LPAR	35.60	-90.30	Lowlands	233	760
HBAR	35.56	-90.66	Lowlands	149	660
PEBM	36.11	-89.75	Lowlands	237	720
PENM	36.45	-89.63	Lowlands	272	500
HENM	36.72	-89.47	Lowlands	299	320
PARM	36.67	-89.75	Lowlands	276	250

Table 4-3 Soil groups used for dynamic testing (Chang et al., 1989)

Soil Group	Description	Range of depth of borings (m)
A2	Terrace sand and gravel (SP-SW-SM-SC-GP)	1.5 – 13.4
A3	Jackson fine sand (SP)	7.6 – 21.6
B2	Jackson clay (CL-CH)	2.5 – 7.6

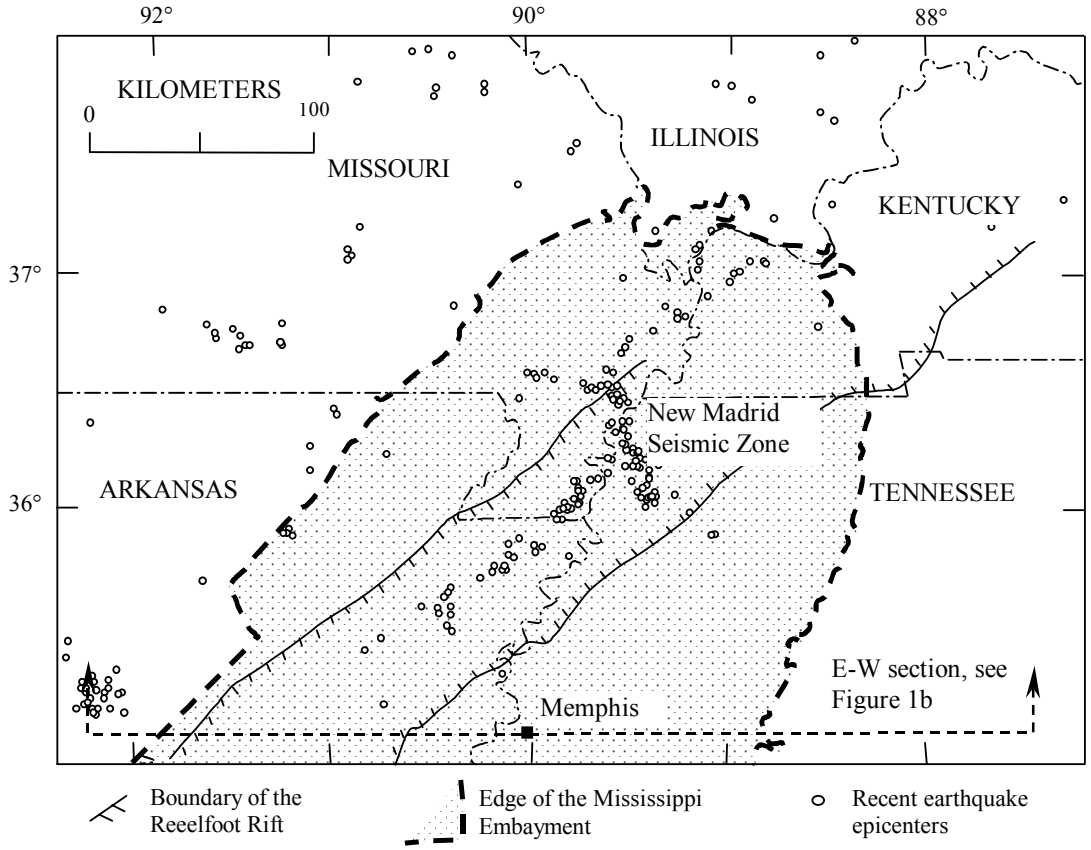

a. Plan view of the Mississippi embayment and major structures within it. Circles denote the clustered pattern of earthquake epicenters that define the New Madrid Seismic Zone within the Reelfoot Rift margins.

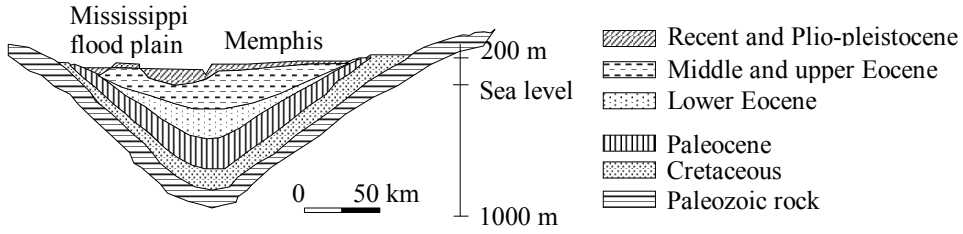

b. E-W section through Memphis (after Ng. et al., 1989). Note: Vertical dimension is highly exaggerated, and the embayment trough has a shallow slope of less than 1/150.

Figure 4-1. The Mississippi embayment.

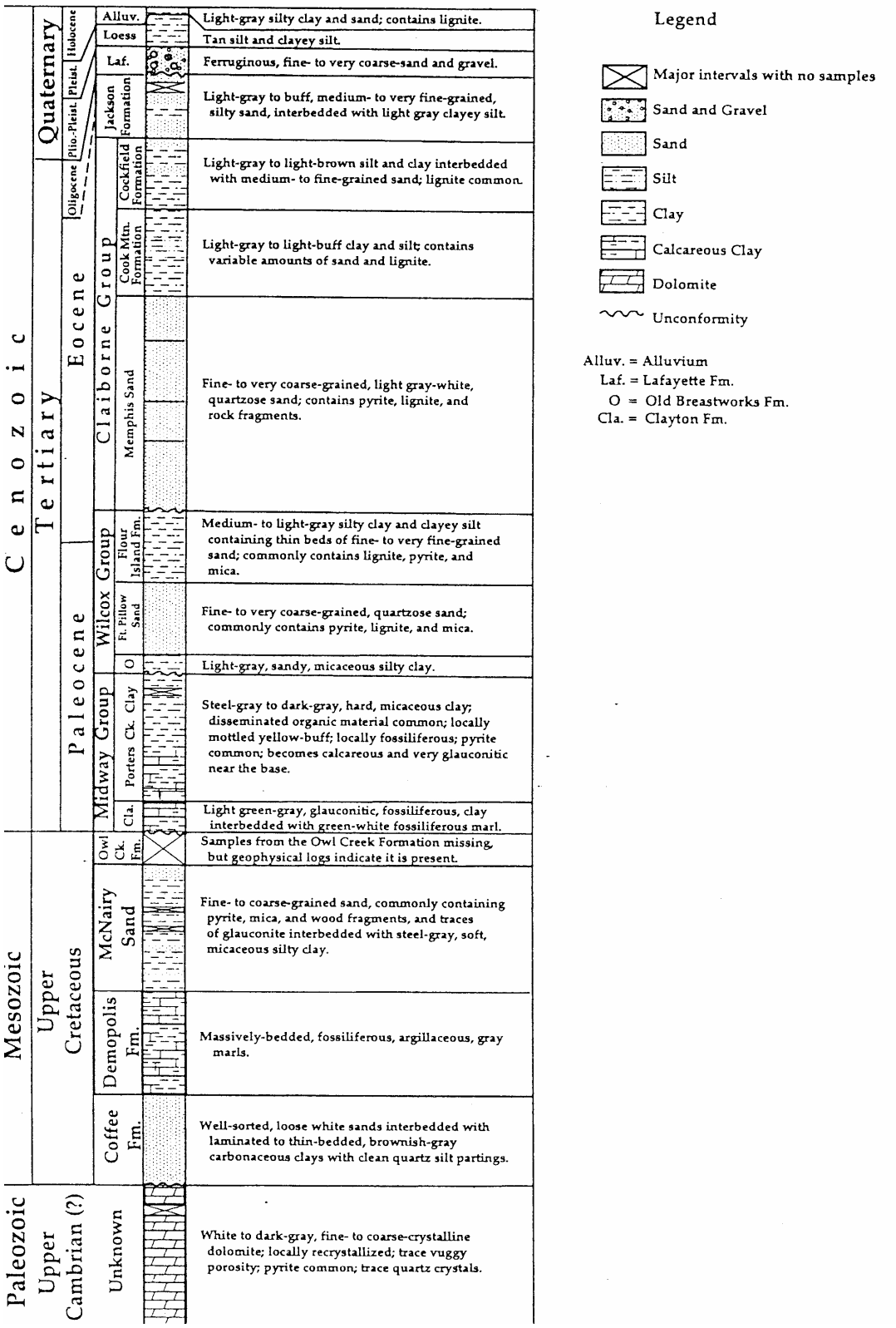

Figure 4-2 Geologic column of the Mississippi embayment (Crone, 1981).

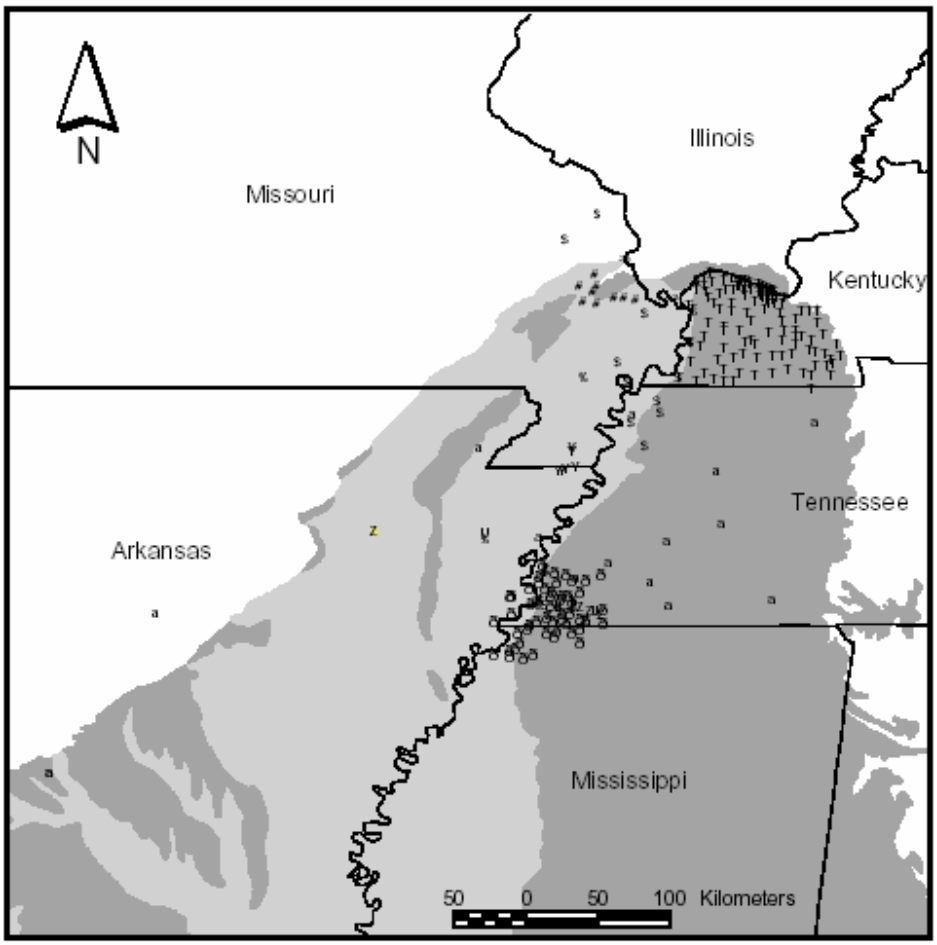

Age of Near-Surface Geologic Deposits
in the Mississippi Embayment

Holocene
Pleistocene

Shear Wave Velocity Measurements

S	Casey et al., 1999	O	Williams, 2000
/	Casey, 1999	[	Schneider, 1999
3	Cooling et al., 1999	Y	Schneider and Mayne, 1998a
Z	Hebeler, 2001	S	Schneider and Mayne, 1998b
%	Liu et al., 1997	#	Bauer, personal communication
·	Liao et al., 2000	a	Pezeshk, personal communication
T	Street et al., 1997	$	Silva, personal communication
Ö	Street, 1999	U	Zavala, personal communication

Figure 4-3 Classification of Mississippi embayment soils based on near-surface geologic deposits and locations of shear velocity profiles measured (Romero and Rix, 2001).

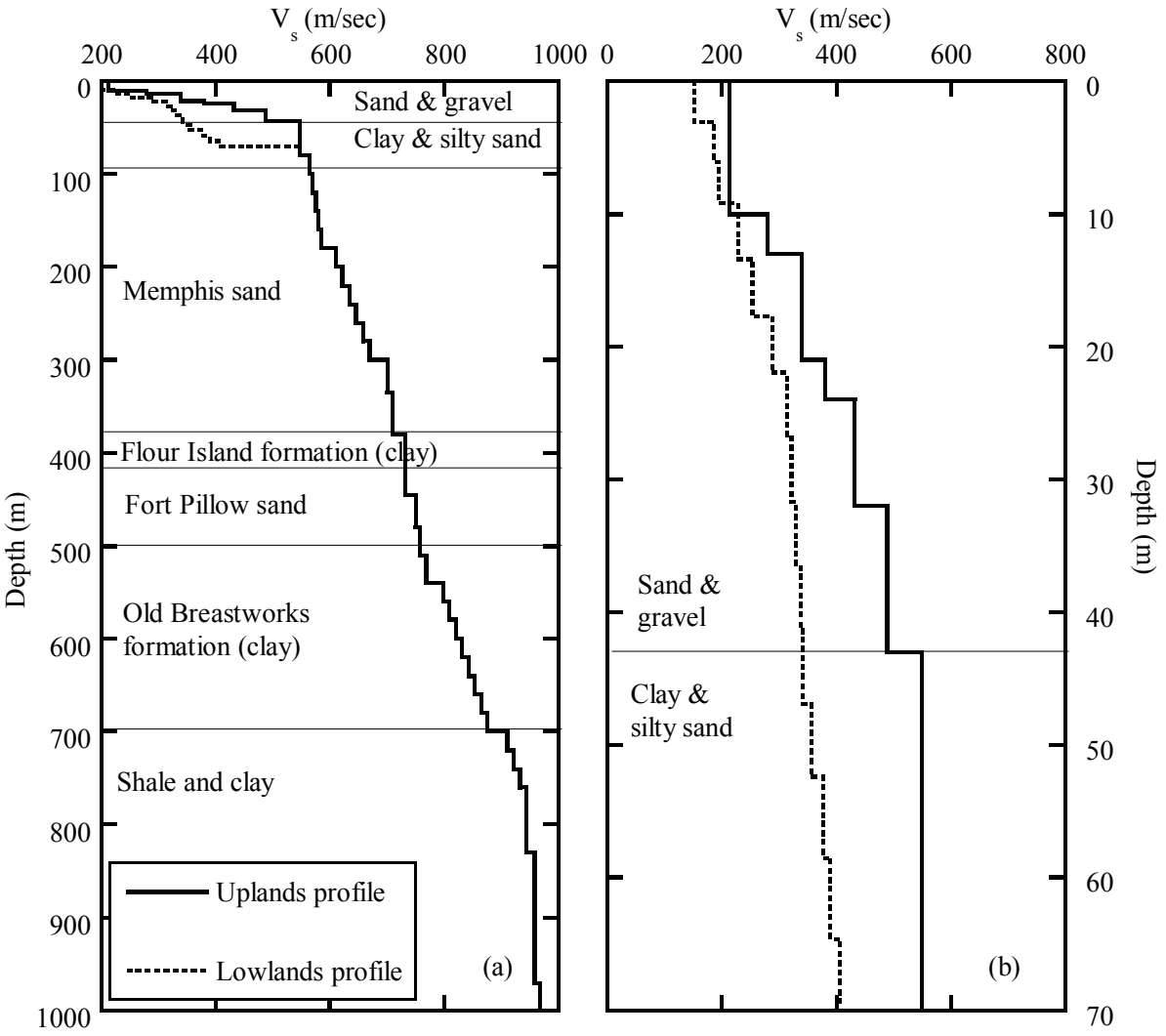

Figure 4-4. Simplified Mississippi embayment stratigraphy and generic shear wave velocity profiles (Uplands and Lowlands) a) up to 1000 m and b) up to 70m. The profiles are the same below the depth of 70m (Romero and Rix, 2001).

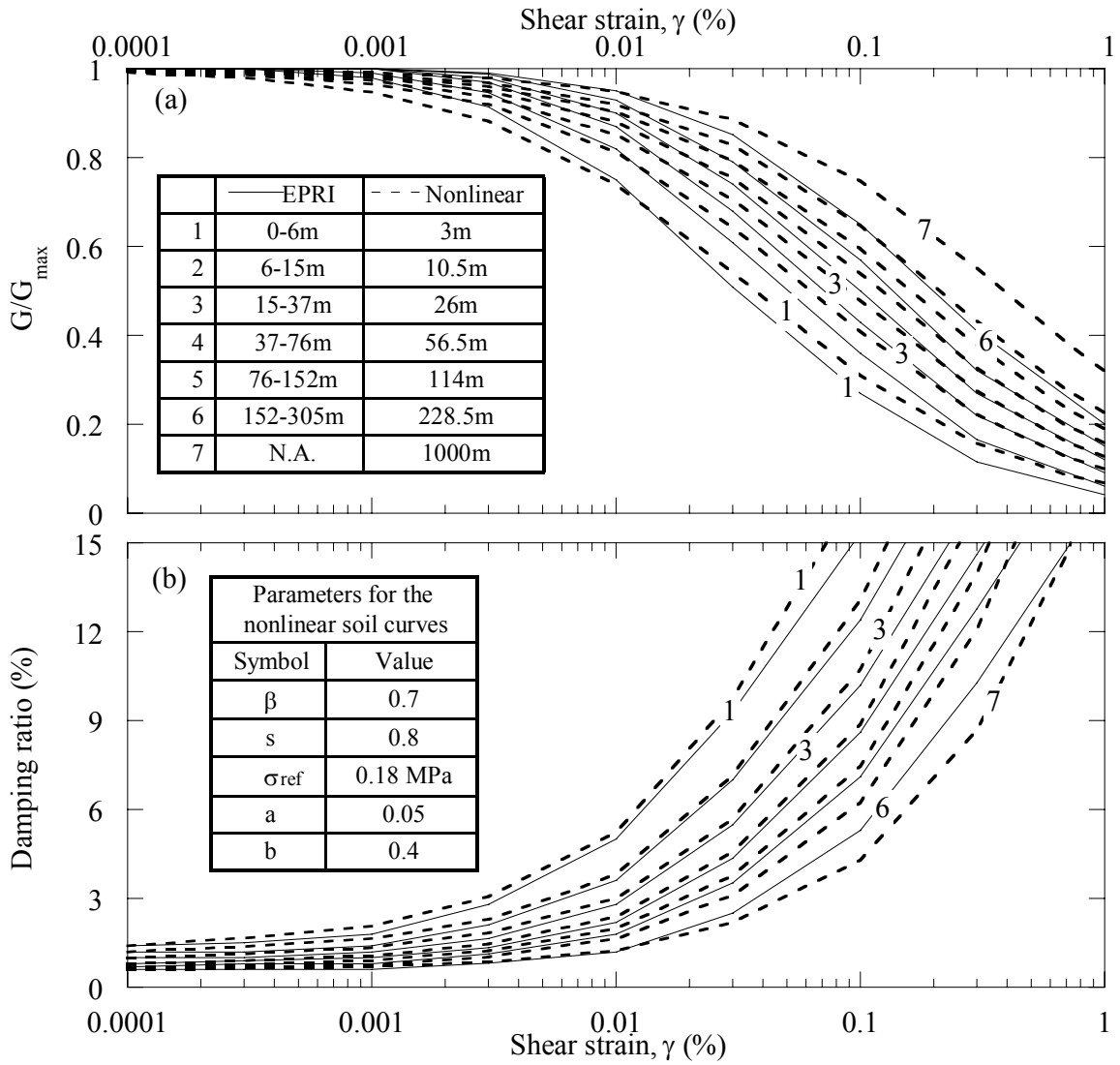

Figure 4-5 Comparison of the EPRI curves (EPRI, 1993) with modulus reduction and damping curves from the nonlinear soil model (extended modified hyperbolic model) with parameters selected to match EPRI curves..

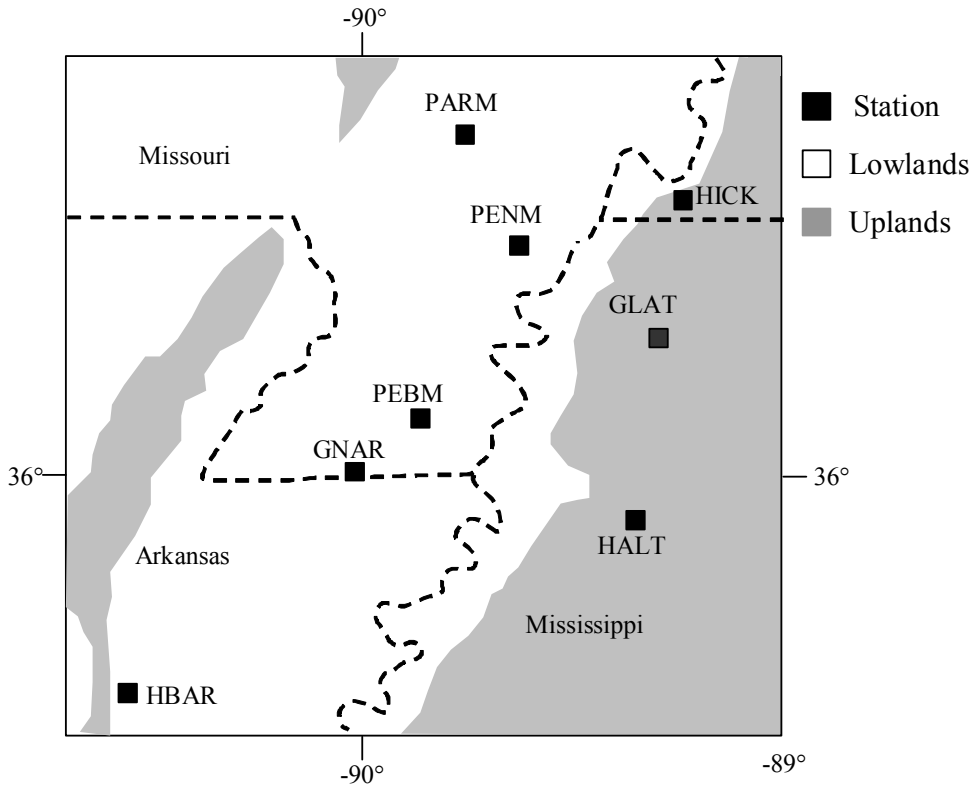

Figure 4-6 Locations of the recording stations in the embayment. White background represents the Lowlands and gray background represents the Uplands.

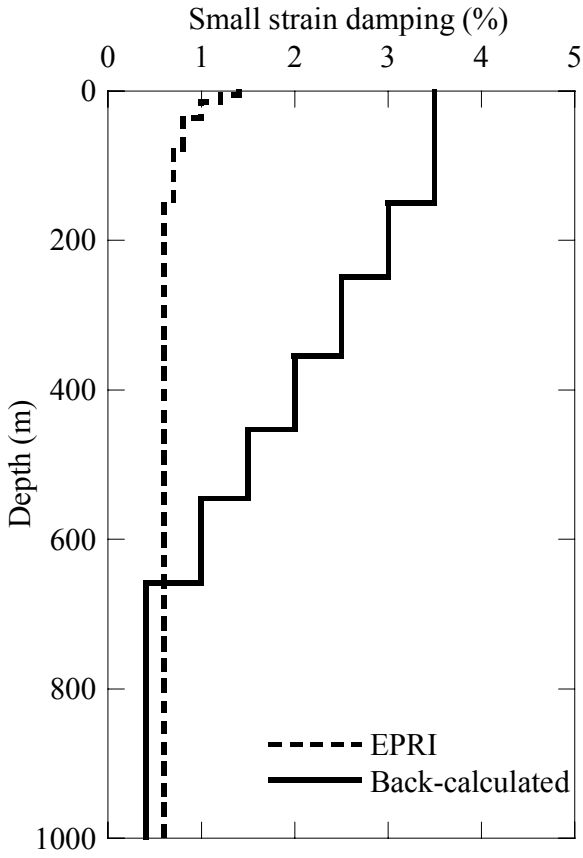

Figure 4-7 Comparison of a) back-calculated viscous damping profile and b) profile developed by EPRI (1993).

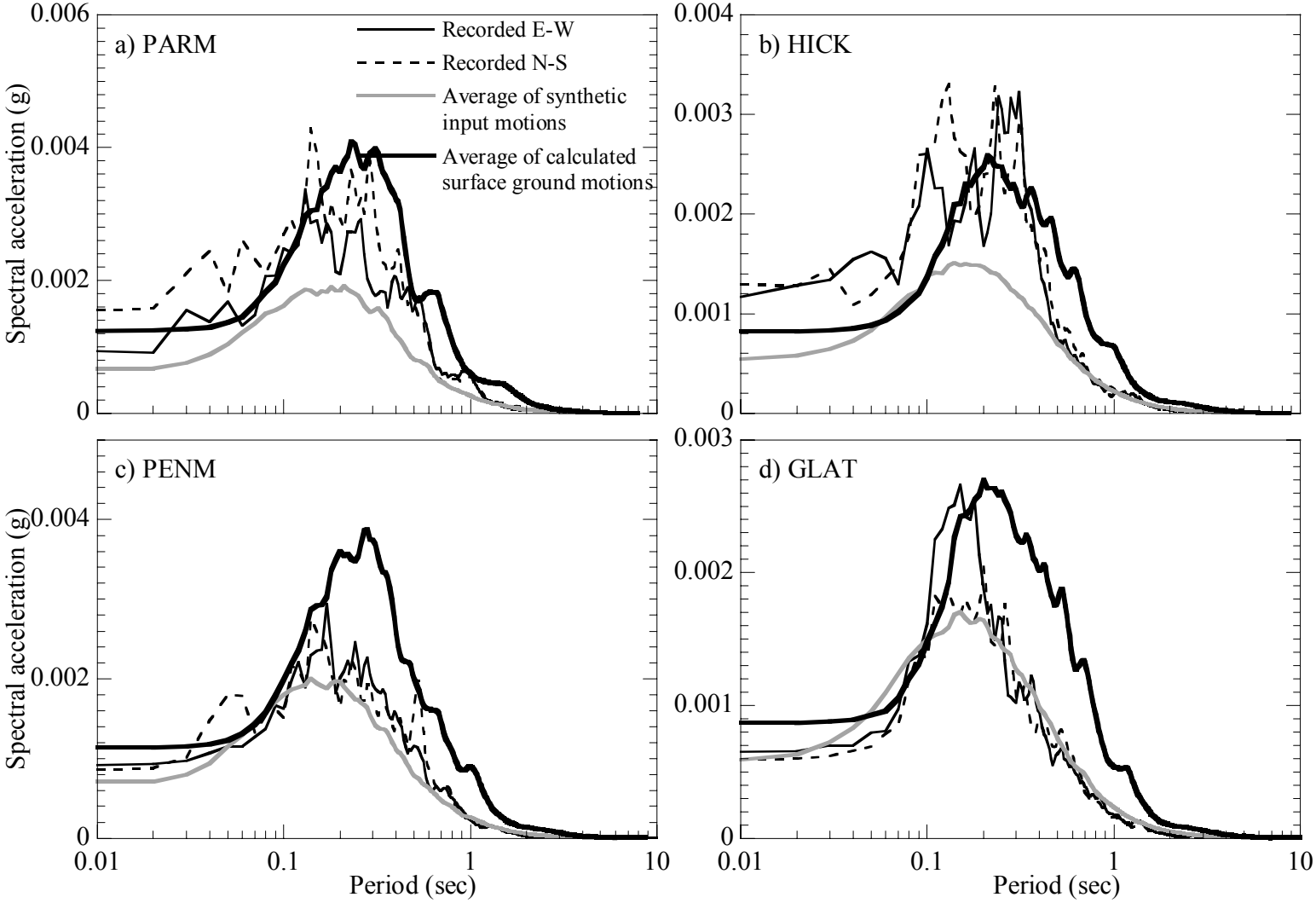

Figure 4-8 Comparison of recorded motions with calculated motions using the back-calculated viscous damping profile for stations a) PARM (250m), b) HICK (500m), c) PENM (500m), and d) GLAT (610m). All of the stations are at soil columns less than 650 m in depth.

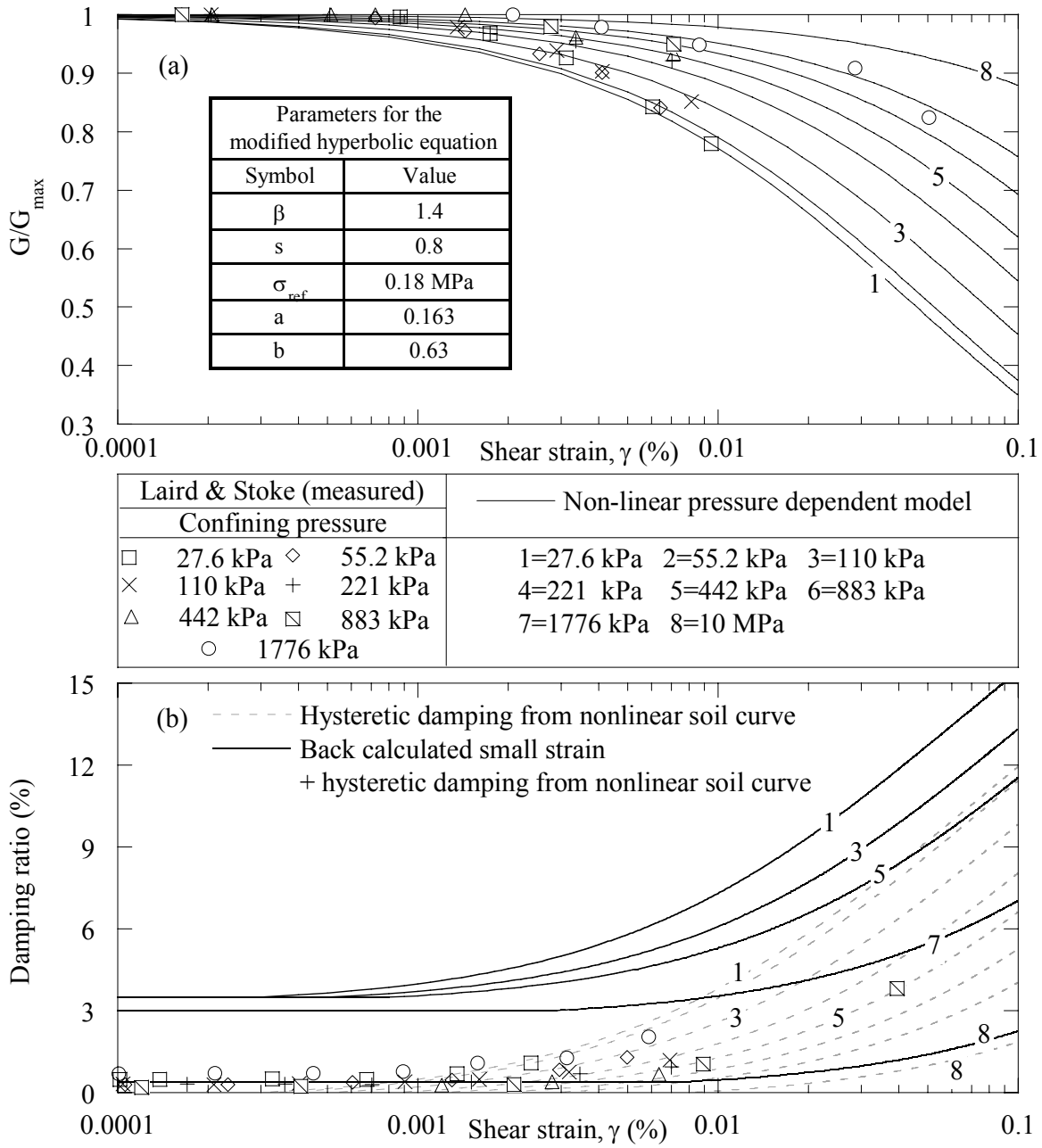

Figure 4-9 Influence of confining pressure on a) shear modulus degradation and b) damping ratio curves in DEEPSOIL nonlinear model used for site response analyses in the Mississippi Embayment. Data from Laird and Stokoe (1993) shown for comparison.

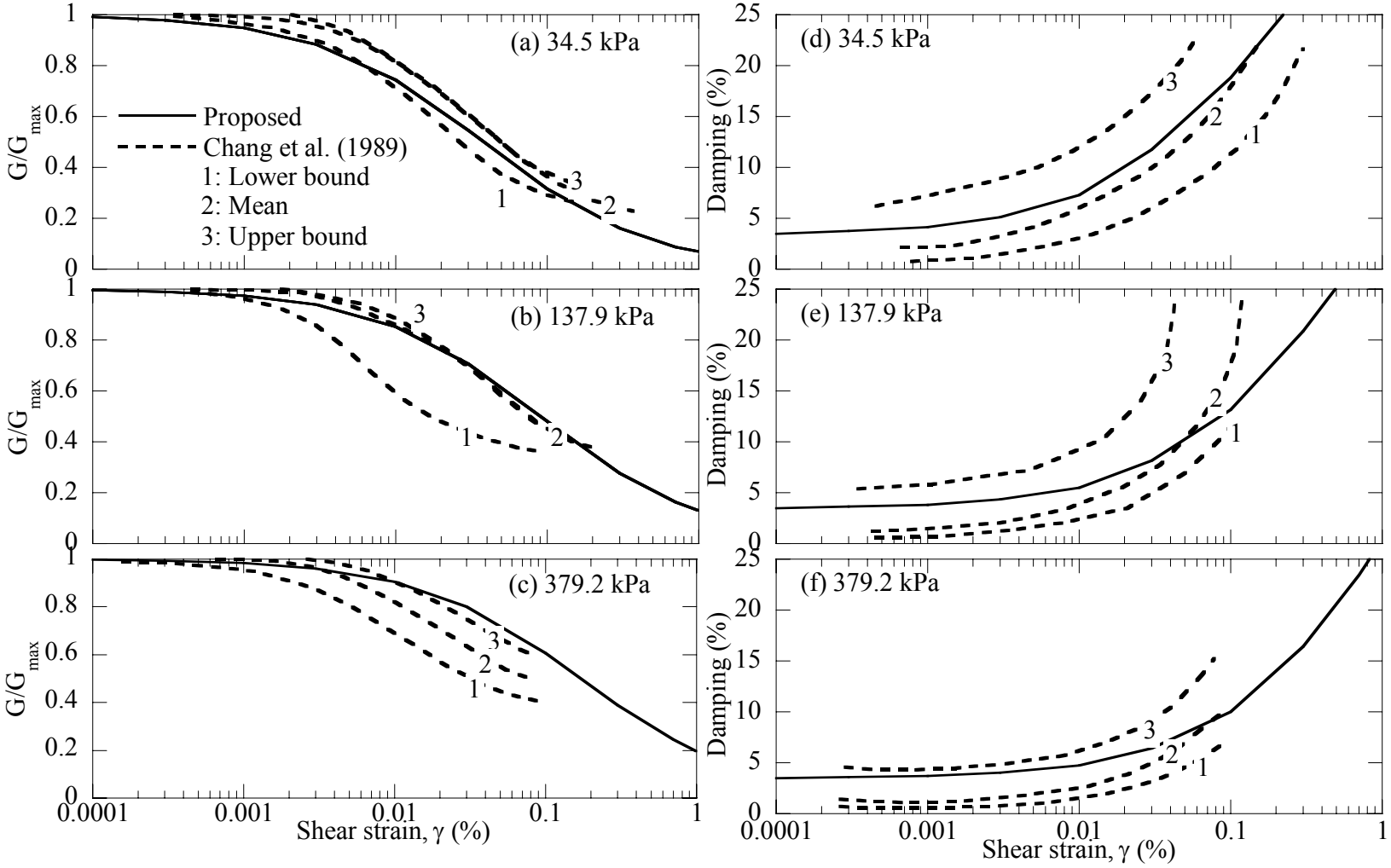

Figure 4-10 Comparison of the proposed dynamic material properties with the laboratory test data of soil group A2 by Chang et al. (1989).

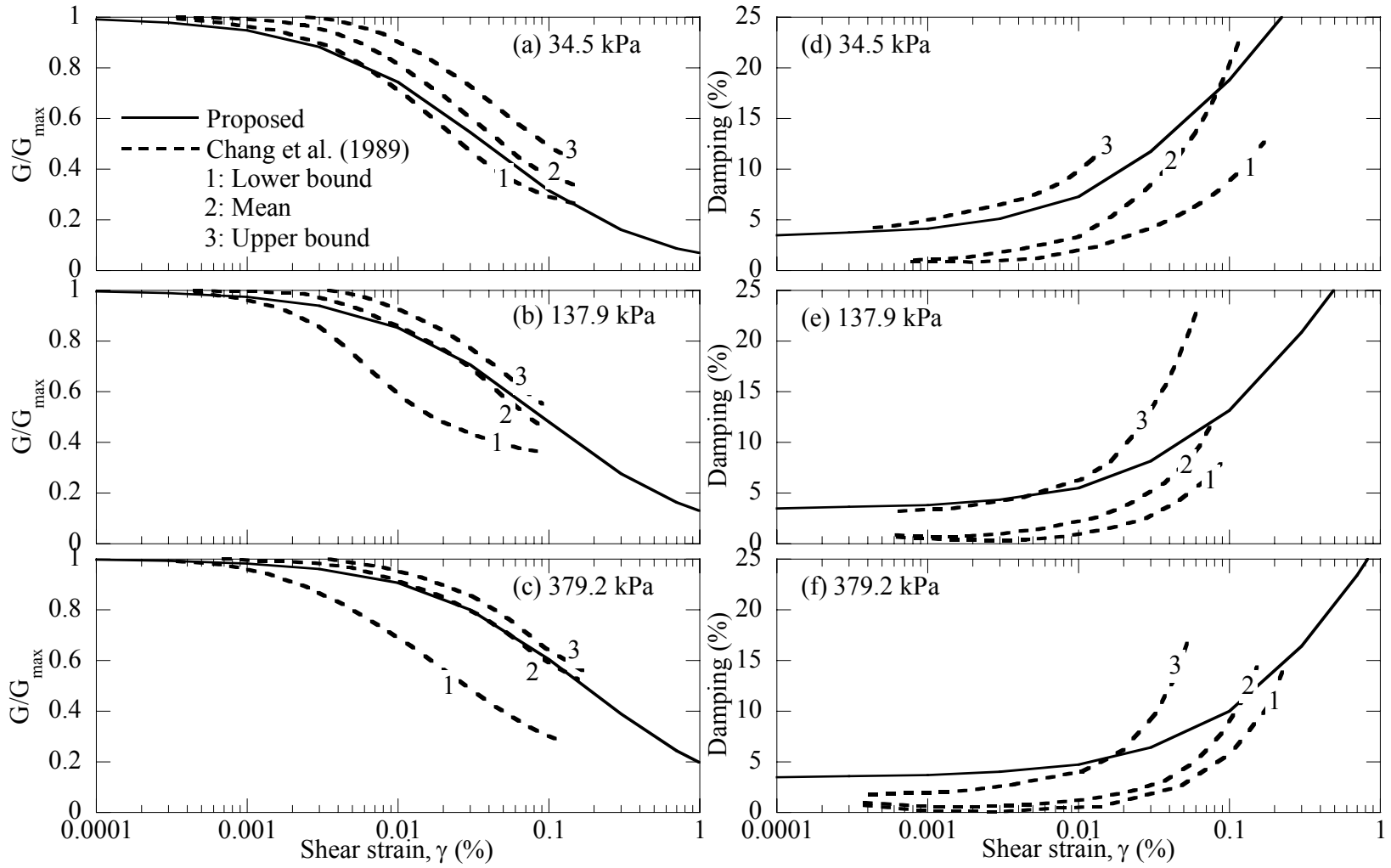

Figure 4-11 Comparison of the proposed dynamic material properties with the laboratory test data of soil group A3 by Chang et al. (1989).

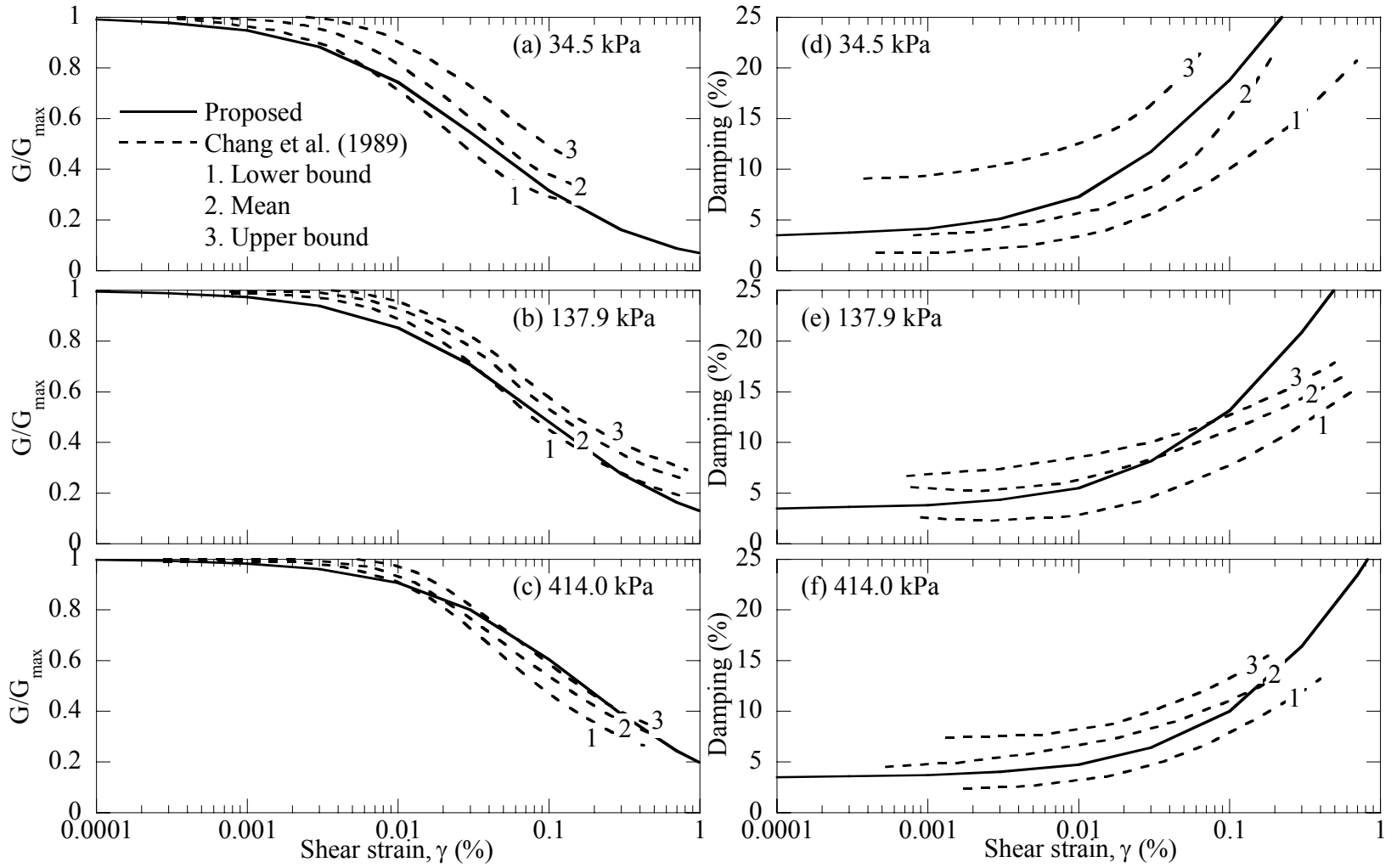

Figure 4-12 Comparison of the proposed dynamic material properties with the laboratory test data of soil group B2 by Chang et al. (1989).

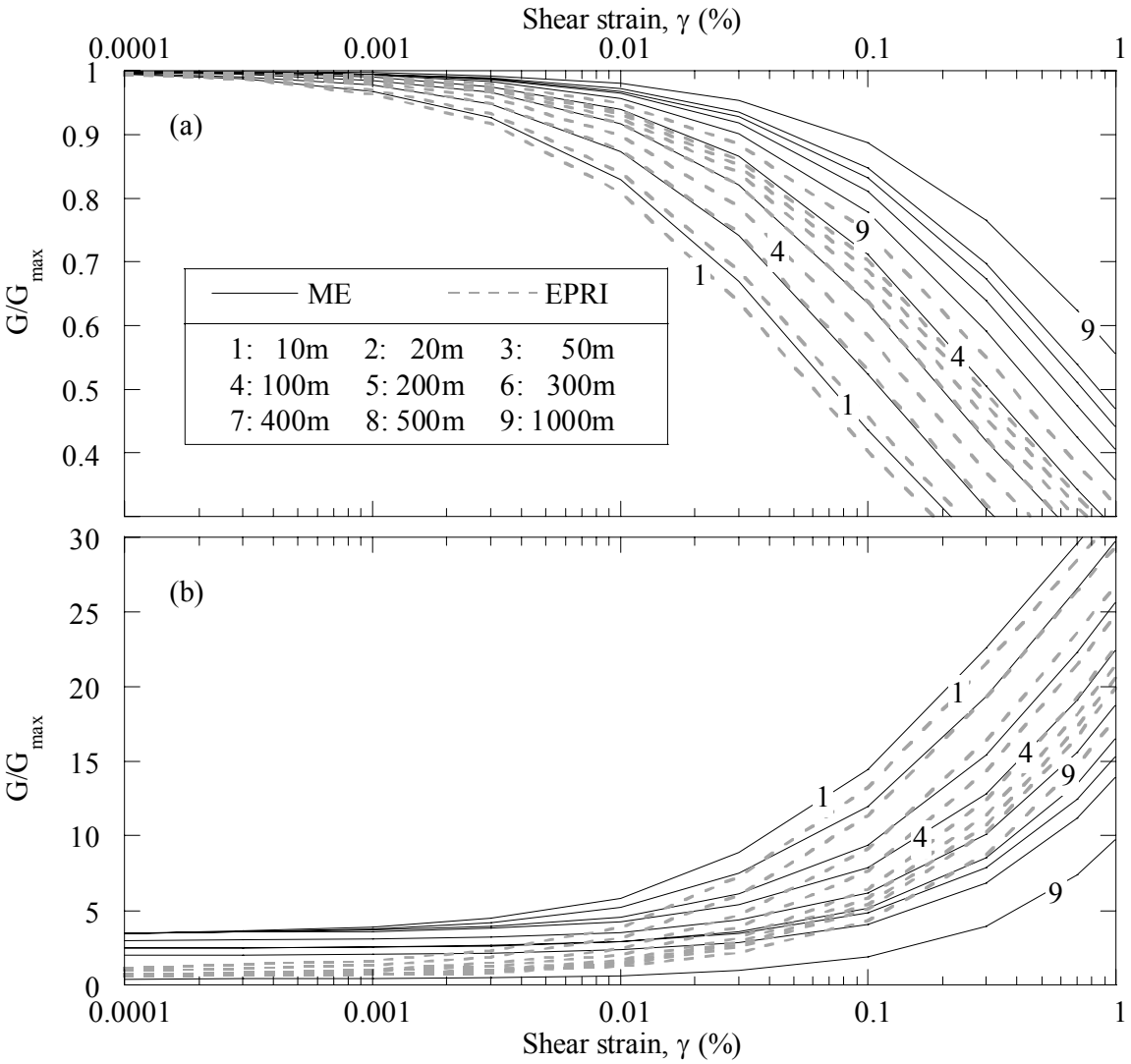

Figure 4-13 Comparison of the proposed dynamic material properties (solid lines) with the modified hyperbolic curves to fit EPRI (1993) curves (dashed lines).

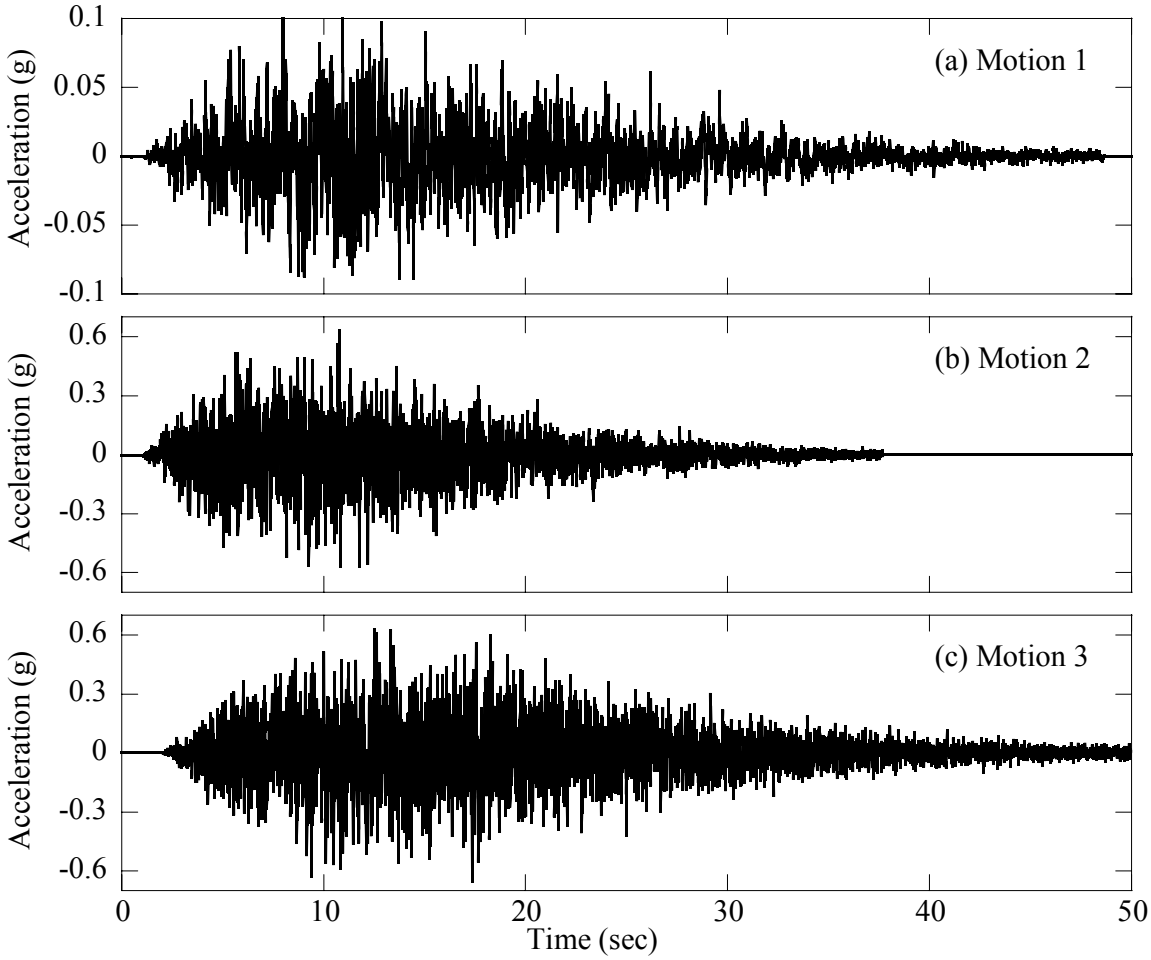

Figure 4-14 Synthetic motions time histories generated using SMSIM version 2.2 (Boore, 2002): a) M = 7.7, R = 168 km, b) M = 7.7, R = 29 km, and c) M =8.0 R = 32 km.

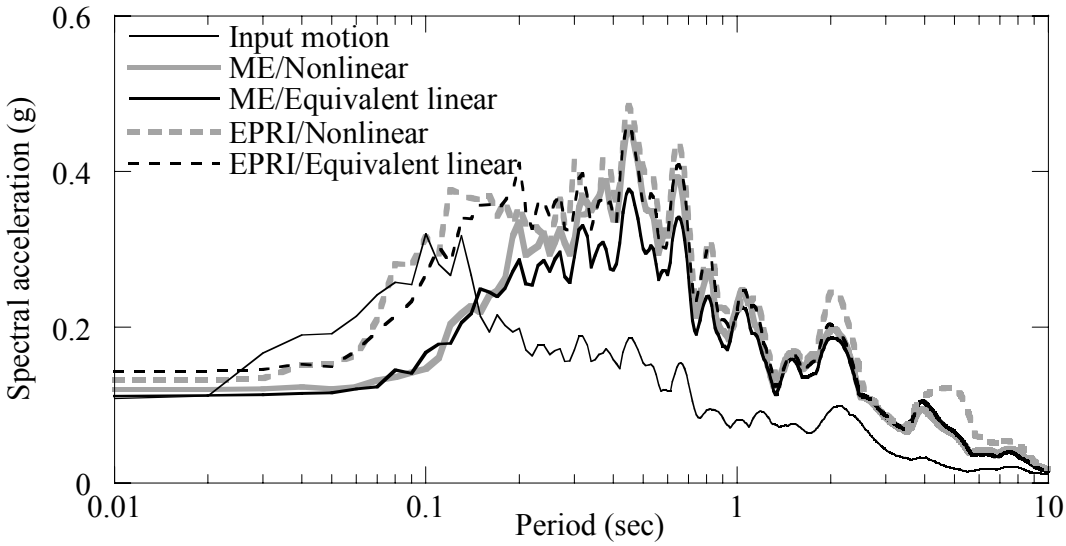

Figure 4-15 Comparison of surface response spectra using proposed ME curves and EPRI curves (EPRI, 1993), 1000 m profile with Uplands shear velocity profile (Romero and Rix, 2001). Input motion: Motion 1 (M= 7.7, R= 168 km, PGA = 0.1g) from SMSIM (Boore, 2002).

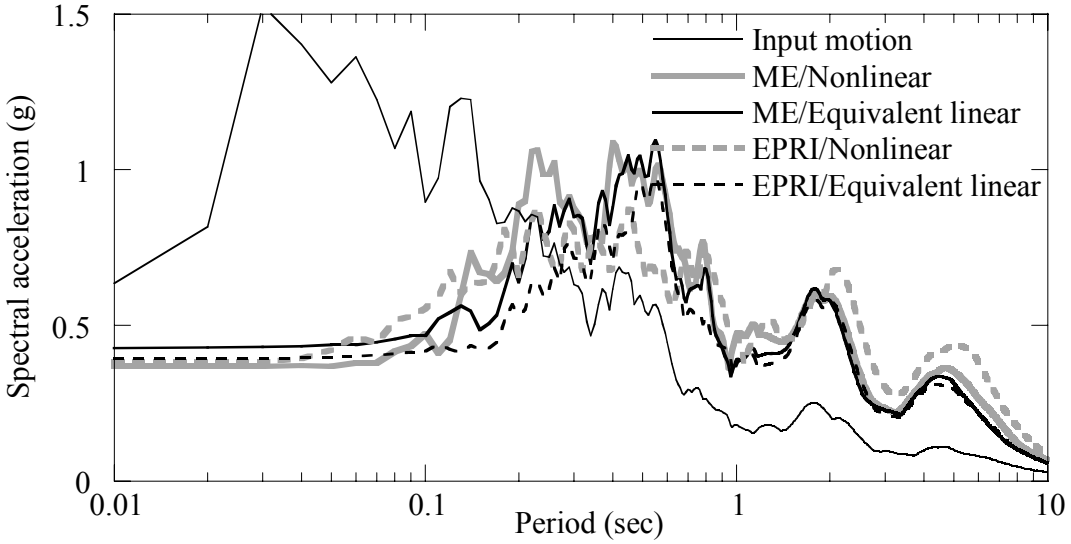

Figure 4-16 Comparison of surface response spectra using proposed ME curves and EPRI curves (EPRI, 1993), 1000 m profile with Uplands shear velocity profile (Romero and Rix, 2001). Input motion: Motion 2 (M= 7.7, R= 29 km, PGA = 0.62g) from SMSIM (Boore, 2002).

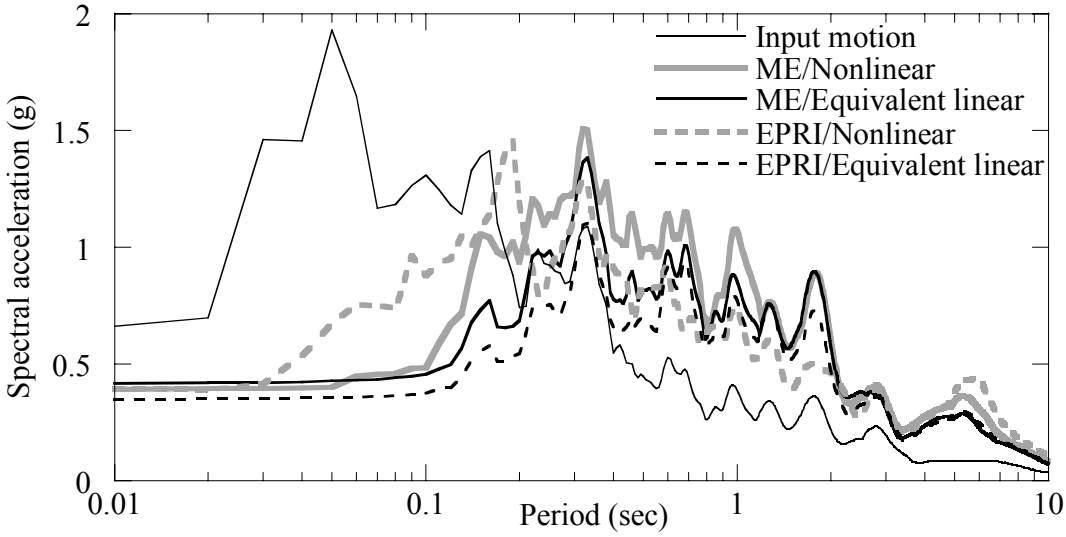

Figure 4-17 Comparison of surface response spectra using proposed ME curves and EPRI curves (EPRI, 1993), 1000 m profile with Uplands shear velocity profile (Romero and Rix, 2001). Input motion: Motion 3 (M= 8.0, R= 32 km, PGA = 0.65g) from SMSIM (Boore, 2002).

CHAPTER 5 SEISMIC HAZARD ANALYSIS AND SITE COEFFICIENTS IN THE MISSISSIPPI EMBAYMENT

5.1 Introduction

Seismic hazard analysis is commonly performed to provide a quantitative estimation of earthquake hazard at a specific site (Kramer, 1996), thus providing the necessary design ground motion parameters. Depending on the methodology of characterizing the hazard, seismic hazard analysis is referred to as a) deterministic (DSHA) or b) probabilistic seismic hazard analysis (PSHA). The different procedures implemented in each of the analyses in characterizing the highly uncertain seismic events have resulted in "political debate" on which methodology should be used (Bommer, 2002; Krinitzsky, 1993). In this chapter, the basic methodology and underlying assumptions of both deterministic and probabilistic seismic hazard analysis are presented. The similarities and differences, advantages and disadvantages of each methodology are discussed.

In the United States, U.S. Geological Survey (USGS) hazard maps are widely used to determine the seismic hazard. The maps are developed using PSHA, with some deterministic assumptions. USGS maps show four ground parameters (peak ground acceleration, 0.2, 0.3, and 1.0 sec spectral acceleration) at three levels of probability of exceedance earthquake scenarios (2%, 5%, and 10 % probability of exceedance in 50 years) and are developed for a reference site condition of "firm-rock" (average shear velocity of 760 m/sec in the top 30 m and identified as Site B (B/C boundary) according to National Earthquake Hazard Reduction Program (NERHP) site classification). This reference site condition used to produce the USGS hazard maps indicates that the computed hazard does not represent the actual site condition. USGS hazard maps are used with the NEHRP site coefficients (FEMA, 1997) to account for the local site effects. Detailed summary and underlying assumptions incorporated in the development of the USGS hazard maps and NEHRP site coefficients are presented.

In design of structures, especially in performance based design, not only the ground motion parameters but actual design ground motion time histories are often needed. An alternative probabilistic seismic hazard analysis procedure was developed by Wen and Wu

(2001). The procedure generates seismic motion time histories that as a sum result in the hazard level estimated through USGS PSHA.

5.2 Deterministic seismic hazard analysis

In deterministic seismic hazard analysis (DSHA), the ground motion characteristics are determined by choosing a controlling earthquake scenario and estimating the corresponding ground motion parameters.

DSHA consists of the following four steps (Reiter, 1990):

1. Identification and characterization of all earthquake sources.
2. Selection of source-to-site distance for each source zone.
3. Selection of the controlling earthquake, in terms of the ground motion parameter.
4. Definition of hazard at the site, usually in terms of ground motion parameters.

First step of DSHA is the identification of all earthquake sources. After the sources are identified, the earthquake potential (the maximum magnitude possible) of the site is characterized. Next, the closest distance to the site is calculated to select the controlling earthquake scenario for each source. The magnitude and distance selected in steps1 and 2 are used with the attenuation relationships to obtain ground motion parameters for each source. Attenuation relationships, also referred to as predictive relationships, are widely used to estimate ground motion parameters at a given magnitude and distance (from the source to the site) (e.g. Campbell, 2002; Toro et al., 1997). They are often developed empirically through available recordings or through numerical simulations when the earthquake data are insufficient. The relationships provide estimates of peak ground motion parameters as functions of magnitude, distance, and in some cases other parameters (such as earthquake source, wave propagation, and/or local site conditions). Since attenuation relationships always contain some amount of scatter in the data, the uncertainty in estimation of the ground motion parameter is accounted for by introducing a standard deviation to the attenuation relationship. The scenario with highest ground motion parameter is selected as the controlling earthquake. While the procedures described in Kramer (1996) and Reiter (1990) state that the mean values from the attenuation relationships are used, Krinitzsky (2002) suggests use of plus one standard deviation when estimating the ground motion parameter.

5.3 Probabilistic seismic hazard analysis

PSHA, first developed by Cornell (1968), provides a framework in which the uncertainties in the size, location, and rate of recurrence of earthquakes and the variation of ground motion characteristics with earthquake size and location can be considered in the evaluation of seismic hazard by relating the ground motion parameter with average return period (Kramer, 1996). The main benefit of the probabilistic seismic hazard analysis is that it allows computation of the mean annual rate of exceedance of a ground motion parameter at a particular site based on the aggregate risk from potential earthquakes of many different magnitudes occurring at many different source-site distances. The main difference between DSHA and PSHA is that PSHA adds another dimension of time.

The procedure of PSHA can be described in four main steps:

1. Source characterization (spatial characterization).
2. Characterization of seismicity of sources through recurrence relationships.
3. Estimation of ground motion parameters through use of predictive relationships.
4. Combination of the uncertainties in earthquake location, earthquake size, and ground motion parameter estimation in the form of seismic hazard curves.

Probabilities calculated in steps 1 through 3 are combined in step 4. Each of the steps is discussed in more detail in the following section.

5.3.1 Source characterization

5.3.1.1 Spatial characterization

The procedure for identification of the source is identical to DSHA. However, instead of choosing the closest distance from the source to the site, the distance probability density function (PDF) is calculated to account for the uncertainty in the location of future seismic events. The geometry of the earthquake source is idealized as a) 1D point source (e.g. very short fault plane), b) 2D area source (e.g. fault planes) or c) 3D volumetric source, as shown in Figure 5-1 (Kramer, 1996). In calculating the distance PDF, earthquakes are usually assumed to have equal probability of occurrence within the source zone (uniform distribution). However, non-uniform distribution may be used if sufficient information is available to justify its use.

For 1D source that lies at a distance of r from the site, the PDF is 1 if the distance to the site is r and 0 otherwise. For 2D and 3D sources, distance PDF varies with distance. PDF for a

3D source is calculated in the same manner. Schematic drawings of the PDF of the three idealized sources are shown in Figure 5-2.

5.3.1.2 Magnitude characterization

Next step in characterization of the source is determination of the magnitude of the source. The probability of a certain magnitude occurring within a given period of time is described by a recurrence law, which forms the backbone of the PSHA methodology. A major assumption in PSHA is that the recurrence law obtained from historic seismicity is applicable for prediction of future seismic events. There are three main recurrence relationships commonly in use.

One is the standard Gutenberg-Richter recurrence relationship (Guttenberg and Richter, 1944). Based on the gathered data for southern Californian earthquakes, a relationship was developed between the recurrence rate and magnitude and expressed as:

$$\log \lambda_m = a' - b'm = \exp\left(\alpha' - \beta' m\right) \tag{5-1}$$

where λ_m = mean annual rate of exceedance of magnitude m, $10^{a'}$ is the mean yearly number of earthquakes of magnitude greater than or equal to zero, and b' is a parameter to control the relative likelihood of large and small earthquakes. The equation is often expressed in exponential term, where $\alpha' = 2.303a'$ and $\beta' = 2.303b'$. The Gutenberg-Richter law is schematically shown in Figure 5-3a.

The standard Gutenberg-Richter relationship covers an infinite range of earthquakes. It will produce earthquake magnitudes that are physically not possible. Bounded Gutenberg-Richter recurrence law has been proposed to confine the range of the magnitudes to eliminate the contribution of very small earthquakes at the lower end and unrealistic high magnitude earthquakes at the high end (McGuire and Arabasz, 1990). The lower limit has been limited to a lower threshold magnitude, m_0, under which has negligible influence on the structures. Then the recurrence relationship, for the condition of $m > m_0$ (only limiting the lower end), can be written as:

$$\lambda_m = \nu \exp\left[-\beta'\left(m - m_0\right)\right] \tag{5-2}$$

where $\nu = exp(\alpha' - \beta' m_0)$. This equation is equivalent to (5-1) except that $exp(\alpha')$ represents mean yearly number of earthquakes of magnitude greater than or equal to m_0.

The high end of the recurrence law is also bounded with m_{max}, representing the maximum magnitude that can occur at the source. The mean annual rate of exceedance incorporating both low and high end $\left(m_0 \le m \le m_{\max}\right)$ can be expressed as:

$$\lambda_m = \nu \frac{\exp\left[-\alpha'\left(m - m_0\right)\right] - \exp\left[-\beta'\left(m_{\max} - m_0\right)\right]}{1 - \exp\left[-\beta'\left(m_{\max} - m_0\right)\right]} \tag{5-3}$$

Figure 5-3b shows the shape of bounded Gutenberg-Richter law in comparison to the standard Gutenberg-Richter law.

Standard and bounded Gutenberg-Richter laws are based on historical data. They do not represent the behavior of a single source or fault. Paleoseismic and geologic data show that individual faults repeatedly generate earthquakes near their maximum magnitude. These are known as characteristic faults. In cases where the rates of such characteristic earthquakes do not agree with the Gutenberg-Richter laws, it can be combined with the Gutenberg-Richter law (Schwartz and Coppersmith, 1984; Schwartz, 1988). Such recurrence law is called a characteristic recurrence law. The characteristic recurrence law is governed by historical seismicity data at low magnitude and geologic data at high magnitudes, as shown in Figure 5-4.

5.3.2 Estimation of ground motion parameter

In PSHA the probability of exceedance of a ground motion parameter for a given magnitude and distance is calculated, instead of the actual value of the ground motion parameter. The probability that ground motion parameter Y would exceed y^* can be calculated as:

$$P\left[Y > y^* \mid m, r\right] = 1 - F_Y(y^*) \tag{5-4}$$

where $F_Y(y^*)$ is the value of the cumulative distribution function (CDF) of Y at m and r. The value of $F_Y(y^*)$ depends on the standard deviation or probability distribution of the ground motion parameter. It is generally assumed that the variation of the ground motion is lognormally distributed and therefore lognormal standard deviations are developed for various attenuation relationships (Campbell, 2002; Toro et al., 1997).

An upper bound is usually imposed to eliminate the contribution of very unlikely events at high standard deviations. For example, U.S. Geological Survey uses an upper bound of plus three standard deviations (Frankel et al., 1996).

5.3.3 Combination of uncertainties and seismic hazard curves

The probabilities computed in steps 1 through 3, sections 5.3.1 to 5.3.2, are used to develop the seismic hazard curve, which relates the annual probability of exceedance for various values of the selected ground motion parameter. Sample seismic curves of peak ground acceleration for various cities in the U.S., developed by USGS (Frankel et al., 1996), are shown in Figure 5-5. The seismic hazard curve is used to determine the ground motion parameter for the selected annual probability of exceedance to be used in seismic design.

In developing the seismic hazard curve, the probabilities calculated in characterizing the sources and estimating the ground motion parameters are combined through use of the following equation:

$$\lambda_{y^*} = \sum_{i=1}^{N_S} \sum_{j=1}^{N_M} \sum_{k=1}^{N_R} \lambda_i P\left[Y > y^* \mid m_j, r_k \right] P\left[M = m_j \right] P\left[R = r_k \right] \tag{5-5}$$

where N_S = number of sources, N_M = magnitude distribution, N_R = number of segments of the distance probability function, λ_i is the annual recurrence rate of the source exceeding the minimum magnitude considered in PSHA. The equation is developed to account for various sources contributing to the hazard at the site.

A range of y^* is selected to develop a smooth seismic hazard curve, as shown in Figure 5-5. Then, the design rate of exceedance is chosen, which is represented as the horizontal line. In design codes, 50 year probability of exceedance is commonly used. In 1997 NEHRP Provisions, two hazard levels, which are 10% and 2% probability of exceedance in 50 years, are considered. Since it is assumed that the earthquakes follow a Poissonian process in PSHA, the annual rate of exceedance of the two hazard levels can be calculated using the following equation:

$$PE_{annual} = 1 - (1 - PE_t)^{1/t} \tag{5-6}$$

where PE_{annual} is the annual probability of exceedance and PE_t is the probability of exceedance in t years. The ground motion parameter that intersects with the design rate of exceedance (horizontal line) is the design ground motion parameter.

Iterating the above procedure for various ground motion parameters enables development of the uniform hazard response spectrum (UHRS).

5.3.4 Logic tree

In case where more than a single model (or assumption) is incorporated, a logic tree is used. The logic tree enables use of alternative models by assigning a weighting factor for each

model. The sum of the weights of various models should be one. A typical logic tree is shown in Figure 5-6, which shows how uncertainties in attenuation relationship, magnitude distribution, and maximum magnitude may be incorporated by applying weights for each assumption.

5.3.5 Deaggregation

PSHA uses aggregate contribution of various potential earthquake sources to calculate the annual rate of exceedance of a given site. The resulting hazard does not represent a single earthquake scenario associated with a specific magnitude and distance. It is, however, possible to calculate the relative contributions of the individual seismic sources to the hazard. The results are commonly displayed in terms of relative contributions for a range of magnitude, distance, and epsilon, ε, which represents the number of standard deviation from the median ground motions estimated from attenuation relationships. It allows estimation of earthquake scenarios that have high likelihood of occurrence. This process is referred to as deaggregation or disaggregation.

The annual rate of exceedance as a function of magnitude and distance can be written as:

$$\lambda_{y^*}(m_j, r_k) \approx P\left[M = m_j\right] P\left[R = r_k\right] \sum_{i=1}^{N_S} \lambda_i P\left[Y > y^* \mid m_j, r_k\right] \tag{5-7}$$

It is equivalent to removing the terms of summation from Equation (5-5) and allows determining the annual exceedance probability of a given magnitude and distance. The relative contribution of the given magnitude and distance can be calculated by comparing it to the aggregate annual rate of exceedance of the site.

5.4 USGS seismic hazard mapping in the central and eastern United States

USGS probabilistic seismic hazard maps for the United States (Frankel et al., 1996; Frankel et al., 2002) are developed to be used as the design maps in the 1997 edition of the NEHRP Recommended Provisions for Seismic Regulations for New Buildings and Other Structures (FEMA, 1997). The hazard maps show four ground motion parameters, which are PGA and spectral acceleration at 0.2, 0.3 and 1.0 sec periods, with 10%, 5%, and 2% probabilities of exceedance in 50 years. The ground motion is that which would be expected at a firm-rock site, with near surface shear velocity of 760 m/sec (B/C boundary according to NEHRP).

USGS hazard maps are developed following the basic procedures of PSHA. Since the basic steps and methodology of PSHA have already been discussed in the previous section, the focus of this section is on details of how the sources and ground motion relations are defined.

5.4.1 Source Characterization

USGS hazard maps use two different models for characterizing the sources: the gridded seismic sources and characteristic earthquakes. The gridded seismicity sources are intended to cover the recorded historical seismicity. These sources represent seismicity from unknown faults to which a specific value of recurrence interval and magnitude size cannot be assigned. The characteristic sources represent sources at which the recurrence interval, magnitude, and geologic shape can be approximately estimated based on the geologic evidence. USGS hazard maps use four alternative models for the gridded seismicity hazard calculation, as shown in Figure 5-7. Models 1 to 3 are based on spatially smoothed historical seismicity and Model 4 is "background zones" to quantify hazard in areas with little or no historic seismicity. The models are combined in a logic tree to quantify a', b' (to define the recurrence rate) for every 0.1° x 0.1° grids in the U.S. (Frankel et al., 1996; Frankel et al., 2002). m_{max} is used to constrain the earthquake potential of the gridded sources and is assigned to each of the grids. The map of the m_{max} (moment magnitude) values for the gridded seismicity models is shown in Figure 5-8. The minimum magnitude used in calculation is body wave magnitude of 5. The formulae by Johnston (1996b) and Boore and Atkinson (1987) are used to convert the body wave magnitude to moment magnitude in both 1996 and 2002 maps.

Characteristic earthquakes are generated separately from the gridded seismicity and given a full weight (Frankel et al., 2002). Among the various seismic source zones treated as characteristic zones, (NMSZ, Charleston, Wabash Valley, Eastern Tennessee Seismic Zone, Meers Fault, Charlevoix, Cheraw Fault), only NMSZ will be discussed in this study since it contributes to most of the seismic hazard in the ME. USGS uses three fictitious NMSZ faults to determine the location of the characteristic earthquakes, as shown in Figure 5-9. The S-shaped faults do not represent the actual faults, but rather intended to encompass the area of highest historic seismicity. The upper and lower faults are close to the borders of the Reelfoot Rift.

M = 8.0 is selected for the characteristic earthquakes in 1996 maps, based on Johnston (1996a). Instead of using a single estimate of the characteristic event, a logic tree for moment

magnitude is used in 2002 maps, whereby 4 estimates of maximum magnitude: M = 7.4 (0.15 wt); M = 7.5 (0.2 wt); M = 7.7 (0.5 wt); and M = 8.0 (0.15 wt). The new lowered estimates are based on recent studies by Bakun and Hopper (2002) and Hough et al. (2000). Incorporating this logic tree results in identical hazard as when using a M = 7.7 scenario.

In 1996 maps, three faults have the same weights. For 2002 maps, different weights are used for the three faults, in which the center fault gets twice the weight (0.5 wt) of the two adjacent faults (0.25 each).

The return period of the characteristic earthquake is based on paleoliquefaction evidence. A return period of 1000 years has been used for 1996 maps. Based on the paleoliquefaction evidence of two to three previous earthquakes prior to 1811-1812 events (Tuttle and Schweig, 2000), the return period is reduced to 500 years in 2002 maps.

In development of the USGS hazard maps, three closest distances from the site to each of the three faults are calculated. The main reason why the distance probability density function is not used, which results in equal probability of occurrence of epicenters, is because for every 500 years on average, the earthquake that occurs in NMSZ faults is not a single event but a sequence of events along the entire length of the fault (Frankel, 2003). For example, in the 1811-12 sequence, the largest earthquakes were on Dec. 16, 1811, Jan. 23, 1812, and Feb. 7, 1812. Based on intensity patterns, it is thought that these events occurred on the southern, northern, and central segments, respectively, of the New Madrid zone. Paleoliquefaction evidence (Tuttle and Schweig, 2000) indicates that such multiple earthquakes also have occurred in the previous sequences.

Thus, each segment along one of the three fictitious faults ruptures every 500 years and the segments do not rupture independently. Since it is assumed that each segment ruptures during a sequence, the nearest distance to the entire fictitious fault is used in the hazard calculation (Frankel, 2003).

5.4.2 Attenuation relationships

USGS maps use attenuation relationships at B/C boundary to estimate ground motion parameters. Two attenuation relations are used for the central and eastern U.S. (CEUS) in a logic tree form in 1996 maps whereas five attenuation relations are used in 2002 maps (Frankel et al., 2002). The relations incorporated are Toro et al. (1997) and Frankel et al. (1996) for 1996 maps

and , a) Toro et al., (1997), b) Frankel et al. (1996), c) Atkinson and Boore (1995), d) Campbell (2002), and e) Somerville et al. (2001) for 2002 maps. Toro et al. and Frankel et al. models use single-corner frequency point source model in the stochastic ground motion simulation, whereas Atkinson and Boore use double-corner frequency model. Campbell uses a hybrid model, which uses both stochastic simulation and empirical data. Finally, the model by Somerville is a broadband model. The 1996 maps use same weight for the two attenuation relationships incorporated. In 2002 maps, different weights are assigned for gridded seismicity hazard calculations (Toro et al.: 0.286 wt, Frankel et al.: 0.286 wt, Atkinson and Boore: 0.286 wt, and Campbell: 0.143 wt) and characteristic earthquakes (Toro et al.: 0.25 wt, Frankel et al.: 0.25 wt, Atkinson and Boore: 0.25 wt, Campbell: 0.125 wt, and Somerville: 0.125 wt).

Uncertainty in the ground motion is accounted for in the attenuation relationship through use of standard deviations. The attenuation relationship has lognormal standard deviations of 0.75 for PGA, 0.2 and 0.3 sec spectral acceleration whereas 1.0 sec spectral acceleration has a standard deviation of 0.8.

An important constraint of the attenuation relationships is that caps are imposed on the maximum PGA, 0.2 sec, and 0.3 sec spectral accelerations. This is necessary due to overestimation of ground motion parameter using attenuation relationships obtained through single-corner stochastic simulation method for characteristic events occurring at very close distance to the site (less than 20 km). Maximum median PGA is 1.5 g for both 1996 and 2002 maps. Different caps are used for 0.2 and 0.3 sec spectral accelerations, whereby 3.75 g and 3.0 g are used for 1996 and 2002 maps respectively. In addition, the distribution of ground motions is truncated at 3 standard deviations for all periods. The capping only influences 2% in 50 year values for the area directly above the three NMSZ faults.

5.5 PSHA and development of ground motion time history

Performance based design of structures requires not only the ground motion parameters, but actual design ground motion time histories. Wen and Wu (2001) propose a procedure similar to the conventional PSHA but that allows generation of seismic motions. PSHA is performed for three cities in the CEUS, which are Memphis (Tennessee), St. Louis (Missouri), and Carbondale (Illinois).

Future seismic events and ground motions were simulated within a reference area (within 500 km from the site, except for characteristic earthquakes) over a 10 year period using the tectonic and seismological data from USGS Open-File Report 96-0532 (Frankel et al., 1996). 9000 simulations of 10 year period are carried out to provide sufficient number of ground motions for statistical analysis with satisfactory accuracy. The ground motions generated are used to develop the uniform hazard response spectra. More details are given in the following sections.

5.5.1 Source characterization

5.5.1.1 Gridded seismic sources

The annual occurrence rate of earthquakes are based on seismicity database from USGS Open-File-Report 96-532 (Frankel et al., 1996). The seismicity data of USGS, defined for every 0.1° × 0.1° grid within CEUS, are used. Within each grid, the number of earthquakes within 10-year period, corresponding magnitudes and hypocenters are assigned using the following process.

a. Number of earthquakes within each grid

The number of earthquakes within each grid is determined by generating a random variable u_k, with a uniform distribution between 0 and 1 as follows:

$$\sum_{X=0}^{n_k-1}\frac{(t\lambda_k)^X}{X!}e^{-t\lambda_k} < u_k \le \sum_{X=0}^{n_k}\frac{(t\lambda_k)^X}{X!}e^{-t\lambda_k} \tag{5-8}$$

where n_k is the number of simulated earthquakes within the selected grid, t = 10-year period.

b. Magnitude characterization

The random variable u_k can be related to the magnitude through the following equation:

$$m_b = m_o - \log_{10}\left(1-u_k\left(1-10^{m_o-m_{\max}}\right)\right) \tag{5-9}$$

where m_o and m_{max} are minimum and maximum magnitudes of the grid, and m_b is the assigned magnitude.

c. Location selection

Within each grid, two random numbers of uniform distribution are chosen along latitude and longitude directions within each cell to randomize the location of the source.

5.5.1.2 Characteristic earthquakes

A rectangular shaped zone is used to confine the locations of epicenters of future characteristic earthquakes. A comparison with the fictitious NMSZ faults used by USGS is

shown in Figure 5-10. The characteristic earthquakes are also assumed to follow a Poisson process, with a mean return period of 1000 years. The epicenters are randomly generated within the rectangular zone.

The main difference with the procedure of USGS is that the epicenters are randomly generated within the NMSZ zone, whereas USGS picks the closet distance to each of the 3 fictitious faults, due to reasons discussed in section 5.4.1. Therefore, the hazard level is much higher when using the USGS procedure. The discrepancy between the two methods increases with increase in contribution of the characteristic events.

5.5.2 Estimation of ground motion parameters

An attenuation relationship is not needed in the procedure by Wen and Wu (2001) since actual ground motion time histories are generated. The magnitude and location information from the source characterization process is used to generate synthetic ground motions using stochastic models SMSIM (Boore, 2002) and FINMSIM (Beresnev and Atkinson, 1998). SMSIM, a point-source stochastic model, is used to simulate earthquakes at gridded seismic sources. In the simulation, only the double-corner frequency source model is used. FINSIM, a finite fault model developed to better simulate near-source effects, is used to simulate characteristic events. FINSIM has been shown to give similar results to broadband model (Somerville et al., 2001) incorporated in 2002 USGS hazard maps, but is computationally less expensive. More details of the stochastic models are described in Appendix C.

5.5.3 Comparison with USGS hazard maps

The UHRS developed for three cities are compared to the 1996 USGS mapped hazards (Wen and Wu, 2001). Among the three cities simulated, only Memphis is located within the ME and thus only UHRS of Memphis are shown. When comparing the 2% in 50 years UHRS, the UHRS developed by Wen and Wu (2001) falls below 1996 USGS hazard spectrum, as shown in Figure 5-11. This is because of the lower hazard estimated for characteristic events. 10% in 50 years UHRS agrees well with the USGS. The main contribution of 10% in 50 years hazard is from gridded seismic sources, and this illustrates that the hazard defined from the simulation is close to USGS hazard maps.

Even though the results are compared to 1996 USGS hazard maps, the simulation procedure is not intended to match the USGS hazard maps. The purpose of the study is to generate uniform hazard ground motion spectra that best represent the seismic hazard in CEUS.

5.6 Estimate of site coefficients/surface ground motions in Mississippi embayment

USGS hazard maps represent hazard at a reference rock site (average shear wave velocity of 760 m/sec at top 30 m also defined as B/C boundary). The site coefficients defined in 1997 NEHRP Provisions (FEMA, 1997) are developed to be used with the mapped ground motion parameters (S_s and S_1) from USGS hazard maps to account for site effects. The basis for development of the site coefficients, how the coefficients are used to construct the design response spectrum, and recent studies to revise the coefficient for the Mississippi embayment are discussed in the following sections.

5.6.1 Site coefficients in NEHRP Provisions

5.6.1.1 Basis for development of site coefficients

The Applied Technological Council (ATC) 3 project was the first effort to include the site effects in the U.S. seismic code (ATC, 1978). Based on the average spectral shapes for various soil conditions developed by Seed et al. (1976), and shown in Figure 5-12a, ATC developed simplified design response spectra for three soil profile types (S1 to S3), as shown in Figure 5-12b. The soil profile types are listed in Table 5-1. Soil type 4 (S4), which represents deep clay deposits, has been added based on the experience of 1985 Mexico City earthquake (Seed et al., 1988). Only the long-period sections of the spectra are amplified in the design response spectrum, through use of the site coefficient, *S*. The design spectra are later incorporated into the Uniform Building Code.

Additional earthquake case histories, including the 1985 Mexico City and 1989 Loma Prieta earthquakes, reveal that the site amplification is dependent on the level of shaking. Low levels of shaking results in significant amplification whereas the amplification is low for severe level of shaking. Another important finding is that the amplification level is different for short-period and long-period. The limitation of the site coefficients of ATC prompted development of new site coefficients.

In 1994 and 1997 NEHRP Provisions (FEMA, 1997), a different site classification scheme was incorporated. In evaluating site effects, the amplification is expressed either as the Ratio of Fourier Spectrum (RFS) or Ratio of Response Spectrum (RRS). Based on the assumption that the energy of the wave is preserved, Joyner suggested that the site amplification (in terms of RRS) at a given period is proportional to $V_s^{-0.5}$, where V_s is the shear wave velocity of the soil profile. Borcherdt (1994) used empirical data from 1989 Loma Prieta earthquake to develop a relationship between mean shear wave velocity of the soil profile and site amplification factor, as shown in Figure 5-13. The amplification factors are based on the statistical studies of RFS and RRS of the Loma Prieta earthquake for several site conditions normalized to nearby rock sites. The figure shows two site coefficients, F_a and F_v, which represent short-period (0.2 sec) and long-period amplification (1.0 sec) respectively. Two site coefficients are used to incorporate the finding that the amplification factor is different for different periods. It is concluded that the amplification factors are approximately proportional to $\bar{V}_s^{-0.4}$ for short periods and to $\bar{V}_s^{-0.6}$ for periods at 1 sec and longer, as shown in Figure 5-13 ($\bar{V}_s$ stands for average shear wave velocity at top 30 m of the soil profile). Both F_a and F_v decrease toward 1.0 as $\bar{V}_s$ approaches 1000 m/sec, which is the reference rock site.

The data from 1989 Loma Prieta earthquake gave recordings with low rock acceleration equal or less than about 0.1g. Since earthquake data at higher levels of shaking were not available, numerical simulations were performed to extrapolate the amplification factors at higher accelerations. Equivalent linear (SHAKE, Schnabel et al., 1972), as well as nonlinear analyses were performed up to rock acceleration higher than 0.4 g. The basic assumptions used are those typically used in one-dimensional site response analyses, and thus, the conclusions are restricted to sites where these conditions are fulfilled (i.e., flat sites with horizontal layering of significant extension and far from rock outcrops and with a clear soil-rock interface at a depth not exceeding several hundred feet). The parametric study used hundreds of soil profiles and soil properties and several dozen input rock motions scaled to peak ground accelerations between less than 0.1g to more than 0.4g (Dobry et al., 1994; Seed et al., 1994). Figure 5-14 shows empirical correlations between site coefficients F_a and F_v and shear wave velocity $\bar{V}_s$ of the site for various levels of rock shaking (Borcherdt, 1994). The regression curves suggest a linear relationship between logarithms of amplification and mean shear velocity.

These findings prompted the development of site coefficients in 1994 and 1997 NEHRP Provisions (FEMA, 1997), as summarized in Table 5-2, Table 5-3 and Table 5-4. Table 5-2 lists the soil classification scheme in 1997 NEHRP (FEMA, 1997). Soil class is defined by the average shear velocity of the top 30 m of the soil profile. Five classes are specified depending on the average stiffness at the upper 30 m of the profile (Site A to E) and one special class for soils requiring site-specific evaluation (Site F), which include soil vulnerable to potential failure or collapse during seismic excitation (e.g. liquefiable soils), peats and/or highly organic clays, and very high plasticity clays. Table 5-3 and Table 5-4 show short-period and long-period site coefficients as functions of site class and level of rock shaking.

5.6.1.2 1997 NEHRP design response spectrum and site coefficients

The site coefficients are used to develop the design spectrum. The design spectrum is made up of three curves, representing the short period, constant spectral response acceleration, and long period sections. The site coefficients are multiplied to the mapped spectral acceleration at 0.2 sec, *Ss*, and at 1 second, S_1, obtained from USGS Seismic Hazard Maps 1 through 24.

$$S_{MS} = F_a S_S \qquad (5\text{-}10)$$
$$S_{Ml} = F_v S_l$$

where S_{MS} = maximum considered earthquake spectral response acceleration for short period (0.2 sec), S_{Ml} = maximum considered earthquake spectral response acceleration for 1 second period, F_a = site coefficient at short period, and F_v = site coefficient at 1 second.

The maximum considered earthquake, which represents the 2% in 50 years earthquake, spectral response accelerations are used to develop the recommended spectrum. The response spectrum curve is developed as follows:

1. Define T_0 and T_s.

$$T_0 = 0.2 S_{M1}/S_{MS} \qquad (5\text{-}11)$$
$$T_S = S_{M1}/S_{MS}$$

2. For periods less than or equal to T_0, the spectral response acceleration, S_a, shall be computed as:

$$S_a = 0.6\frac{S_{MS}}{T_0}T + 0.4 S_{MS} \qquad (5\text{-}12)$$

3. For periods greater than or equal to T_S, the spectral response acceleration, S_a, shall be taken as:

$$S_a = \frac{S_{M1}}{T} \tag{5-13}$$

A schematic plot of the NEHRP response spectrum is shown in Figure 5-15.

5.6.1.3 Limitations of NEHRP site coefficients

Although the NEHRP procedure is very easy to use, it has several shortcomings. The main limitation of the current procedure is that site coefficients obtained deterministically are used with mapped spectral accelerations that are obtained from probabilistic hazard analysis. The spectral accelerations from USGS maps do not come from a single source or motion, but from multiple possible sources. In other words, the spectral accelerations are combined hazards from large and small earthquakes, for which different site coefficients should be used.

Another limitation of the current site coefficients is that they are intended to be used for a uniform 30 m thick profile. They do not represent the site effects at deeper profiles, e.g. the deep deposits of the ME.

5.6.2 Quarter-wave length approach by Wen and Wu (2001)

The need to account for the site effects in performing PSHA has been recognized by Wen and Wu (2001). The bedrock ground motions generated through PSHA (described in section 5.5) at three selected cities are propagated through site specific profiles. Quarter-wavelength-method (QWM, Joyner et al., 1981) is used to propagate the ground motions generated through PSHA at selected three cities in the central United States. The propagated ground motions are compiled and used to develop UHRS at each of the three cities. The UHRS and the corresponding 1997 NEHRP design response spectrum for Site C, both at Memphis, are shown in Figure 5-16. The simulated UHRS are consistently lower than NEHRP spectra for all three probabilities of exceedance considered. Even though the UHRS are compared to the NEHRP spectra, the assessment of appropriateness of the 1997 NEHRP site coefficients based on the comparison is not possible since the discrepancy originates from the different input ground motion characterization, as can be observed from lower hazard estimated compared to USGS hazard maps (Figure 5-11).

The research presented a new methodology in assessing the site effects probabilistically in the Mississippi embayment. In comparison, NEHRP procedure characterizes the site effects deterministically. The main limitation of this research is that QWM is used to propagate the waves. QWM is a linear solution, and will significantly overestimate response for high levels of

shaking since nonlinear site effects are not accounted for. Another downside of the research is that the research results only show results for three cities selected and have not been generalized for different site conditions encountered in the Mississippi embayment. Generalized site coefficients, as the NERHP site coefficients, are needed to provide simplified seismic guidelines for various locations in the embayment.

5.6.3 Equivalent linear approach by Romero and Rix (2001)

Romero and Rix (2001) perform site response analyses to estimate the effect of deep deposits of the embayment on ground motion propagation. A detailed parametric study is performed to assess the effects of the following geotechnical factors: a) depth of nonlinear behavior, b) effect of embayment depth, c) age of near surface deposits, and the following seismological factors: a) moment magnitude, b) stress drop, and c) epicentral distance. Eight earthquake scenarios are chosen to cover the wide range of ground motions, ranging in magnitude from 5.5 to 8 and epicentral distance from 10 to 200 km. The ground motions are synthetic motions generated using RASCALS (Schneider et al., 2001), which uses a single corner point source model. Thirty simulations are performed for each scenario.

The generic shear velocity profiles, developed in the study, as well as site specific soil profiles are used. The dynamic curves developed by EPRI (1993) are used. Both the shear velocity profiles and the dynamic curves are randomized to account for the inherent uncertainties. The ground motions are also propagated using the program RASCALS (Schneider et al., 2001). RASCALS provide Fourier and response spectra, but does not provide output ground motion time histories.

It is assumed that the nonlinear behavior is constrained to the upper 150 m. Below 150 m, the soil would behave linear elastically with only small strain damping to attenuate the waves. Several analyses, with various assumptions on the extent of nonlinear behavior, are performed to validate the assumptions. Four depths of nonlinear behavior, which are 30 m, 150 m, 300 m, and 1000 m, are evaluated.

The results of the parametric study are summarized in terms of PGA, response spectra and Fourier amplitude spectra, RRS, and RFS. The results of RRS and RFS are compared to various other parametric studies, including Dobry et al. (1994) and EPRI (1993), and amplification factors proposed by Atkinson and Boore (1997).

Dobry et al. (1994) developed RRS based on observed site effects during 1985 Michoacan and 1989 Loma Prieta earthquakes. RRS is composed of two constant regions. From period 0 – 0.5 sec at which RRS of 1.3 is determined and periods longer than 1.5 sec at which RRS of 2.3 is computed. The RRS developed by Dobry et al. (1994) is constant for all motions, whereas in reality the amplification decreases with increasing input motion level due to higher nonlinear effects. The RRS for various M = 6.5 scenarios (R ranging from 10 km to 200 km) is compared to the RRS of Dobry et al. (1994), as shown in Figure 5-17. It is concluded that the RRS of Dobry et al. (1994) are adequate at all periods at R = 10 km, except at resonant periods and underestimates response for longer distance events (weak motions).

The RRS for the hard rock site is also compared to the amplification factors recommended by EPRI (1993) and Atkinson and Boore (1997), as shown in Figure 5-18. EPRI (1993) proposed amplification factors as a function of median rock PGA, frequency, and depth of soil column for representative profiles in the eastern North America. Atkinson and Boore (1997) developed spectral amplification factors for hard rock sites in eastern North America. The RRS developed by Atkinson and Boore (1997) is higher at periods lower than 0.25 sec since QWM is used, whereas Romero uses equivalent linear analysis to propagate the seismic waves. EPRI (1993) uses a procedure similar to Romero in developing the amplification factors. The differences are attributed to differences in the shear wave velocity profiles and the variation of soil column depth.

The results of the parametric study are also compared to the 1997 NEHRP design response spectra, Figure 5-19. The surface response spectra using the input motion corresponding to M =8, R = 50 km scenario earthquake was compared with 1997 NEHRP response spectra (S_s = 0.35g and S_1 = 0.18g). The earthquake scenario is chosen since it is considered to have the highest contribution to the seismic hazard in Memphis. The results of 1000m Uplands, Lowlands and B/C boundary profiles are compared to NEHRP design spectra for Site B, D, and E. Uplands and Lowlands both fall under Site D category in NEHRP. The surface spectra are normalized to PGA, so that only the shapes of the spectra are compared. The 1000 m profile results in significant shifting to higher periods compared to B/C boundary or rock outcrop. It is concluded that the NEHRP spectra do not model the shifting of peak spectral accelerations to longer periods for softer profiles, thereby significantly underestimating the spectral shape at longer periods. However, an exact comparison is not possible since all of the

spectra are normalized. The B/C boundary uses the same shear velocity as the NEHRP Provisions (average shear velocity = 760 m/sec), but the resulting response spectrum falls below the design spectrum. This shows that even though same assumptions are used, the design spectrum cannot be reproduced by a single motion.

The main limitation of the research is that the site effects are assessed deterministically, as in NEHRP Provisions (FEMA, 1997). Another limitation is that generic dynamic properties that are used are not constrained by information about soil response in the embayment. In addition, the equivalent linear analysis is also essentially a linear solution and does not capture the true nonlinear behavior of soils for strong ground motions.

5.6.4 Toro and Silva approach (2001)

Toro and Silva (2001) perform PSHA at Memphis, Tennessee and St. Louis, Missouri. The PSHA methodology is similar to USGS procedure. The extensive geological, geophysical, and seismological works that have been conducted within the NMSZ to identify the seismogenic faults in the NMSZ have been incorporated (Johnston and Schweig, 1996, Van Arsdale and Johnston, 1999). Site response analyses are performed to characterize the effects of the embayment deposits and develop amplification factors. Identical soil profiles and properties, as well as methodology for generating input ground motions, to Romero and Rix (2001) are assumed. Amplification factors are developed for various rock motion amplitude, soil type, and depth. The amplification factors are used to develop surface seismic hazard maps in the embayment. The amplification factors are multiplied to the mapped hazard at the reference rock site to develop regional seismic hazard maps of the embayment with site effects.
The procedure is identical to Romero and Rix (2001), and therefore has the same limitations.

5.7 Summary

This chapter summarizes how the seismic hazard at a given site is characterized. Two methods of seismic hazard analysis, deterministic seismic hazard analysis (DSHA) and probabilistic seismic hazard analysis (PSHA), are described. In the U.S., USGS hazard maps, developed from PSHA, are widely used. USGS hazard maps depict four ground motion parameters at three probabilities of exceedance. A detailed description of the assumptions and methodology behind the USGS hazard maps are presented. An alternative method of seismic hazard analysis is presented which preserves all of the characteristics of a PSHA, but allows

generation of actual ground motion time histories in addition to ground motion parameters (Wen and Wu, 2001).

USGS hazard maps represent hazard at a reference rock site. The mapped ground motion parameters are combined with site coefficients of 1997 NEHRP Provisions to characterize the hazard at a soil profile. The site coefficients are developed deterministically through compiled empirical data to represent five generic soil classes categorized in NEHRP Provisions. The deep Mississippi embayment cannot be represented with generic site coefficients of NEHRP. In addition, the NEHRP site coefficients are obtained deterministically and are not necessarily compatible with probabilistically derived response spectra in USGS hazard maps.

Wen and Wu (2001) developed a novel procedure whereby the site effects can be determined probabilistically. However, the use of QWM, a linear solution, is unrealistic for propagating strong ground motions. Romero and Rix (2001) and Toro and Silva (2001), on the other hand, have used equivalent linear analysis which enables more realistic simulation of strong ground motion propagation. However, the deterministic methodology used to assess site effects is not consistent with the probabilistic USGS hazard maps. In addition, the equivalent linear analysis, even though superior to the QWM, is also essentially a linear solution and does not capture the true nonlinear behavior of soils. The generic dynamic soil properties used are not constrained using embayment specific data.

Table 5-1 Site profile types and site coefficients in seismic codes prior to 1994 NEHRP Provisions (Dobry et al., 1994).

Soil profile type	Description	Site coefficient S
S1	A soil profile with either (1) rock of any characteristic, either shale-like or crystalline in nature, that has a shear wave velocity greater than 2,500 ft/sec or (2) stiff soil conditions where the soil depth is less than 200 ft and the soil types overlying the rock are stable deposits of sands, gravels, or still clays.	1.0.
S2	A soil profile with deep cohesionless or stiff clay conditions where the soil depth exceeds 200 feet and the soil types overlying rock are stable deposits of sands, gravels, or still clays.	1.2
S3	A soil profile containing 20 to 40 ft in thickness of soft-to medium-stiff clays with or without intervening layers of cohesionless soils.	1.5
S4	A soil profile characterized by a shear wave velocity of less than 500 ft/sec containing more than 40 ft of soft clays or silts.	2.5

Table 5-2 Site classification (FEMA, 1997).

Site class	Description	$\overline{v}_s$	$\overline{N}$ or $\overline{N}_{ch}$	$\overline{s}_u$
A	Hard rock	> 1500 m/s	N.A.	N.A.
B	Rock	760 to 1500 m/s	N.A.	N.A.
C	Very dense soil and soft rock	360 to 760 m/s	> 50	> 100 kPa
D	Stiff soil	180 to 360 m/s	15 to 50	50 to 100 kPa
E	Soft soil	< 180 m/s	< 15	< 50 kPa
F	Soils requiring site-specific evaluations	Soils requiring site-specific evaluation		

Table 5-3 Values of F_a as a function of site class and mapped short-period maximum considered earthquake spectral acceleration (FEMA, 1997).

Site class	Mapped maximum considered earthquake spectral response acceleration at short periods				
	$S_s \leq 0.25$	$S_s = 0.50$	$S_s = 0.75$	$S_s = 1.0$	$S_s \geq 1.25$
A	0.8	0.8	0.8	0.8	0.8
B	1.0	1.0	1.0	1.0	1.0
C	1.2	1.2	1.1	1.0	1.0
D	1.6	1.4	1.2	1.1	1.0
E	2.5	1.7	1.2	0.9	a
F	a	a	a	A	a

Note: Use straight line interpolation for intermediate values of S_S.
[a] Site-specific geotechnical investigation and dynamic site response analyses shall be performed.

Table 5-4 Values of F_v as a function of site class and mapped 1 second period maximum considered earthquake spectral acceleration (FEMA, 1997).

Site class	Mapped maximum considered earthquake spectral response acceleration at long periods				
	$S_1 \leq 0.1$	$S_1 = 0.2$	$S_1 = 0.3$	$S_1 = 0.4$	$S_1 \geq 0.5$
A	0.8	0.8	0.8	0.8	0.8
B	1.0	1.0	1.0	1.0	1.0
C	1.7	1.6	1.5	1.4	1.3
D	2.4	2.0	1.8	1.6	1.5
E	3.5	3.2	2.8	2.4	a
F	a	a	A	a	a

Note: Use straight line interpolation for intermediate values of S_1.
[a] Site-specific geotechnical investigation and dynamic site response analyses shall be performed.

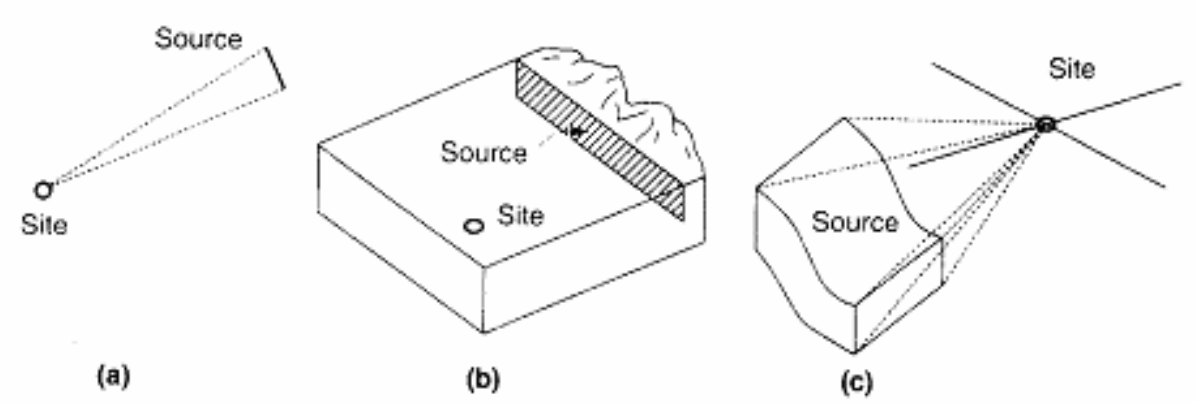

Figure 5-1 Geometrical idealization of the source: a) short fault that can be modeled as a one-dimensional point source, b) shallow fault that can be modeled as a two-dimensional linear source, c) three-dimensional source zone (Kramer, 1996).

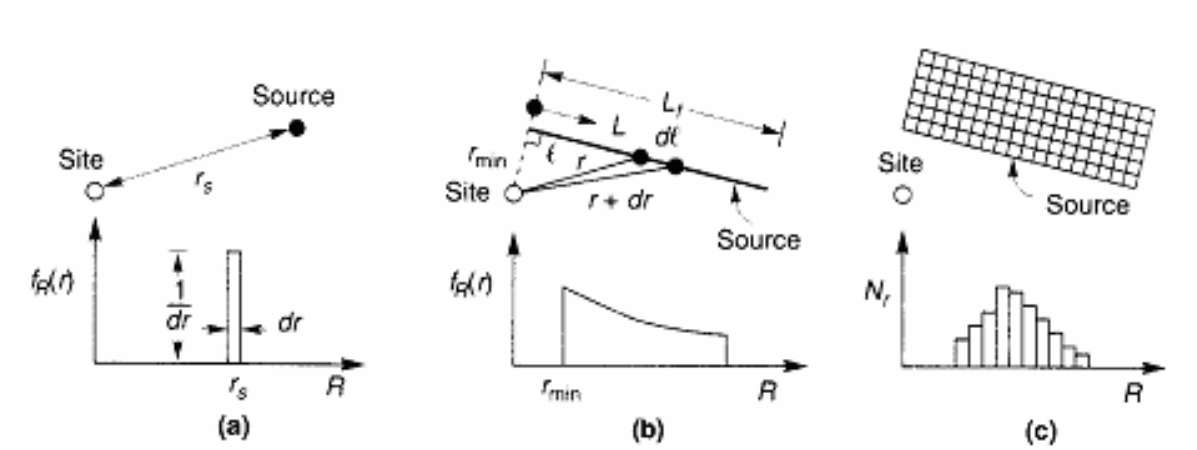

Figure 5-2 Probability density functions of various sources: a) 1-D source, b) 2-D source, c) 3-D source (Kramer, 1996).

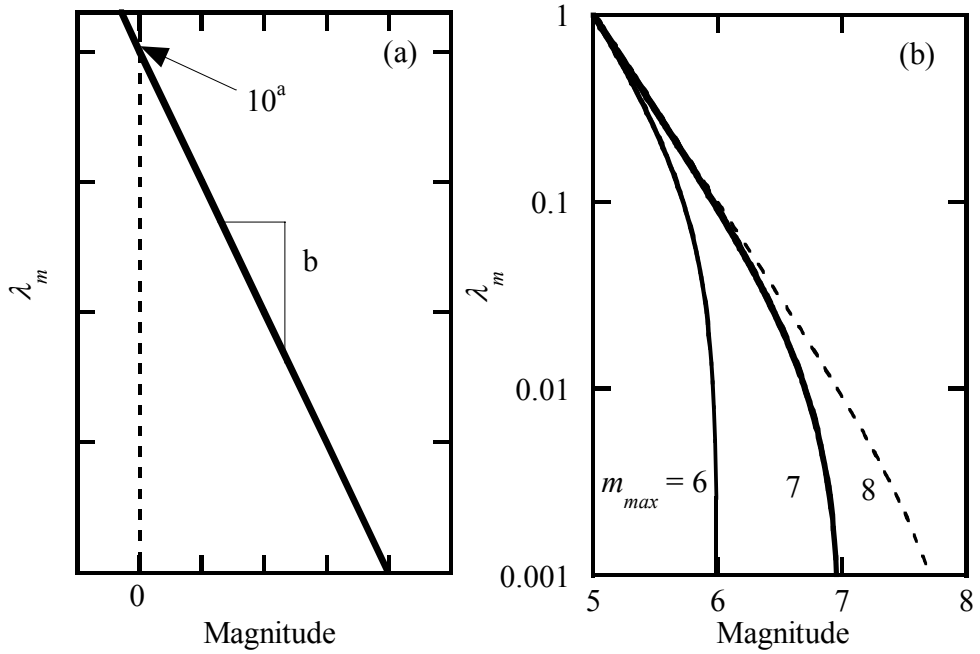

Figure 5-3 Schematic drawing of a) Gutenberg-Richter and b) bounded Gutenberg-Richter relationship.

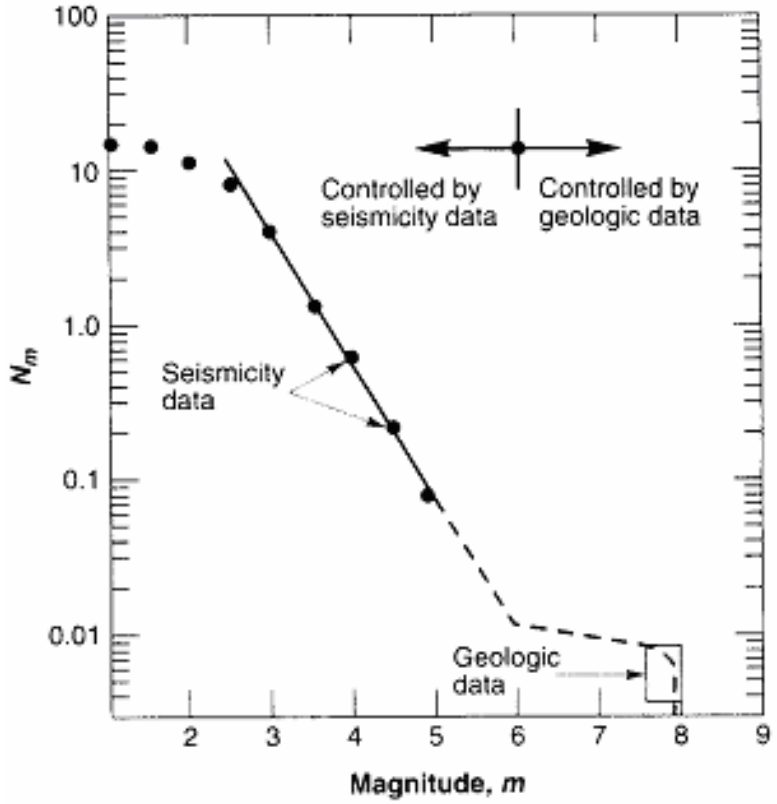

Figure 5-4 Schematic drawing of characteristic earthquake recurrence law (Youngs and Coppersmith, 1985).

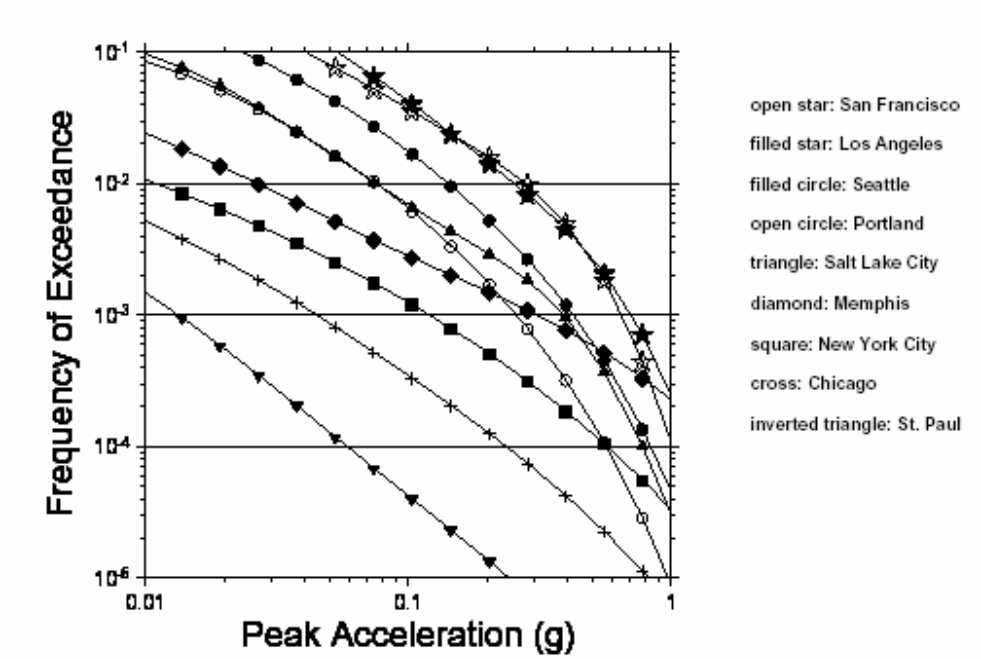

Figure 5-5 Seismic hazard curves of PGA for various selected Cities in the U.S. (Frankel et al., 1996)

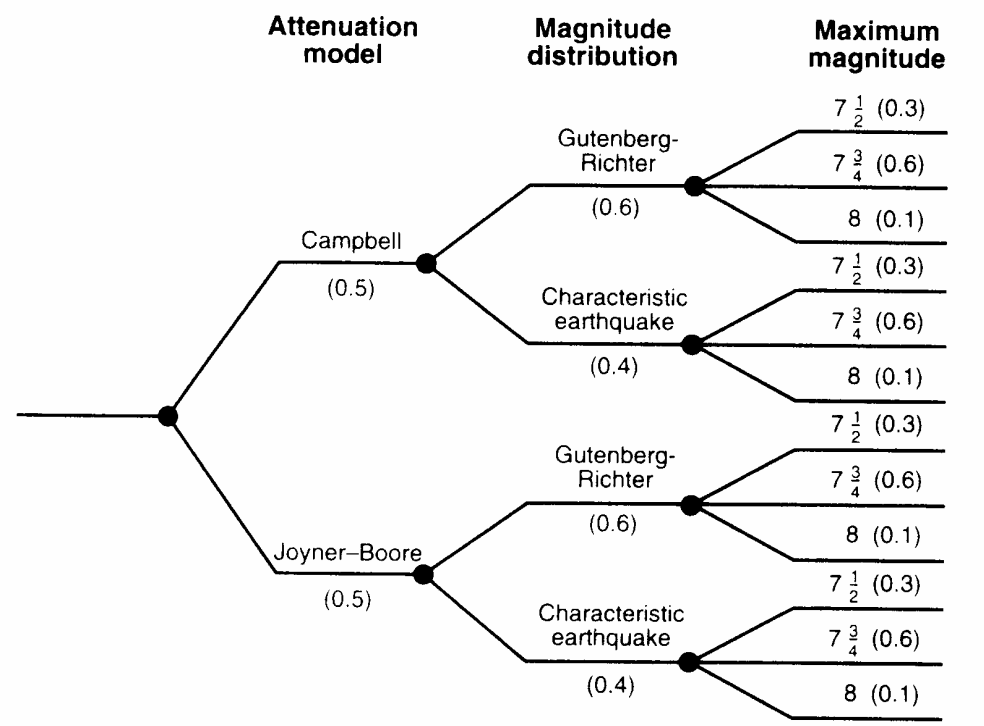

Figure 5-6 Logic tree for incorporation of various models in PSHA (Kramer, 1996).

.

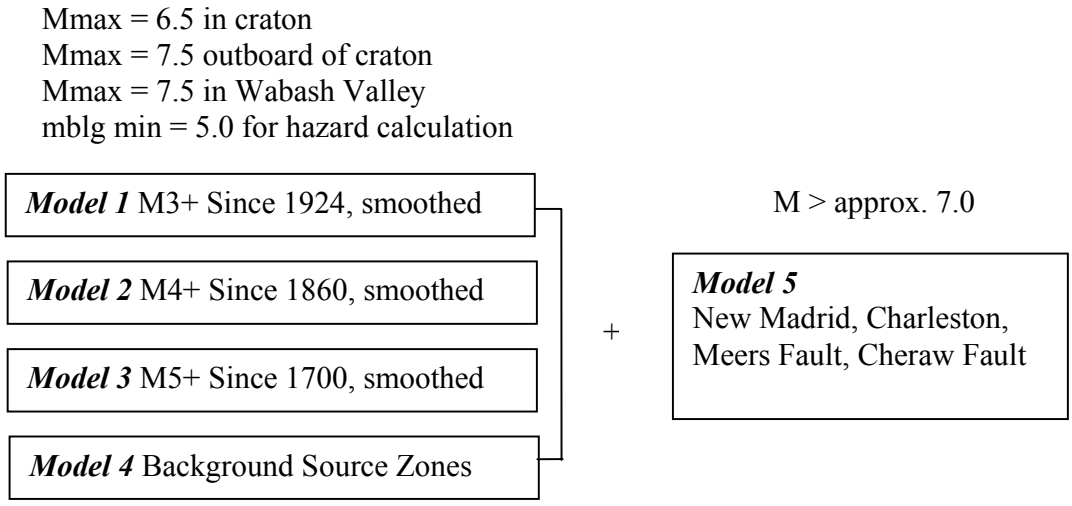

Figure 5-7 Alternative models of seismic hazard for central and eastern U.S. (Frankel et al., 1996).

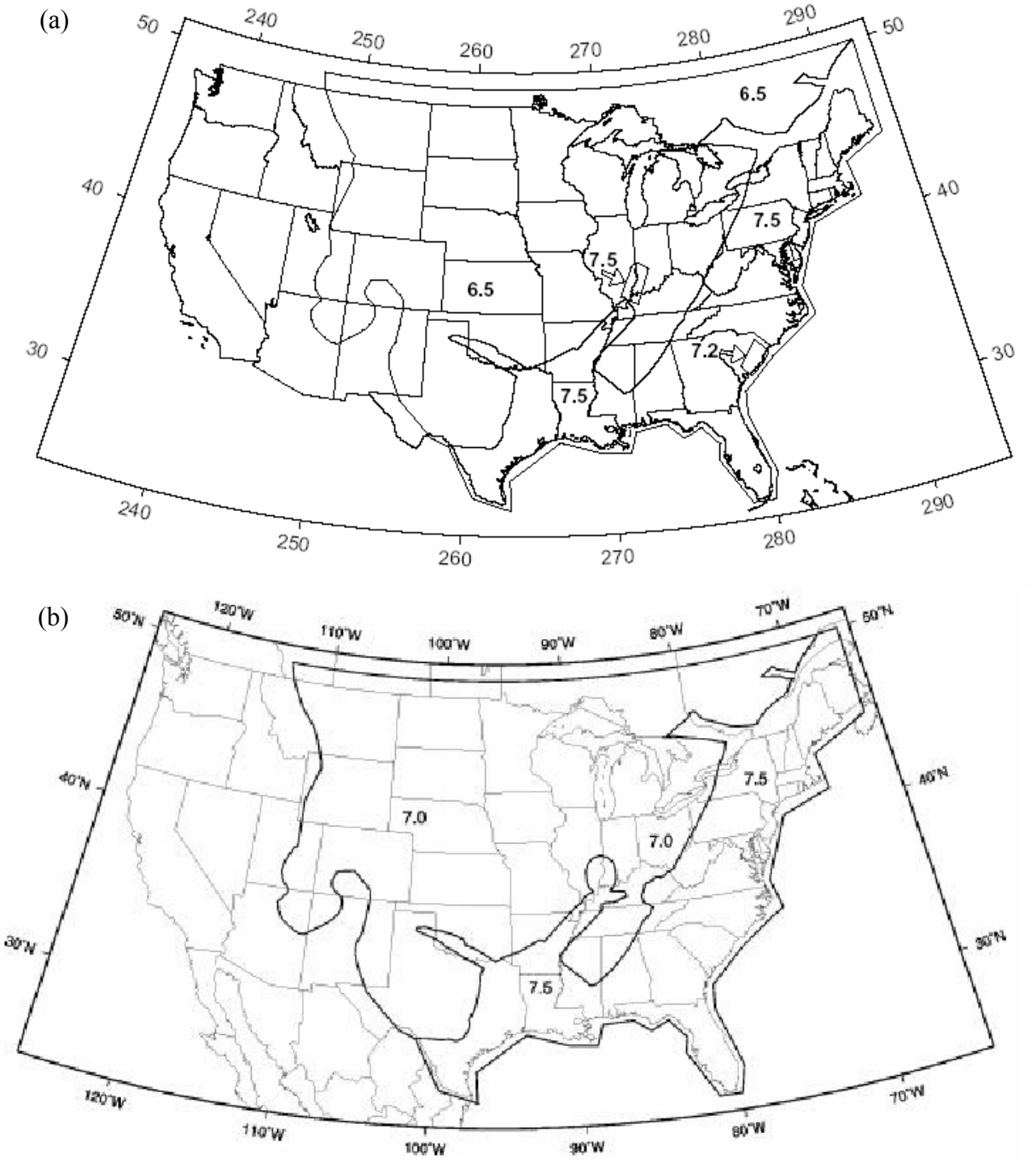

Figure 5-8 Maximum magnitude zones used in central and eastern U. S: a) 1996 maps, b) 2002 maps.

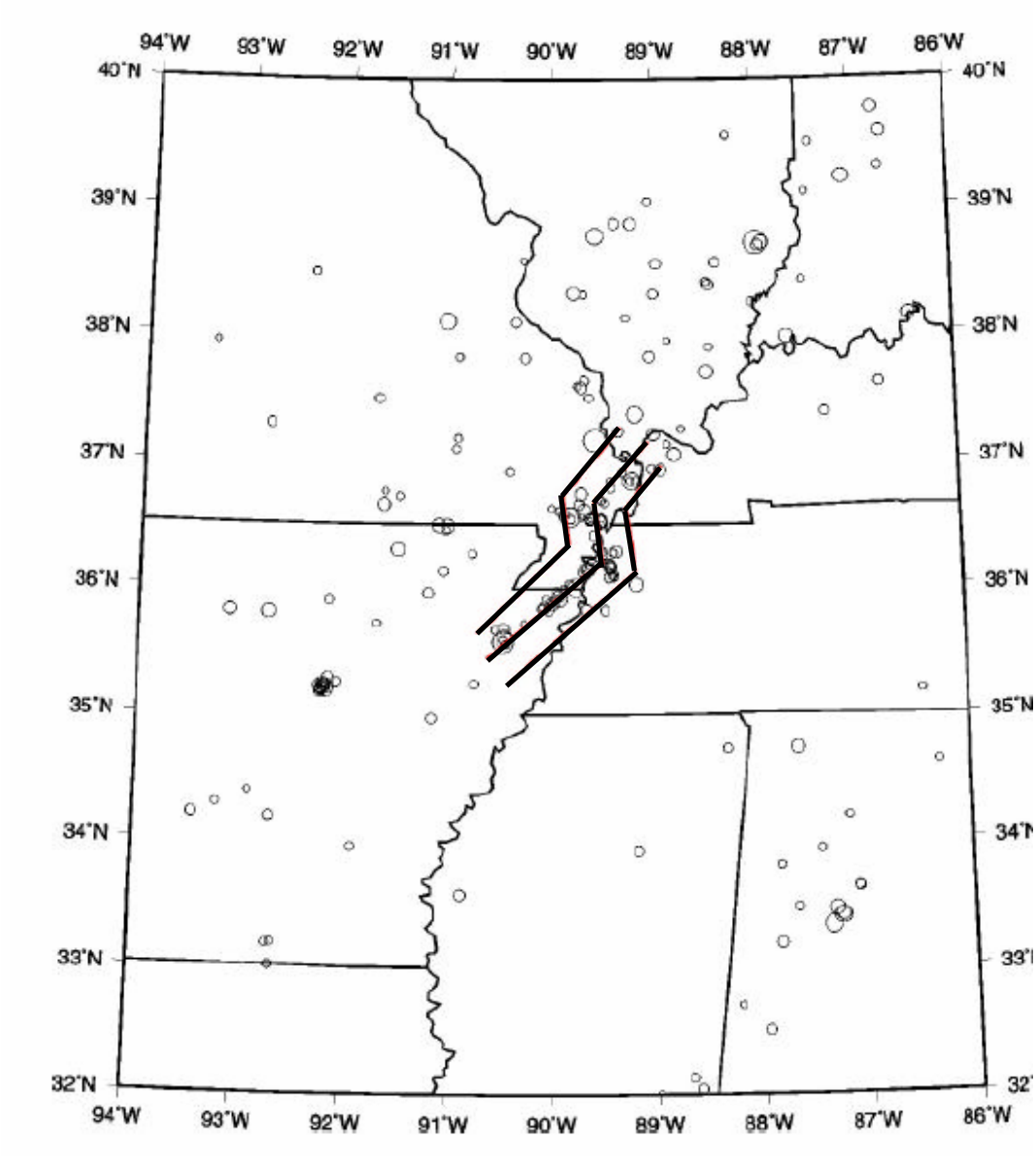

Figure 5-9 Three NMSZ fictitious faults used to define the characteristic earthquake in the Mississippi embayment (Frankel et al., 2002).

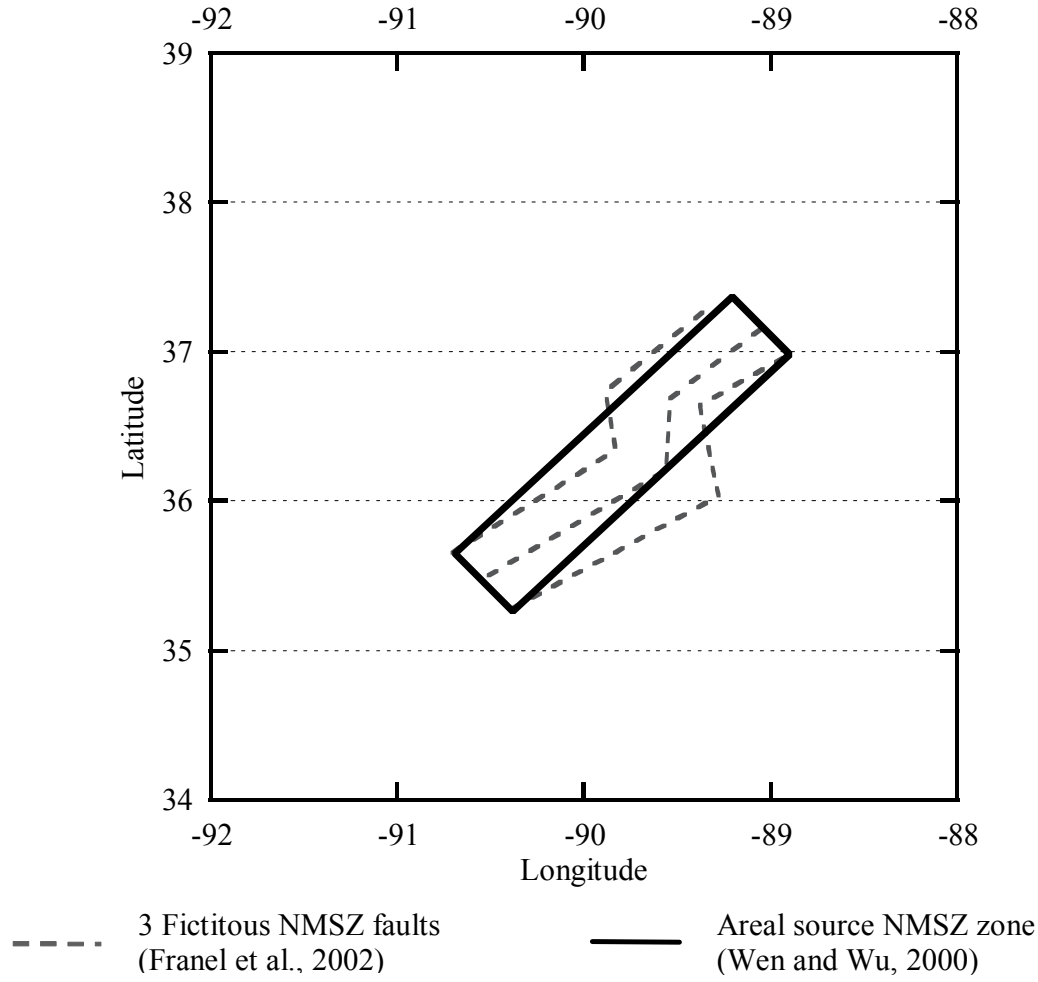

Figure 5-10 Three NMSZ fictitious faults used to define the characteristic earthquake in the Mississippi embayment (Frankel et al., 2002) and areal source zone used by Wen and Wu (2001).

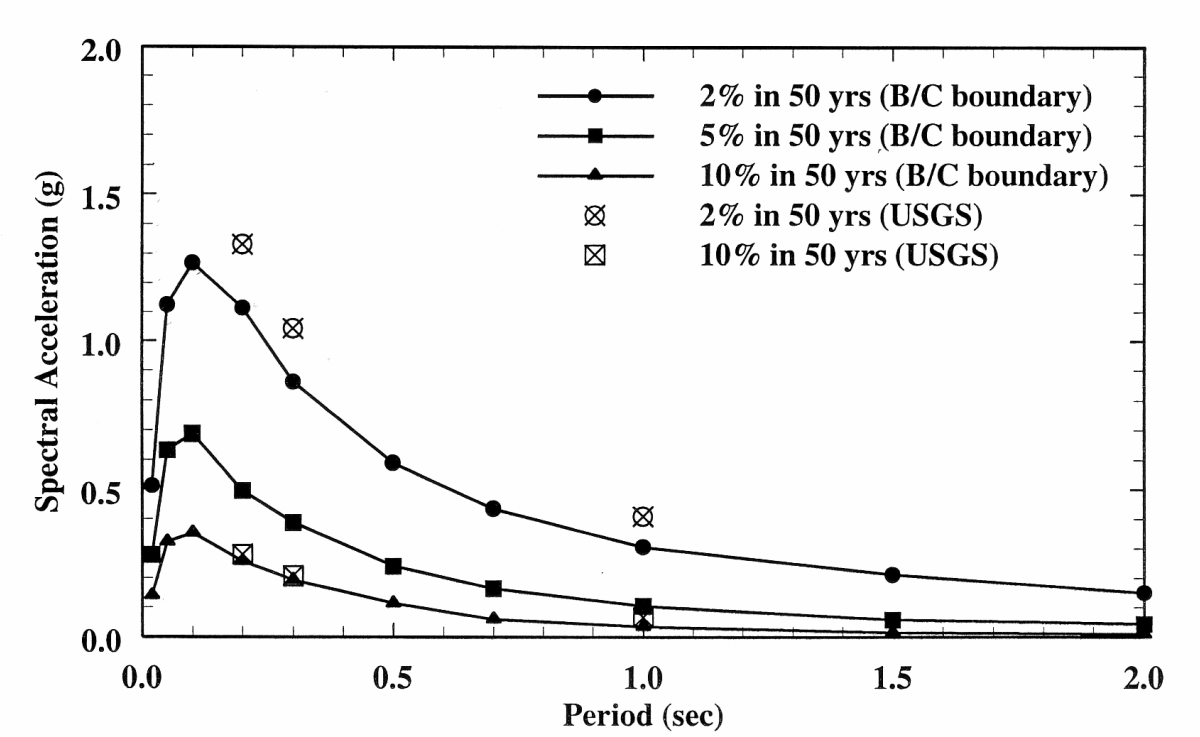

Figure 5-11 Comparison of simulated uniform hazard response spectra by Wen and Wu (2001) and USGS mapped values for B/C boundary at Memphis. 2% uniform hazard response spectrum is lower than USGS hazard map whereas 10% spectrum agrees well with USGS hazard map.

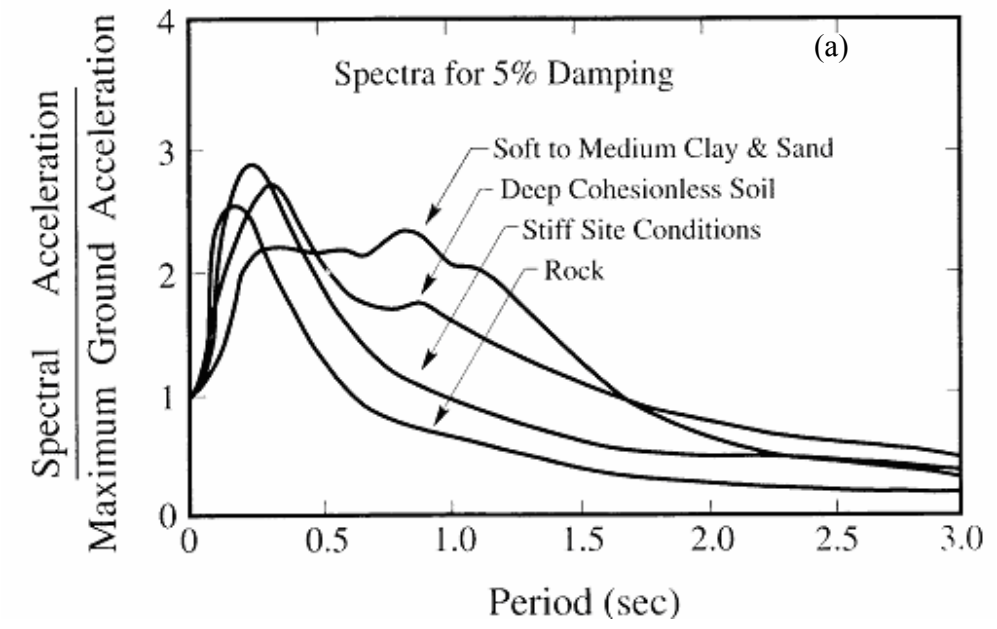

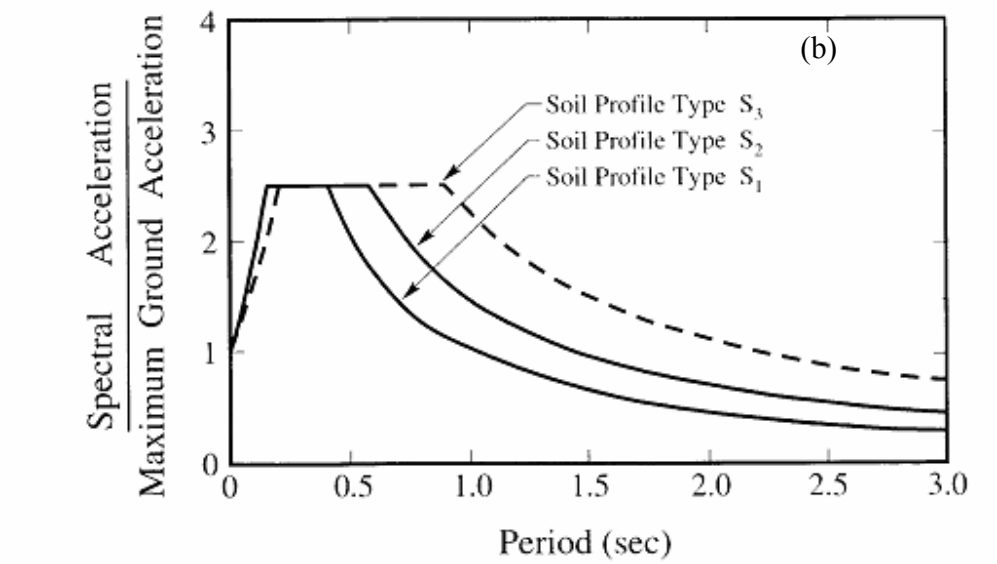

Figure 5-12 a) Average acceleration spectra for different site conditions and b)spectral shapes proposed by ATC 3 for soil profile types S1, S2, S3 (summarized in Table 5-1).

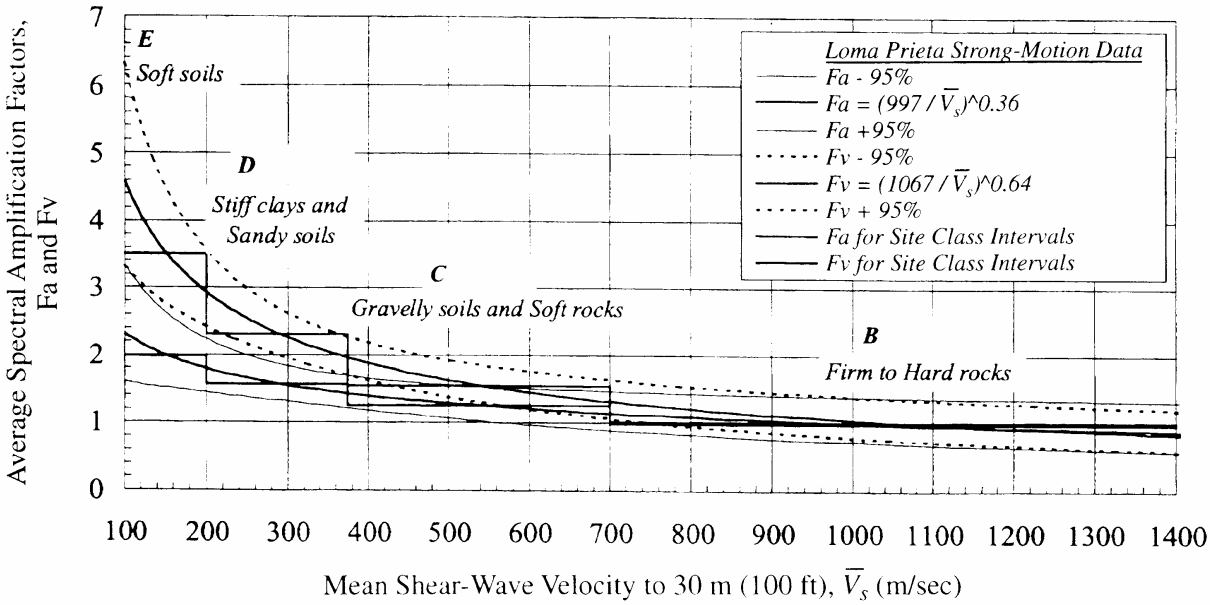

Figure 5-13 The relationship between short-period F_a and long-period F_v amplification factors with respect to Firm to Hard rock (Site B) versus mean shear velocity. The regression equations derived from the Loma Prieta earthquake based on Ratios of Fourier Spectra of nearby soil and rock recordings are used (Borcherdt, 1994).

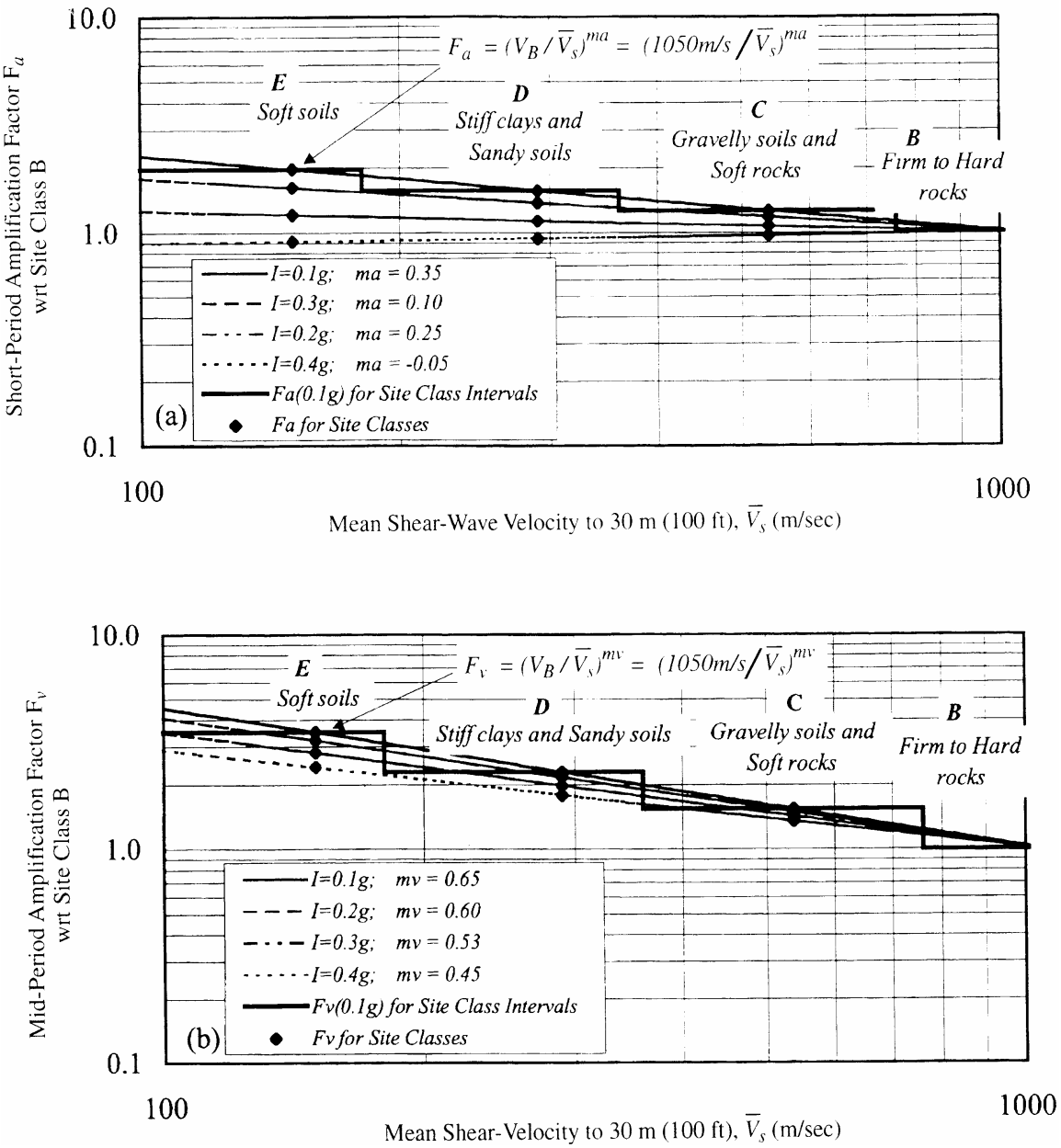

Figure 5-14 a) Short-period F_a and b) long-period F_v (termed mid-period in the above figure) amplification factors with respect to Fir to Hard rock (Site B) plotted with mean shear wave velocity Vs, using the indicated equations with exponents ma and mv for the various levels of the input ground motion (Borcherdt, 1994) The exponents ma and mv represent the slope of the straight lines. *I* in this figure represent the input ground motion level on rock in units of g.

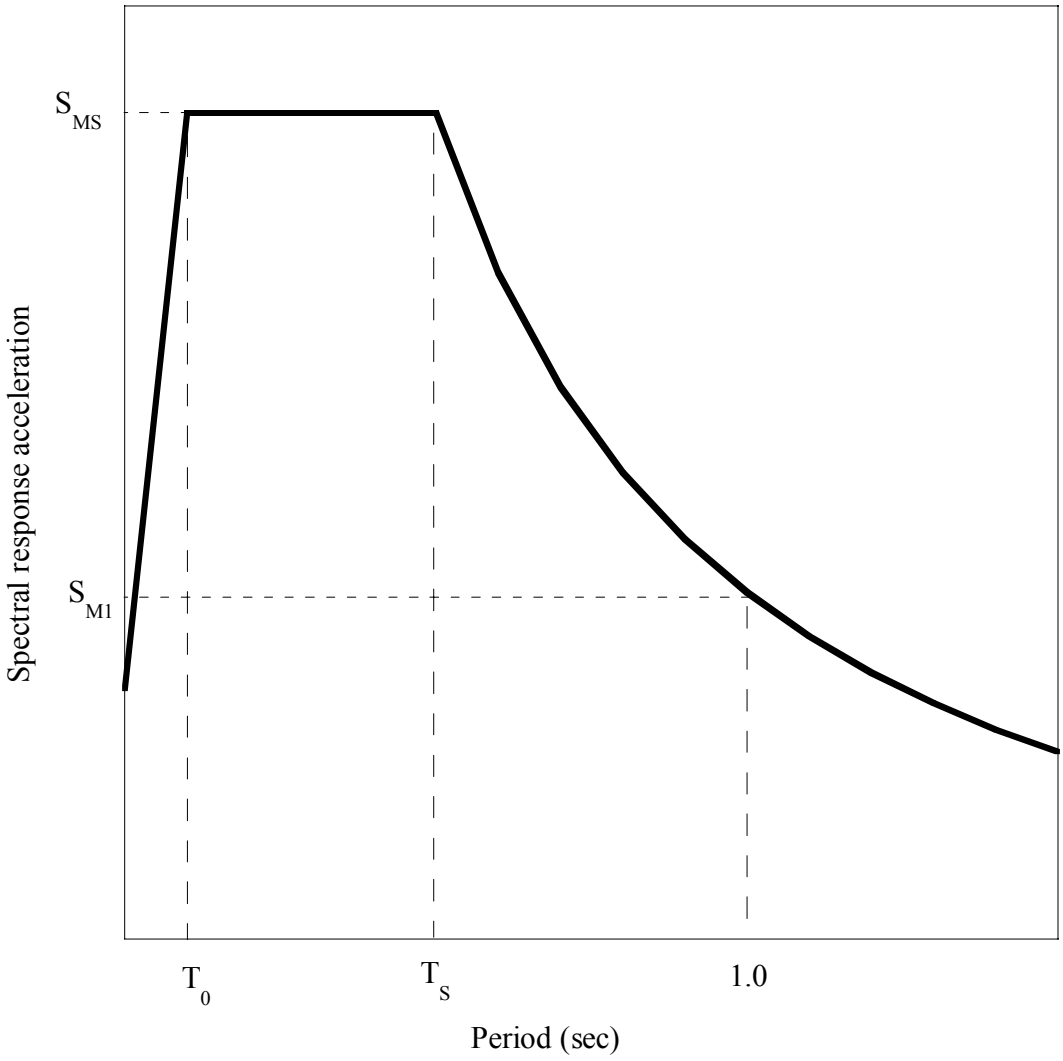

Figure 5-15 1997 NEHRP recommended response spectrum.

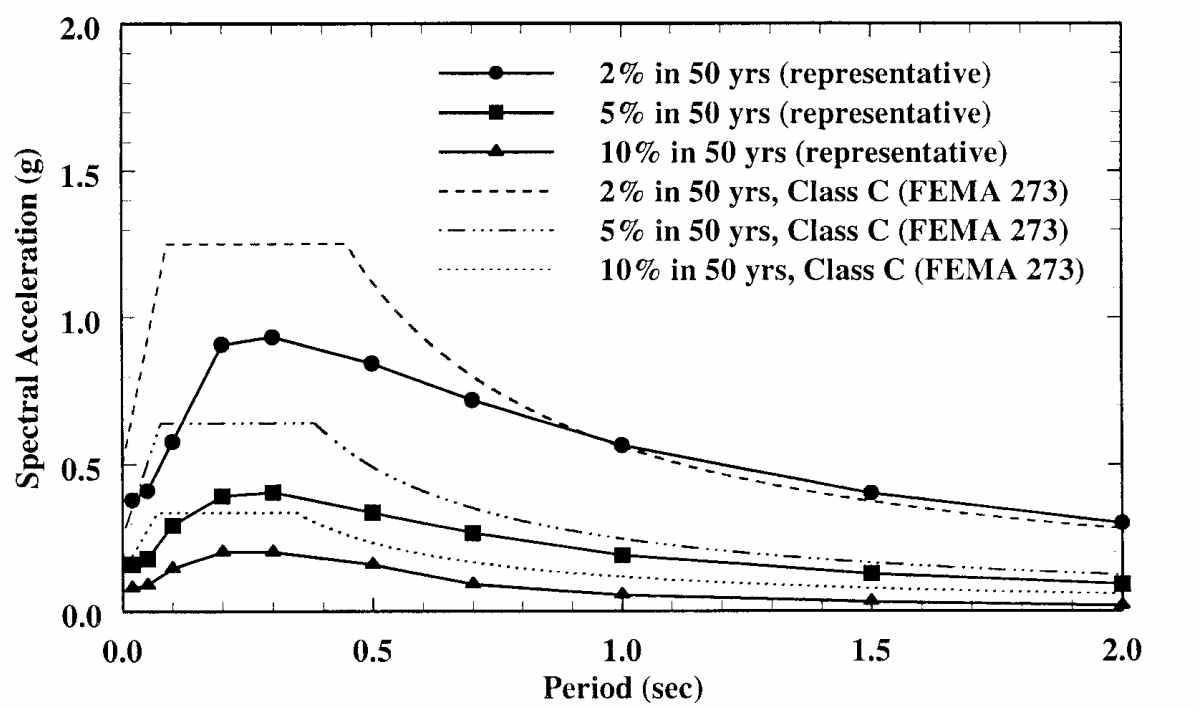

Figure 5-16 Comparison of simulated uniform hazard response spectra by Wen and Wu (2001) and NEHRP Site C design response spectra at Memphis. The simulated UHRS are consistently lower than NEHRP spectra at low periods (up to 1.0 sec).

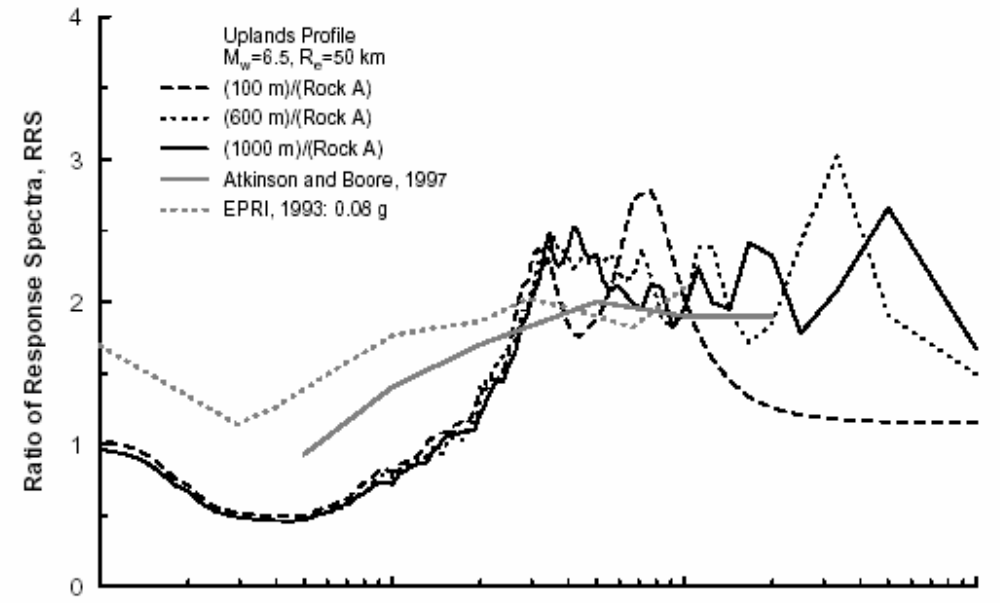

(a) Uplands Profiles

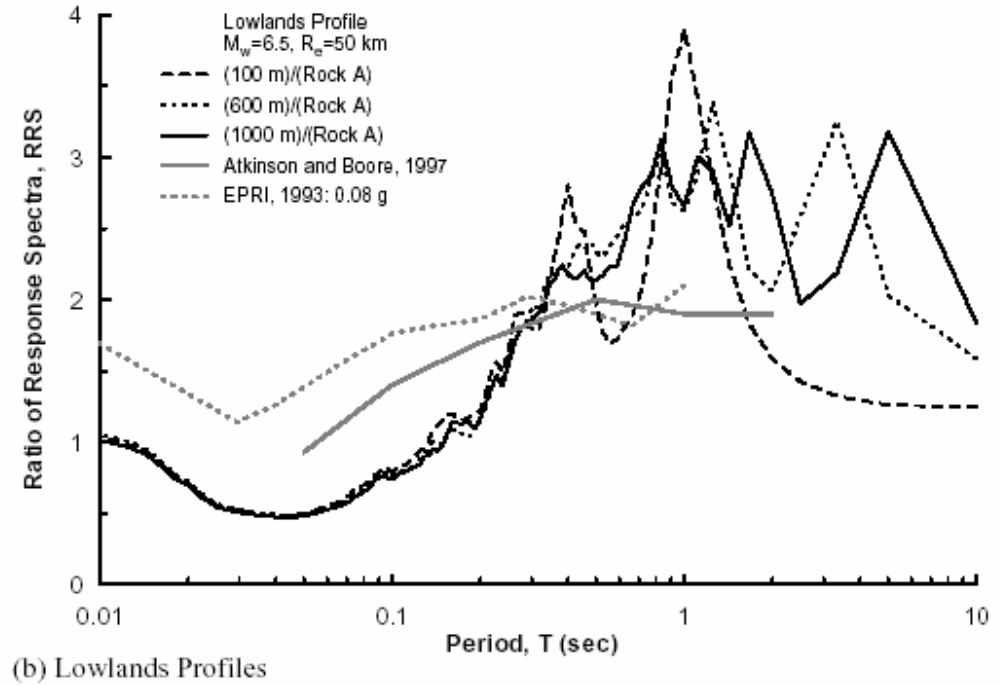

(b) Lowlands Profiles

Figure 5-17 RRS for the a) Uplands and b) Lowlands profiles compared to a hard rock (Site A) for 100m, 600 m, and 1000 m by Romero and Rix (2001) and the amplification factors developed by Atkinson and Boore (1997) and EPRI (1993).

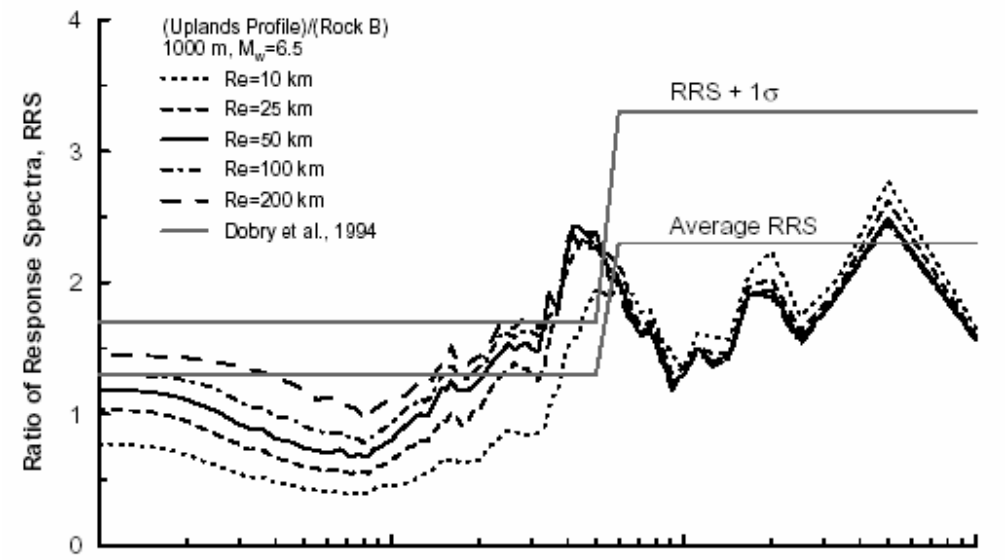

(a) Uplands Profiles

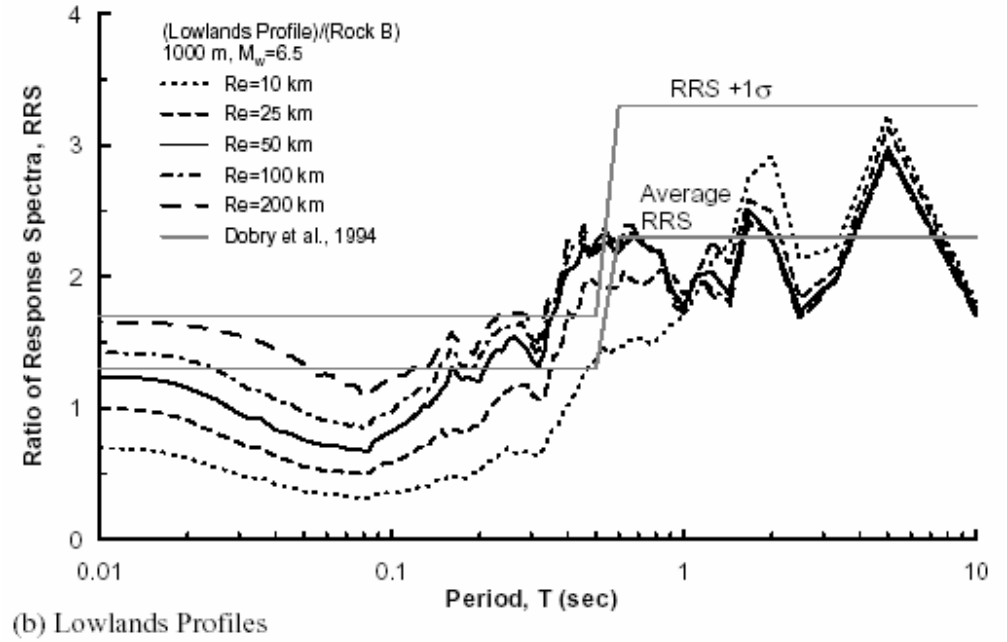

(b) Lowlands Profiles

Figure 5-18 RRS for the a) Uplands and b) Lowlands profiles by Romero and Rix (2001) for M = 6.5 and R = 10, 25, 50, 200 km compared with the RRS by Dobry et al. (1994).

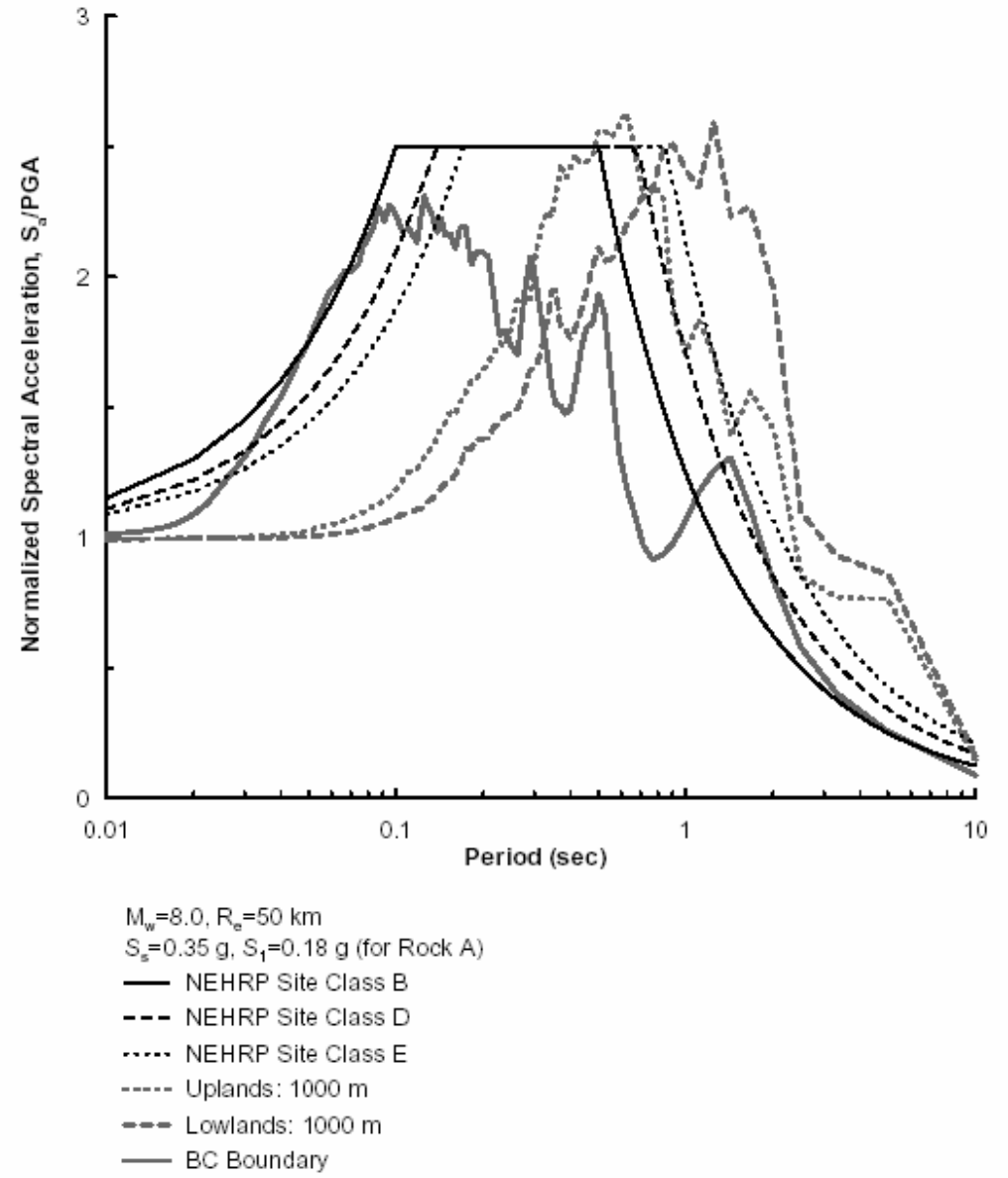

Figure 5-19 Comparison of normalized NEHRP design response spectra and calculated normalized response spectra for Uplands, Lowlands, and B/C boundary profiles (Romero and Rix, 2001).

CHAPTER 6 SEISMIC HAZARD ANALYSIS WITH NONLINEAR SITE EFFECTS AND ESTIMATION OF DEPTH DEPENDENT SITE COEFFICIENTS

6.1 Introduction

The seismic hazard from a PSHA is an aggregate risk from potential earthquakes of many different magnitudes occurring at many different source-site distances. Each of the potential earthquake scenarios is different in terms of its ground motion parameters, such as PGA and spectral accelerations. The site coefficients, defined as a function of the ground motion parameters, will be different for the various earthquake scenarios. Applying different site coefficients for different ground motions will preserve the probabilistic nature of the PSHA. This is seldom done in practice and the combined sum of the future seismic hazards, represented in selected ground motion parameters, is treated as originating from a single source (e.g. NEHRP Provisions, FEMA, 1997).

An integrated probabilistic seismic hazard analysis procedure that incorporates non-linear site effects, PSHA-NL, is developed and used to characterize the influence of thick deposits of the upper ME on seismic site coefficients. PSHA-NL follows the methodology of the 2002 USGS hazard maps and generates a compatible set of ground motion records. The motions are propagated using nonlinear and equivalent linear site response analyses and used to derive surface uniform hazard response spectra. A set of generic site coefficients are derived and summarized in a format similar to NEHRP site coefficients, with an added dimension of ME deposits thickness to the Paleozoic rock, a physically meaningful impedance boundary.

6.2 Proposed procedure to develop probabilistic site coefficients

An integrated probabilistic seismic hazard analysis which accounts for non-linear site effects (PSHA-NL) is developed. The combination enables the development of fully probabilistic site coefficients that account for the geologic structure of the upper ME and are compatible with USGS hazard maps. The proposed procedure comprises the following elements:

- *I: Site selection :* Several representative locations are selected within the ME to cover the range of spectral accelerations in the ME and NEHRP Provisions.
- *II: Probabilistic seismic hazard analysis with non-linear site effects PSHA-NL:*

- Step 1. Source characterization: Seismic sources are generated during a selected number of simulation years based on the seismicity information from USGS hazard maps. This step develops sets of magnitude and source-to-site distance that are fed into Step 2.
- Step 2. Generate ground motion time histories: Ground motion time histories are developed from the sets of magnitudes and source-to-site distances developed in Step 1.
- Step 3. Site response: The suite of generated motions in Step 2 is propagated through site specific profiles using non-linear and equivalent linear site response analyses to account for the site effects. The surface response spectra are calculated and aggregated into surface uniform response spectra (UHRS).

➢ *III: Determination of site coefficients:* Site coefficients consistent with the probabilistic approach are developed from the computed UHRS.

6.3 Selection of site locations

The upper ME is a deep basin ranging in thickness from very shallow (less than 30m) up to 1 km in depth. Seismic hazard varies, from less than 0.65g up to higher than 1.5g for 0.2 sec spectral accelerations for 2% in 50 years probability of exceedance. Ideally, analyses should be performed throughout the ME to cover the range of embayment depths and seismic hazards. The computational cost of the required series of analyses is presently prohibitive. Therefore, locations are selected to represent the range of spectral acceleration levels expected within the ME and covered in NEHRP Provisions (FEMA, 1997). Six locations are selected in the ME as summarized in Table 6-1 and shown in Figure 6-1. The high seismic hazard levels of the ME do not allow representation of the full range of spectral accelerations of the NEHRP Provisions using 2% in 50 years hazard levels.

The selected locations are not intended to represent geologically specific sites and the sediment thickness at the selected sites is hypothetically varied from 30 m to 1000 m to represent the sediment thickness range encountered in the ME.

6.4 Probabilistic seismic hazard analysis with non-linear site effects (PSHA-NL) at the Mississippi embayment

A new PSHA procedure that integrates the site effects, PSHA-NL, is developed and applied to the ME. The procedure is composed of three main steps, which are 1) source characterization, 2) ground motion time history generation, and 3) site response. Step 1 and 2, an extension of the work of Wen and Wu (2001), approximate the USGS hazard maps. The main difference from USGS hazard maps is that actual seismic motion time histories are developed. Step 3 is performed to characterize the effect of the embayment deposits on ground motion propagation. The output of the procedure is a suite of surface ground motions and UHRS that are later used to develop the ME site coefficients. The procedure is shown in Figure 6-2 and Figure 6-3 and described in detail in the following sections.

6.4.1 Step 1 Source characterization

The USGS hazard maps define two types of seismic sources, which are a) characteristic and b) gridded seismic sources. The characteristic sources represent sources at which the recurrence interval and magnitude can be estimated based on geologic evidence. The gridded seismic sources are intended to cover the historical seismicity and large background source zones. The background source zones are used to assign hazard in areas with little historical seismicity but with the potential to generate damaging earthquakes. The gridded seismic sources do not have fixed recurrence interval and magnitude. The seismicity of the gridded sources is described by the recurrence rate, which is a continuous function that relates annual rate of exceedance and magnitude. The seismicity is defined for every $0.1° \times 0.1°$ grid in the central and eastern U.S (Frankel et al., 1996). The characteristic and gridded sources are treated separately and added to the final seismic hazard.

The proposed procedure utilizes the seismicity information, for both characteristic and gridded seismic sources, from USGS hazard maps, but develops actual sources that occur within a finite number of simulation years (N). Wen and Wu (2001) suggest that 90,000 simulation years are required to result in occurrence rates compatible with USGS hazard maps. The same number of simulation years is used in this study.

6.4.1.1 Characteristic earthquakes

The characteristic earthquakes are assumed to occur in the NMSZ. USGS NMSZ fault geometries are used which consist of three fictitious faults, shown in Figure 6-1. The faults' contribution to the hazard are weighted such that the center fault has a 1/3 wt in 1996 maps and 0.5 in 2002 maps, and each of the two outer faults has a 1/3 wt in 1996 maps and 0.25 wt in 2002 maps (Figure 6-2 and Figure 6-3). The characteristic events are not randomly generated, as when simulating the gridded seismic sources. The recurrence rate of characteristic events is fixed at 1000 years for 1996 maps and 500 years in 2002 maps. Therefore, the number of occurrences within the simulation period can be calculated using the fixed recurrence rate. The period of simulation in this study is 90,000 years. The number of occurrences of characteristic earthquakes is for the simulation period is 90 for 1996 maps and 180 for 2002 maps. Since the faults have different weights, the number of sources for each of the fault should be assigned accordingly. For 1996 maps, 30 sources should be generated for each fault. For 2002 maps, 90 sources should be generated at center fault and 45 at adjacent faults.

USGS uses the closest distances to each of the three faults to calculate the cumulative seismic hazard at the site. The rationale for choosing the closest distance instead of assuming equal probability of occurrence along the entire fault has been presented in section 5.4.1. This means that only a single scenario (single M and R) is possible at each of the three fault. M = 8.0 is assigned for 1996 maps whereas M = 7.7 is used for 2002 maps.

6.4.1.2 Gridded seismic sources

The recurrence rates proposed in the USGS hazard maps (Frankel et al., 1996; Frankel et al., 2002)are used to characterize the seismicity of the gridded seismic sources in this study. The occurrence in time during a ten-year period is calculated according to a Poisson process, using the USGS defined recurrence rate. The magnitude, given the occurrence of an earthquake, is then assigned according to the magnitude distribution for gridded seismic events proposed by USGS. The simulation is repeated for a total of 9000 10-year simulations to result in 90,000 simulation years. The numbers of generated sources during the 90,000 simulation years range from 9000 to 10,000.

6.4.2 Step 2 Ground motion time history generation

USGS hazard maps use attenuation relationships to estimate ground motion parameters from the characterized sources. The main difference between the proposed PSHA procedure and USGS hazard maps is that instead of using the attenuation relationships, actual ground motion time histories are developed from the sets of magnitude and source-to-site distance information obtained from the source characterization process. The generation of actual ground motion time histories eliminates the need to use attenuation relationships, provided that the characteristics of the ground motion approximate the attenuation relationships.

Only single-corner point source model is needed to reproduce the 1996 maps. 2002 maps, on the other hand, incorporate three additional attenuation relationships in estimation of the ground motion parameter which include double-corner point source model, broadband model, and hybrid model using both empirical data and stochastic model (Frankel et al., 2002). Only the point source stochastic model is used in this study (Figure 6-2 and Figure 6-3), due to the lower contribution and difficulty in incorporating the models in the simulation. Both single corner and double corner point source models are used, whereby single corner and double corner models are assigned the same weight, for both gridded and characteristic seismic sources (Figure 6-3).

In this study, the newest version of SMSIM (version 2.2) is incorporated. Details on the stochastic model are described in Appendix C.

The stochastic model SMSIM (version 2.2) (Boore, 2002), which has been used in development of the point source model based attenuation relationships, are used to develop ground motion time histories using the USGS defined input parameters. Details on the stochastic model are described in Appendix C. The motions are generated at hard rock site class A representing Palezoic bedrock.

6.4.2.1 UHRS development

The procedure for developing the UHRS is shown in Figure 6-4. The response spectrum of each of the propagated ground motions are calculated and compiled. Each of the points in the response spectrum represents the ground motion parameter *Y*. The annual probability of the source exceeding a particular value y^* can be calculated using equation.

$$\lambda_k = \lambda_i \cdot P\left[Y > y^*\right] = \lambda_i \cdot \left[1 - F\left(\frac{y^* - Y}{\sigma_{\ln Y}}\right)\right] \tag{6-1}$$

where λ_i for all of the generated motions is 1/total simulation years; σ_{lnY} is the lognormal standard deviation, $\left[1-F\left(\frac{y^*-Y}{\sigma_{\ln Y}}\right)\right]$ is CDF of Y to exceed y^*. The annual probability of exceedance is calculated for a range of y^*. This procedure is repeated for all of the ground motions generated. The results are summed up. From the summation of all probabilities, the ground motion parameter corresponding to the desired design probability of exceedance is calculated.

6.4.2.2 Comparison with USGS hazard maps

The attenuation relationships incorporated in the USGS hazard maps use the Fourier amplification function, Figure 6-5, to represent amplification at B/C boundary (Frankel et al., 2002). The ground motions generated (hard rock motions at Palezoic bedrock) are converted to B/C boundary motions to compare with USGS hazard maps. A maximum cap is imposed on the converted ground motions, as in the 2002 USGS hazard maps. Whereas USGS hazard maps impose different caps for PGA and 0.2 sec spectral acceleration, only the PGA is capped in the proposed simulation since the proposed simulation procedure uses ground motion time history. The ground motion can only be scaled to a single selected ground motion parameter.

At all sites the UHRS are developed for probability of exceedance of 2% in 50 years. Additionally UHRS are developed at site 1 for higher probabilities of exceedence to cover the lower range of spectral accelerations used in NEHRP Provisions (S_s = 0.25g, S_s = 0.5g, and S_1 = 0.1g). UHRS with probabilities of exceedence of 3.6%, 4.9%, and 7.7% in 50 years have S_s = 0.25g/ S_1=0.057g, S_s = 0.40g/ S_1=0.10g , and S_s = 0.50g/ S_1=0.145g, respectively.

The simulated UHRS at B/C boundary are compared to the 1996 and 2002 USGS mapped hazard and NEHRP Site B design response spectrum. USGS hazard maps provide 4 ground motion parameters (PGA, 0.2, 0.3, and 1.0 sec SA). The NEHRP Site B design spectrum is used to represent the hazard at other periods at B/C boundary. Seismic hazard corresponding to 2% and 10% in 50 years probability of exceedance seismic hazards are compared.

Figure 6-6 and Figure 6-7 show 2% in 50 years hazard of proposed simulation and USGS hazard maps. When comparing the 1996 and 2002 maps, the calculated seismic hazards are similar. The lower recurrence rate of 2002 maps (from 1000 years to 500 years) is countered

balanced with lower magnitude of characteristic event (from 8.0 to 7.7). The simulated UHRS re in very good agreement with both 1996 and 2002 maps.

Figure 6-8 and Figure 6-9 show 10% in 50 years hazard of proposed simulation and USGS hazard maps. The 1996 maps are significantly lower than 2002 maps. The increased recurrence rate of characteristic event does not highly influence the 2% in 50 years hazard but has pronounced influence on 10% in 50 years hazard. Again, the simulated UHRS compare very well with the USGS hazard maps.

For all sites, the simulated UHRS agree very well with both 1996 and 2002 USGS hazard maps. This demonstrates that the proposed simulation can closely reproduce the seismic hazard determined by USGS, but at the same time allow generation of ground motion time histories.

6.4.2.3 Comparison of characteristic events with UHRS

The PSHA allows determination of UHRS using aggregate risk of all possible future earthquake sources. However, PSHA does not provide a specific or worst case scenario and resulting ground motion time histories. Deaggregation is commonly used to estimate the seismic contribution of various sources in terms of magnitude and distance. An earthquake scenario that has the highest contribution to the seismic hazard is selected and representative ground motion time histories are developed. For 2% in 50 years hazard in the ME, the worst-case scenario is always the characteristic earthquake due to proximity of the NMSZ. In other words, the characteristic event which occurs at a distance closest to the given site within the three NMSZ faults is the worst case scenario. Figure 6-10 and Figure 6-11 compare the response spectra of the characteristic scenario ground motions with the 2% in 50 years 2002 UHRS. Since two source models, single corner and double corner source models, are incorporated in generation of the earthquake ground motions, response spectra for both of the models are shown. The response spectra are average of the ground motions simulated.

For Site 1, at which the seismic hazard is the lowest, the characteristic event is significantly lower than the UHRS. Characteristic event becomes closer to UHRS with increase in seismic hazard. At site 6, the characteristic event using single corner is almost identical to the UHRS. At Site 6, single corner characteristic event is higher than UHRS. This comparison illustrates that UHRS cannot be represented by a characteristic event, as commonly done in practice through deaggregation.

6.4.3 Step 3 Site response analysis

The generated ground motions at hard rock are propagated to the ground surface to account for the effects of embayment deposits. The seismic wave propagation is simulated using 1-D site response analysis code DEEPSOIL, described in the companion paper. Two generic soil profiles of the Mississippi embayment developed by Romero et al. (2001), Figure 4-4, are used in the simulation. Both profiles fall within NEHRP Site D category, whereby the Uplands and Lowlands profiles have an average shear wave velocity of 314 m/s and 249 m/s respectively in the top 30 m. The profiles are generic to the Mississippi embayment and do not represent conditions at a specific location.

Two sets of soil properties are used in the study; a) the proposed dynamic soil properties for the ME derived in CHAPTER 4 and b) the generic dynamic soil properties developed by EPRI (1993) to account for the uncertainty of the dynamic properties of the embayment . The proposed properties are constrained using the in-situ laboratory tests and weak motion recordings in the embayment and will be referred to as ME properties. The properties developed by EPRI will be referred to as EPRI properties. The dynamic soil properties are not randomized in performing site response analysis, as in Romero et al. (2001). It is not possible to assign variability parameters for the randomization process of the embayment soils due to the lack of laboratory test data. Application of non-site-specific variability parameters will result in sets of dynamic curves that do not represent embayment soils.

The characteristic ground motions are propagated using nonlinear analysis as the PGA of the resulting ground motions at the selected sites range between 0.06g to 1.0g. The ground motions from gridded seismic sources are propagated using equivalent linear analysis as 99.6% to 98.6% of the ground motions have a PGA lower than 0.1 g. Both the nonlinear and equivalent linear analyses are performed using DEEPSOIL. The response spectra of the surface motions are used to develop the UHRS.

6.5 Evaluation of UHRS

Figure 6-12a show 2% in 50 years UHRS for site 1 (S_s = 0.66g, S_1 = 0.2g), for depths from 30 m to 1000 m using the Uplands profile and ME properties. The 30 m UHRS compares well with the NEHRP design response spectrum (F_a =1.28, and F_v = 2). However, the UHRS continuously decreases with increasing deposit thickness at short periods (approximately up to

0.5 sec). The rate of reduction is quite pronounced up to a thickness of 300 m, but more subtle at greater depths. This is due to low strain levels and viscous damping at depth. The amplification at long periods, on the other hand, increases significantly. The amplification shifts to longer periods due to a shift to higher resonant periods with increase in column thickness. The UHRS plots demonstrate the need to incorporate soil profile thickness dependent design site coefficients. The short period site coefficient decreases, whereas the long period site coefficient increases with soil column thickness.

Figure 6-12b shows 2% in 50 years RUS (ratio of uniform hazard spectra: defined as the ratio of surface UHRS to B/C boundary UHRS) for site 1. RUS, based on probabilistically derived UHRS, is different from the widely used deterministic amplification factor RRS, which is defined as the ratio of surface response spectrum to the bedrock response spectrum. RRS has been used to obtain deterministic site coefficients of NEHRP Provisions (FEMA, 1997).

The RUS are compared to the NEHRP site coefficients (F_a and F_v). The NEHRP F_a and F_v site coefficients (F_a =1.28, and F_v = 2) are plotted to compare with RUS in Figure 6-12b. Even though the F_a and F_v are used as amplification factors at two discrete points (0.2 and 1.0 sec spectral accelerations), constant ranges of F_a and F_v are plotted because constant values of F_a and F_v are applied to short period (approximately 0.1 to 0.5 sec in ME) and long period (0.5 sec and higher), respectively. The NEHRP F_a matches well with the 30 m RUS, but F_v is higher than 30 m UHRS at periods 0.5 sec and higher. Figure 6-12a show that NEHRP design spectrum compares well with the 30 m UHRS when using the NEHRP proposed long period site coefficient even though the coefficients are higher than the simulated amplification ratio at long periods. Figure 6-13 and Figure 6-17 show the computed UHRS and RRS for sites 2 to 6. For all sites, the same trend as in site 1 is observed.

NEHRP site coefficients, based on site classes using the top 30 m shear wave velocity, are compared to RUS for all selected sites with 30 m thick profiles in Figure 6-18. For all sites, NEHRP F_a at short periods are similar to, but provides a slightly lower estimate than the RUS (Figure 6-18). The long-period coefficient F_v, however, differs from the calculated RUS at all sites. Whereas the calculated RUS show constant amplification of 1 at all sites for 30 m profiles, NEHRP site coefficients range from 1.6 to 2.0.

F_v not only controls the long period amplification, but also controls the T_0 and T_s which determine the shape of the design spectrum, Equation (5-11). If the simulated long period

amplification of 1 is used, it will reduce the values of T_0 and T_s. This is demonstrated using site 1 as an example and shown in Figure 6-19. Using NEHRP values F_a = 1.28 and F_v = 2.0 results in overall good match with the simulated UHRS at Site 1.Using F_a = 1.28, but using F_v = 1 from RUS will significantly shift the response spectrum to lower periods. It will match the simulated long period spectral acceleration at 1.0 sec, but underestimate the important periods from approximately 0.3 sec to 1.0 sec. In the following analyses, F_v has been chosen to obtain a good match with UHRS.

6.6 Influence of material properties and soil profile

Figure 6-21 to Figure 6-25 compare 2% in 50 years UHRS of site 1 to 6 using all combinations of shear wave velocity profiles (Uplands and Lowlands profiles) and material properties (ME and EPRI properties). Lowlands profile results in lower short period amplification than Uplands and slight shifting to higher periods due to the lower shear wave velocity at the upper 70 m of the profile.

The effect of the material properties is much more pronounced compared to the effect of the shear wave velocity profile. EPRI properties have much lower small strain damping compared to the ME properties and has significant influence on propagation of weak ground motions, as demonstrated in the companion paper. Therefore, the UHRS and corresponding F_a is larger at short period when using EPRI properties than when using ME properties. The thickness dependency is also less due to overall lower small strain damping ratio when using the EPRI properties. The long period amplification is very similar when using EPRI or ME properties except for 1000 m profile, where the lower confining pressure dependency of EPRI properties results in softer behavior of the soil column and the long period amplification is much larger than when using ME properties.

6.7 Computed UHRS based site coefficients

Soil profile thickness dependent site coefficients for the ME are developed based on the UHRS. It is difficult to assign site coefficients using RUS since a) various peaks exist within both constant F_a and F_v ranges and b) selection of site coefficients not only controls the amplification but also the T_0 and T_s, or the shape of the design response spectrum. Instead of directly using RUS, the site coefficients are chosen such that a reasonable envelope of the UHRS is obtained. Design spectra using the proposed site coefficients and the computed UHRS for the

selected sites are shown in Figure 6-27 to Figure 6-31. The design spectra for all six sites are shown in Figure 6-32.

This procedure is used to develop the site coefficients for all analyses, using Uplands/Lowlands profiles, and using both the ME/EPRI properties. Proposed site coefficients are summarized in Table 6-2 and Figure 6-33 for Uplands and Table 6-3 and Figure 6-34 for Lowlands profiles. The proposed coefficients are summarized in a similar format to NEHRP Provisions, with the addition of dependency on the embayment thickness. Based on the results using both the ME and EPRI properties, upper and lower bound for Uplands and Lowlands are developed. F_a are lower when using the ME properties for all soil profile thicknesses used in this study and therefore are the lower bound. Decrease in F_a for 1000 m profile is approximately 30% when using ME properties, but is approximately 20% when using EPRI properties. The values of F_v and the rate of decrease in F_v using the ME properties are higher than when using EPRI properties, and thus is the upper bound.

The nonlinear site coefficients derived in the simulation show consistent behavior with change in thickness of the soil column. Therefore it is possible to develop simple functions to relate the thickness of the soil profile to upper / lower bound site coefficients. The functions are listed in Table 6-4. The functions are identical for Uplands and Lowlands profiles, indicating that the rate of change of the site coefficients with thickness is only dependent on the material properties.

The proposed site coefficients are for the Mississippi embayment and Site D only. However, the PSHA-NL methodology is general and can be applied to any sites in the US, provided that the site dynamic properties are available. It should be recognized that the proposed design spectra do not envelope the peaks of the UHRS. Therefore, site-specific analysis is recommended in design of critical structures to account for the resonant periods at which the hazard is the highest. Site-specific analysis is also warranted in design of long period longitudinal structures in deep embayment deposits, since the design spectrum will underestimate very long period amplification.

6.8 Summary and conclusions

A new methodology for determining probabilistic site coefficients is developed and applied to the Mississippi embayment. Initially, PSHA is performed to reproduce the USGS hazard maps, while generating a compatible set of ground motion time histories. The generated motions are propagated through generic profiles of the Mississippi embayment, taking into account non-linear site effects of individual motions. Two generic shear velocity profiles (Uplands and Lowlands) and two sets of dynamic properties (ME properties and EPRI properties developed in a companion paper) are used to account for the uncertainty in the soil properties. Surface uniform hazard response spectra are computed and used to develop site coefficients. The coefficients show a strong dependence on Mississippi embayment deposit thickness to the Paleozoic rock, a physically meaningful impedance boundary. The proposed site coefficients are presented in NEHRP style coefficients with the added dimension of embayment thickness. Results indicate that proposed coefficient for embayment thickness of 30m compare well with NEHRP site coefficients. However, for deep soil profiles of the ME, the proposed site coefficients are lower at short periods and higher at long periods than the 1997 NEHRP site coefficients.

Table 6-1 Selected locations for PSHA.

Site No	S_s (g)	S_1 (g)	PGA (g)	Latitude (°)	Longitude (°)	F_a[2]	F_v[2]
1	0.656	0.20	0.307	37.0	-87.5	1.28	2
2	0.75	0.22	0.34	35.5	-88.6	1.2	1.96
3	1.00	0.30	0.568	35.5	-89.2	1.1	1.8
4	1.25	0.34	0.66	36.0	-90.9	1.0	1.72
5	1.50	0.40	0.796	37.5	-89.5	1.0	1.6
6	1.84	0.50	1.01	36.8	-88.8	1.0	1.5

[1] From 2% in 50 years 2002 USGS hazard maps

[2] From 1997 NEHRP Provisions

Table 6-2 Recommended site coefficients of the Mississippi embayment for Uplands.

a) F_a as a function of soil profile thickness and mapped 0.2 second period spectral acceleration 2002 USGS hazard maps.

Thickness (m)	Mapped 0.2 sec spectral acceleration from 2002 USGS hazard maps														
	S_s = 0.25g			S_s = 0.50g			S_s = 0.75g			S_s = 1.0g			$S_s \geq$ 1.25g		
	NEHRP	Upper bound [2]	Lower bound [1]	NEHRP	Upper bound [2]	Lower bound [1]	NEHRP	Upper bound [2]	Lower bound [1]	NEHRP	Upper bound [2]	Lower bound [1]	NEHRP	Upper bound [2]	Lower bound [1]
30	1.6	1.6	1.5	1.4	1.5	1.4	1.2	1.35	1.3	1.1	1.25	1.2	1.0	1.2	1.15
100	1.6	1.54	1.4	1.4	1.44	1.3	1.2	1.29	1.2	1.1	1.19	1.1	1.0	1.14	1.05
200	1.6	1.48	1.3	1.4	1.38	1.2	1.2	1.23	1.1	1.1	1.13	1.0	1.0	1.08	0.95
300	1.6	1.42	1.2	1.4	1.32	1.1	1.2	1.17	1.0	1.1	1.07	0.9	1.0	1.02	0.85
500	1.6	1.37	1.15	1.4	1.27	1.05	1.2	1.12	0.95	1.1	1.02	0.85	1.0	0.97	0.8
1000	1.6	1.32	1.1	1.4	1.22	1.0	1.2	1.07	0.9	1.1	0.97	0.8	1.0	0.92	0.78

b) F_v as a function of soil profile thickness and mapped 1.0 second period spectral acceleration from 2002 USGS hazard maps.

Thickness (m)	Mapped 1.0 sec spectral acceleration from 2002 USGS hazard maps														
	S_1 = 0.1g			S_1 = 0.2g			S_1= 0.3g			S_1= 0.4g			$S_1 \geq$ 0.5g		
	NEHRP	Upper bound [1]	Lower bound [2]	NEHRP	Upper bound [1]	Lower bound [2]	NEHRP	Upper bound [1]	Lower bound [2]	NEHRP	Upper bound [1]	Lower bound [2]	NEHRP	Upper bound [1]	Lower bound [2]
30	2.4	2.4	2.4	2.0	2.0	2.0	1.8	1.8	1.8	1.6	1.7[2]	1.7	1.5	1.6	1.6
100	2.4	2.7	2.5	2.0	2.3	2.1	1.8	2.1	1.9	1.6	2	1.8	1.5	1.9	1.7
200	2.4	2.8	2.6	2.0	2.4	2.2	1.8	2.2	2	1.6	2.1	1.9	1.5	2	1.8
300	2.4	2.9	2.7	2.0	2.5	2.3	1.8	2.3	2.1	1.6	2.2	2	1.5	2.1	1.9
500	2.4	2.95	2.75	2.0	2.55	2.35	1.8	2.35	2.15	1.6	2.25	2.05	1.5	2.15	1.95
1000	2.4	3.0	2.8	2.0	2.6	2.4	1.8	2.4	2.2	1.6	2.3	2.1	1.5	2.2	2

[1] and [2] denote results using ME properties and EPRI properties, respectively.

Note: Use straight-line interpolation for intermediate values of S_S and S_1.

Table 6-3 Recommended site coefficients of the Mississippi embayment for Lowlands.

a) F_a as a function of soil profile thickness and mapped 0.2 second period spectral acceleration from 2002 USGS hazard maps.

Thickness (m)	Mapped 0.2 sec spectral acceleration from 2002 USGS hazard maps														
	S_s = 0.25g			**S_s = 0.50g**			**S_s = 0.75g**			**S_s = 1.0g**			**$S_s \geq$ 1.25g**		
	NEHRP	Upper bound [2]	Lower bound [1]	NEHRP	Upper bound [2]	Lower bound [1]	NEHRP	Upper bound [2]	Lower bound [1]	NEHRP	Upper bound [2]	Lower bound [1]	NEHRP	Upper bound [2]	Lower bound [1]
30	1.6	1.5	1.4	1.4	1.4	1.3	1.2	1.3	1.2	1.1	1.2	1.1	1.0	1.15	1.0
100	1.6	1.44	1.3	1.4	1.34	1.2	1.2	1.24	1.1	1.1	1.14	1.0	1.0	1.09	0.9
200	1.6	1.38	1.2	1.4	1.28	1.1	1.2	1.18	1.0	1.1	1.08	0.9	1.0	1.03	0.8
300	1.6	1.32	1.1	1.4	1.22	1.0	1.2	1.12	0.9	1.1	1.02	0.8	1.0	0.97	0.7
500	1.6	1.27	1.05	1.4	1.17	0.95	1.2	1.07	0.85	1.1	0.97	0.75	1.0	0.92	0.65
1000	1.6	1.22	1.0	1.4	1.12	0.9	1.2	1.02	0.8	1.1	0.92	0.7	1.0	0.87	0.6

b) F_v as a function of soil profile thicknes and mapped 1.0 second period spectral acceleration from 2002 USGS hazard maps.

Thickness (m)	Mapped 1.0 sec spectral acceleration from 2002 USGS hazard maps														
	S_1 = 0.1g			**S_1 = 0.2g**			**S_1= 0.3g**			**S_1= 0.4g**			**$S_1 \geq$ 0.5g**		
	NEHRP	Upper bound [1]	Lower bound [2]	NEHRP	Upper bound [1]	Lower bound [2]	NEHRP	Upper bound [1]	Lower bound [2]	NEHRP	Upper bound [1]	Lower bound [2]	NEHRP	Upper bound [1]	Lower bound [2]
30	2.4	2.5	2.5	2.0	2.1	2.1	1.8	1.9	1.9	1.6	1.8	1.8	1.5	1.7	1.7
100	2.4	2.8	2.6	2.0	2.4	2.2	1.8	2.2	2	1.6	2.1	1.9	1.5	2	1.8
200	2.4	2.9	2.7	2.0	2.6	2.3	1.8	2.3	2.1	1.6	2.2	2	1.5	2.1	1.9
300	2.4	3.0	2.8	2.0	2.7	2.4	1.8	2.4	2.2	1.6	2.3	2.1	1.5	2.2	2
500	2.4	3.05	2.85	2.0	2.75	2.45	1.8	2.45	2.25	1.6	2.35	2.15	1.5	2.25	2.05
1000	2.4	3.1	2.9	2.0	2.8	2.5	1.8	2.5	2.3	1.6	2.4	2.2	1.5	2.3	2.1

[1] and [2] denote results using ME properties and EPRI properties, respectively.

Note: Use straight-line interpolation for intermediate values of S_S and S_1.

Table 6-4 Functions of the recommended embayment thickness dependent site coefficients of the Mississippi embayment.

F_a		
Thickness Range	Upper bound[2]	Lower bound[1]
Up to 30 m	F_{a30m}	F_{a30m}
30 m – 300 m	F_{a30m} -0.0006 d	F_{a30m} - 0.001d
300 – 500 m	F_{a30m} -0.18-0.00025(d-300)	F_{a30m} -0.3-0.00025(d-300)
500 – 1000 m	F_{a30m} -0.23-0.0001(d-500)	F_{a30m} -0.35-0.0001(d-500)

F_v		
Thickness Range	Upper bound[1]	Lower bound[2]
Up to 30 m	F_{v30m}	F_{v30m}
30 m – 100 m	F_{v30m} +0.003d	F_{v30m} +0.001d
100 m – 300 m	F_{v30m} +0.3+0.001(d-100)	F_{v30m} ++0.1+0.001(d-100)
300 – 500 m	F_{v30m} +0.5+0.00025(d-300)	F_{v30m} +0.3+0.00025(d-300)
500 – 1000 m	F_{v30m} +0.55+0.0001(d-500)	F_{v30m} +0.35+0.0001(d-500)

[1] and [2] denote results using ME properties and EPRI properties, respectively.
d = thickness (m)
Note that the functions are same for Uplands and Lowlands.

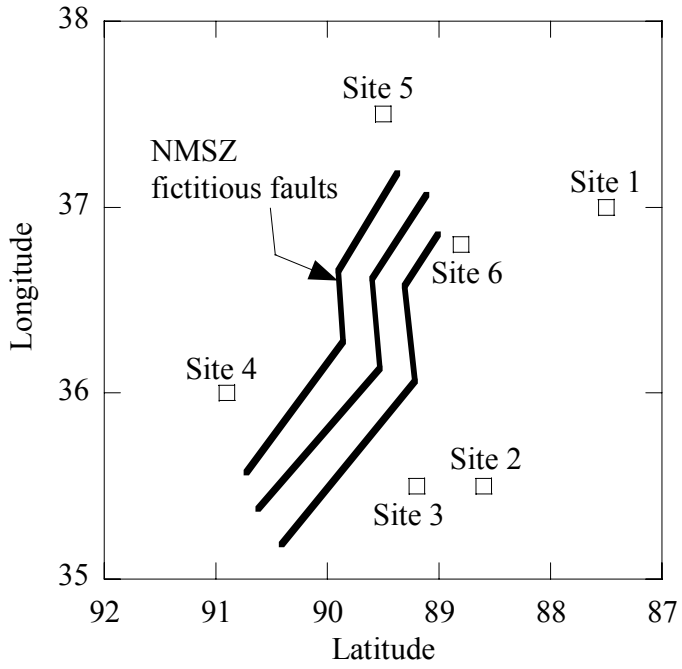

Figure 6-1 Fictitious faults representing NMSZ and selected locations in the Mississippi embayment for PSHA.

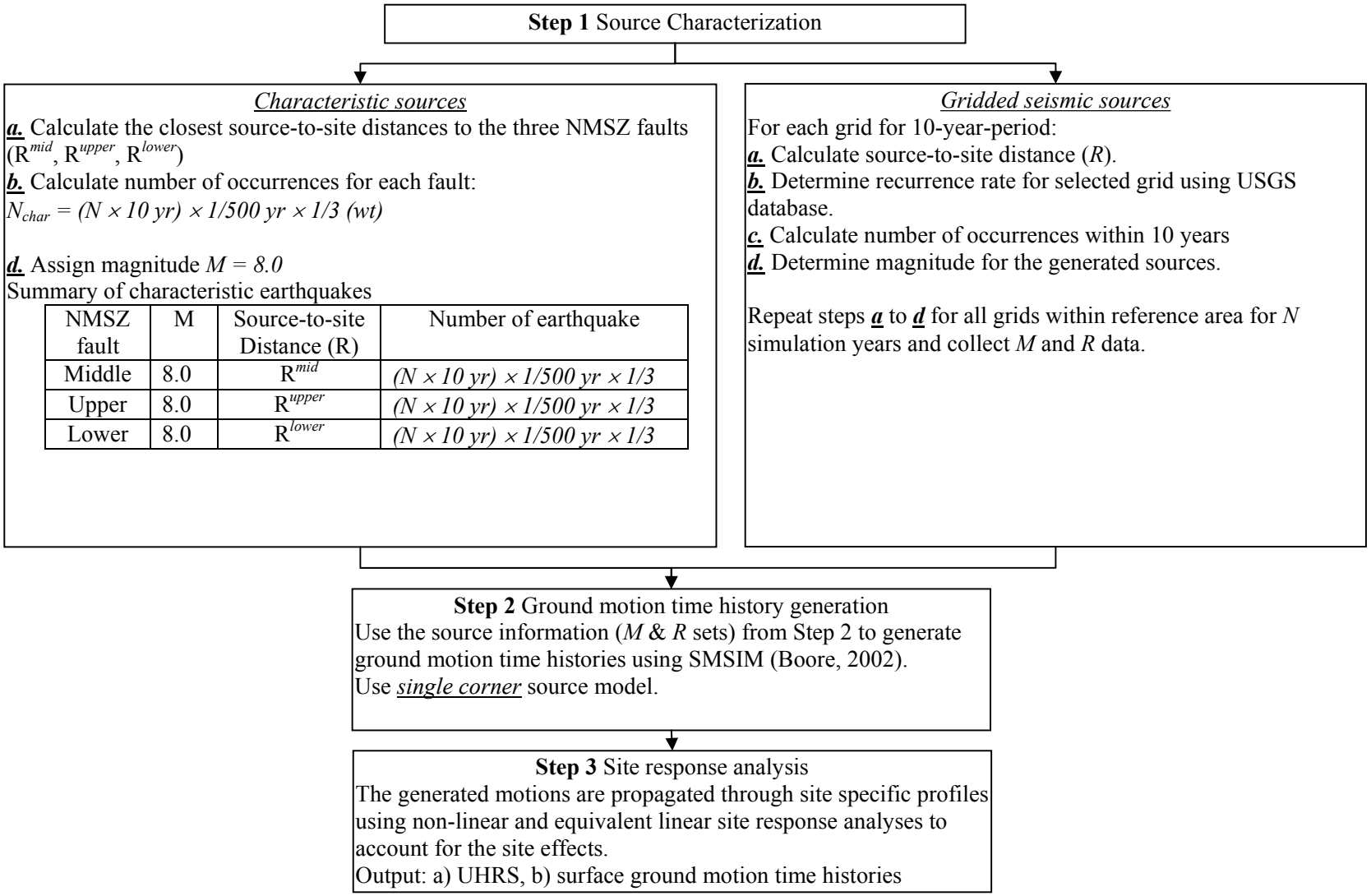

Figure 6-2 Flowchart to approximate 1996 USGS hazard maps and perform PSHA-NL.

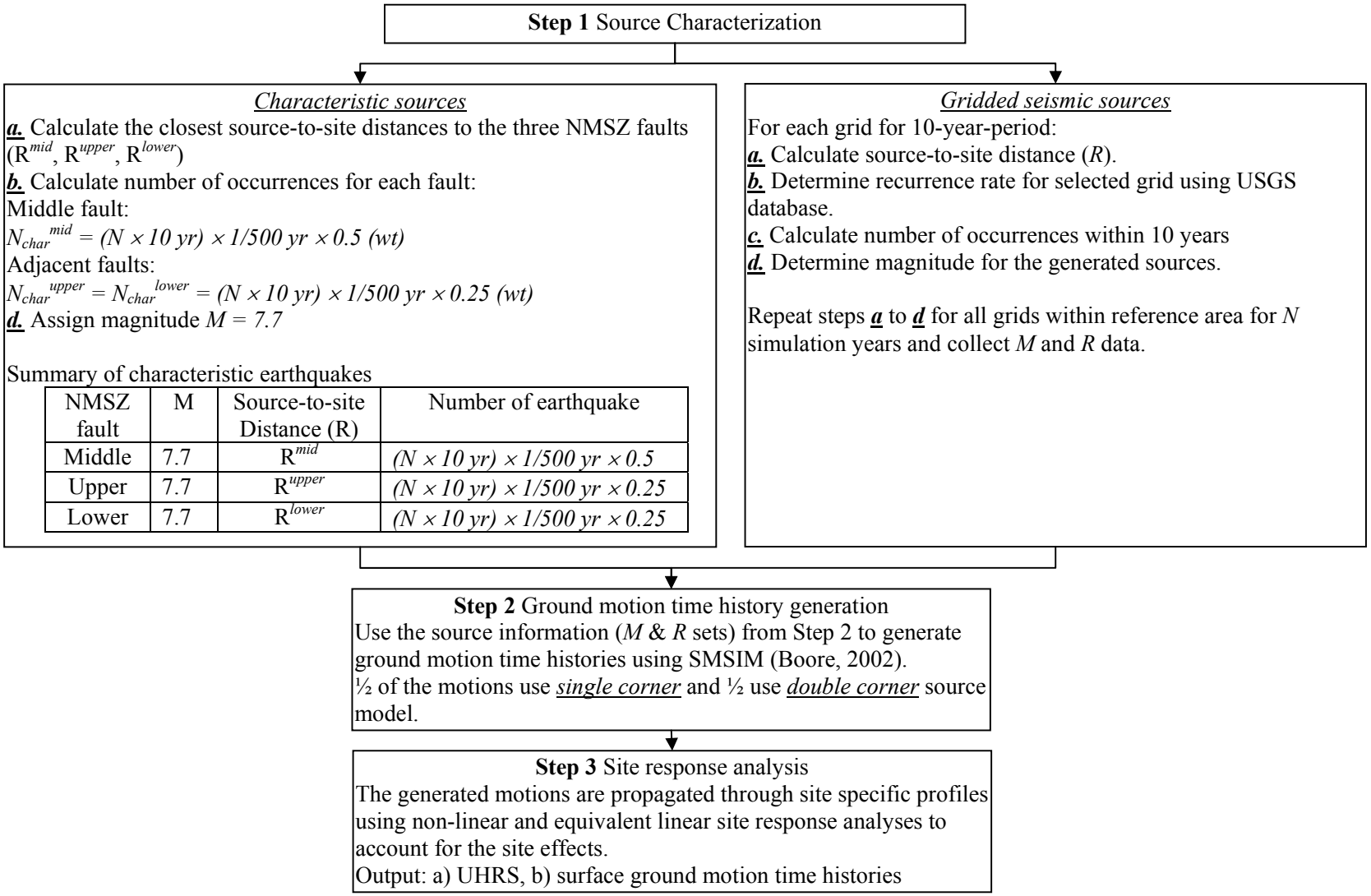

Figure 6-3 Flowchart to approximate 2002 USGS hazard maps and perform PSHA-NL.

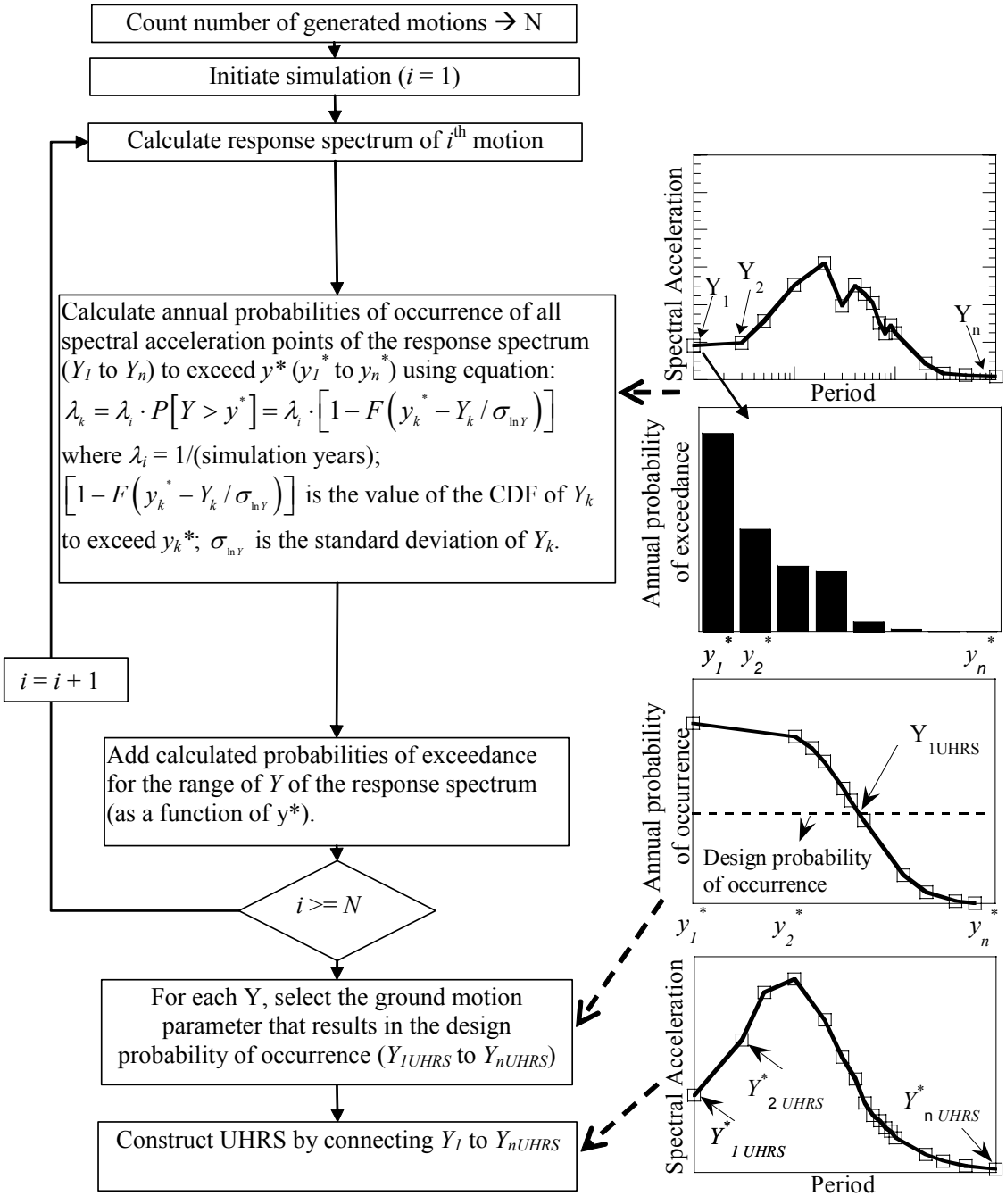

Figure 6-4 Flowchart for calculating UHRS.

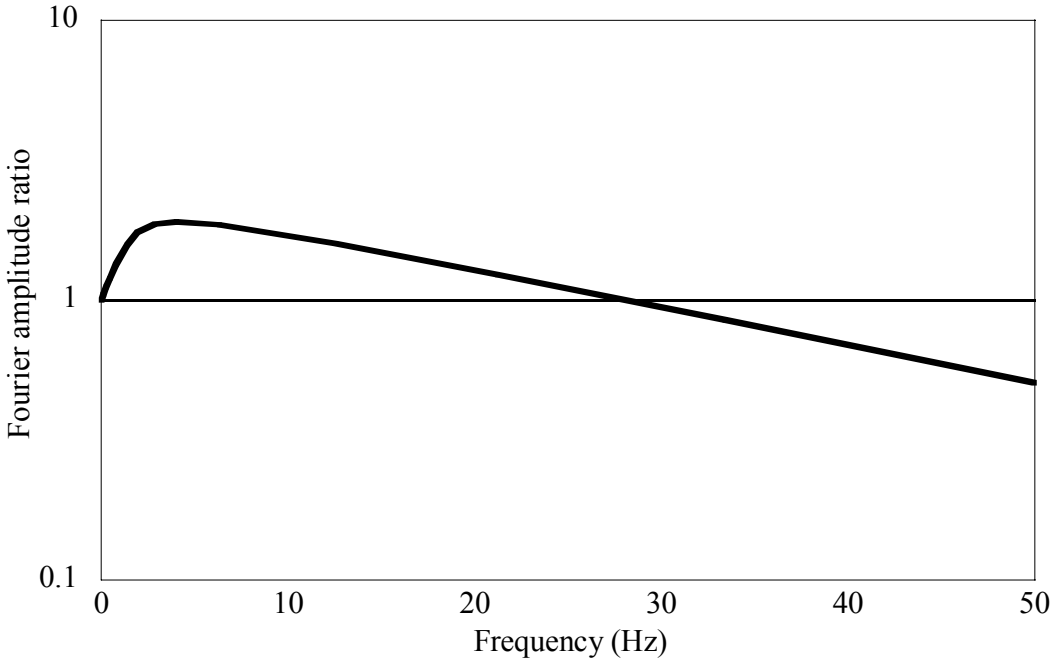

Figure 6-5 Fourier amplification function to convert hard rock to B/C boundary motions (Frankel et al., 2002).

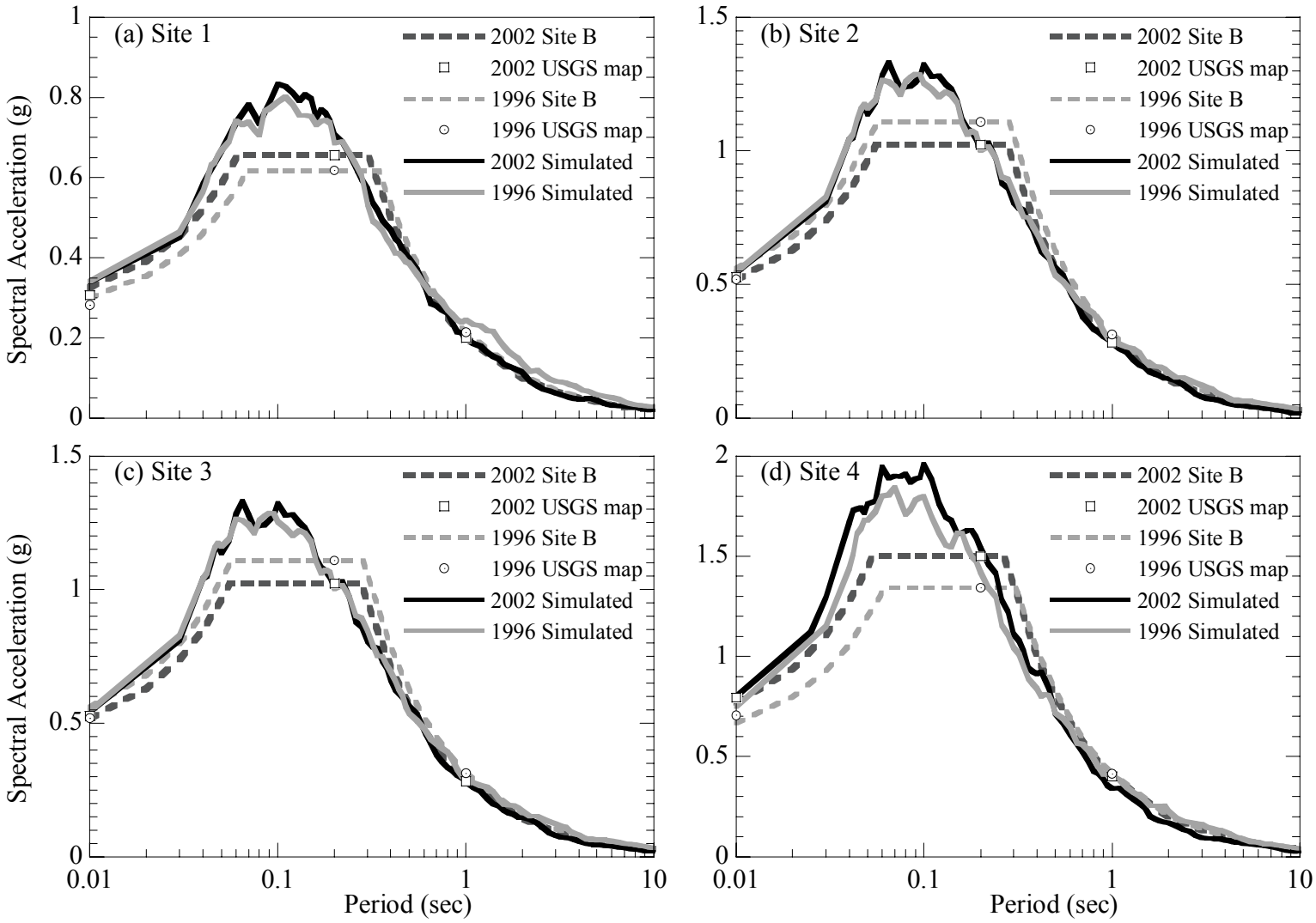

Figure 6-6 Comparison of 2% probability of exceedance in 50 years simulated UHRS at B/C boundary with 1996 and 2002 USGS hazard maps: a) Site 1, b) Site 2, c) Site 3, d) Site 4.

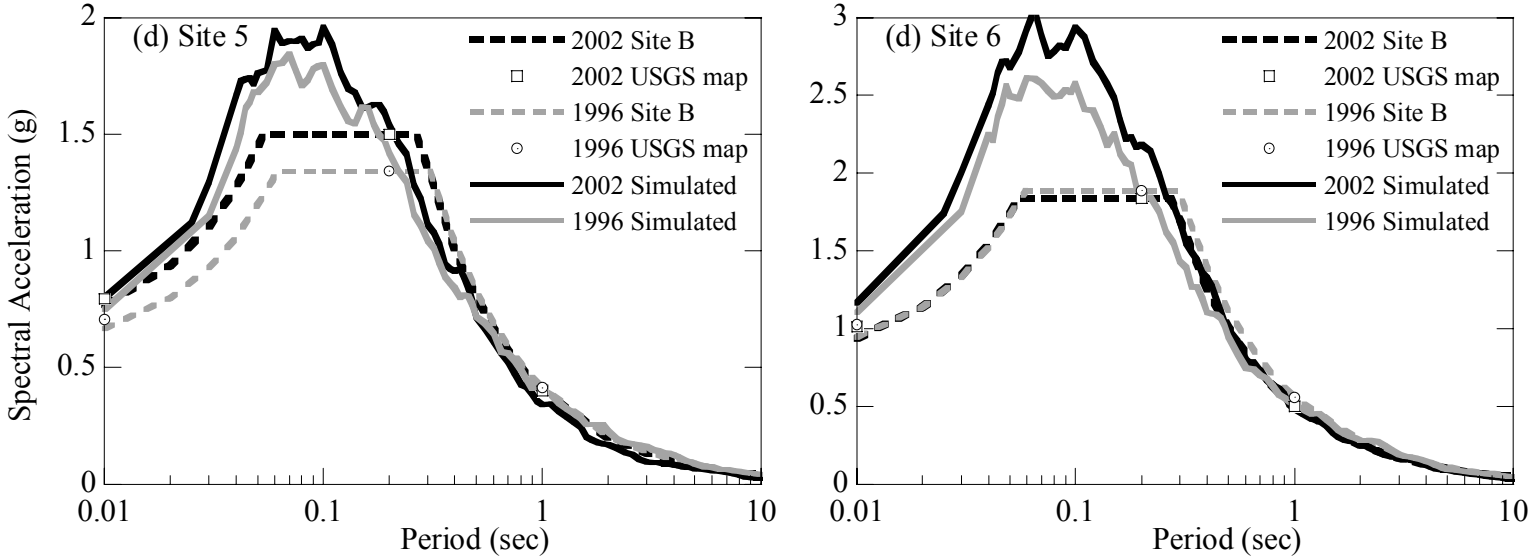

Figure 6-7 Comparison of 2% probability of exceedance in 50 years simulated UHRS at B/C boundary with 1996 and 2002 USGS hazard maps: a) Site 5 and b) Site 6.

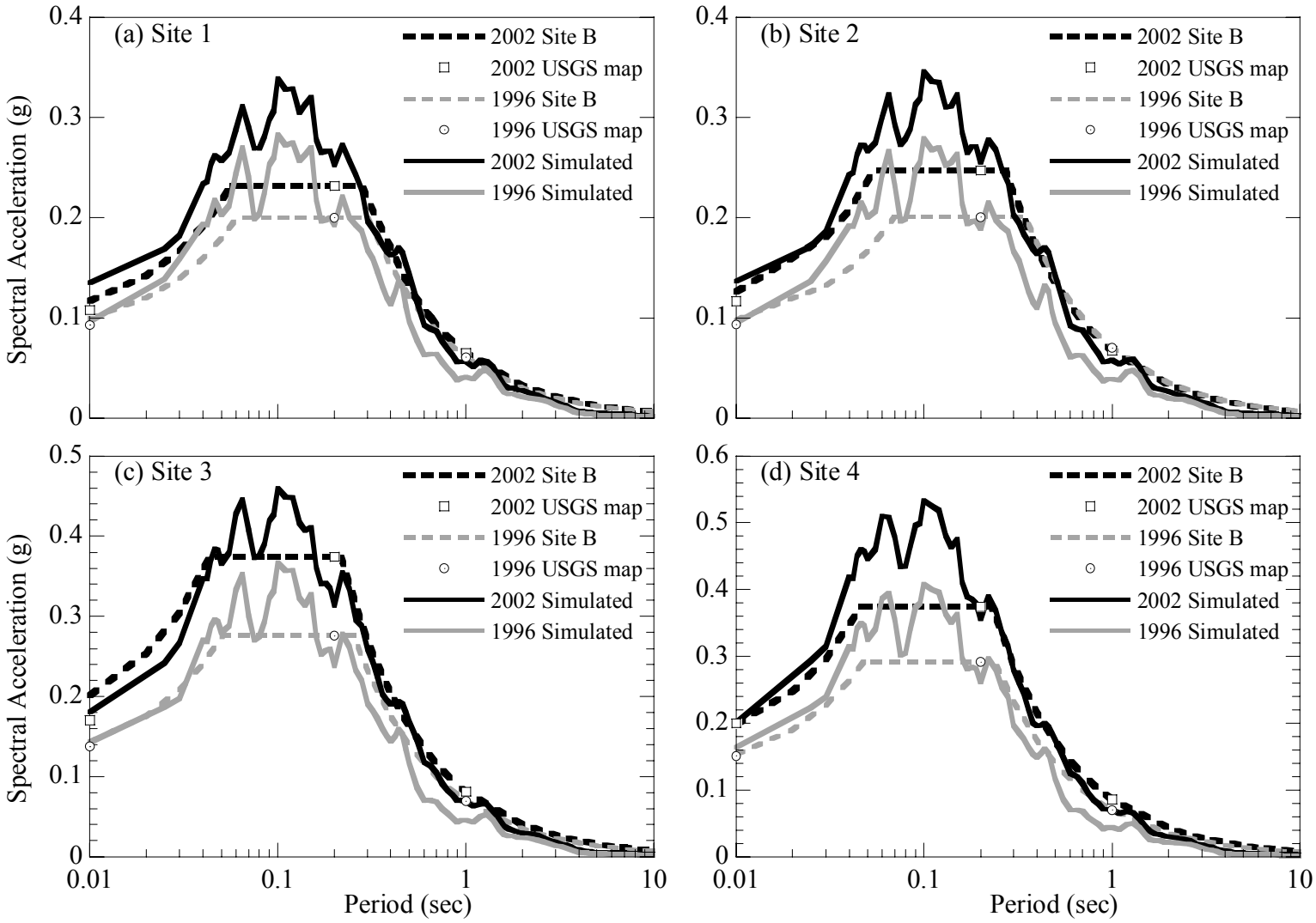

Figure 6-8 Comparison of 10% probability of exceedance in 50 years simulated UHRS at B/C boundary with 1996 and 2002 USGS hazard maps: a) Site 1, b) Site 2, c) Site 3, d) Site 4.

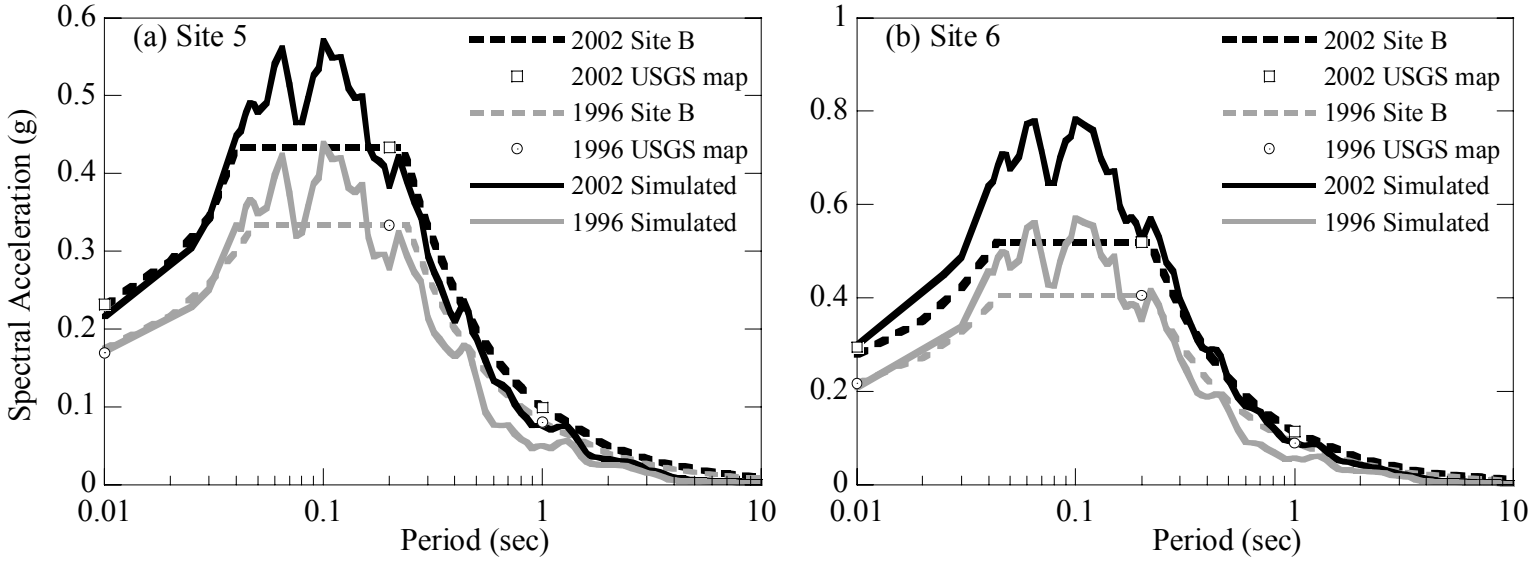

Figure 6-9 Comparison of 10% probability of exceedance in 50 years simulated UHRS at B/C boundary with 1996 and 2002 USGS hazard maps: a) Site 5 and b) Site 6.

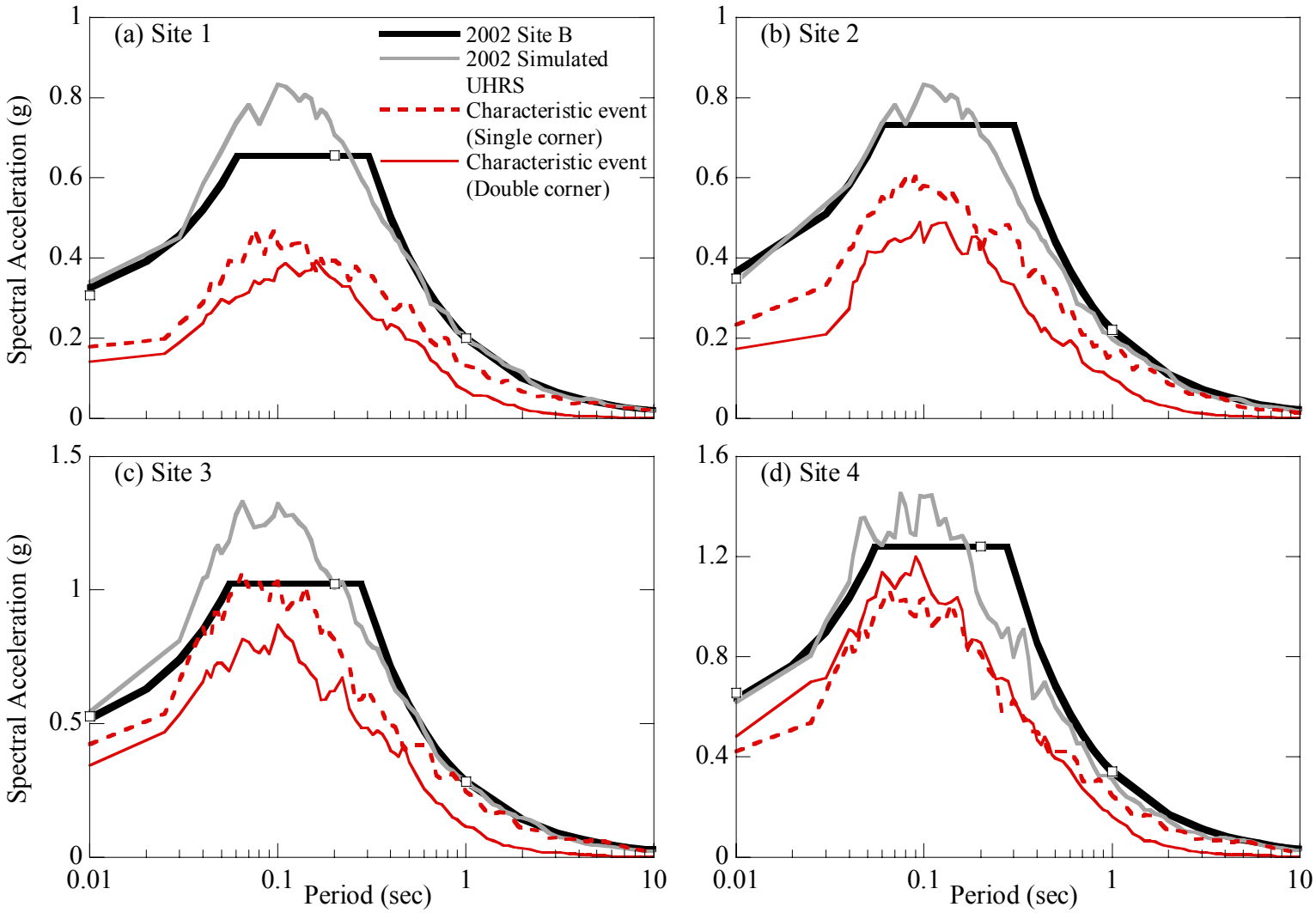

Figure 6-10 Comparison of UHRS with the characteristic scenario which has the highest contribution to the 2% probability of exceedance in 50 years hazard (equivalent to characteristic earthquake): a) Site 1, b) Site 2, c) Site 3, d) Site 4.

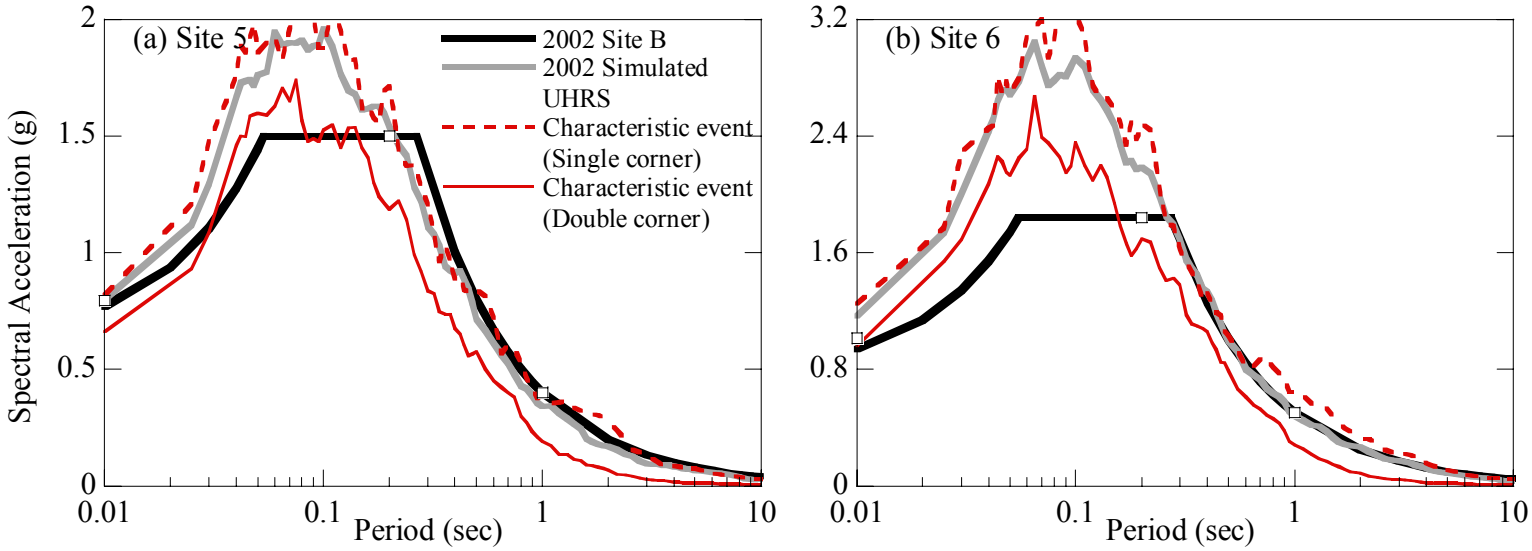

Figure 6-11 Comparison of UHRS with the deterministic scenario which has the highest contribution to the 2% probability of exceedance in 50 years hazard (equivalent to characteristic earthquake): a) Site 5, b) Site 6.

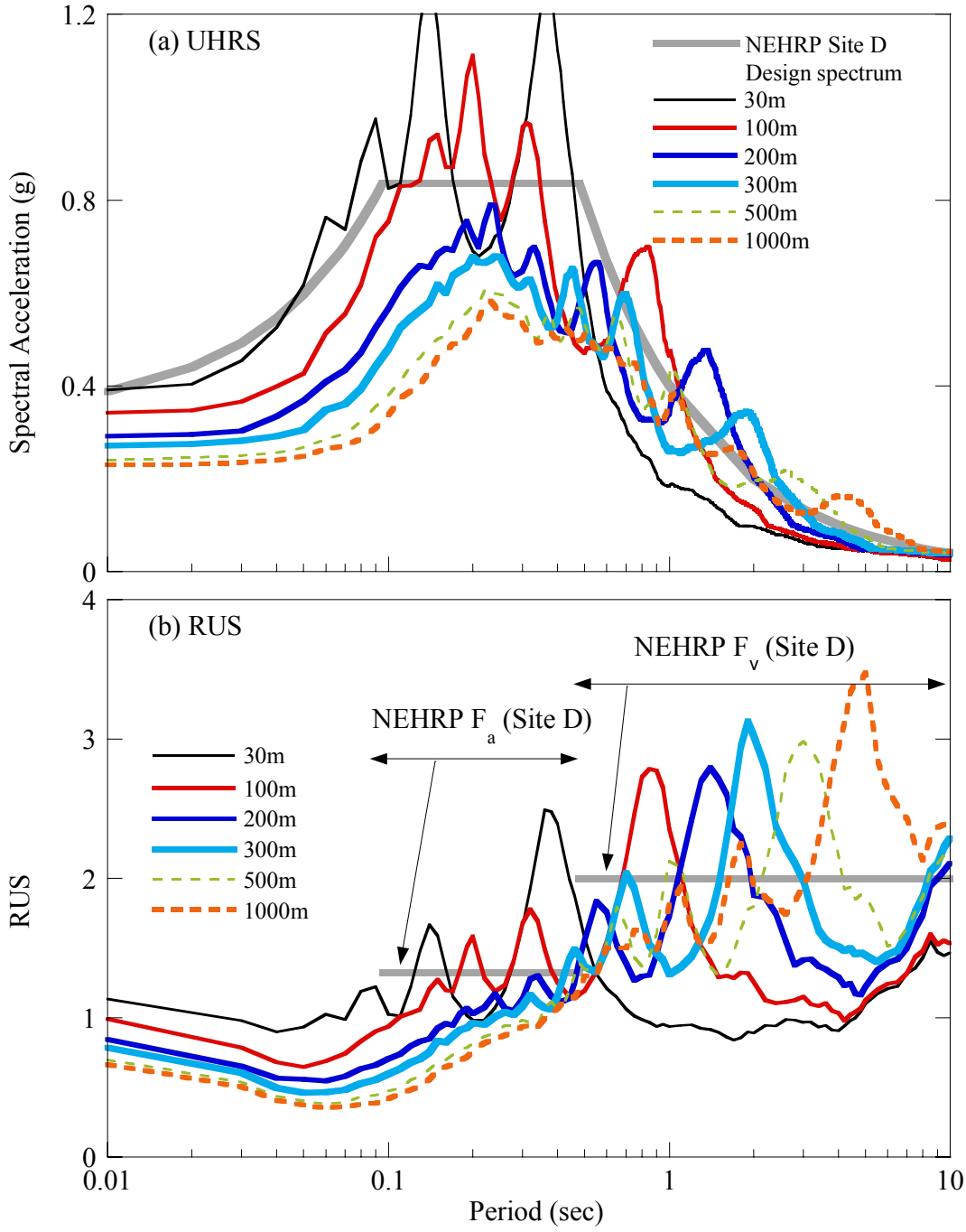

Figure 6-12 Site 1, 2% in 50 years, a) UHRS and b) RUS using Uplands profile / ME properties and six profiles ranging in thickness from 30 m to 1000 m. NEHRP Site D Design response spectrum is shown in thick gray line in plot (a). RUS is ratio of surface UHRS to BC UHRS.

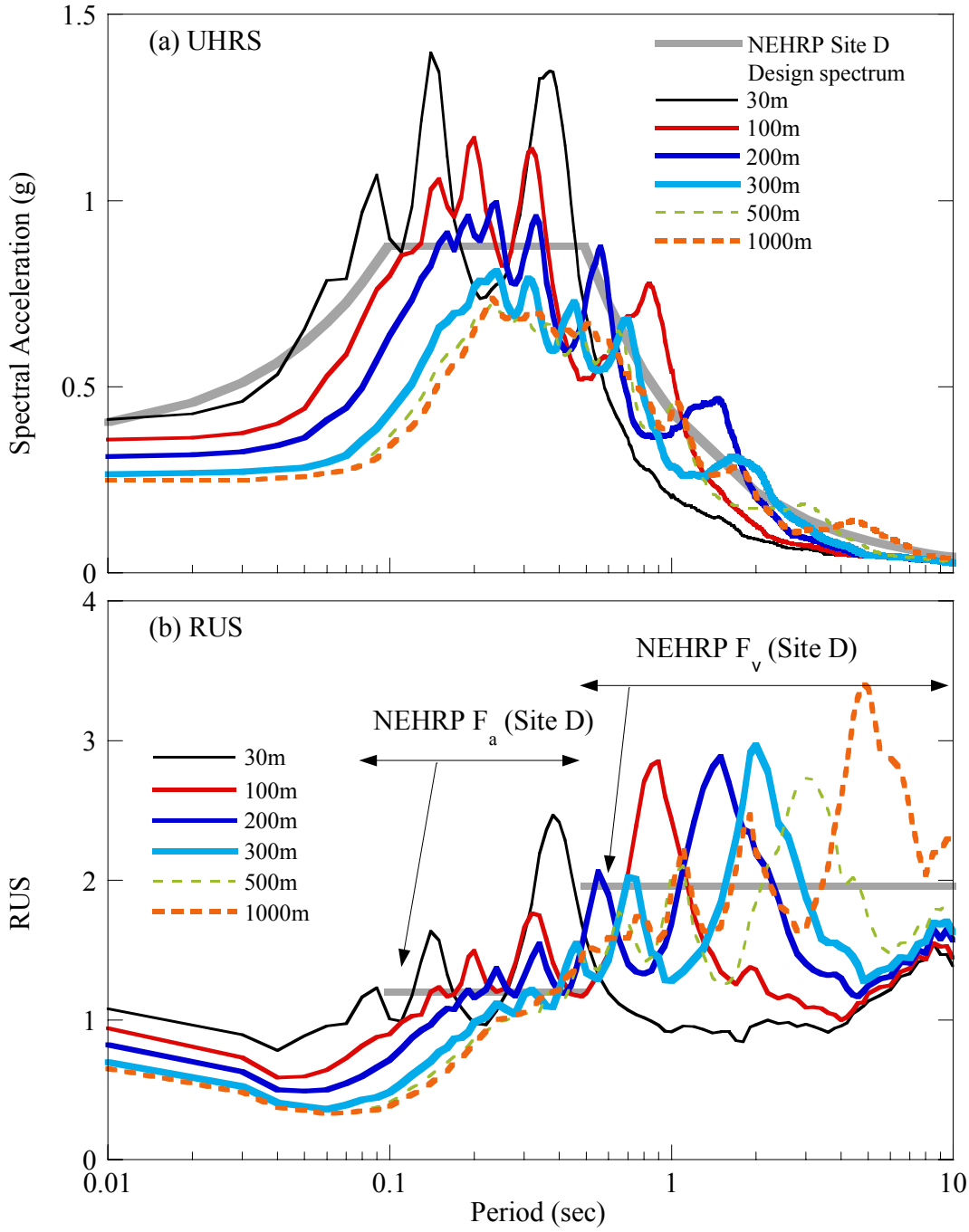

Figure 6-13 Site 2, 2% in 50 years, a) UHRS and b) RUS using Uplands profile / ME properties and six profiles ranging in thickness from 30 m to 1000 m. NEHRP Site D Design response spectrum is shown in thick gray line in plot (a). RUS is ratio of surface UHRS to BC UHRS.

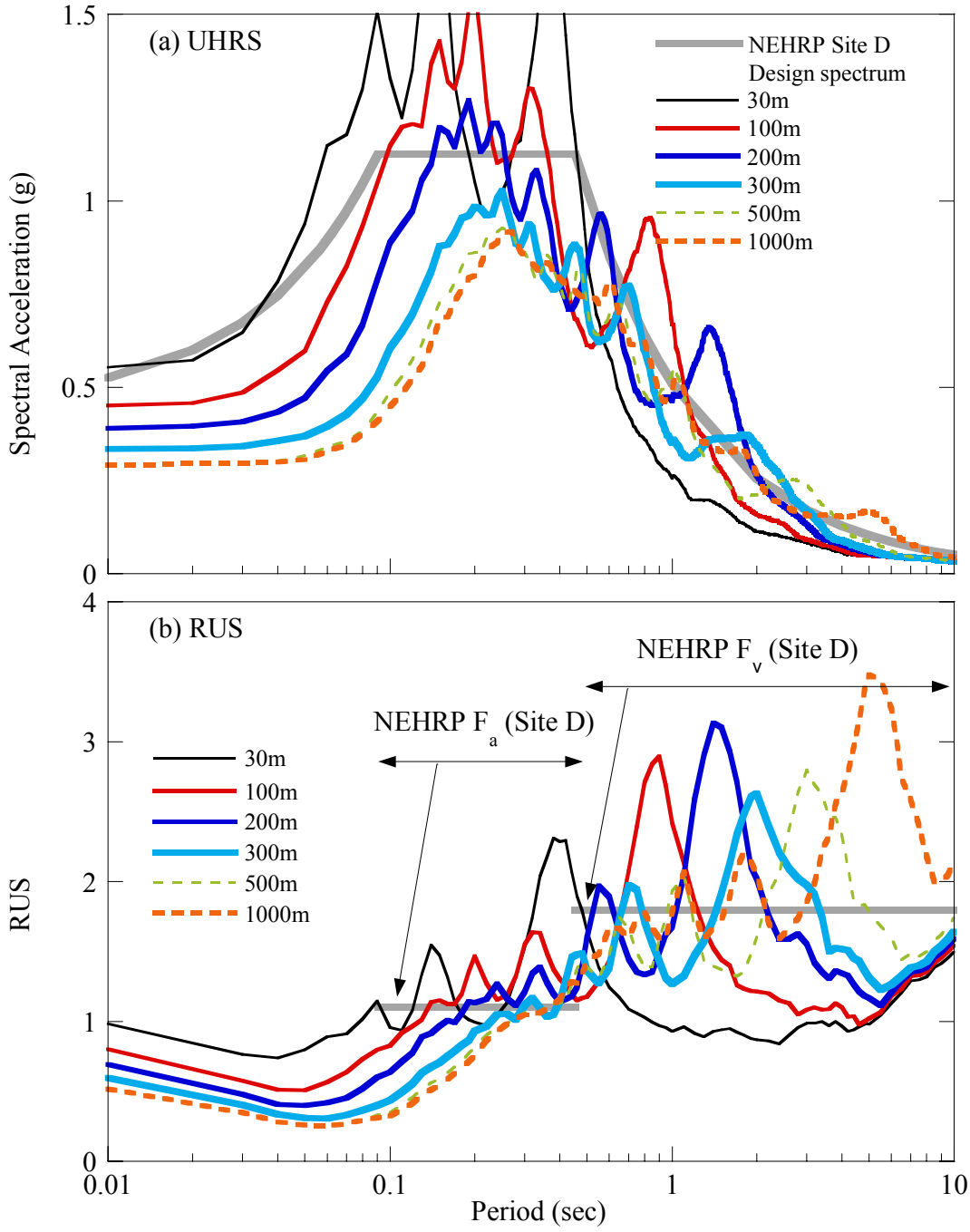

Figure 6-14 Site 3, 2% in 50 years, a) UHRS and b) RUS using Uplands profile / ME properties and six profiles ranging in thickness from 30 m to 1000 m. NEHRP Site D Design response spectrum is shown in thick gray line in plot (a). RUS is ratio of surface UHRS to BC UHRS.

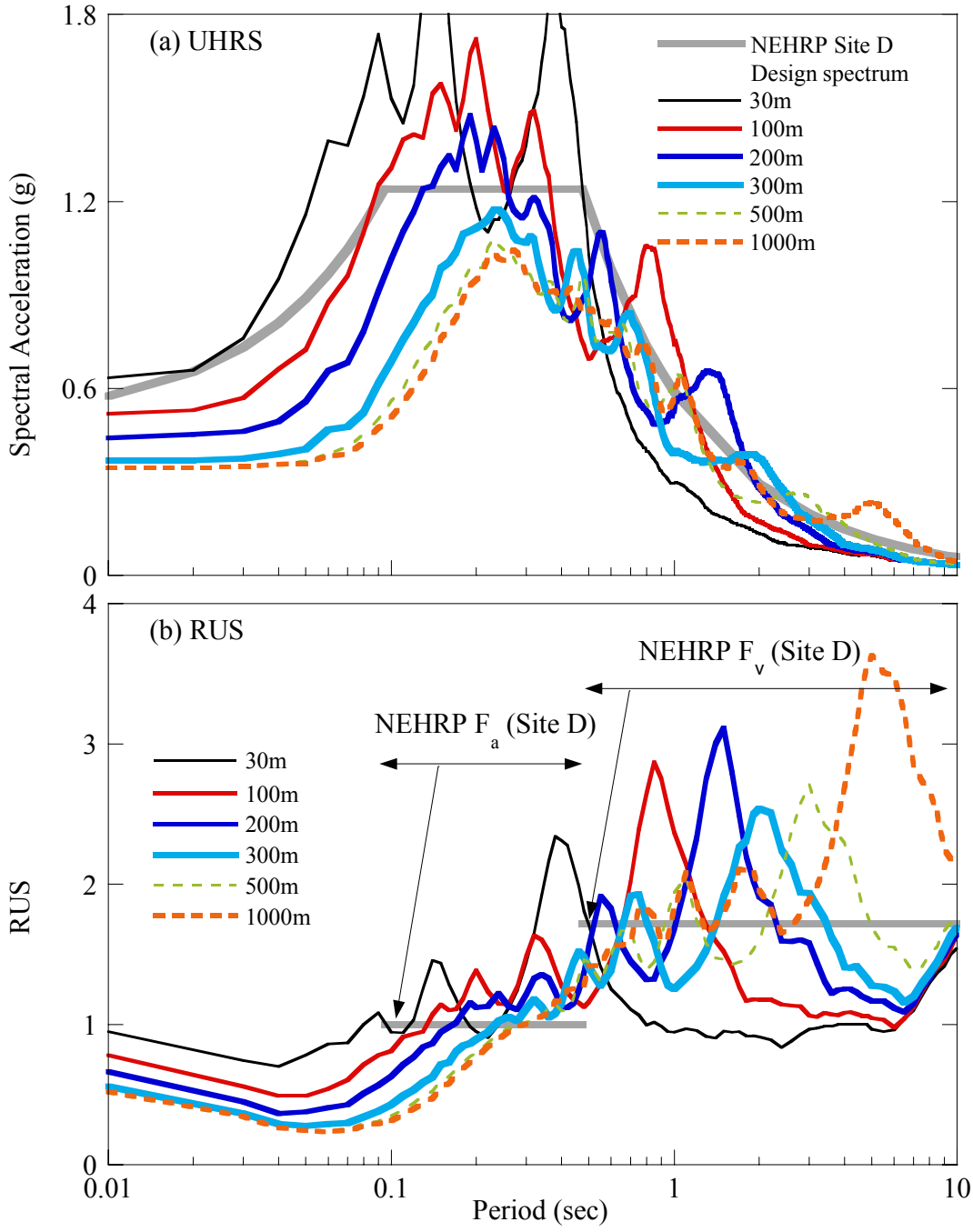

Figure 6-15 Site 4, 2% in 50 years, a) UHRS and b) RUS using Uplands profile / ME properties and six profiles ranging in thickness from 30 m to 1000 m. NEHRP Site D Design response spectrum is shown in thick gray line in plot (a). RUS is ratio of surface UHRS to BC UHRS.

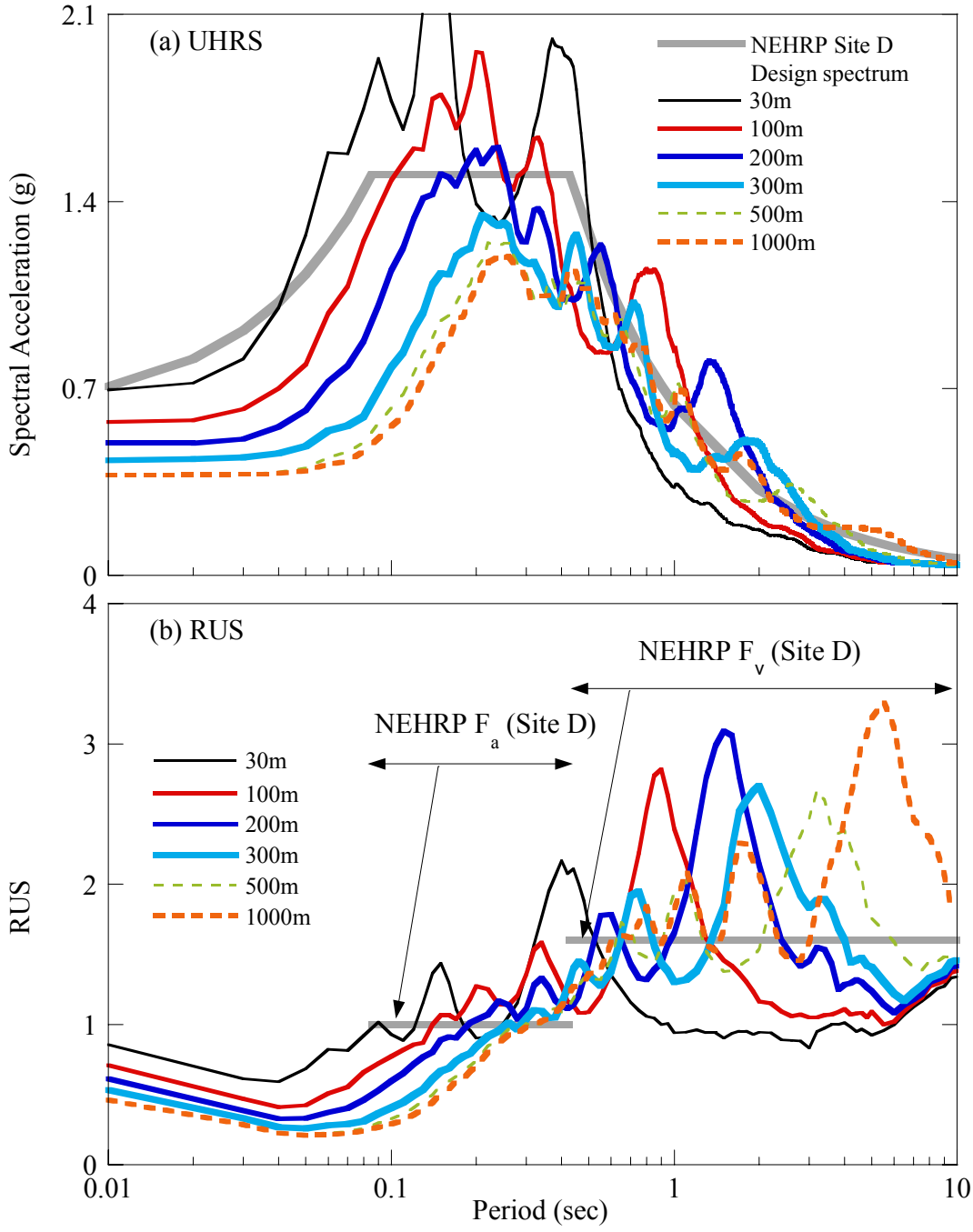

Figure 6-16 Site 5, 2% in 50 years, a) UHRS and b) RUS using Uplands profile / ME properties and six profiles ranging in thickness from 30 m to 1000 m. NEHRP Site D Design response spectrum is shown in thick gray line in plot (a). RUS is ratio of surface UHRS to BC UHRS.

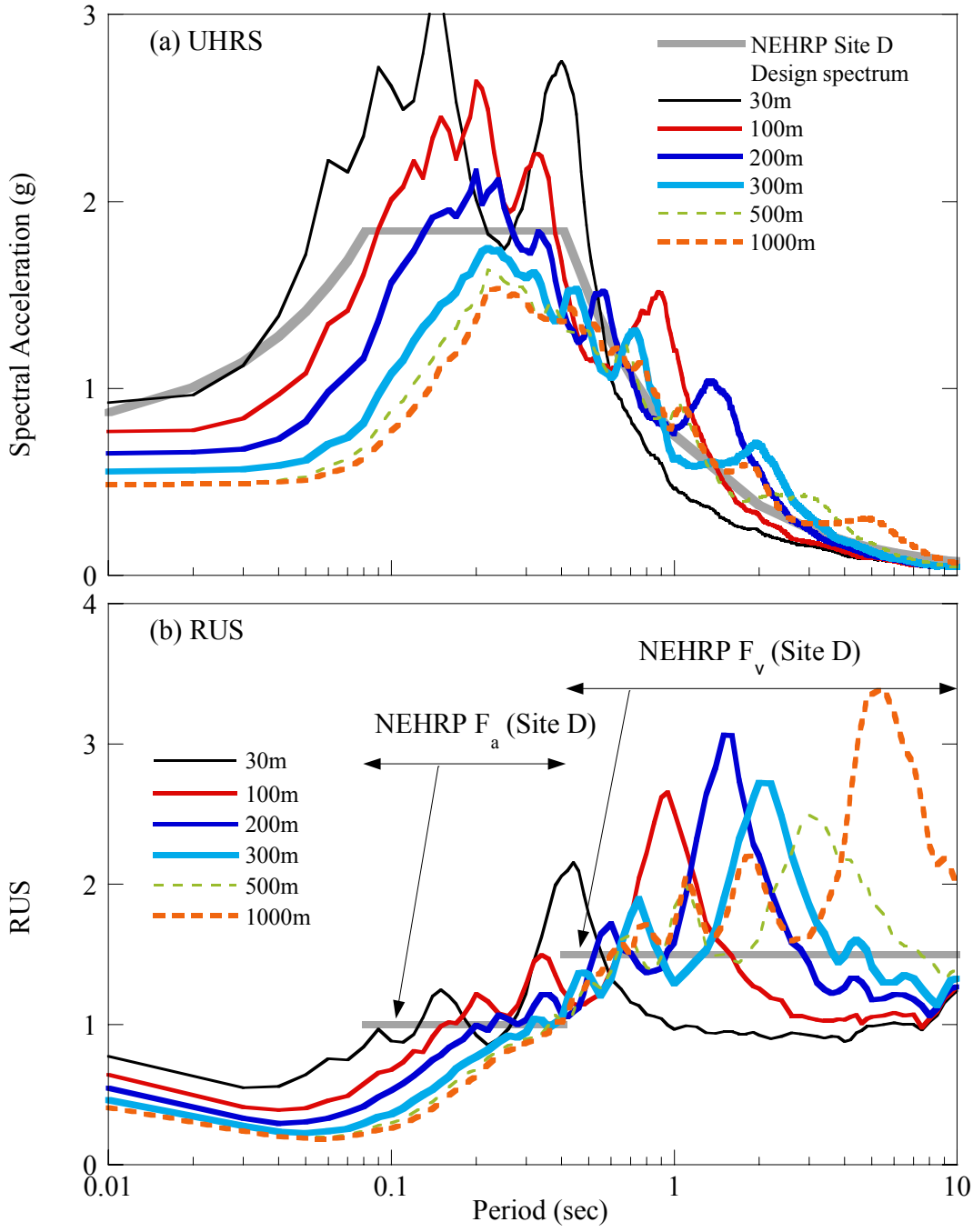

Figure 6-17 Site 6, 2% in 50 years, a) UHRS and b) RUS using Uplands profile / ME properties and six profiles ranging in thickness from 30 m to 1000 m. NEHRP Site D Design response spectrum is shown in thick gray line in plot (a). RUS is ratio of surface UHRS to BC UHRS.

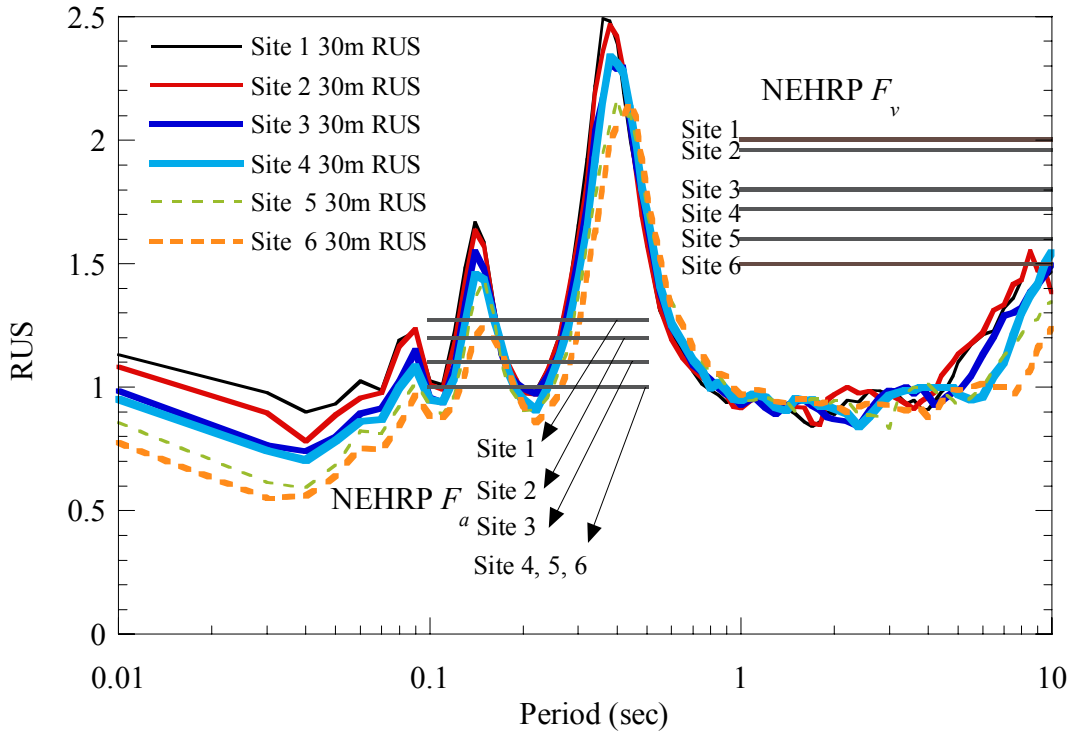

Figure 6-18 Comparison of RUS using 30 m Uplands profile and ME properties vs. NEHRP F_a and F_v for Site 1 to 6.

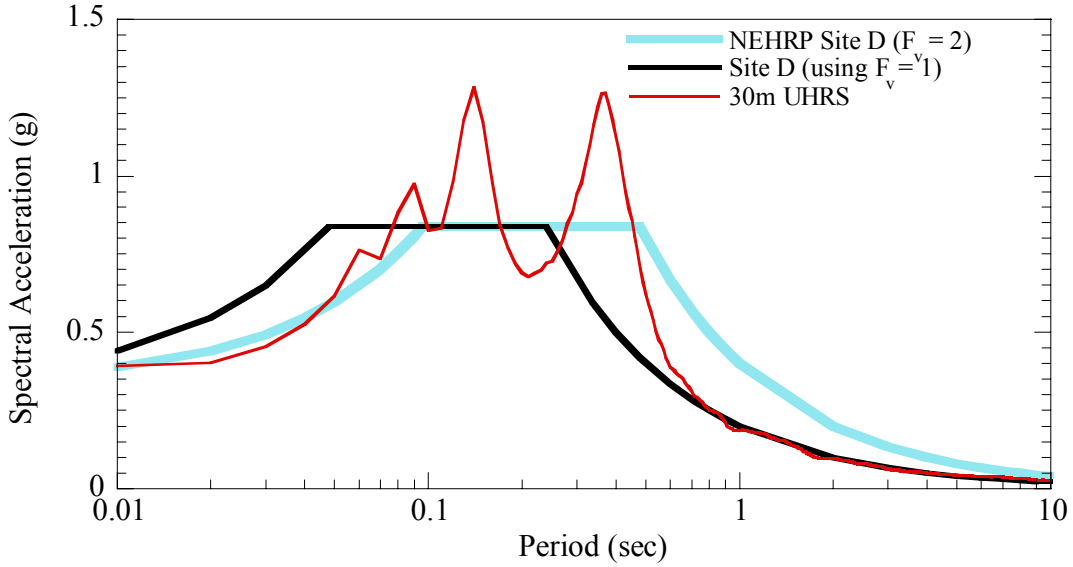

Figure 6-19 Comparison of design spectra using F_v based on S_1 of Site 1 (F_v = 2) and F_v from the simulated RUS (F_v = 1).

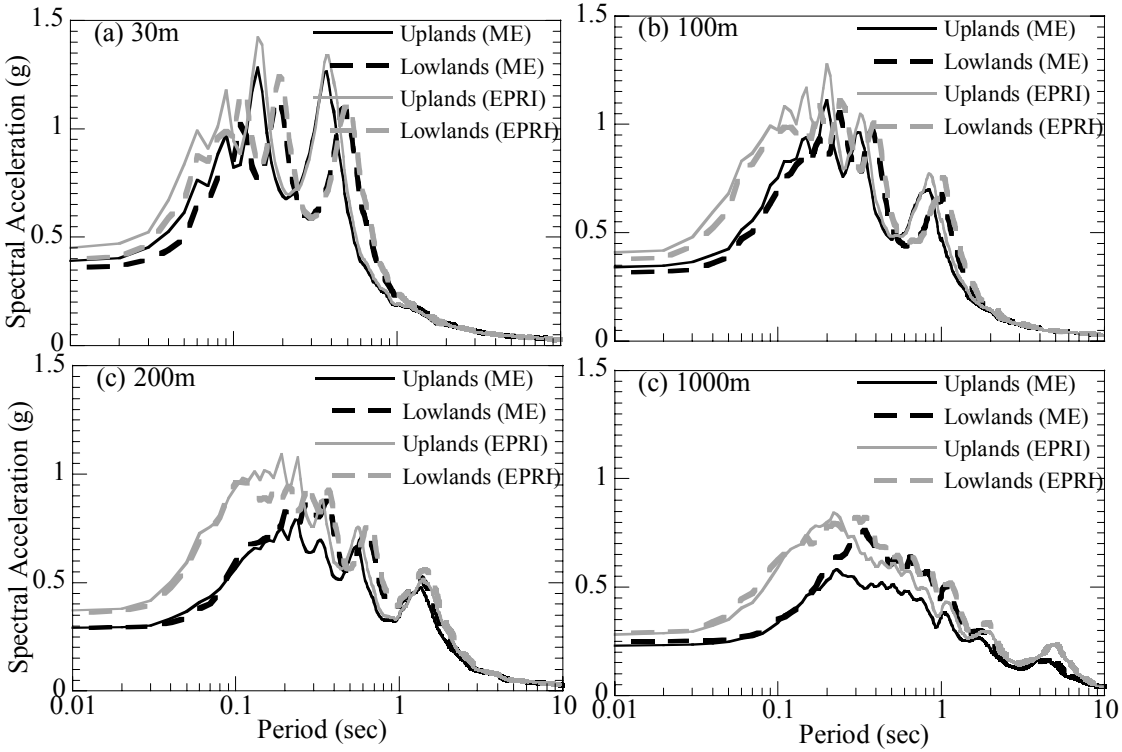

Figure 6-20 Comparison of UHRS (2% in 50 years) for Site 1 using various combinations of Uplands and Lowlands profiles and ME and EPRI soil properties.

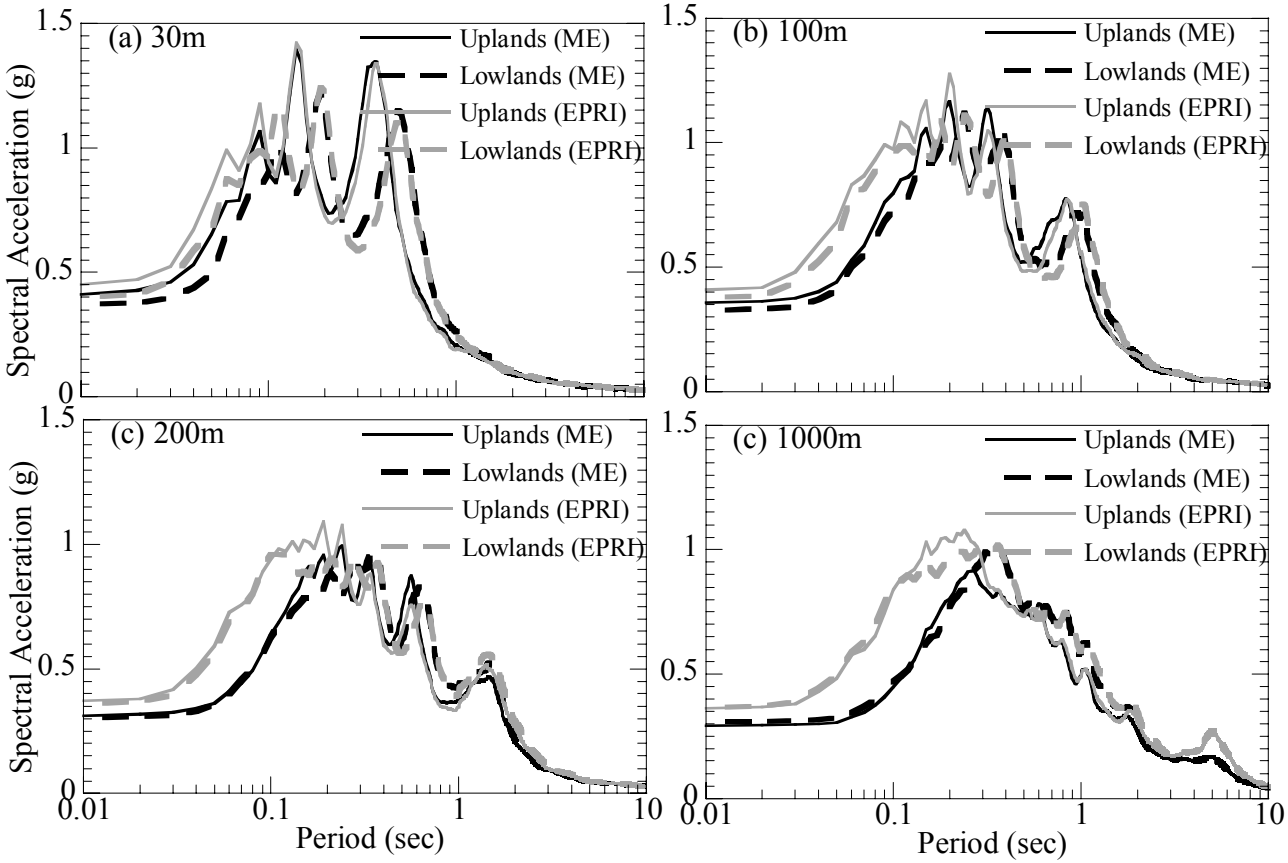

Figure 6-21 Comparison of UHRS (2% in 50 years) for Site 2 using various combinations of Uplands and Lowlands profiles and ME and EPRI soil properties.

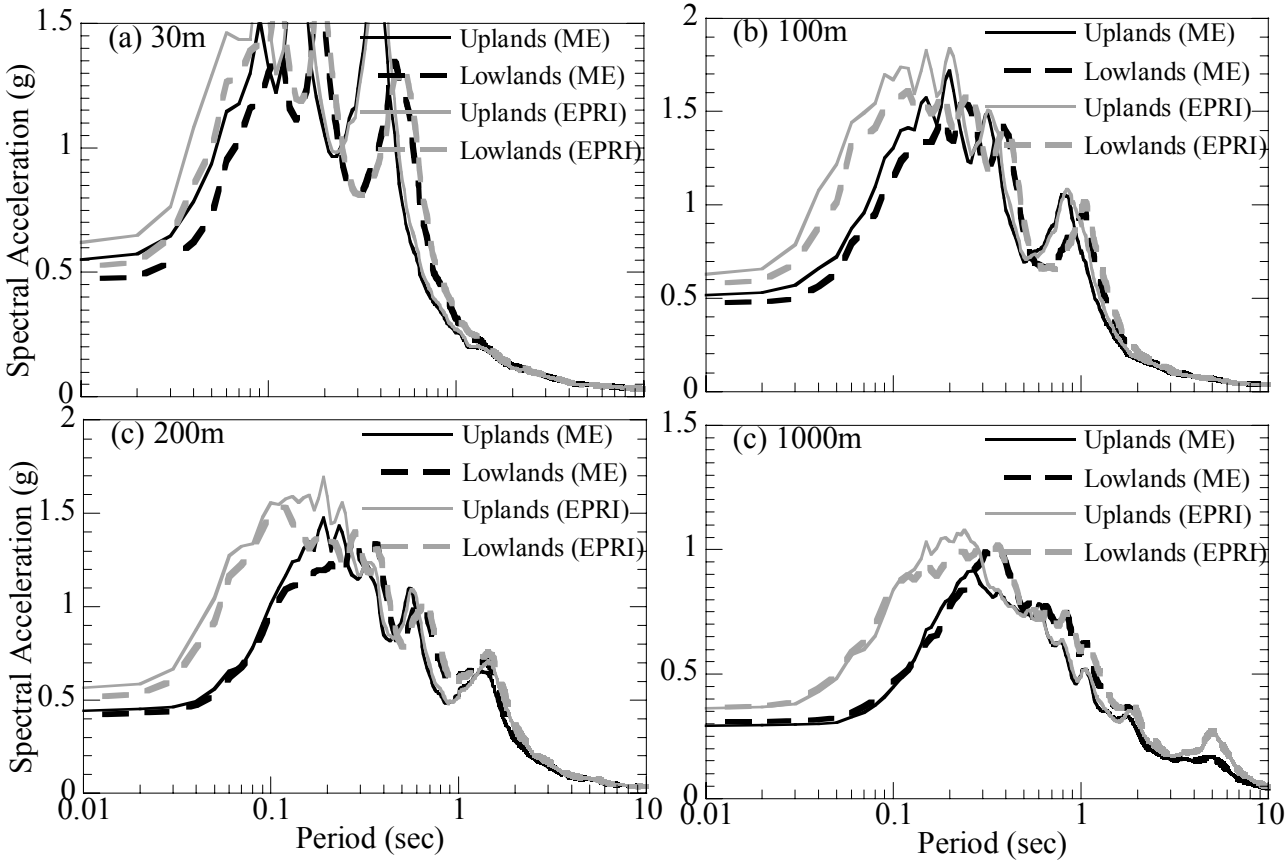

Figure 6-22 Comparison of UHRS (2% in 50 years) for Site 3 using various combinations of Uplands and Lowlands profiles and ME and EPRI soil properties.

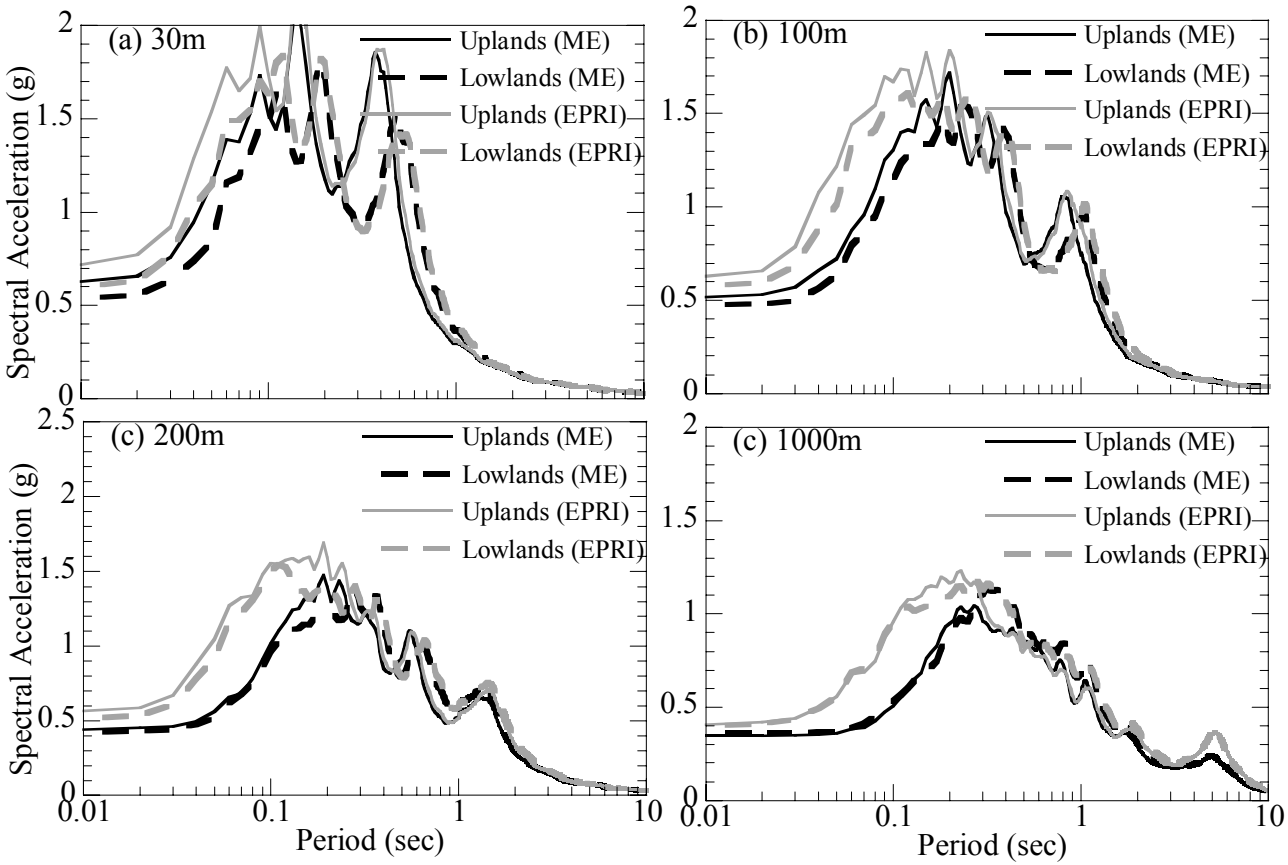

Figure 6-23 Comparison of UHRS (2% in 50 years) for Site 4 using various combinations of Uplands and Lowlands profiles and ME and EPRI soil properties.

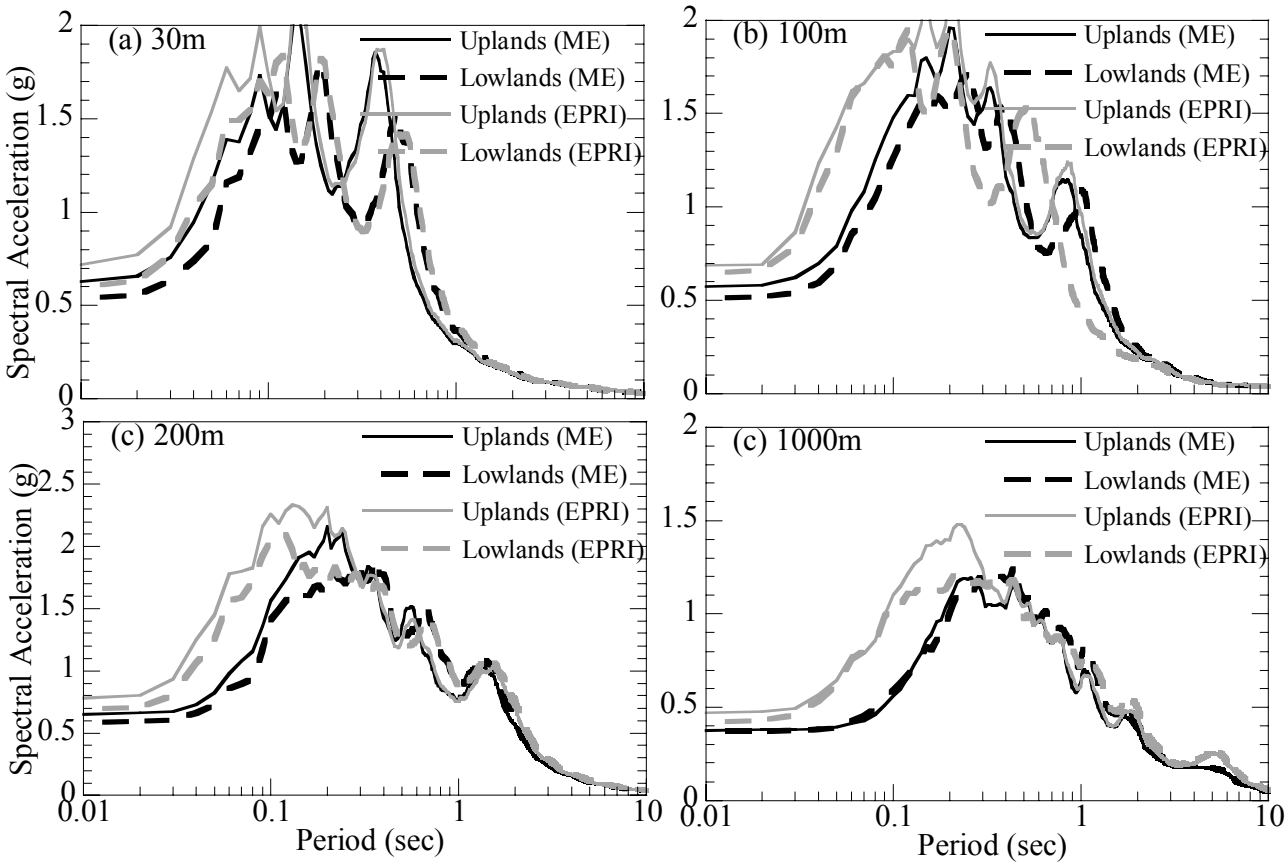

Figure 6-24 Comparison of UHRS (2% in 50 years) for Site 5 using various combinations of Uplands and Lowlands profiles and ME and EPRI soil properties.

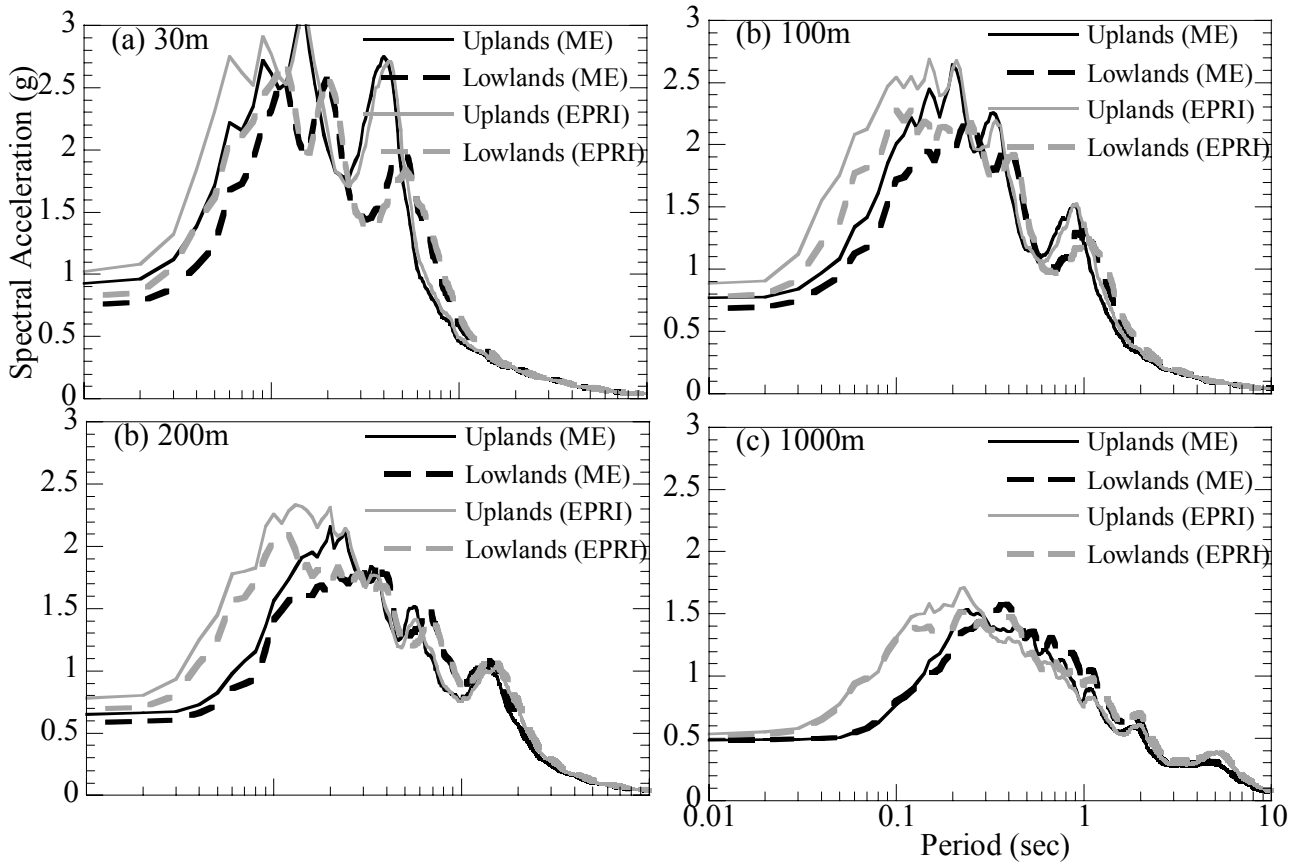

Figure 6-25 Comparison of UHRS (2% in 50 years) for Site 6 using various combinations of Uplands and Lowlands profiles and ME and EPRI soil properties.

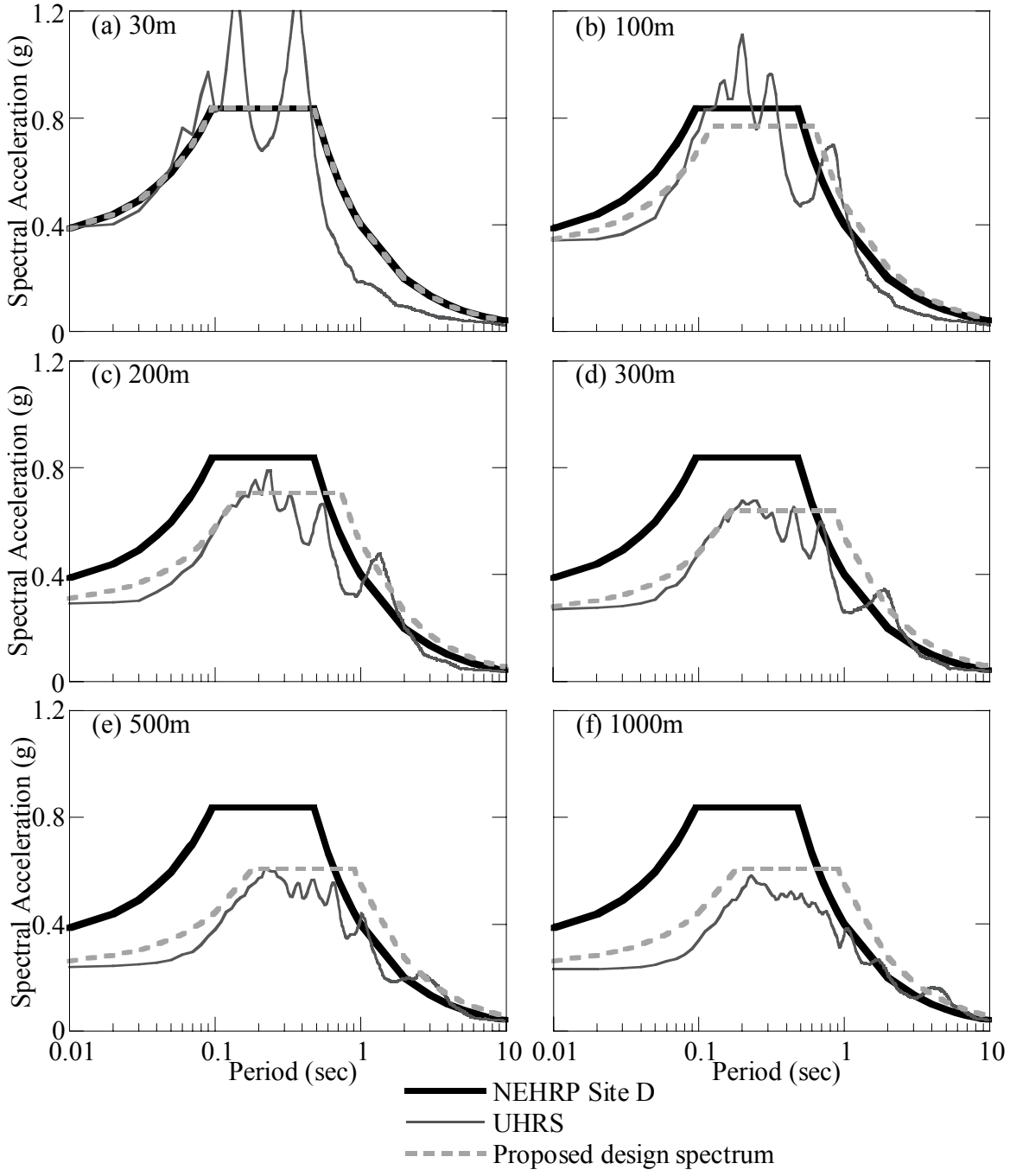

Figure 6-26 UHRS (2% in 50 years) and design spectra with depth dependent site coefficients for Site 1 using Uplands profile and ME dynamic properties.

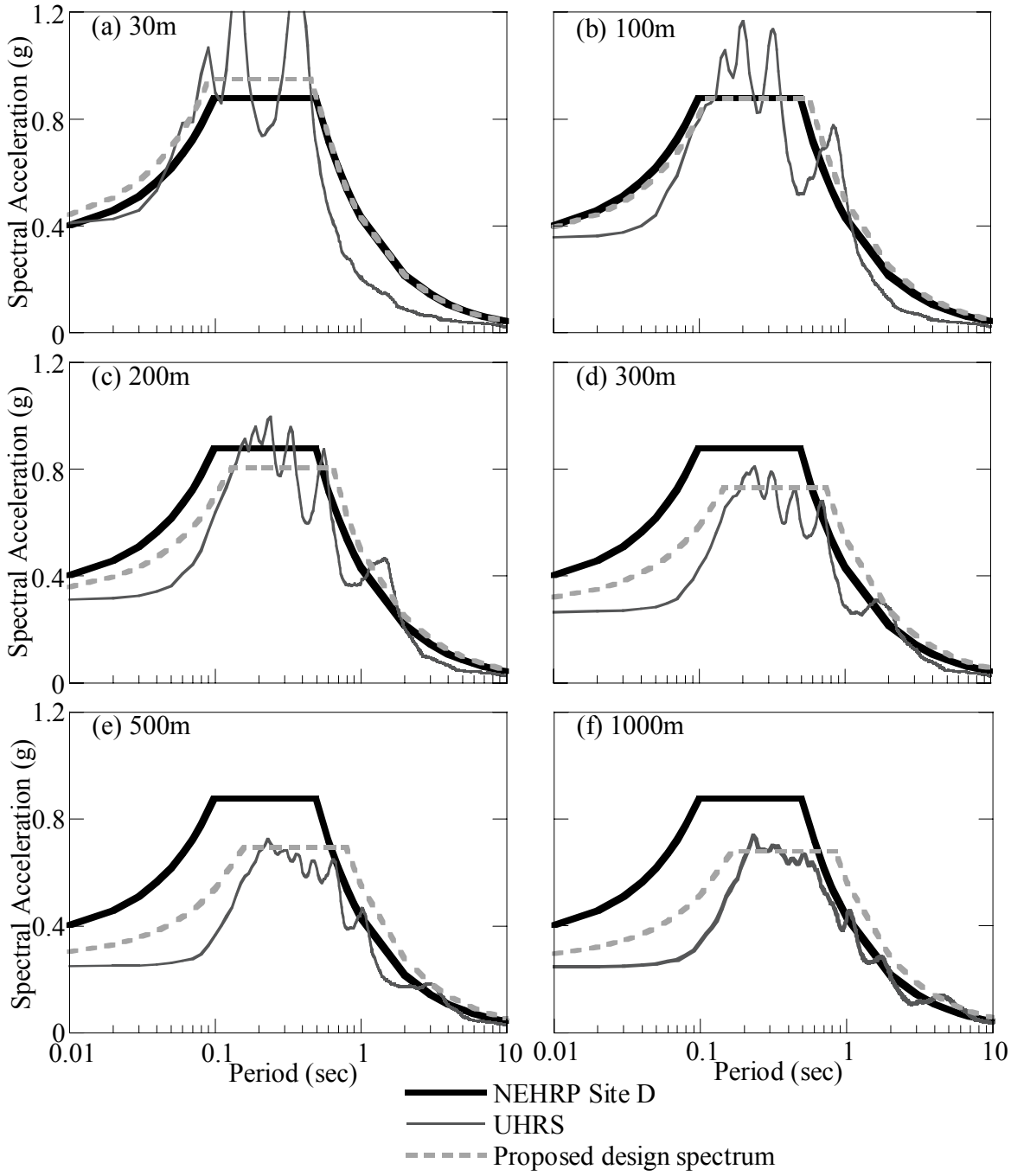

Figure 6-27 UHRS (2% in 50 years) and design spectra with depth dependent site coefficients for Site 2 using Uplands profile and ME dynamic properties.

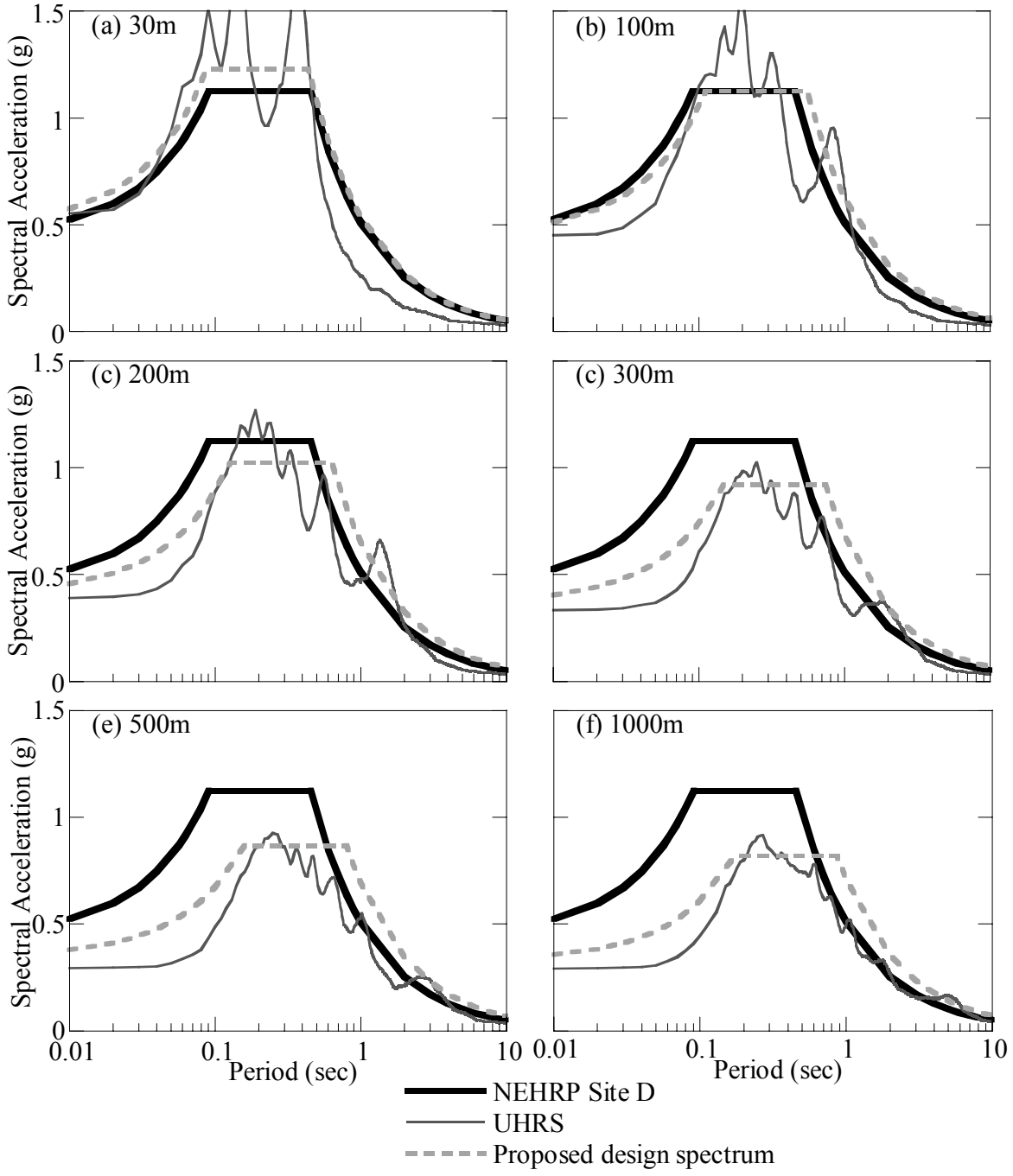

Figure 6-28 UHRS (2% in 50 years) and design spectra with depth dependent site coefficients for Site 3 using Uplands profile and ME dynamic properties.

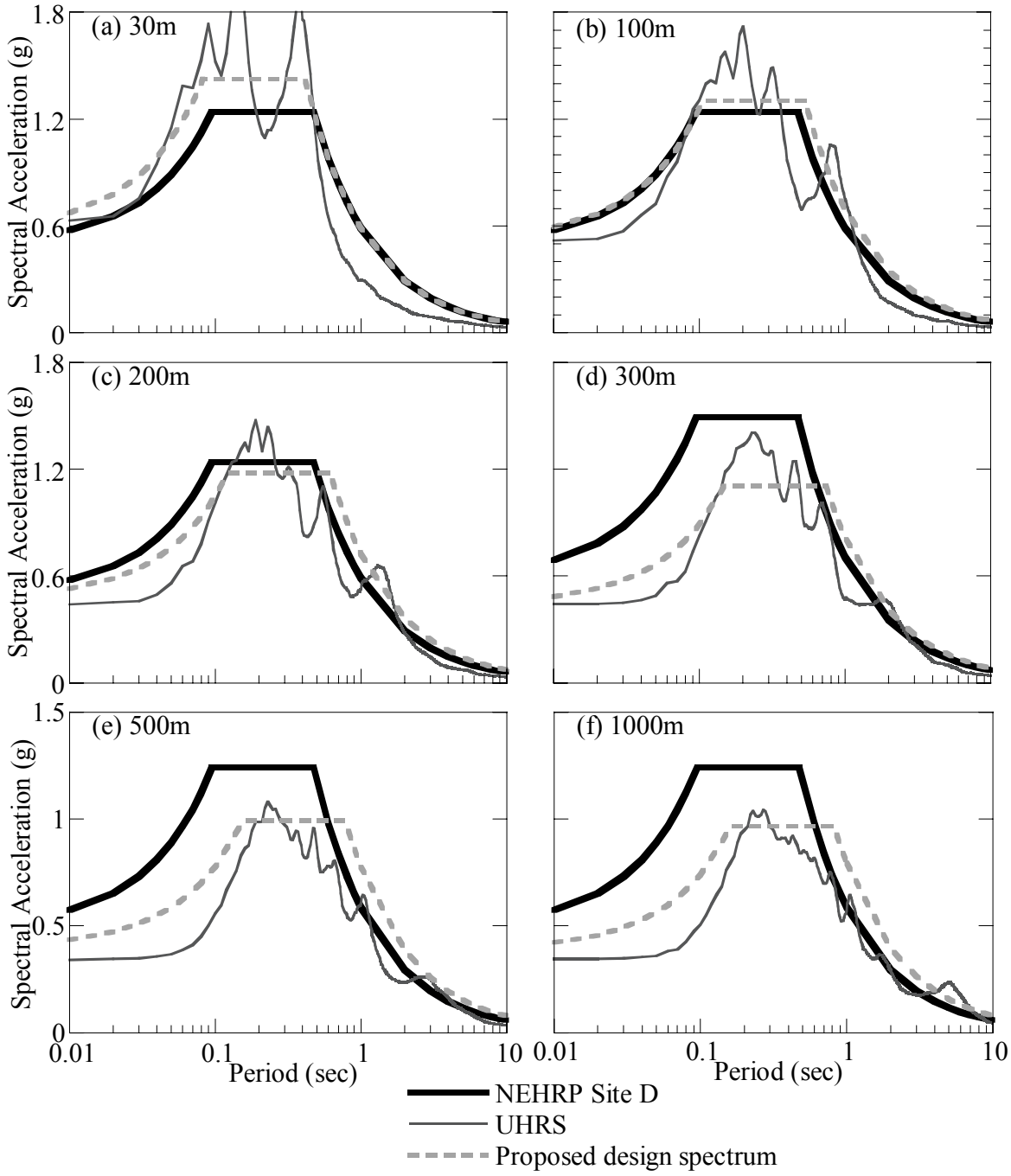

Figure 6-29 UHRS (2% in 50 years) and design spectra with depth dependent site coefficients for Site 4 using Uplands profile and ME dynamic properties.

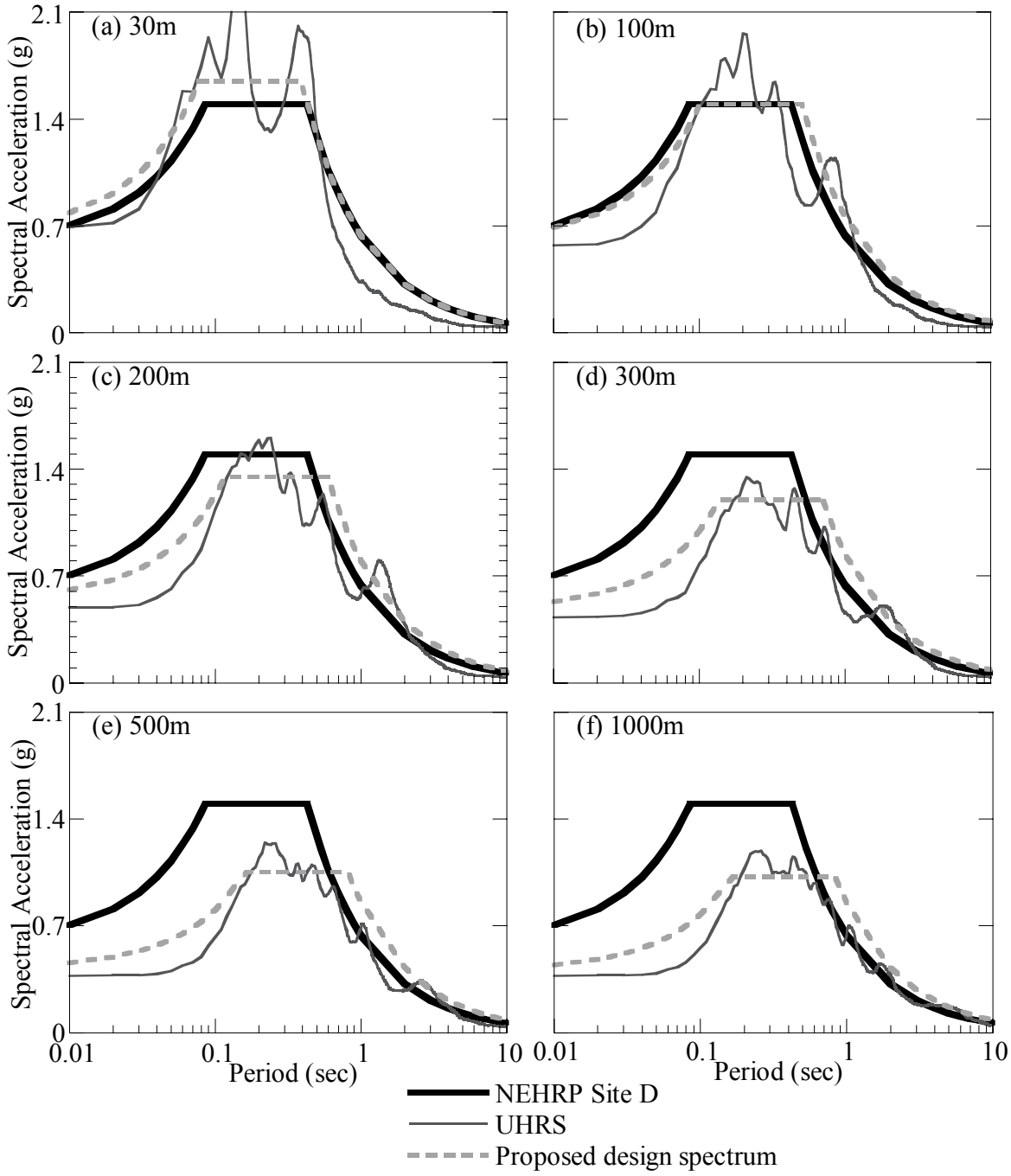

Figure 6-30 UHRS (2% in 50 years) and design spectra with depth dependent site coefficients for Site 5 using Uplands profile and ME dynamic properties.

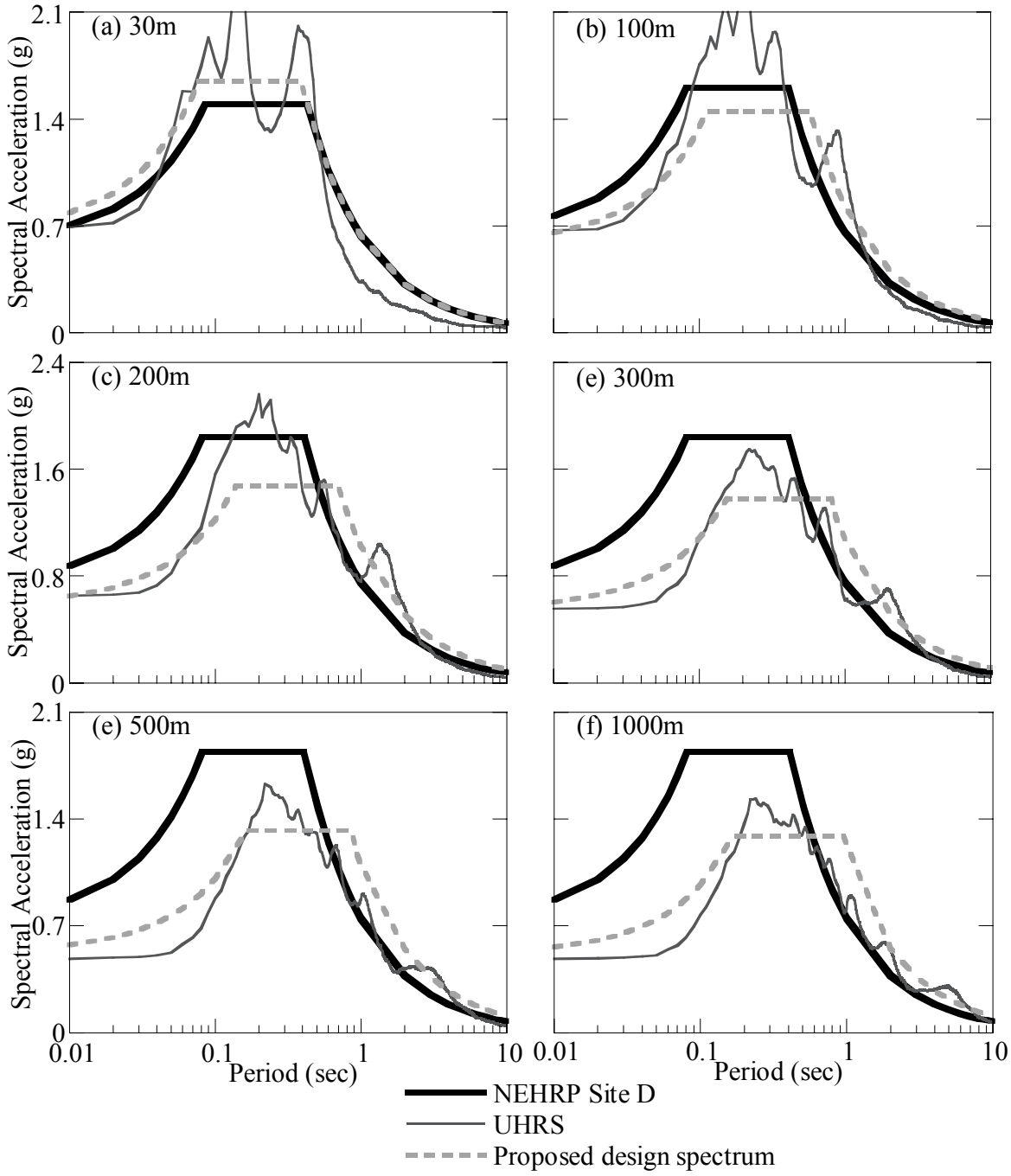

Figure 6-31 UHRS (2% in 50 years) and design spectra with depth dependent site coefficients for Site 6 using Uplands profile and ME dynamic properties.

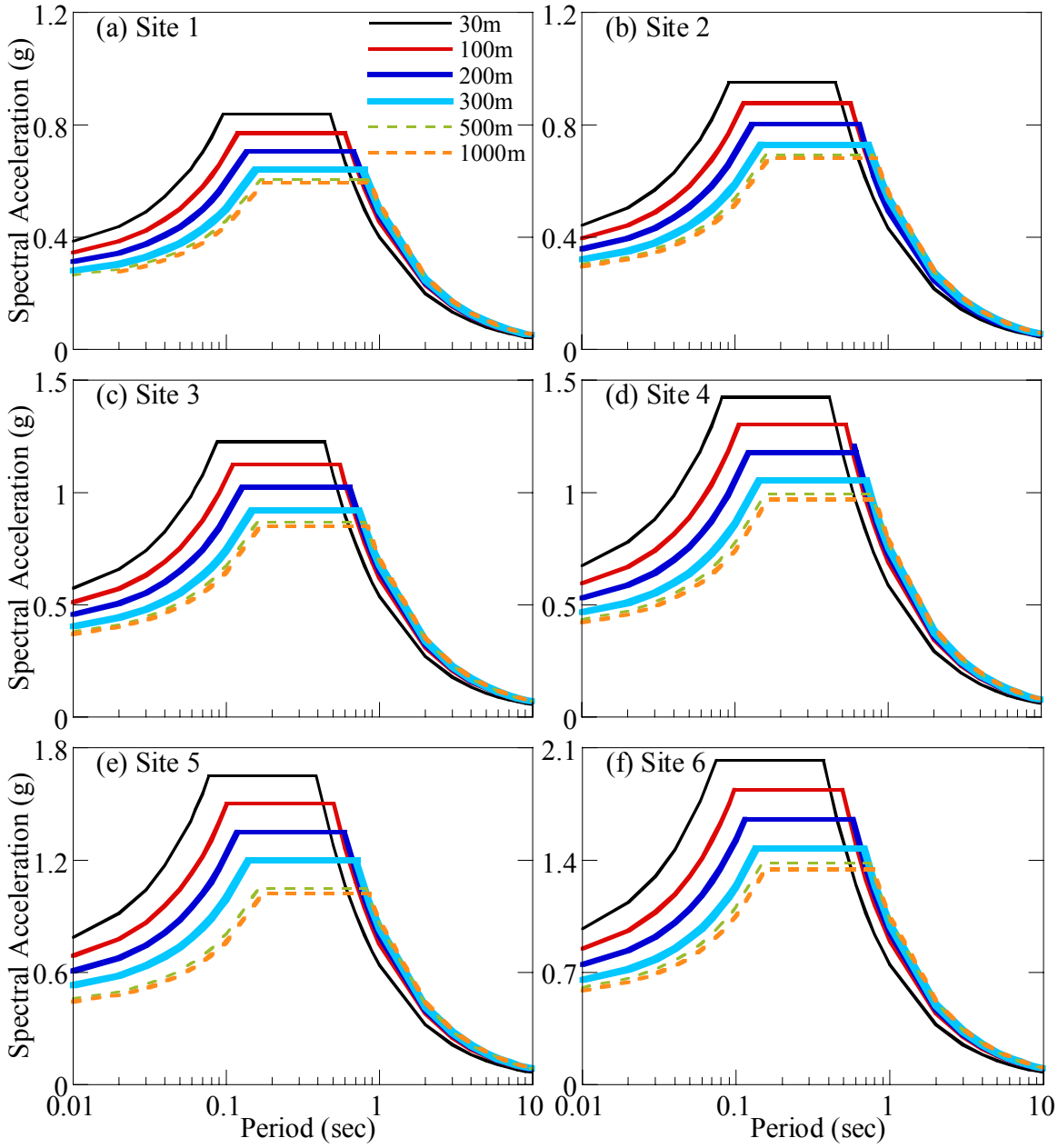

Figure 6-32 Proposed design spectra developed using probabilistic depth dependent site coefficients for Site 1 to 6 for Uplands profile with ME dynamic properties.

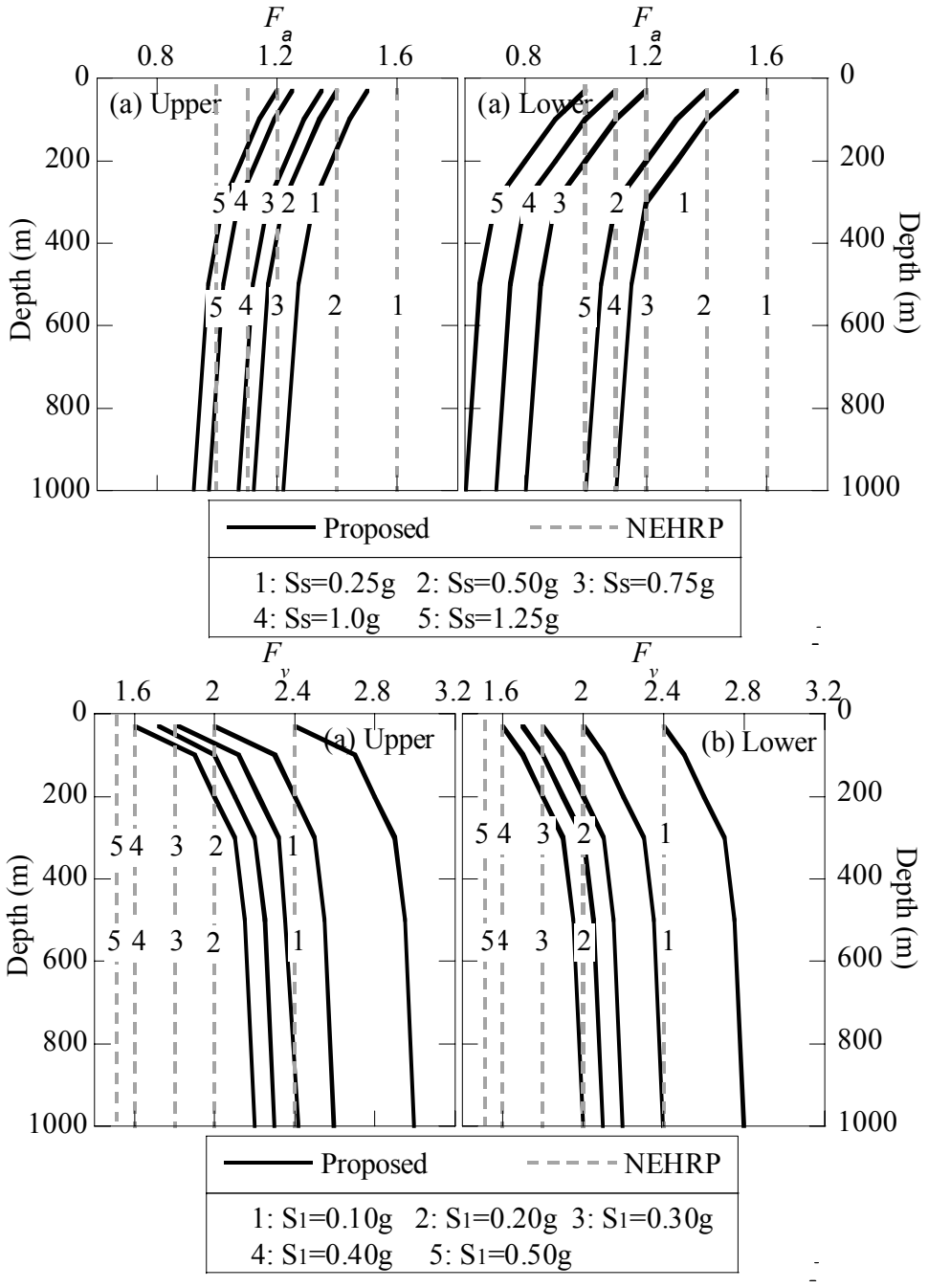

Figure 6-33 Recommended site coefficients for Uplands: (a) F_a Upper bound, (b) F_a Lower bound, (c) F_v Upper bound, (d) F_v Lower bound.

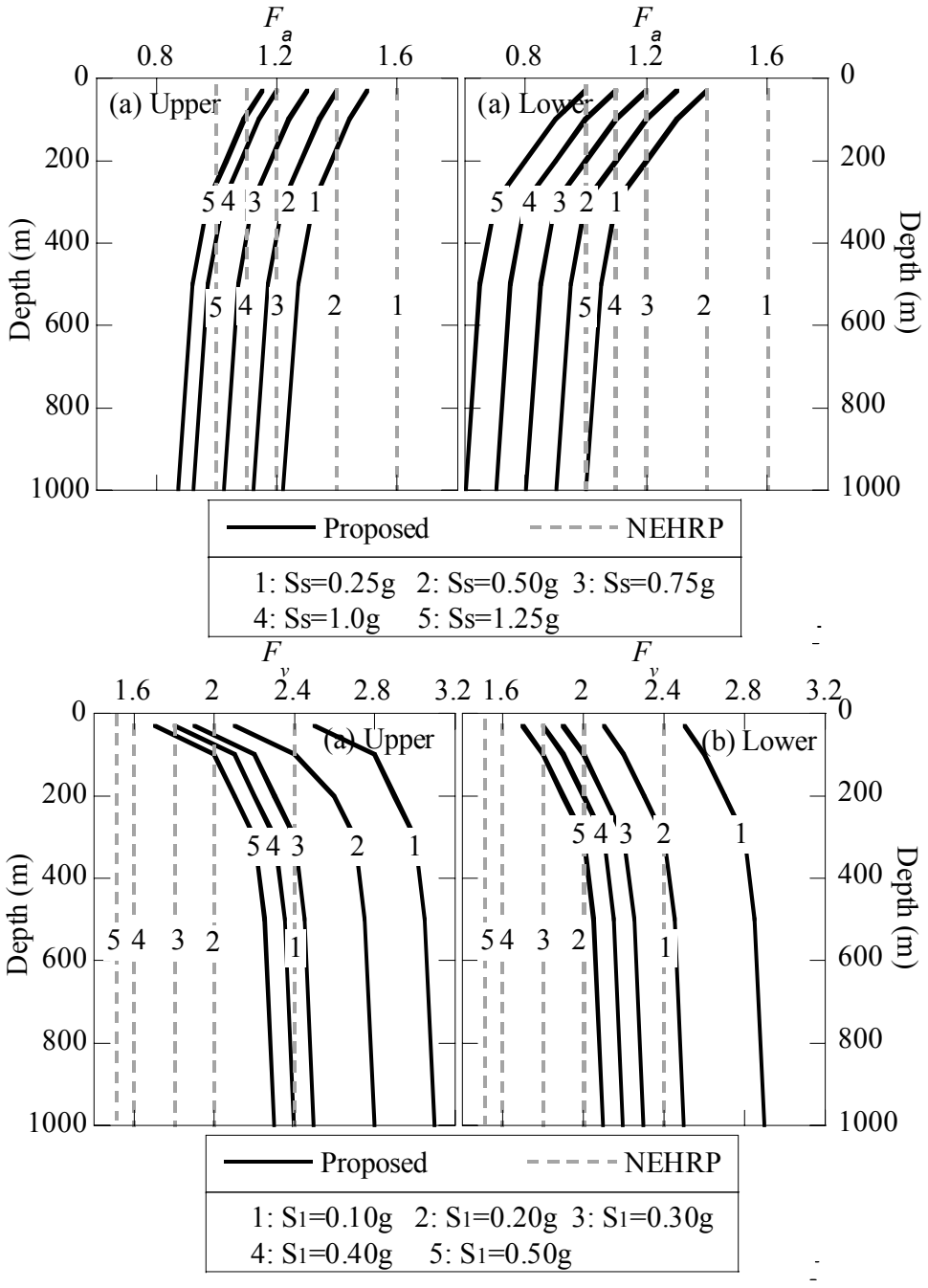

Figure 6-34 Recommended site coefficients for Lowlands: (a) F_a Upper bound, (b) F_a Lower bound, (c) F_v Upper bound, (d) F_v Lower bound.

CHAPTER 7 CONCLUSIONS AND RECOMMENDATIONS FOR FUTURE RESEARCH

The goal of this research is to assess and quantify the effect of the deep deposits of the Mississippi embayment on seismic ground motion propagation. The study is divided into 3 main sections: 1) development of a new nonlinear site response analysis model to simulate strong ground motion propagation through very deep deposits; 2) development of dynamic soil properties for Mississippi embayment deposits to be used in site response analysis; and 3) development of probabilistic seismic hazard analysis with nonlinear site effects to generate site coefficients for the embayment. This research incorporates the nonlinear site response model and the estimated dynamic properties in the developed probabilistic seismic hazard analysis (PSHA) for obtaining probabilistic site coefficients.

7.1 Development of nonlinear site response model

7.1.1 Summary and conclusions

A new one-dimensional nonlinear site response analysis program, DEEPSOIL, for deep and shallow deposits is developed. The model's new features include a) confining pressure dependent soil model, b) new viscous damping formulations to better simulate wave propagation through thick deposits, and c) increased numerical accuracy.

Feature 1: Confining pressure dependent soil model

The confining pressure is a very important parameter that influences the dynamic soil behavior in a deep soil column. A pressure dependent constitutive soil model has been developed and incorporated in DEEPSOIL. The model extends the modified hyperbolic equation to allow coupling with the confining pressure.

Feature 2: New Viscous damping formulation

In a nonlinear analysis, viscous damping is often added to represent damping at very small strains where many soil models are primarily linear. The accuracy of a conventional solution deteriorates with increase in depth of the soil profile. This is due to the artificial damping introduced through the uncontrolled frequency dependent viscous damping.

An important feature of DEEPSOIL is incorporation of full and extended Rayleigh damping formulations to reduce the dependence of frequency on damping. DEEPSOIL is the first 1D site response analysis program to incorporate the extended Rayleigh damping

formulation. In addition to the viscous damping formulation, selection of the optimum frequencies/modes for the viscous damping formulations is an equally important part of performing a nonlinear analysis. However, the importance of the selection procedure is often neglected and is done in an ad hoc manner without a clear guideline. A descriptive guideline is developed to effectively choose the significant frequencies/modes for the Rayleigh damping formulations. The significance of the selection of the frequencies/modes is discussed.

The viscous damping matrix is composed of the mass and stiffness matrices, in addition to the coefficients that are calculated from the natural modes of the soil column. Even though the stiffness of the soil column changes continuously during the course of the loading, a constant initial stiffness is used in a conventional viscous damping formulation. In this research, the stiffness and the natural modes of the soil column are updated at each time step.

Feature 3: Increased numerical accuracy

The numerical accuracy of the solution has been greatly increased using a flexible sub-incrementation scheme that effectively calculates the number of steps depending on the induced strain level. The flexible scheme is also proven to be very effective in terms of computational cost.

In addition to the new nonlinear site response model analysis model with the various enhancements over a conventional code, DEEPSOIL also features the equivalent linear analysis. The formulation is very similar to SHAKE (Schnabel et al. 1972), but the limitation of the number of layers, material properties, and input motion data points have been removed.

The performance of the developed model is evaluated through comparisons with other non-linear site response analysis models, equivalent linear site response analysis model, and field recordings from the Loma Prieta Earthquake.

The developed features are packaged in a graphical user interface. The interface guides the user through the steps required to perform a nonlinear or equivalent linear analysis. The selection process of the frequencies/modes and of the nonlinear parameters of the confining pressure dependent soil model is greatly simplified.

7.1.2 Recommendations for future work

There are several areas that can further enhance the nonlinear model:

1. Enhanced constitutive model: DEEPSOIL uses the extended modified hyperbolic model to simulate the nonlinear behavior. While the use of the simplified model is justified in

performing site response analysis in the Mississippi embayment, a more robust model that can simulate more complex behaviors of soils is needed for site specific analysis if more detailed data is available on the cyclic behavior of the soil. In addition, the developed constitutive model currently only allows total stress analysis. One of the main advantages of performing nonlinear site response analysis is that an effective stress analysis can be performed, provided a constitutive model that can simulate pore pressure build-up or dissipation is incorporated. A new constitutive soil model that can simulate pore pressure changes during the seismic loading should be incorporated.

2. Extension of the 1D model: DEEPSOIL approximates the wave propagation as 1D vertical propagation of horizontal shear waves. There might be a need to extend the formulation to allow 2D and 3D wave propagation. This will allow account for the surface topographical effects.
3. Automatic determination of the frequencies/modes for Rayleigh damping formulation: The proposed viscous damping formulations significantly increase the accuracy of the wave propagation solution. However, it involves trial-and-error procedure in selecting optimum frequencies/modes for the damping formulation. This procedure has been greatly simplified by providing a graphical interface to select the frequencies/modes in DEEPSOIL. However, a more robust scheme to automatically select the optimum frequencies/modes is needed to make the nonlinear program accessible to more users.

7.2 Estimation of dynamic properties

7.2.1 Summary and conclusions

Estimation of the dynamic properties, although critical in site response analysis, is difficult in deep deposits of the Mississippi embayment. CHAPTER 4 reviews efforts to characterize dynamic properties of the Mississippi embayment soils and develops properties for use in DEEPSOIL. Results from cyclic laboratory tests performed by Laird and Stokoe (1993) at confining pressures up to 3 MPa are used to characterize the pressure dependent behavior of soils due to the lack of data specific to the Mississippi embayment. The estimated dynamic properties are further constrained using laboratory test results of shallow embayment soils. Viscous damping soil properties are constrained using weak motion recordings from a recent earthquake

near the embayment. This study is the first attempt to incorporate the weak motion recordings to constrain the viscous damping properties of the embayment.

The back-calculated damping is much higher than the estimated damping from laboratory tests. The back-calculated viscous damping is combined with hysteretic damping from the laboratory tests. The proposed curves are compared to the limited ME in-situ soil laboratory tests. The proposed curves fall within the bounds of the in-situ test results, whereby the estimated pressure dependency and viscous damping ratios are greater than those from the in-situ soil sample test results.

7.2.2 Recommendations for future work

There are several methods to improve the estimation of dynamic properties.

1. Use more recent recordings of the embayment to further constrain the viscous damping properties.
2. In addition, recordings at shallower sites will enable better definition of depth dependent properties.
3. Obtain more in-situ soil samples in the embayment and perform laboratory test at high confining pressure to better understand the dynamic behavior of in-situ soils.

7.3 Development of probabilistic seismic hazard analysis procedure with nonlinear site effects and estimation of probabilistic site coefficients

7.3.1 Summary and conclusions

A new PSHA analysis procedure is developed that combines the non-linear site response analysis (DEEPSOIL) to develop fully probabilistic site coefficients within the Mississippi embayment. The procedure deviates from the conventional procedure of characterizing the site coefficients deterministically. It fully restores the probabilistic nature of the USGS hazard maps and allows the quantification of the site effect.

The developed procedure initially performs PSHA that reproduces the USGS hazard maps, but at the same time generates actual ground motion time histories. It is important that the USGS hazard maps are accurately simulated to isolate site effects. The generated motions are propagated through site specific profiles, allowing taking into account the site effects of

individual motions. The resulting UHRS at the surface are used to develop probabilistic site coefficients.

The developed procedure is applied to the Mississippi embayment to determine the probabilistic site coefficients and assess the effect of embayment depth. Two soil profiles (Uplands and Lowlands) and two dynamic properties (ME proposed and EPRI properties) are used to account for the uncertainty of the soil properties. All four possible combinations of soil profiles and properties are used. The results are summarized in identical format to NEHRP Provisions (FEMA 1997) to be used in design, with the added dimension of depth. In addition, the upper bound and lower bound of both the short period and long period site coefficients are determined for both Uplands and Lowlands.

Results indicate that the deterministic NEHRP site coefficients provide reasonable estimate for 30 m profiles. This is because the contribution of the characteristic event is significant in the Mississippi embayment. The short period coefficients are highly overestimated whereas the long period coefficients are underestimated for deep deposits. New depth dependent site coefficients are developed in the same format as NEHRP site coefficients, with the added dimension of depth.

7.3.2 Recommendations for future work

1. It is necessary to incorporate the various source models in simulating the 2002 USGS hazard maps. This means that the broadband (or finite fault) model and hybrid model, in addition to the point source model, should be included in the simulation.
2. Results indicate that the current NEHRP spectrum has several limitations. A new methodology for constructing the design spectrum is needed that addresses the following limitations:
    a) Using the current definition of long period site coefficient resulted in significant shifting of the design spectrum. There is a need to define T_0 and T_s that are not influenced by the ratio of F_a / F_v, but on the natural modes of the soil column.
    b) The current formulation results in higher long period estimate at long periods for 30 m soil profile.

3. The probabilistic site coefficients are developed for the Mississippi embayment. The developed numerical procedure can be applied to elsewhere in the U.S. Additional studies in other areas, e.g. California, are warranted to further assess NEHRP site coefficients.

APPENDICES

A SOLUTION OF DAMPED SINGLE DEGREE OF FREEDOM SYSTEM TO HARMONIC EXCITATION

A.1 Kelvin-Voigt model

Equation of motion under harmonic excitation of a single degree of freedom (SDOF) system using Kelvin-Voigt model is written as (Chopra, 1995):

$$m\ddot{u} + c\dot{u} + ku = P_0 e^{i\omega t} \tag{A-1}$$

where m = mass, c = viscous damping; k = stiffness; $\ddot{u}$ = acceleration; $\dot{u}$ = relative velocity; u = relative displacement; P_0 = amplitude, ω = frequency of harmonic excitation.

Dividing Equation (A-1) by m, the equation becomes

$$\ddot{u} + 2\frac{c}{2\sqrt{mk}}\omega_n \dot{u} + \omega_n{}^2 u = \frac{P_0}{m} e^{i\omega t} \tag{A-2}$$

$2\sqrt{mk}$ is termed critical damping coefficient c_c. Equivalent damping ratio, ξ, is defined as the ratio of the damping coefficient to the critical damping coefficient:

$$\xi = \frac{c}{c_{cr}} = \frac{c}{2\sqrt{km}} = \frac{c\omega_n}{2k} \tag{A-3}$$

where $\omega_n = \sqrt{k/m}$ = natural frequency of the system.

Energy loss due to viscous damping is:

$$E_d = \pi c\omega u_0{}^2 = 2\pi\xi\frac{\omega}{\omega_n} k u_o{}^2 \tag{A-4}$$

which is proportional to the frequency ω of imposed forces.

Equivalent damping ratio is calculated as:

$$\xi = \frac{1}{4\pi}\frac{1}{\omega/\omega_n}\frac{E_d}{E_s} \tag{A-5}$$

where $Es = 1/2ku_0{}^2$.

The steady state solution of Equation (A-1) is:

$$u = \frac{P_0/k}{\sqrt{[1-(\omega/\omega_n)^2]^2 + [2\xi(\omega/\omega_n)]^2}} e^{i\omega t} \tag{A-6}$$

and the phase angle between imposed loading and response is

$$\phi = \tan^{-1}\frac{2\xi(\omega/\omega_n)}{1-(\omega/\omega_n)^2} \tag{A-7}$$

A.2 Hysteretic model

Equation of motion under harmonic excitation of a SDOF system using the hysteretic model is written as (Udaka, 1975):

$$m\ddot{u} + k(1 + i2\xi)u = P_0 e^{i\omega t} \tag{A-8}$$

The amplitude of response is:

$$u = \frac{P_0 / k}{\sqrt{[1-(\omega/\omega_n)^2]^2 + (2\xi)^2}} \tag{A-9}$$

and the phase angle between imposed force and response is

$$\phi = \tan^{-1} \frac{2\xi}{1-(\omega/\omega_n)^2} \tag{A-10}$$

A.3 Udaka model (1975)

Equation of motion under harmonic excitation of a SDOF system using the Udaka model is written as (Udaka, 1975):

$$m\ddot{u} + k(1 - 2\xi^2 + i2\xi\sqrt{1-\xi^2})u = P_0 e^{i\omega t} \tag{A-11}$$

The amplitude of response is:

$$u = \frac{P_0 / k}{\sqrt{[1-(\omega/\omega_n)^2]^2 + [2\xi(\omega/\omega_n)]^2}} \tag{A-12}$$

and the phase angle between imposed force and response is

$$\phi = \tan^{-1} \frac{2\xi\sqrt{1-\xi^2}}{1-2\xi^2-(\omega/\omega_n)^2} \tag{A-13}$$

The amplitude of the response is identical to Kelvin-Voigt model, Equation (A-6).

B NUMERICAL INTEGRATION OF DYNAMIC EQUATIONS OF MOTION

B.1 Numerical solution methods

The most widely used numerical solution methods for solving the dynamic equation of motion, Equation (2-35), are a) central difference, b) Newmark β, and c) Wilson θ method. The central difference method is an explicit method, whereas Newmark and Wilson methods are implicit methods.

The two most important aspects of the numerical schemes is their a) stability and b) accuracy (Chopra 1995). The central difference method is only stable if the following requirement is satisfied:

$$\frac{\Delta t}{T_n} < \frac{1}{\pi} \tag{B-1}$$

Wilson θ methods are unconditionally stable, whereas the stability of the Newmark β method depends on the type of the method. More details on the Newmark β are described in the following.

B.2 Newmark β method

Newmark (Newmark, 1959) developed various time-stepping methods based on the following equations:

$$\begin{aligned} \dot{u}_{i+1} &= \dot{u}_i + \left[(1-\gamma)\Delta t\right]\ddot{u}_i + (\gamma \Delta t)\ddot{u}_{i+1} \\ u_{i+1} &= u_i + (\Delta t)\dot{u}_i + \left[(0.5-\beta)(\Delta t)^2\right]\ddot{u}_i + \left[\beta(\Delta t)^2\right]\ddot{u}_{i+1} \end{aligned} \tag{B-2}$$

The parameters β and γ determine the variation of acceleration at a time step. The accuracy and stability depends on the value of the parameters selected. Two special cases of Newmark method is a) average acceleration ($\beta = \frac{1}{4}$ and $\gamma = \frac{1}{2}$) and b) linear acceleration ($\beta = \frac{1}{6}$ and $\gamma = \frac{1}{2}$) methods. In average acceleration method, the acceleration is constant over a time step, whereas the acceleration varies linearly in linear acceleration method. Iteration is required to solve Equation (B-2) for a nonlinear system since unknown $\ddot{u}_{i+1}$ appears on the right side. For a linear system, it is possible to modify the equation and solve without iteration.

Figure B-1 compares the accuracy of the three solution methods, in terms of amplitude decay (AD, also referred to as artificial damping) and period elongation (PE). Linear and average

acceleration methods are two types of Newmark β methods. AD and PE are defined in Figure B-1b. Only Wilson θ method (using θ = 1.4) introduces AD. In terms of PE, Newmark β method (linear method) results in the lowest PE, whereas the central difference introduces the highest error. The average Newmark β method is used in the study.

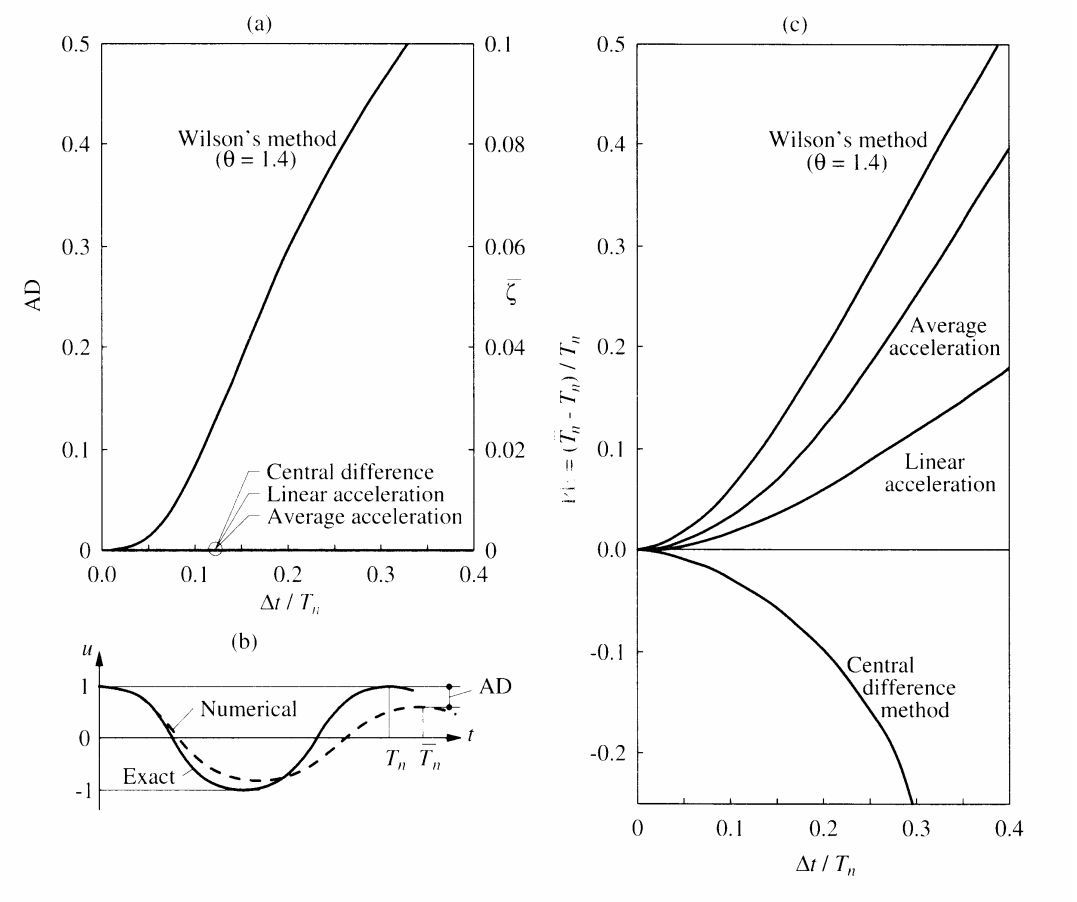

Figure B-1 Comparison of accuracy of numerical methods to solve dynamic equation of motion: a) AD (amplitude decay) versus $\Delta t / T_n$, b) definition of AD and PE (period elongation), c) period elongation versus $\Delta t / T_n$ (Chopra, 1995).

C POINT SOURCE STOCHASTIC MODEL

Point source models are composed of three components: a) earthquake source model, b) attenuation model, and c) low-pass filter. The most commonly used earthquake source model is based on (Brune, 1970; Brune, 1971) and assumes an instantaneous rupture of a circular fault producing seismic energy. Earthquake source model generates Fourier spectra at the rupture point first. The shape of Fourier spectra is determined by single corner frequency or the combination of double corner frequencies. Then, according to attenuation relationship, which includes radiation damping and material damping, Fourier spectra at observation points is calculated.

The mathematical form for the Fourier amplitude spectrum of the ground motion is:

$$A(M_0, R_h, f) = E(M_0, f) \cdot D(R_h, f) \cdot P(f) \tag{C-1}$$

where $E(M_0, f)$ is the source model; $D(R_h, f)$ is a diminution factor accounting for attenuation; $P(f)$ is high-cut filter; f is cyclic frequency (Hz), R_h is focal distance (km), and M_0 is moment magnitude (dyne-cm). The model assumes that the Fourier amplitude spectrum of an acceleration time history maybe approximated as band-limited, random, Gaussian white noise (BLWN).

C.1 Point source model

C.1.1 Single corner frequency model

The most commonly used earthquake source model is based on Brune (1970) and assumes an instantaneous rupture of a circular fault producing seismic energy. The Brune source model is defined as:

$$E(M_0, f) = C \cdot (2\pi f)^2 \cdot M_0 \cdot \left\{ \frac{1}{1 + \left(\frac{f}{f_c} \right)^2} \right\} \tag{C-2}$$

C is a constant relative to crustal density and shear wave velocity;

f_c is the corner frequencies (Hz) defined as

$$f_c = 4.9 \times 10^6 \beta \left(\frac{\Delta\sigma}{M_0} \right)^{1/3} \tag{C-3}$$

β is shear wave velocity and $\Delta\sigma$ is the stress drop (Boore 1983).

Therefore, the Brune source spectrum is dependent on two key parameters: (1) the size of earthquake given by seismic moment and (2) the energy released during the event defined by the stress drop. The stress drop is measured by the strength of high-frequency energy (Atkinson and Beresnev, 1997) and represents the available stress that produces seismic waves (Brune, 1970). It is generally computed from the high- frequency energy of the Fourier spectrum of measured spectrum (Atkinson and Beresnev, 1997). The value of stress drop may be used as fitting parameter to adjust the point source model to model observed ground motions that may not fit the Brune model. A stress drop of 100 bars has been widely used for the central and eastern United States and adequately models measured ground motions (Boore, 1983; EPRI, 1993). The stress drop slightly increases the corner frequency and magnitude of Fourier amplitude spectrum. On the other hand, an increase in moment magnitude decreases the corner frequency thereby producing more low-frequency energy.

C.1.2 Double corner frequency model

The one-corner frequency model assumes that the high-frequency spectrum is proportional to the rupture area of the fault (Joyner, 1984). In contrast, the two-corner frequency model assumes this applies for earthquakes with a seismic moment, M_0, less than a critical moment, M_{0c}, where the rupture length and width both increase with magnitude (Joyner, 1984). Above the critical moment, the two corner frequencies, f_A and f_B, are inversely proportional to the rupture length and width, respectively. The mathematical form of two-corner frequency model (Atkinson and Beresnev, 1997) is expressed as:

$$E(M_0, f) = C \cdot (2\pi f)^2 \cdot M_0 \cdot \left\{ \frac{1-\zeta}{1+\left(\frac{f}{f_A}\right)^2} + \frac{\zeta}{1+\left(\frac{f}{f_B}\right)^2} \right\} \quad \text{(C-4)}$$

f_A, f_B=corner frequencies (Hz), which is function of magnitude

ζ=weighting parameter, which is also function of magnitude

C.2 Attenuation model

The diminution factor represents the total attenuation through the geologic media and is given as a function of hypocentral distance and frequency by:

$$D(R_h, f) = D_g(R_h) \cdot D_m(R_h, f) \tag{C-5}$$

in which $D_m(R_h, f)$ is anelastic material attenuation (material damping); $D_g(R_h)$ is geometric attenuation (radiation damping).

The anelastic attenuation considers the decrease of amplitude with increasing frequency and distance due to material damping and is given as:

$$D_m(R_h, f) = \exp\left(\frac{-\pi f R_h}{\beta Q(f)}\right) \tag{C-6}$$

where *Q(f)* represents the quality factor, *Q*, as a function of frequency and is given by:

$$Q(f) = 680 f^{0.36} \tag{C-7}$$

for eastern North America (Atkinson and Boore, 1995).

Geometric attenuation considers the decrease in amplitude of seismic energy as it propagates away from the source. The corresponding attenuation for eastern North America (Atkinson and Boore, 1995) is given by:

$$\begin{aligned} D_g &= 1/R & R < 70km \\ D_g &= 1/70 & 70km \le R < 130km \\ D_g &= 1/70(130/R)^{0.5} & R \ge 130km \end{aligned} \tag{C-8}$$

C.3 Low-pass filter

P(f) is a low pass filter modeling the attenuation of high frequencies from the source spectra. Boore (1983) proposed a forth-order Butterworth filter given by:

$$P(f) = \frac{1}{\sqrt{1 + (f / f_{\max})^8}} \tag{C-9}$$

where f_{max} is the cut-off frequency defined by Hanks (1982). Based on recorded Fourier spectra in California, f_{max} appears to be related to site conditions.

C.4 Motion duration

Total duration T_d (sec) for the strong-motion phase is decomposed into source and path duration:

$$T_d = T_0 + T_p \tag{C-10}$$

where source duration T_0 is related to corner frequency f_A:

$$T_0 = \frac{1}{2 \cdot f_A} (\text{sec}) \tag{C-11}$$

C.5 Input file of SMSIM used in development of USGS hazard maps

```
For Art Frankel, kappa = 0.01, fm=100, ampl. from linear fit to 0.2 km
rho, beta, prtitn, rtp, fs:
    2.8 3.6 0.71 0.55 2.0
spectral shape: source number (1=Single Corner;2=Joyner;3=A93;4=custom),
                pf, pd (1-corner spectrum = 1/(1+(f/fc)**pf)**pd; 0.0 otherwise)
                (usual model: pf=2.0,pd=1.0; Butterworth: pf=4.0,pd=0.5)
                (Note: power of high freq decay --> pf*pd)
    1 2.0 1.0
spectral scaling: stressc, dlsdm, fbdfa, amagc
                (stress=stressc*10.0**(dlsdm*(amag-amagc))
                (fbdfa, amagc for Joyner model, usually 4.0, 7.0)
                (not used for source 3, but placeholders still needed)
    150.0 0.0 4.0 7.0
gsprd: r_ref, nsegs, (rlow(i), slope(i))  (Usually set r_ref = 1.0 km)
    1.0
    3
      1.0   -1.0
      70.0   0.0
      130.0 -0.5
q: fr1, Qr1, s1, ft1, ft2, fr2, qr2, s2, c_q
    1.0 680 0.36 0.06 0.1 1.0 680.0 0.36 3.6
source duration: weights of 1/fa, 1/fb
    1.0 0.0
path duration: nknots, (rdur(i), dur(i), slope of last segment
    1
      0.0 0.0
    0.05
site amplification: namps, (famp(i), amp(i))
    14
    0.01   1.000
    0.1014 1.058
    0.2402 1.129
    0.4468 1.220
    0.7865 1.375
    1.3840 1.649
    1.9260 1.858
    2.8530 2.051
    4.0260 2.172
    6.3410 2.282
   12.5400 2.378
   21.2300 2.419
   33.3900 2.440
   82.0000 2.463
site diminution parameters: fm, akappa, dkappadmag, amagkref
    100.0 0.01 0.0 6.0
low-cut filter parameters: fcut, norder
    0.0 2
rv params: zup, eps_int (int acc), amp_cutoff (for fup), osc_crrctn(1=b&j;2=l&p)
    10.0 0.00001  0.001 1
window params: idxwnd(0=box,1=exp), tapr(<1), eps_w, eta_w, f_tb2te, f_te_xtnd
    1 0.05 0.2 0.05 2.0 1.0
timing stuff: dur_fctr, dt, tshift, seed, nsims, iran_type (0=normal;1=uniform)
    1.3  0.01 1.0 123.0 200 0
remove dc from random series before transforming to freq. domain (0=no;1=yes)?
    0
```

D UNIFORM HAZARD SPECTRA

D.1 UHRS and design response spectra for Lowlands and using ME properties

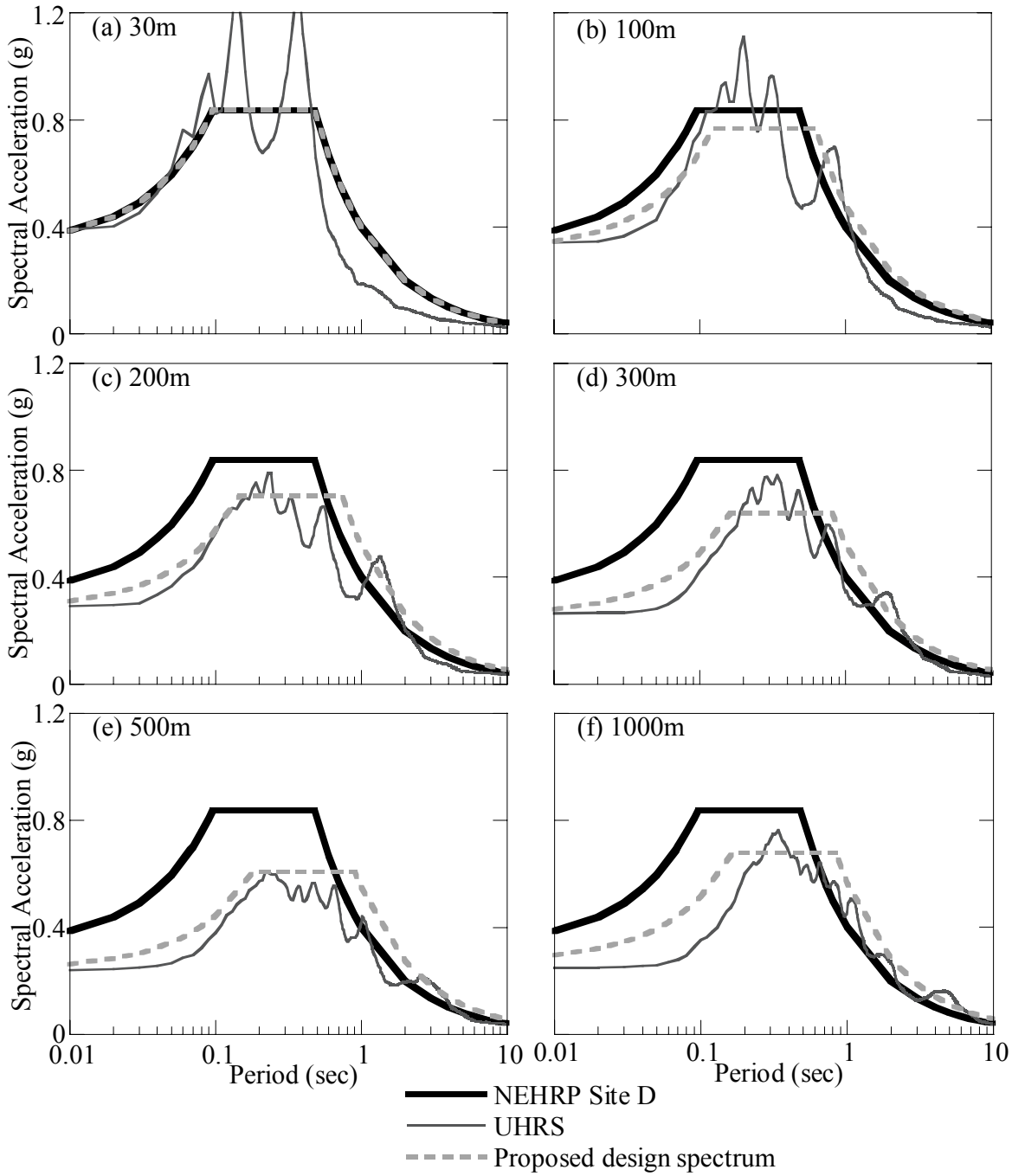

Figure D-1 UHRS (2% in 50 years) and design spectra with depth dependent site coefficients for Site 1 using Lowlands profile and ME dynamic properties.

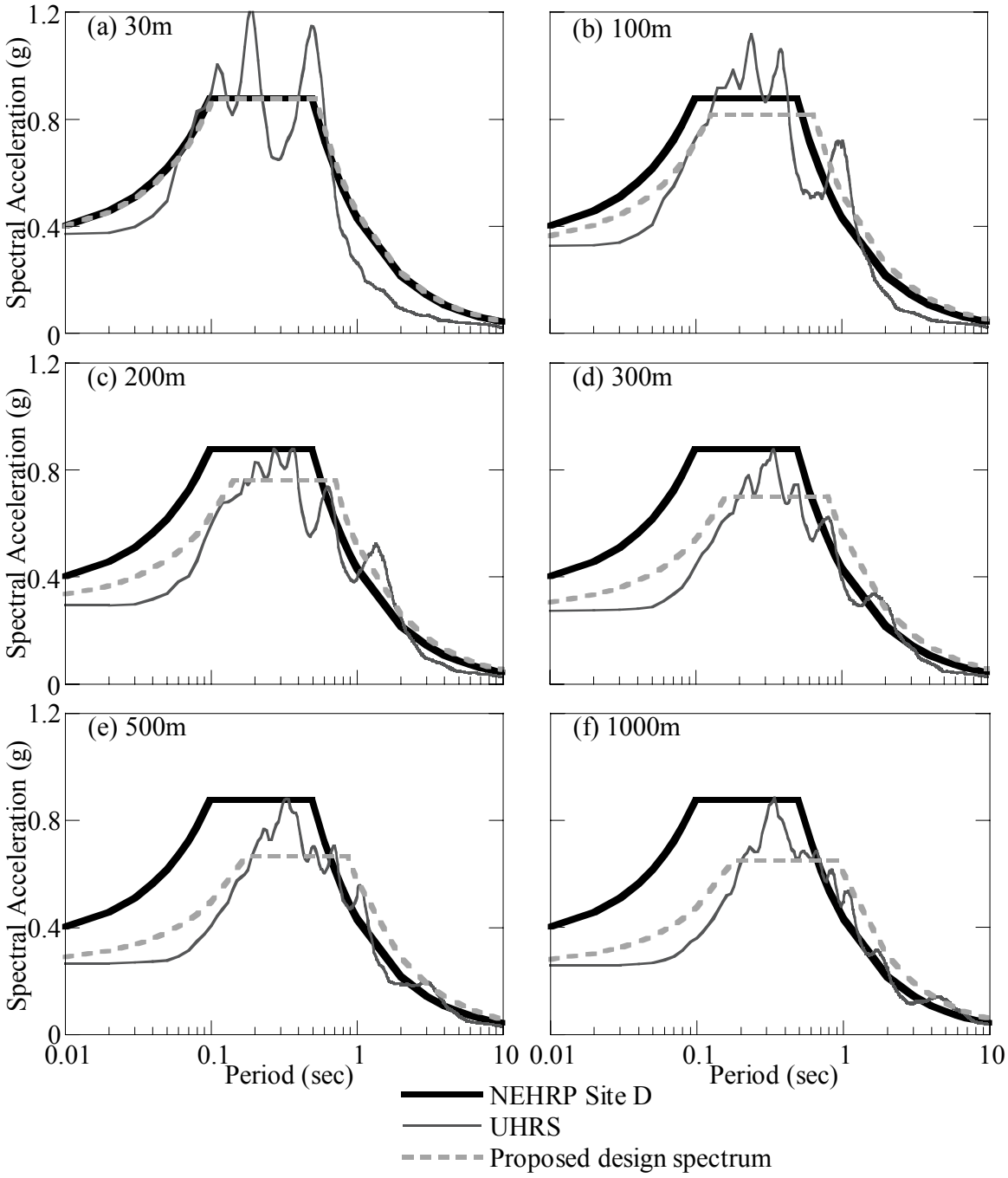

Figure D-2 UHRS (2% in 50 years) and design spectra with depth dependent site coefficients for Site 2 using Lowlands profile and ME dynamic properties.

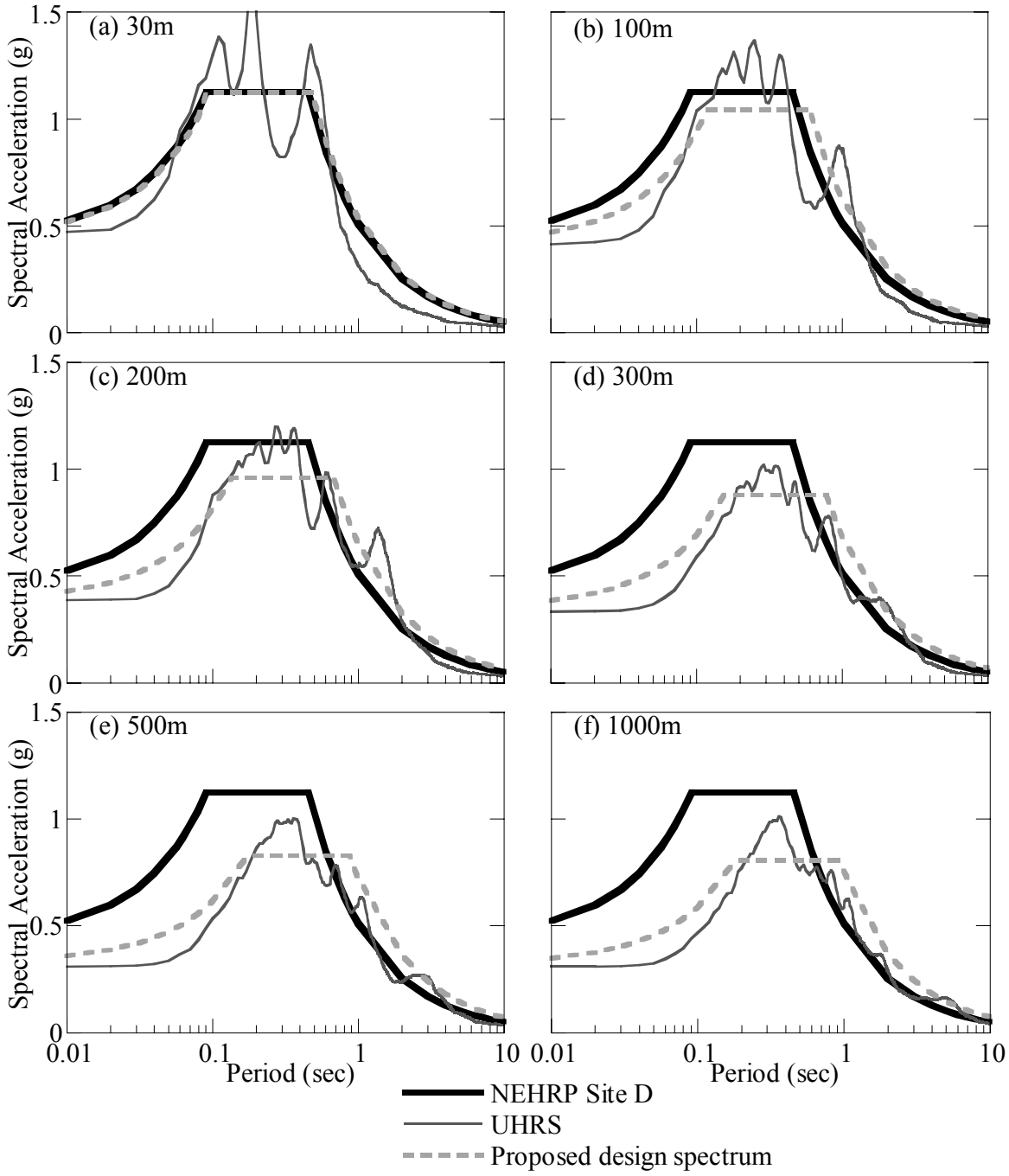

Figure D-3 UHRS (2% in 50 years) and design spectra with depth dependent site coefficients for Site 3 using Lowlands profile and ME dynamic properties.

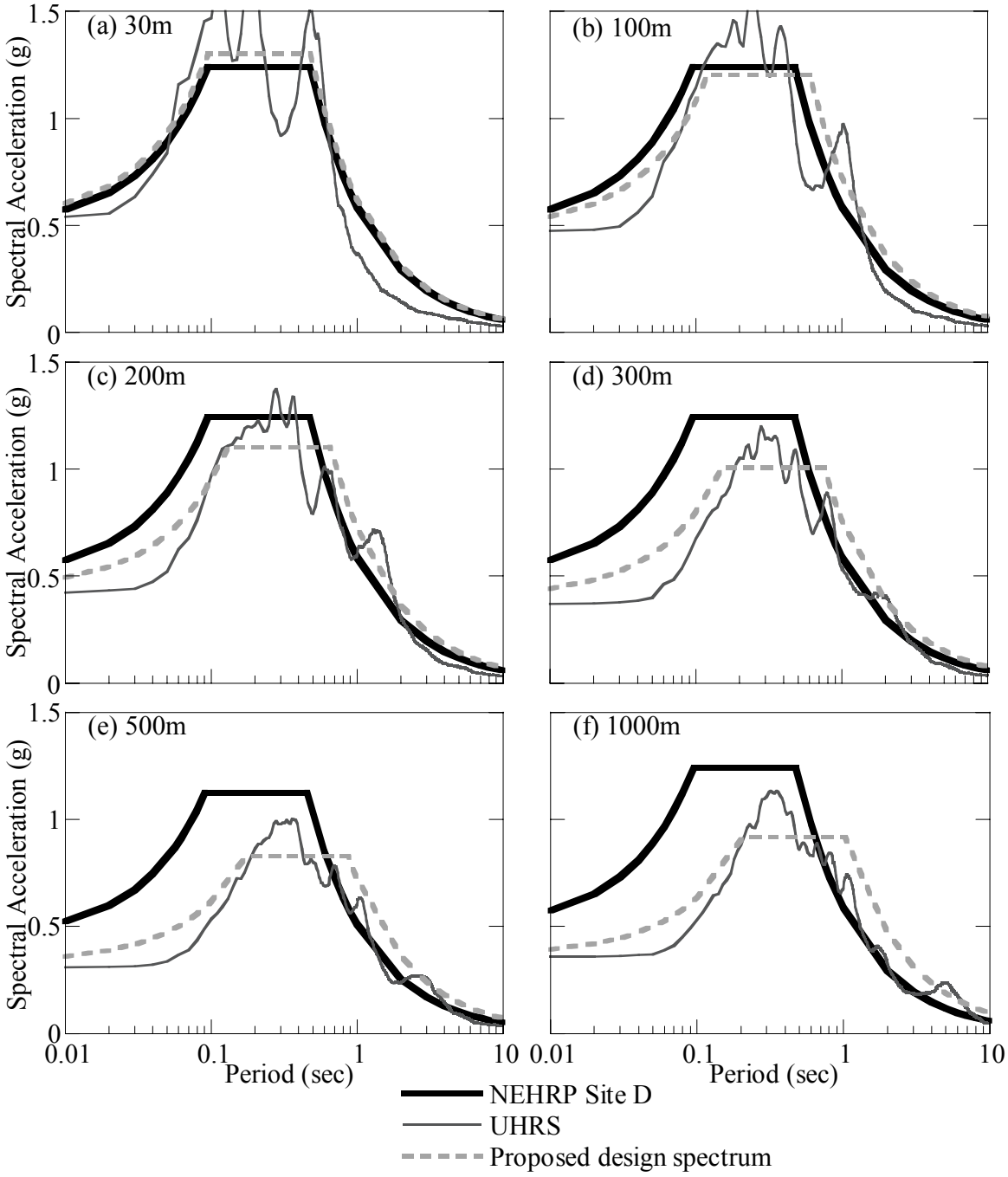

Figure D-4 UHRS (2% in 50 years) and design spectra with depth dependent site coefficients for Site 4 using Lowlands profile and ME dynamic properties.

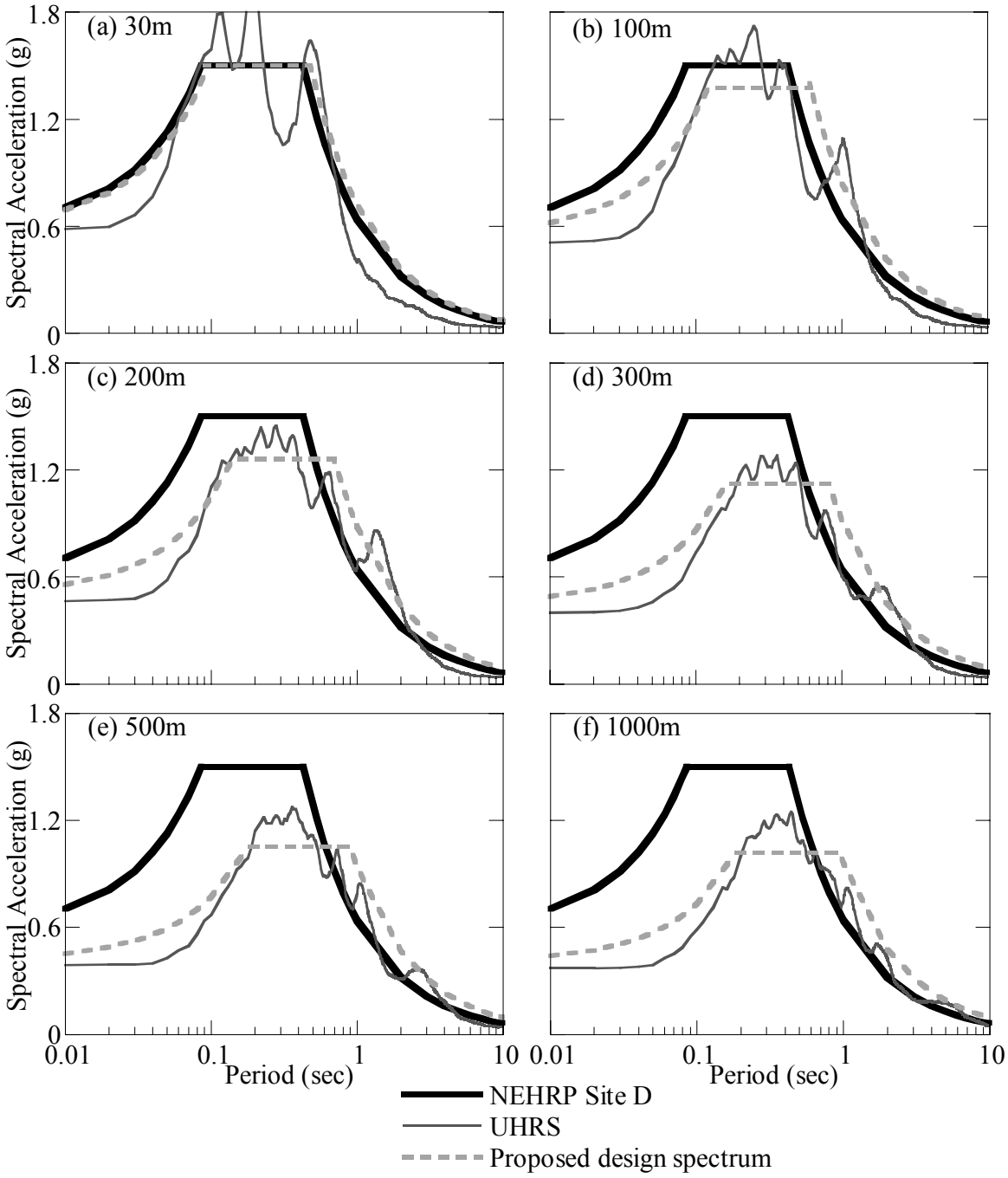

Figure D-5 UHRS (2% in 50 years) and design spectra with depth dependent site coefficients for Site 5 using Lowlands profile and ME dynamic properties.

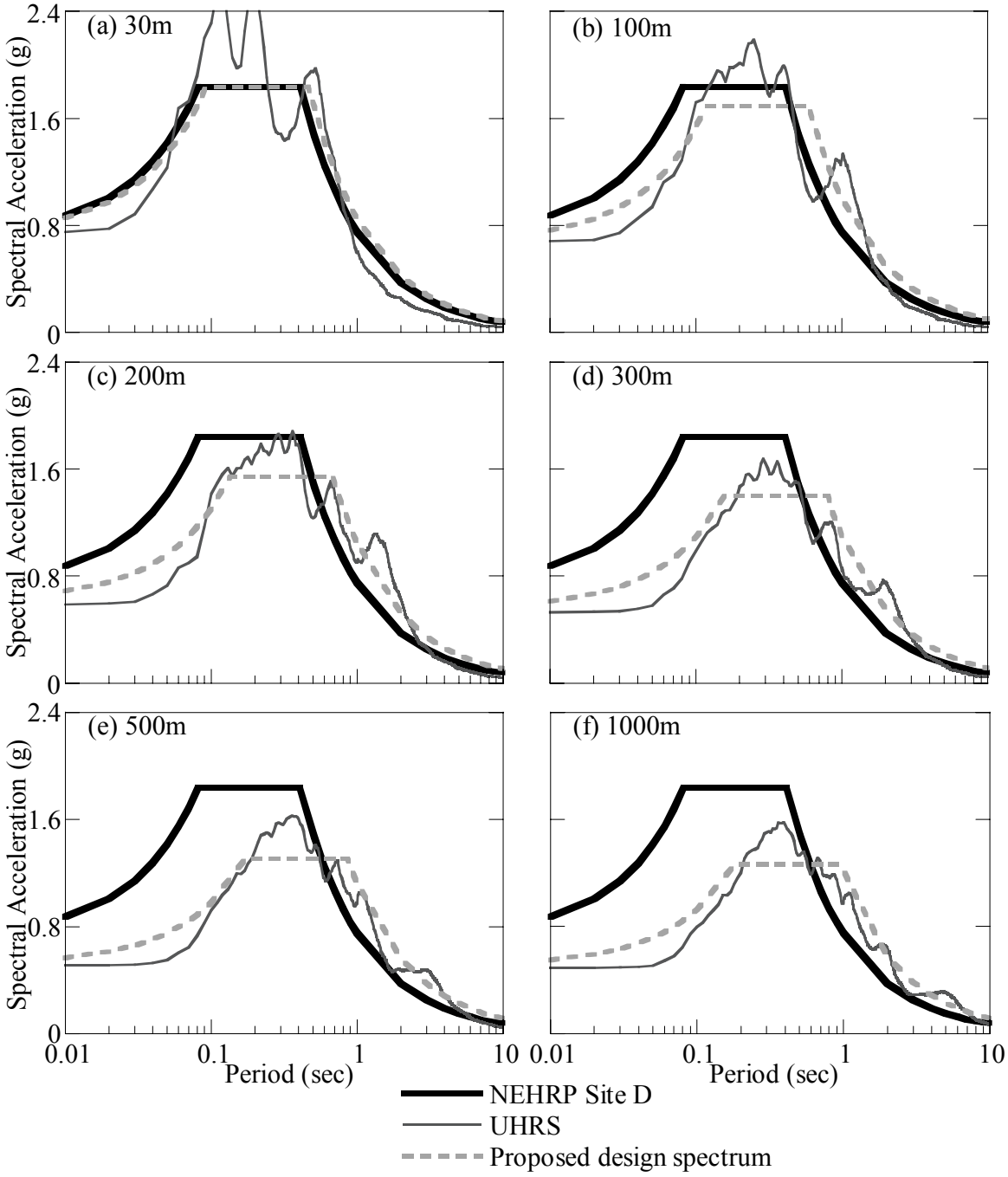

Figure D-6 UHRS (2% in 50 years) and design spectra with depth dependent site coefficients for Site 6 using Lowlands profile and ME dynamic properties.

D.2 UHRS and design response spectra for Uplands and using EPRI properties

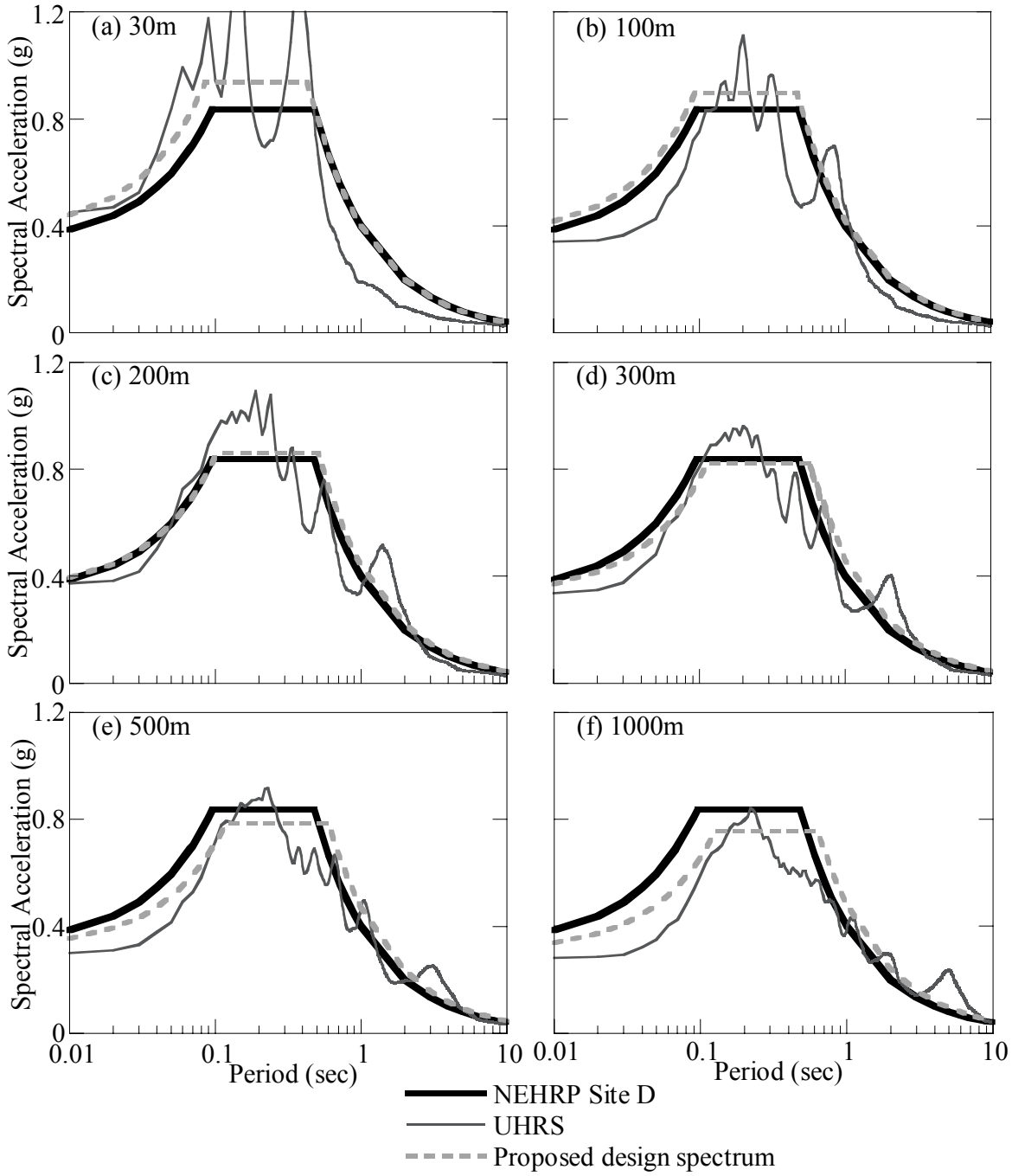

Figure D-7 UHRS (2% in 50 years) and design spectra with depth dependent site coefficients for Site 1 using Uplands profile and EPRI dynamic properties.

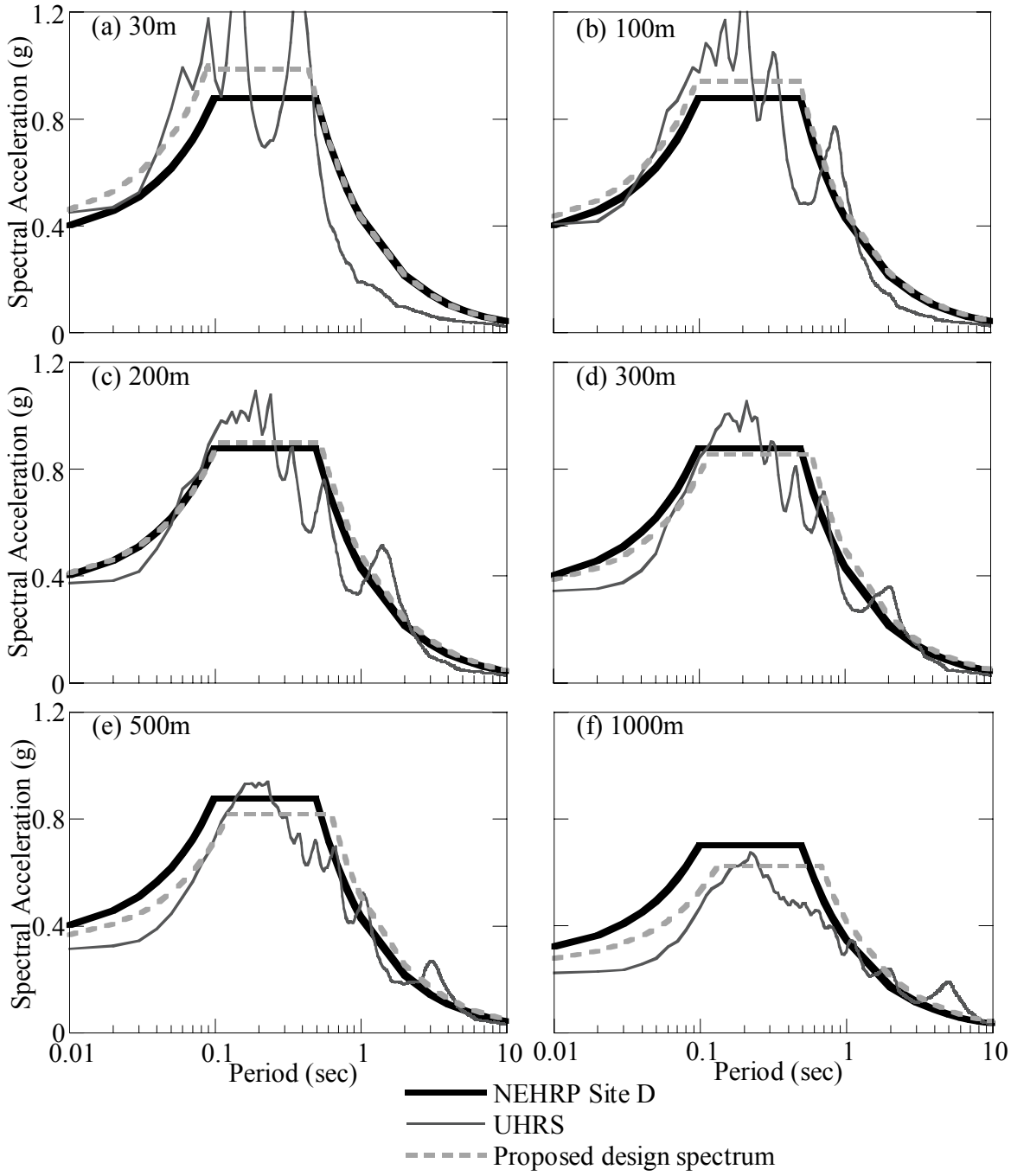

Figure D-8 UHRS (2% in 50 years) and design spectra with depth dependent site coefficients for Site 2 using Uplands profile and EPRI dynamic properties.

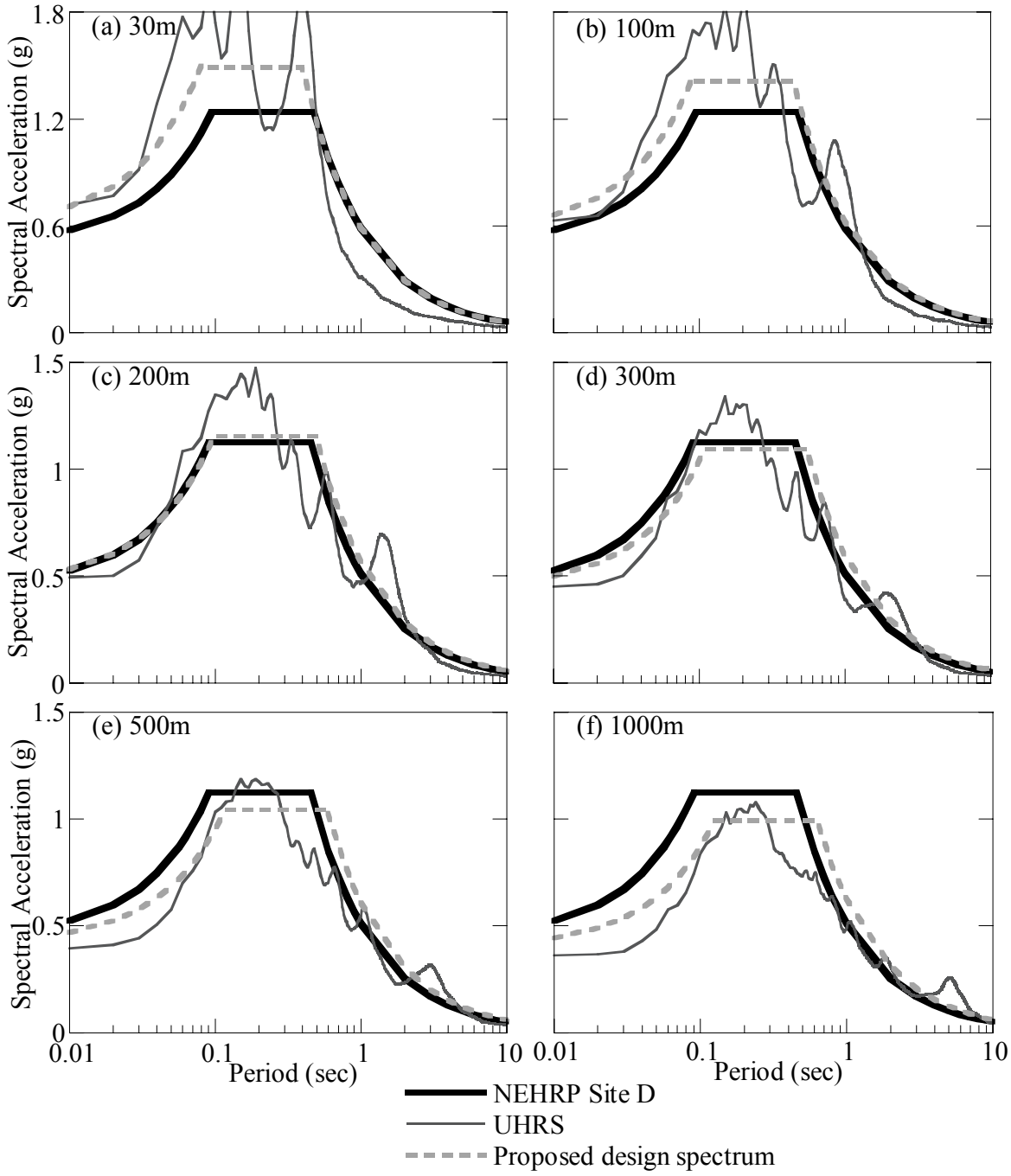

Figure D-9 UHRS (2% in 50 years) and design spectra with depth dependent site coefficients for Site 3 using Uplands profile and EPRI dynamic properties.

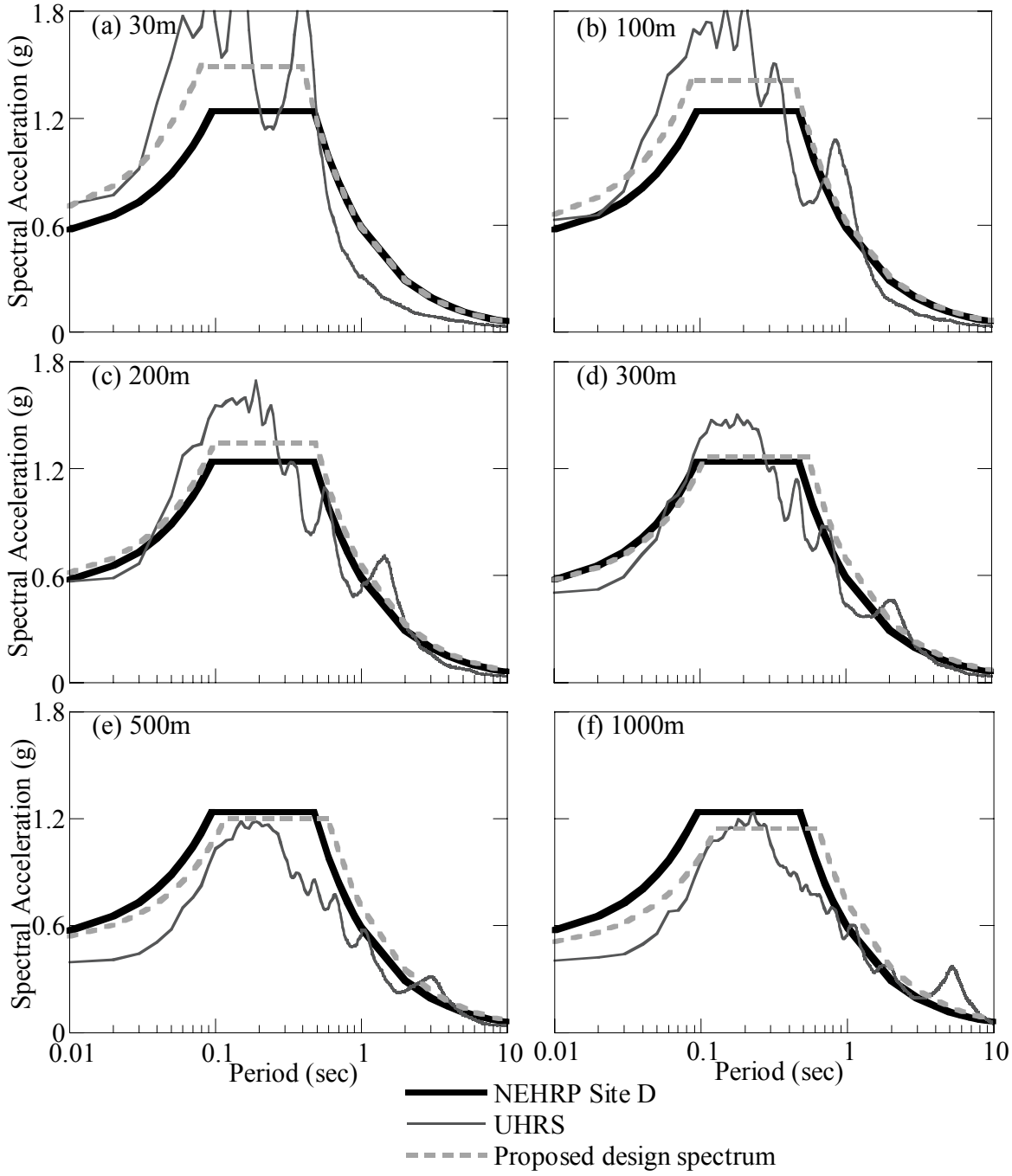

Figure D-10 UHRS (2% in 50 years) and design spectra with depth dependent site coefficients for Site 4 using Uplands profile and EPRI dynamic properties.

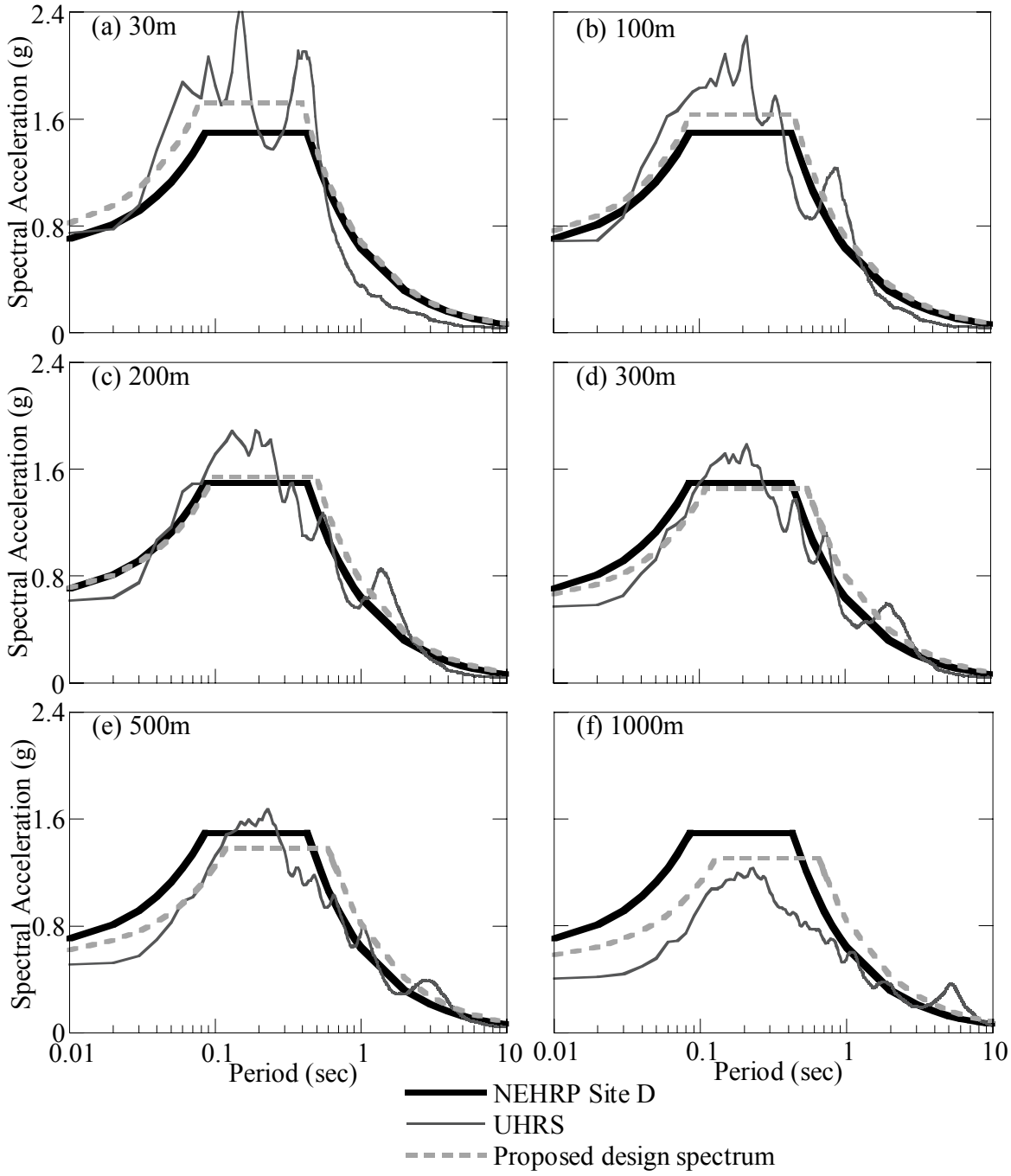

Figure D-11 UHRS (2% in 50 years) and design spectra with depth dependent site coefficients for Site 5 using Uplands profile and EPRI dynamic properties.

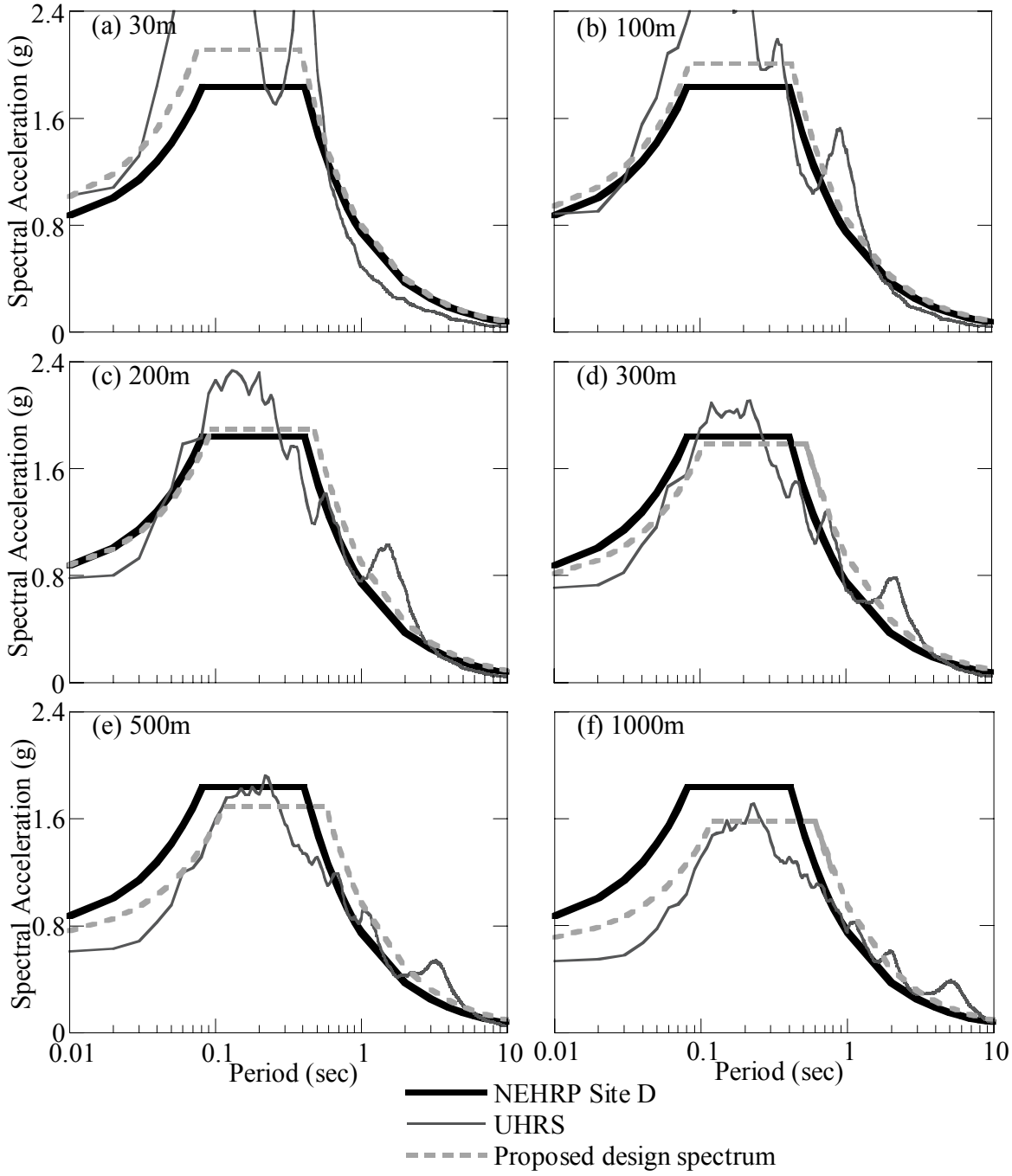

Figure D-12 UHRS (2% in 50 years) and design spectra with depth dependent site coefficients for Site 6 using Uplands profile and EPRI dynamic properties.

D.3 UHRS and design response spectra for Lowlands and using EPRI properties

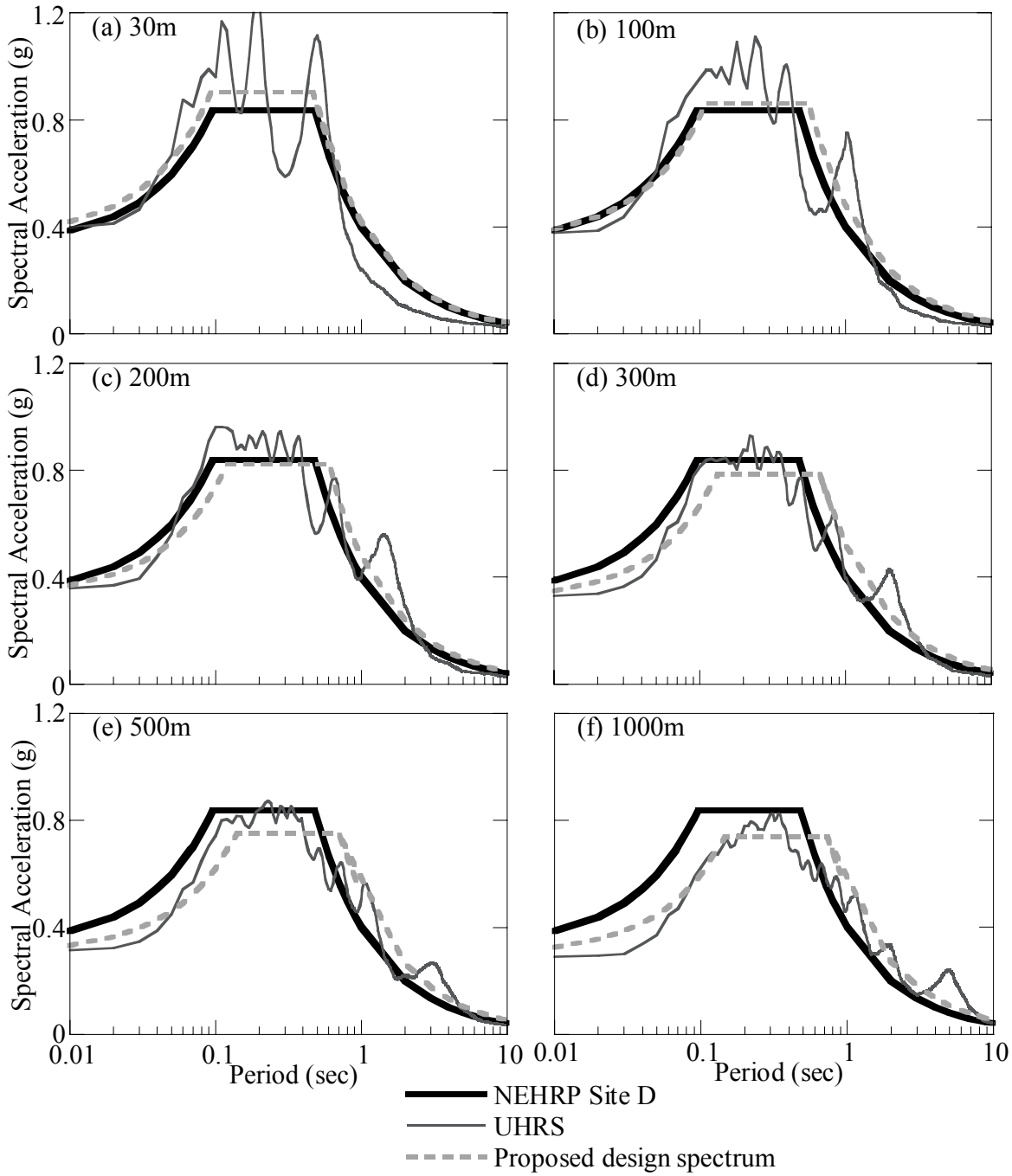

Figure D-13 UHRS (2% in 50 years) and design spectra with depth dependent site coefficients for Site 1 using Lowlands profile and EPRI dynamic properties.

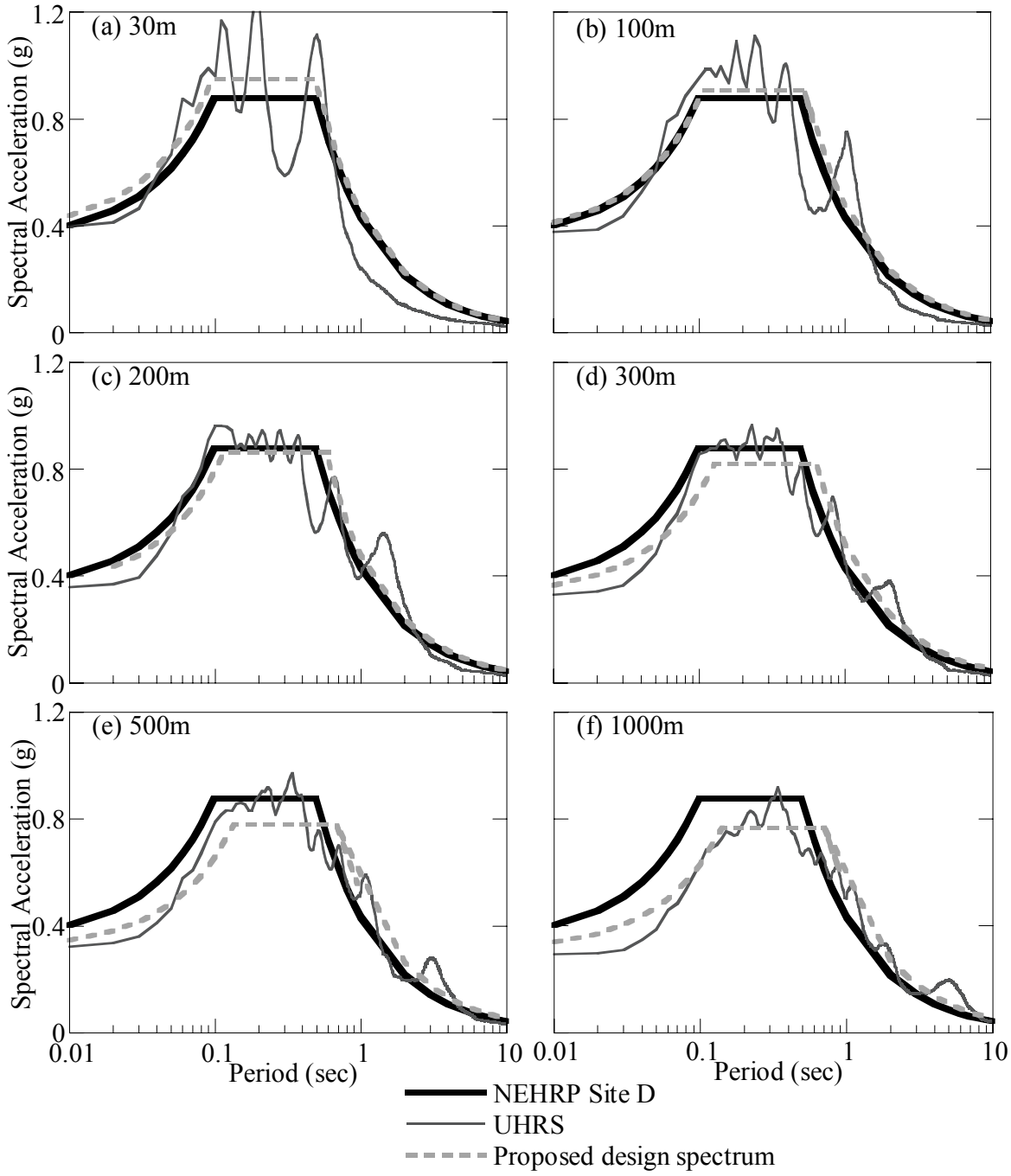

Figure D-14 UHRS (2% in 50 years) and design spectra with depth dependent site coefficients for Site 2 using Lowlands profile and EPRI dynamic properties.

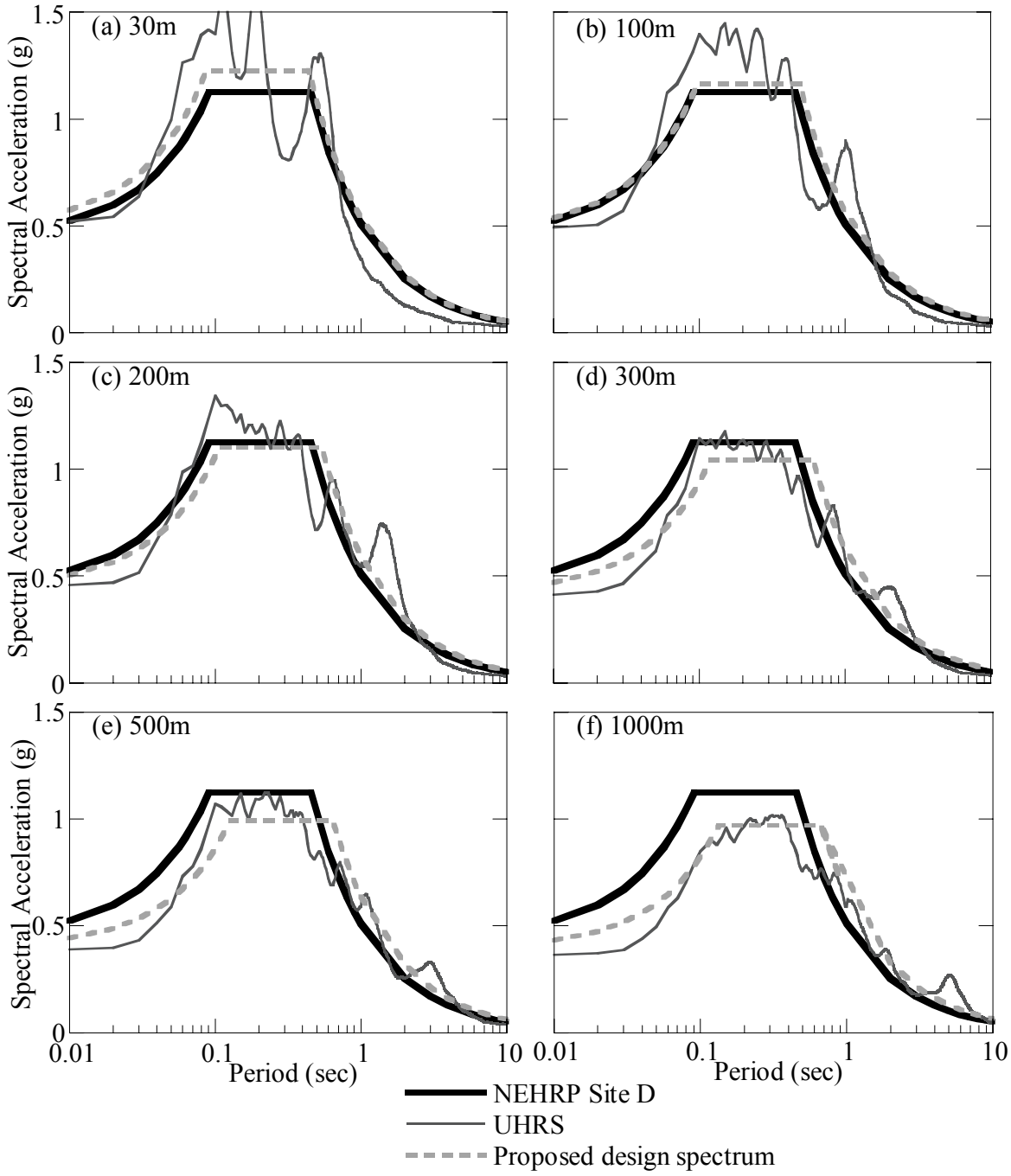

Figure D-15 UHRS (2% in 50 years) and design spectra with depth dependent site coefficients for Site 3 using Lowlands profile and EPRI dynamic properties.

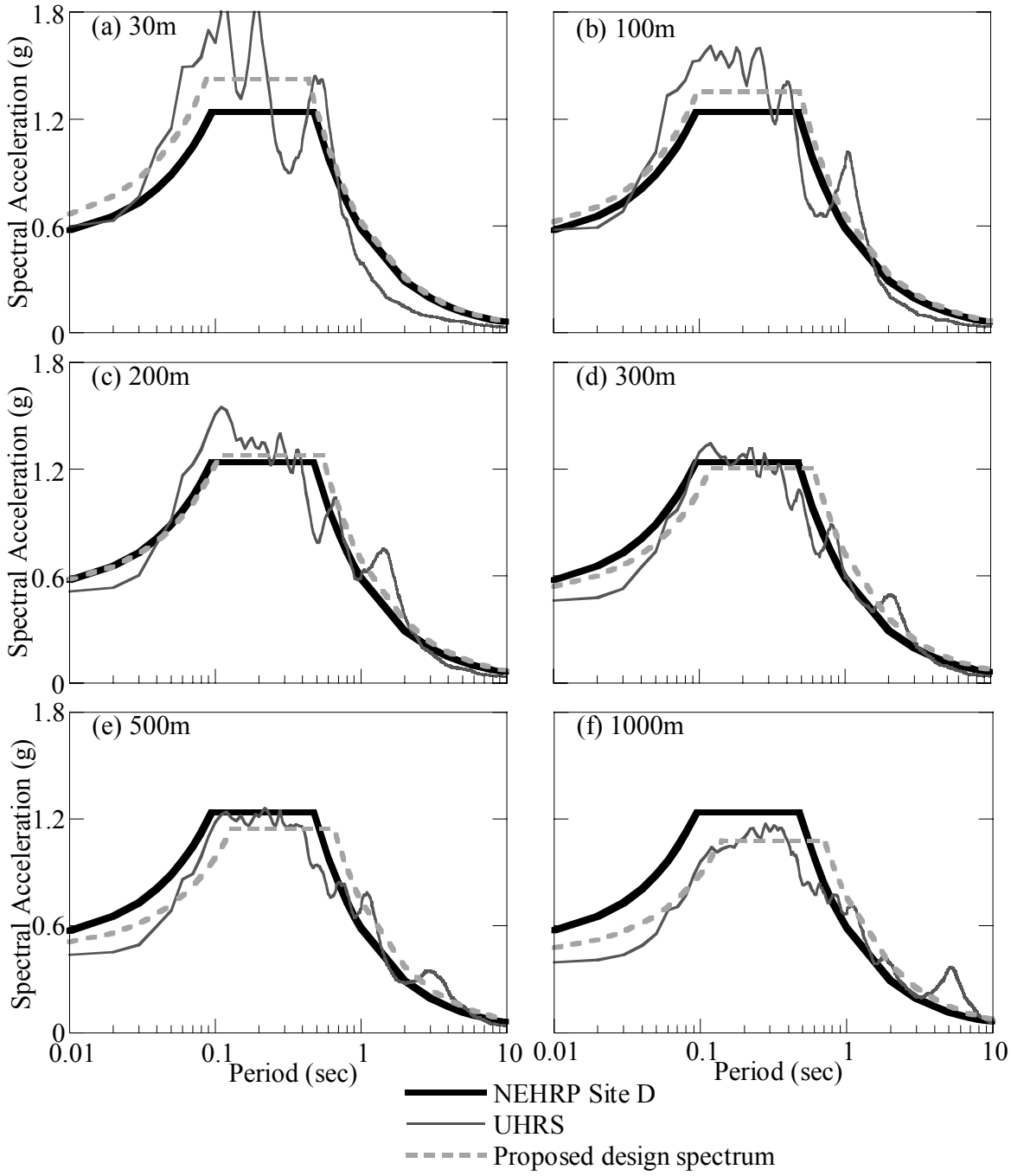

Figure D-16 UHRS (2% in 50 years) and design spectra with depth dependent site coefficients for Site 4 using Uplands profile and EPRI dynamic properties.

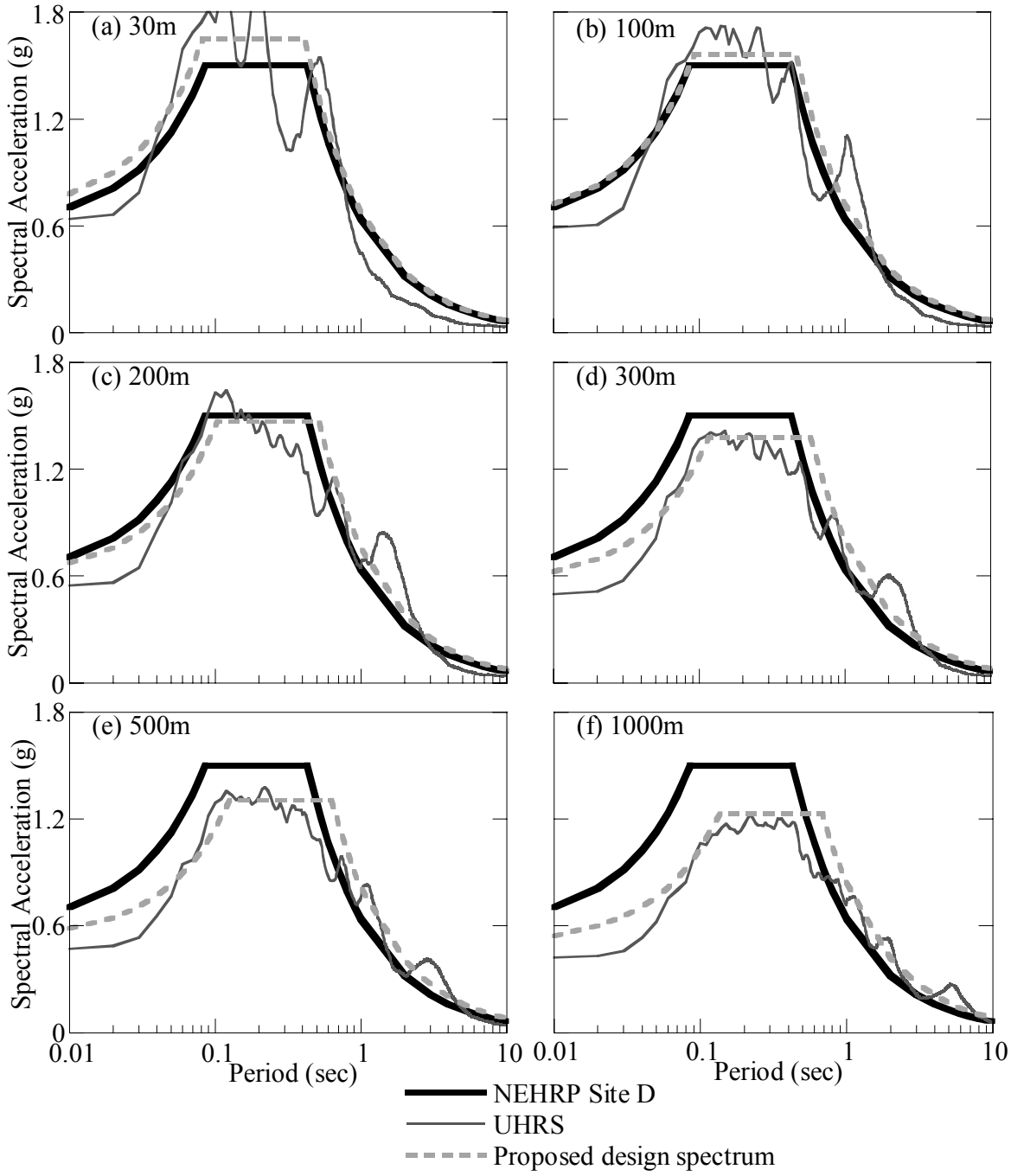

Figure D-17 UHRS (2% in 50 years) and design spectra with depth dependent site coefficients for Site 5 using Uplands profile and EPRI dynamic properties.

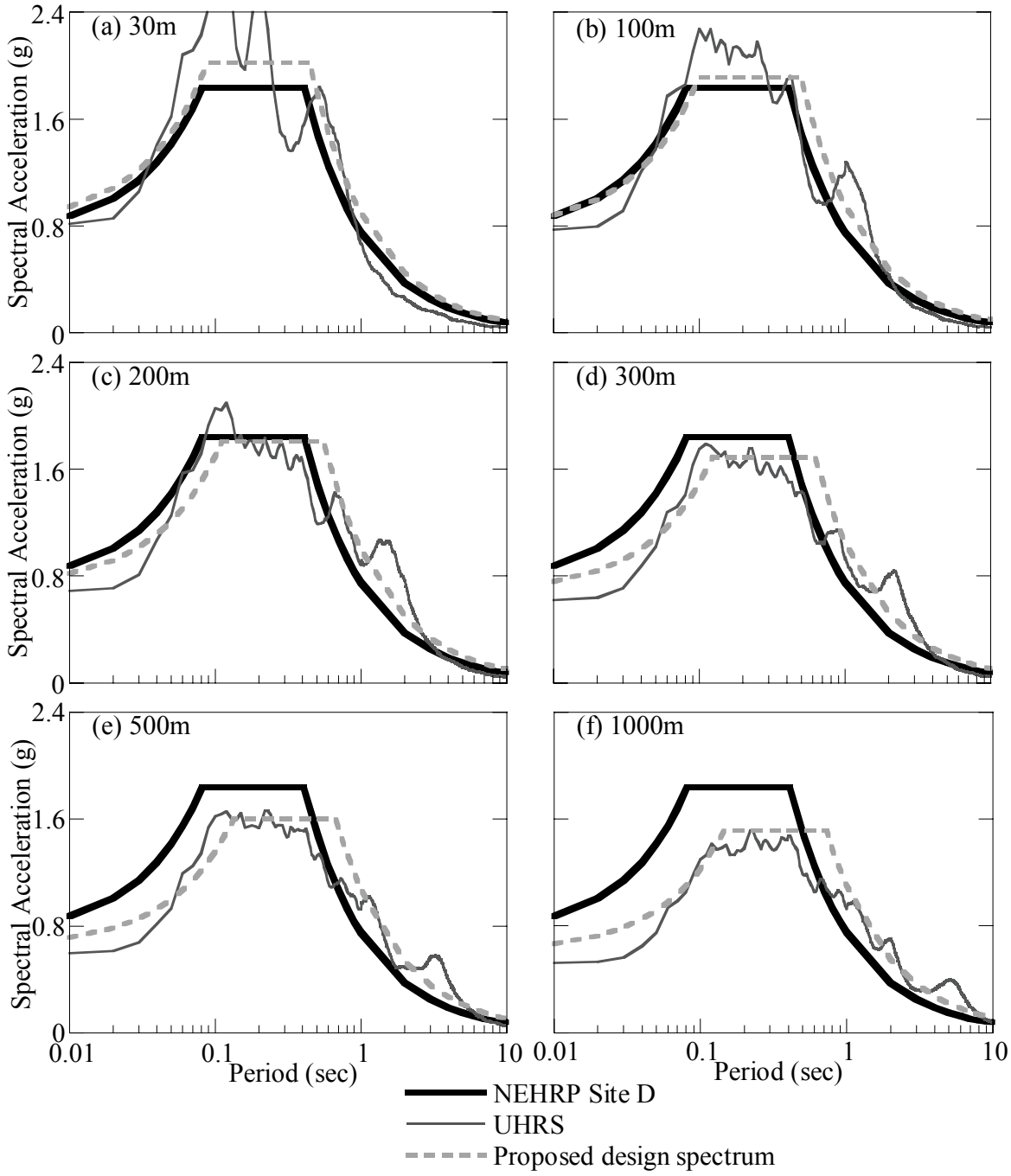

Figure D-18 UHRS (2% in 50 years) and design spectra with depth dependent site coefficients for Site 6 using Uplands profile and EPRI dynamic properties.

REFERENCES

Assimaki, D., Kausel, E., and Whittle, A. J. (2000). "Model for dynamic shear modulus and damping for granular soils." *Journal of Geotechnical & Geoenvironmental Engineering*, 126(10), 859-869.

ATC, A. T. C. (1978). "Tentative provisions for the development of seismic regulations for buildings, ATC 3-06 Report." Redwood City, CA.

Atkinson, G. M., and Beresnev, I. (1997). "Don't call it stress drop." *Seismological Research Letters*, 68(1), 3-4.

Atkinson, G. M., and Boore, D. M. (1995). "Ground motions relations for eastern North America." *Bulletin of Seismological Society of America*, 85, 17-30.

Atkinson, G. M., and Boore, D. M. (1997). "Some comparisons between recent ground motion relations." *Seismological Research Letters*, 68(1), 24-40.

Bakun, W. H., and Hopper, M. G. (2002). "1811-1812 New Madrid, Missouri, and the 1886 Charleston, South Carolina, earthquakes." *in review*.

Beresnev, I. A., and Atkinson, G. M. (1998). "FINSIM - a FORTRAN Program for simulating stochastic acceleration time histories from finite faults." *Seismological Research Letters*, 69(1), 27-32.

Bielak, J., Xu, J., and Ghattas, O. (1999). "Earthquake ground motion and structural response in alluvial valleys." *Journal of Geotechnical & Geoenvironmental Engineering*, 125(5), 413-423.

Bommer, J. J. (2002). "Deterministic vs. probabilistic seismic hazard assessment: an exaggerated and obtrusive dichotomy." *Journal of Earthquake Engineering*, 6(1), 43-73.

Boore, D. M. (1983). "Stochastic simulation of high-frequency ground motions based on seismological models of the radiated spectra." *Bulletin of the Seismological Society of America*, 73(6), 1865-1894.

Boore, D. M. (2002). "SMSIM Fortran programs for simulating ground motions from earthquakes: Version 2.16. A revision of OFR 96-80-A." US Geological Survey, Menlo Park.

Boore, D. M., and Atkinson, G. M. (1987). "Stochastic prediction of ground motion and spectral response parameters at hard-rock sites in eastern North America." *Bulletin of Seismological Society of America*, 77, 440-467.

Borcherdt, R. D. (1994). "Estimates of site-dependent response spectra for design (methodology and justification)." *Earthquake spectra*, 10, 617-653.

Borja, R. D., Duvernay, B. G., and Lin, C. H. (2002). "Ground response in Lotung: total stress analyses and parametric studies." *Journal of Geotechincal and Geoenvironmental engineering*, 128(1), 54-63.

Borja, R. I., and Amies, A. P. (1994). "Multiaxial Cyclic Plasticity Model for Clays." *Journal of Geotechnical and Geoenvironmental Engineering*, 120(6), 1051-1069.

Borja, R. I., Chao, H. Y., Montans, F. J., and Lin, C. H. (1999). "Nonlinear ground response at Lotung LSST site." *Journal of Geotechnical and Geoenvironmental Engineering*, 125(3), 187-197.

Brune, J. N. (1970). "Tectonic stress and the spectra of seismic shear waves from earthquakes." *Journal of Geophysical Research*, 75(26), 4997-5009.

Brune, J. N. (1971). "Correction." *Journal of Geophysical Research*, 76, 5002.

Campbell, K. W. (2002). "Prediction of strong ground motion using the hybrid empirical method: example application to eastern North America." *submitted to Bulletin of Seismological Society of America*.

Chang, T. S., Hwang, H., and Ng, K. W. (1989). "Subsurface conditions in Memphis and Shelby County, Tennessee." *NCEER-89-0021*, National Center for Earthquake Engineering Research, State University of New York at Buffalo, Buffalo, NY.

Chang, T. S., Teh, L. K., and Shang, Y. (1992). "Seismic characteristics of sediments in the New Madrid Seismic Zone." CERI, Memphis State University, Memphis, Tennessee.

Chopra, A. K. (1995). *Dynamics of structures : theory and applications to earthquake engineering*, Prentice Hall, Englewood Cliffs, N.J.

Clough, R. W., and Penzien, J. (1993). *Dynamics of structures*, McGraw-Hill, New York.

Cornell, C. A. (1968). "Engineering seismic risk analysis." *Bulletin of Seismological Society of America*, 58, 1583-1606.

Cox, R. T., and Van Arsdale, R. B. (1997). "Hotspot origin of the Mississippi embayment and its possible impact on the contemporary seismicity." *Engineering Geology*, 46, 5-12.

Crone, A. J. (1981). "Sample description and stratigraphic correlation of the New Madrid test well-1-X, New Madrid County, Missouri." U.S. Geological Survey, Open-File-Report 81-426.

Dafalias, Y. F. (1980). "The concept and application of the bounding surface in plasticity theory." *IUTAM Symposium on Physical Non-linearities in Structural Analysis*, France, 56-63.

Dafalias, Y. F., and Popov, E. P. (1979). "A model for nonlinearly hardening materials for complex loading." *Acta Mechanica*, 21(3), 173-192.

Dobry, R., Martin, G. R., Parra, E., and Bhattacharyya, A. (1994). "Development of site - dependent ratios of elastic response spectra (RRS)." *Proceedings of the 1992 NCEER/SEAOC/BSSC Workshop on Site Response During Earthquakes and Seismic Code Provisions*, G. R. Martin, ed., University of Southern California, Los Angeles, November 18-20, 1992, National Center for Earthquake Engineering Research Special Publication *NCEER-94-SP01*, Buffalo, NY.

Dobry, R., and Vucetic, M. (1987). "Dynamic properties and seismic response of soft clay deposits." *International Symposium on Geotechnical Engineering of Soft Soils*, Mexico City, 51-87.

Elgamal, A. W., and Yang, Z. (2000). "Numerical modeling of liquefaction-induced lateral spreading." *Proceedings of the 12th World Conference on Earthquake Engineering*, Upper Hutt, New Zealand.

Elgamal, A. W., Yang, Z., Parra, E., and Dobry, R. (1999). "Modeling of liquefaction-induced shear deformations." *Second International Conference on Earthquake Geotechnical Engineering*, Lisbon, Portugal, 895-900.

EPRI. (1993). "Guidelines for determining design basis ground motions." *EPRI Tr-102293*, Electric Power Research Institute, Palo Alto, CA.

FEMA. (1997). "NEHRP recommended provisions for seismic regulations for new buildings and other structures, Part I." 337p.

Finn, W. D. L., Lee, K. W., and Martin, G. R. (1977). "An effective stress model for liquefaction." *Journal of the Geotechnical Engineering Division*, 103(GT6), 517-533.

Finn, W. D. L., Ventura, C. E., and Wu, G. (1993). "Analysis of ground motions at Treasure Island site during the 1989 Loma Prieta earthquake." *Soil Dynamics and Earthquake Engineering*, 12, 383-390.

Frankel, A. (2003). "Personal Communications."

Frankel, A., Mueller, C., Perkins, D., Barnhard, T., Leyendecker, E., Safak, E., Hanson, S., Dickman, N., and Hopper, M. (1996). "National seismic hazard maps: Documentation June 1996." *OFR 960532*, US Geological Survey.

Frankel, A., Pertersen, M. D., Mueller, C. S., Haller, K. M., Wheeer, R. L., Leyendecker, E. V., Wesson, R. L., Harmsen, S. C., Cramer, C. H., Perkins, D. M., and Rukstales, K. S. (2002). "Documentation for the 2002 update of the national seismic hazard maps." *OFR 02-420*, US Geological Survey.

Frankel, A. M., C. Perkins, D. Barnhard, T. Leyendecker, E. Safak, E. Hanson, S. Dickman, N. Hopper, M. (1996). "National seismic hazard maps: Documentation June 1996." *Open-File Report 960532*, US Geological Survey.

Gibbs, J. F., Fumal, T. E., Boore, D. M., and Joyner, W. B. (1992). "Seismic velocities and geologic logs from borehole measurements at seven strong-motion stations that recorded the 1989 Loma Prieta earthquake." *USGS Open-File Report 92-287*, USGS, Menlo Park.

Guttenberg, B., and Richter, C. F. (1944). "Frequency of earthquakes in California." *Bulletin of Seismological Society of America*, 35, 117-130.

Hanks, T. C. (1982). "f_{max}." *Bulletin of the Seismological Society of America*, 72(6), 1867-1879.

Hardin, B. O., and Drnevich, V. P. (1972a). "Shear modulus and damping in soils: Design equations and curves." *Journal of Soil Mechanics and Foundations*, 98(SM7), 289-324.

Hardin, B. O., and Drnevich, V. P. (1972b). "Shear modulus and damping in soils: Measurement and parameter effects." *Journal of Soil Mechanics and Foundation Engineering Division*, 98(SM6), 603-624.

Hardin, K. O., Drnevich, V. P., Wang, J., and Sams, C. E. (1994). "Resonant column testing at pressures up to 3.5 MPa (500 psi)." Dynamic geotechnical testing II., R. J. Ebelhar, V. P. Drnevich, and B. L. Kutter, eds., American Society for Testing and Materials. Philadelphia, PA, United.

Hashash, Y. M. A. (1992). "Analysis of deep excavations in clay," Ph.D., Massatchusetts Institute of Technology, Cambridge.

Hashash, Y. M. A., and Park, D. (2001). "Non-linear one-dimensional seismic ground motion propagation in the Mississippi embayment." *Engineering Geology*, 62(1-3), 185-206.

Hashash, Y. M. A., and Park, D. (2002). "Viscous damping formulation and high frequency motion propagation in nonlinear site response analysis." *Soil Dynamics and Earthquake Engineering*, 22(7), pp. 611-624.

Hays, W. W. (1980). "Procedures for Estimating Earthquake Ground Motions,." U.S. Geological Survey Professional Paper 1114.

Herrman, L. R., Kaliakin, V., Shen, C. K., Mish, K. D., and Zhu, Z.-Y. (1986). "Numerical implementation of plasticity model for cohesive soils." *Journal of Engineering Mechanics*, 113(4), 500-519.

Hough, S. E., Armbruster, J. G., Seeber, L., and Hough, J. F. (2000). "On the Modified Mercalli intensities and magnitudes of the 1811-1812 New Madrid earthquakes." *Journal of Geophysical Research*, 105, 23,839-23,864.

Hudson, M., Idriss, I. M., Beikae, M., University of California Davis. Center for Geotechnical Modeling, and National Science Foundation (U.S.). (1994). *QUAD4M : a computer program to evaluate the seismic response of soil structures using finite element procedures and incorporating a compliant base*, Center for Geotechnical Modeling Dept. of Civil and Environmental Engineering University of California Davis, Davis Calif.

Hudson, M., Idriss, I.M., and Beikae, M. 1994. (1994). "QUAD4M - A computer program to evaluate the seismic response of soil structures using finite element procedures and incorporating a compliant base." Center for Geotechnical Modeling, Department of Civil and Environmental Engineering, University of California, Davis, CA., Davis, CA.

Hwang, S. K., and Stokoe, K. H. (1993). "Dynamic properties of undisturbed soil samples from Treasure Island, California." *Geotechnical Engineering Report GR 93-4*, Geotechnical Engineering Center, Civil Engineering Department, University of Texas at Austin.

I.M. Idriss, H. B. S. (1968). "Seismic response of horizontal soil layers." *Soil mechanics and foundations*, 94(4), 1003-1029.

Idriss, I. M. (1990). "Response of Soft Soil Sites During Earthquakes." *Proceedings of the Symposium to Honor H.B. Seed*, Berkeley, CA, 273-289.

Idriss, I. M., and Sun, J. I. (1992). "SHAKE91: A computer program for conducting equivalent linear seismic response analyses of horizontally layered soil deposits." Department of Civil and Environmental Engineering, University of California Davis.

Idriss, I. M. S., H.B. (1968). "Seismic response of horizontal soil layers." *Soil mechanics and foundations*, 94(4), 1003-1029.

Ishibashi, I., and Zhang, X. (1993). "Unified dynamic shear moduli and damping ratios of sand and clay." *Soils and Foundations*, 33(1), 182-191.

Ishihara, K. (1996). *Soil Behavior in Earthquake Geotechnics*, Oxford University Press, Oxford.

Iwasaki, T., Tatsuoka, F., and Takagi, Y. (1978). "Shear moduli of sands under cyclic torsional shear loading." *Soils and Foundations*, 18(1), 32-56.

Johnston, A. C. (1996a). "Moment magnitude assessment of stable continental earthquakes, Par 2: historical seismicity." *Geophysical Journal International*, 125, 639-678.

Johnston, A. C. (1996b). "Seismic moment assessment of stable continental earthquake, III., 1811-1812 New Madrid, 1886, Charleston, and 1755 Lisbon." *Geophysical Journal International*, 124, 381-414.

Joyner, W. B. (1984). "A scaling law for the spectra of large earthquakes." *Bulletin of the Seismological Society of America*, 74(4), 1167-1188.

Joyner, W. B., Warrick, R. E., and Fumal, T. (1981). "The effect of Quaternary alluvium on strong motion in the Coyote Lake, California, Earthquake of 1979." *Bulletin of Seismological Society of America*, 71(4), 1333-1349.

Kokusho, T. (1980). "Cyclic triaxial test of dynamic soil properties for wide strain range." *Soils and Foundations*, 20(2), 45-60.

Konder, R. L., and Zelasko, J. S. (1963). "Hyperbolic stress-strain formulation of sands." *Second pan American Conference on Soil Mechanics and Foundation Engineering*, Sao Paulo, Brazil, 289-324.

Kramer, S. L. (1996). *Geotechnical earthquake engineering*, Prentice Hall, Upper Saddle River, N.J.

Krinitzsky, E. L. (1993). "Earthquake probability in engineering - Part 2: Earthquake recurrence and limitations of Gutenberg-Richter b-values for the engineering of critical structures." *Engineering Geology*, 36, 1-52.

Krinitzsky, E. L. (2002). "How to obtain earthquake ground motions for engineering design." *Engineering Geology*, 65, 1-16.

Laird, J. P., and Stokoe, K. H. (1993). "Dynamic properties of remolded and undisturbed soil samples test at high confining pressure." *GR93-6*, Electric Power Research Institute.

Lanzo, G., and Vucetic, M. (1999). "Effect of soil plasticity on damping ratio at small cyclic strains." *Soils and Foundations*, 39(4), 121-141.

Law, H. K., and Lam, I. P. (1999). "Seismic performance of the Yerba Buena Island Tunnel." *3rd National Conference of the Geo-Institute '99*, Champaign-Urbana, IL, 659-670.

Lee, M. K., and Finn, W. D. L. (1978). "DESRA-2, Dynamic effective stress response analysis of soil deposits with energy transmitting boundary including assessment of liquefaction potential." Soil Mechanics Series, No. 36, Department of Civil Engineering, University of British Columbia, Vancouver, Canada.

Masing, G. (1926). "Eignespannungen und Verfestigung beim Messing." *Second International Congress on Applied Mechanics*, Zurich, Switzerland, 332-335.

Matasovic, N. (1993). "Seismic response of composite horizontally-layered soil deposits," Ph.D. Thesis, University of California, Los Angeles.

Matasovic, N., and Vucetic, M. (1995). "Seismic response of soil deposits composed of fully-saturated clay and sand layers." *First International Conference on Earthquake Geotechnical Engineering*, Tokyo, Japan, 611-616.

McGuire, R. K., and Arabasz, W. J. (1990). "An introduction to probabilistic seismic hazard analysis." *Geotechnical and Environmental Geophysics, Society of Exploration Geophysicists*, 1, 333-353.

McKeown, F. A. (1982). "Investigations of the New Madrid, Missouri, earthquake region." U.S. Geological Survey Professional Paper 1236.

Mesri, G., Febres-Cordero, E., Shields, D. R., and Castro, A. (1981). "Shear stress-strain-time behavior of clays." *Geotechnique*, 31(4), 537-552.

Mroz, Z. (1967). "On the description of anisotropic work hardening." *Journal of Mechanics and Physics of Solids*, 15, 79-93.

Newmark, N. M. (1959). "A Method of Computation for Structural Dynamics." *Journal of the Engineering Mechanics Division*, 85, 67-94.

Ng, K. W., Chang, T. S., and Hwang, H. (1989). "Subsurface Conditions of Memphis and Shelby County." *Technical Report NCEER-89-0021*, National Center for Earthquake Engineering Research, State University of New York at Buffalo, Buffalo, N.Y.

Nicholson, C., Simpson, D. W., Singh, S., and Zollweg, J. E. (1984). "Crustal studies, velocity inversions, and fault tectonics: results from a microearthquake survey in the New Madrid Seismic Zone." *Journal of Geophysical Research*, 89(B6), 4545-4558.

Nuttli, O. W. (1973). "Mississippi Valley earthquakes of 1811 and 1812: intensities, ground motion and magnitudes." *Bulletin of Seismological Society of America*, 63(1), 227-248.

Otto, W. N. (1973). "The Mississippi valley earthquakes of 1811 and 1812: intensities, ground motion and magnitudes." *Bulletin of the seismological society of America*, 63(1), 227-248.

Ou, G. B., and Herrmann, R. B. (1990). "A statistical model for ground motion produced by earthquakes at local and regional distances." *Bulletin of the Seismological Society of America*, 80(6), 1397-1417.

Park, D., and Hashash, Y. M. A. (2003a). "Soil damping formulation in nonlinear time domain site response analysis." *Journal of Earthquake Engineering*, in press.

Park, D., and Hashash, Y. M. A. (2003b). "Soil damping formulation in nonlinear time domain site response analysis." *Journal of Earthquake Engineering*, in press.

Parks, W. S., and Lounsbury, R. W. (1976). "Summary of some current and possible future environment problems related to geology and hydrology at Memphis, Tennesse." *4-76*, U.S. Geological Survey.

Parra, E. (1996). "Numerical modeling of liquefaction and lateral ground deformation including cyclic mobility and dilation response in soil system," Ph.D. Thesis, Rensselaer Polytechnic Institute, Troy, NY.

Pass, D. G. (1994). "Soil characterization of the deep accelerometer site at Treasure Island, San Francisco, California," M.S. Thesis, University of New Hampshire.

Pestana-Nascimento, J. M. (1994). "A unified constitutive model for clays and sands," Sc.D., MIT, Cambridge, MA.

Pezeshk, S., Camp, C. V., Liu, L., J.M. Evans, J., and He., J. (1998). "Seismic Acceleration Coefficients For West Tennessee and Expanded Scope of Work for Seismic Acceleration Coefficients For West Tennessee Phase 2 - Field Investigation. Project Number TNSPR-RES116. Prepared for the Tennessee Department of Transportation and the U.S. Department of Transportation Federal Highway Administration." *Project Number TNSPR-RES116*, University of Memphis.

Prevost, J. H. (1977). "Mathematical modeling of monotonic and cyclic undrained clay behavior." *International Journal of Numerical and Analytical Methods in Geomechanics*, 1(2), 195-216.

Prevost, J. H. (1985). "A simple plasticity theory for frictional cohesionless soils." *Soil Dynamics and Earthquake Engineering*, 4(1), 9-17.

Prevost, J. H. (1998). "DYNAFLOW User's Manual." Department of Civil Engineering and Operations Research, Princeton University.

Pyke, R. M. (1979). "Nonlinear soil models for irregular cyclic loadings." *Journal of the Geotechnical Engineering Division*, 105(GT6), 715-726.

Rathje, E. M., and Bray, J. D. (2001). "One- and two-dimensional seismic analysis of soild-waste landfills." *Canadian Geotechincal Journal*, 38(4), 850-862.

Rayleigh, J. W. S., and Lindsay, R. B. (1945). *The theory of sound*, Dover Publications, New York.

Reiter, L. (1990). *Earthquake hazard analysis : issues and insights*, Columbia University Press, New York.

Roesset, J. M. (1977). "Soil amplification of Earthquakes." Numerical methods in Geotechnical Engineering, J. T. C. C.S. Desai, ed., McGraw-Hill, New York, 649-682.

Romero, S., Hebeler, G., and Rix, G. J. (2001). "Recommended reference profile for Memphis, Tennessee." Engineering Geology.

Romero, S. M., and Rix, G. J. (2001). "Ground motion amplification in the Upper Mississippi Embayment." *GIT-CEE/GEO-01-1*, National Science Foundation Mid America Center, Atlanta.

Roscoe, K. H., and Burland, J. B. (1968). "On the generalized stress-strain behaviour of "wet" clay." Engineering Plasticity, J. Heyman, ed., Cambridge University Press, Cambridge, England, 535-609.

Roscoe, K. H., and Schofield, A. N. (1963). "Mechanical behavior of an idealised 'wet' clay." *Proceedings, 2nd European Conference on Soil Mechanics*, Wiesbaden, Germany, 47-54.

ROSRINE. (2003). "Resolution of Site Response Issues from the Northridge Earthquake." http://geoinfo.usc.edu/rosrine/.

Udaka, T. (1975). "Analysis of Response of Large Embankments to Traveling Base Motions," University of California, Berkeley.

Sakai, H., and Sawad, S. (1996). "Non-iterative computation scheme for analysis of nonlinear dynamic system by finite element method." *Proceedings of Eleventh World Conference on Earthquake Engineering*.

Schnabel, P. B., Lysmer, J. L., and Seed, H. B. (1972). "SHAKE: A computer program for earthquake response analysis of horizontally layered sites." *EERC-72/12*, Earthquake Engineering Research Center, Berkeley, CA.

Schneider, J. A., Mayne, P. W., and Rix, G. J. (2001). "Geotechnical site characterization in the greater Memphis area using cone penetration tests." *Engineering Geology*, 62(1-3), 169-184.

Schwartz, D. P. (1988). "Geology and seismic hazards: Moving into the 1990s." Earthquake engineering and soil dynamics II: Recent advances in ground motion evaluation, Geotechnical special publication 20, ASCE, New York, 1-42.

Schwartz, D. P., and Coppersmith, K. J. (1984). "Fault behavior and characteristic earthquakes: examples from the Wasatch and San Andreas fault zones." *Journal of Geophysical Research*, 89(B7), 5681-5698.

Schweig, E. S., and Van Arsdale, R. B. (1996). "Neotectonics of the upper Mississippi embayment." *Engineering Geology*, 45, 185-203.

Seed, H. B., and Idriss, I. M. (1970). *Soil moduli and damping factors for dynamic response analyses*, College of Engineering University of California Berkeley., Berkeley.

Seed, H. B., and Idriss, I. M. (1983). "Ground motions and soil liquefaction during earthquakes." *EERI Monograph Series, Earthquake Engineering Research Institute*, Berkeley, CA.

Seed, H. B., Murarka, R., Lysmer, J., and Idriss, I. M. (1976). "Relationships Between Maximum Acceleration, Maximum Velocity, Distance from Source and Local Site Conditions for Moderately Strong Earthquakes." *Bulletin of the seismological society of America*, 66(4), 1323-1342.

Seed, H. B., Romo, M. P., Sun, J. I., Jaime, A., and Lysmer, J. (1988). "The Mexico earthquake of September 19, 1985 - relationships between soil conditions and earthquake ground motions." *Earthquake spectra*, 4, 687-729.

Seed, H. B., Wong, R. T., Idriss, I. M., and Tokimatsu, K. (1986). "Moduli and damping factors for dynamic analyses of cohesionless soils." *Journal of Geotechnical Engineering*, 112(11), 1016-1032.

Seed, R. B., Dickenson, S. E., Rau, G. A., White, R. K., and Mok, C. M. (1994). "Observations regarding seismic response analyses for soft and deep clay sites." *Proceedings of the 1992 NCEER/SEAOC/BSSC Workshop on Site Response During Earthquakes and Seismic Code Provisions*, G. R. Martin, ed., University of Southern California, Los Angeles, November 18-20, 1992, National Center for Earthquake Engineering Research Special Publication *NCEER-94-SP01*, Buffalo, NY.

Shedlock, K. M., and Johnston, A. C. (1994). *Investigations of the New Madrid seismic zone*, U.S. Geological Survey, Washington, DC; Denver, CO.

Silva, W. (2000). ROSRINE Study.

Somerville, P., Collins, N., Abrahamson, N., Graves, R., and Saikia, C. (2001). "Ground motion attenuation relations for the central and eastern United States." U.S. Geological Survey.

Sugito, M., Goda, H., and Masuda, T. (1994). "Frequency dependent equi-linearized technique for seismic response analysis of multi-layered ground." *Doboku Gakkai Rombun-Hokokushu/Proceedings of the Japan Society of Civil Engineers*, 493(3-2), 49-58.

Takemiya, H., and Adam, M. (1998). "2D nonlinear seismic ground analysis by FEM-BEM: the case of Kobe in the Hyogo-ken Nanbu Earthquake." *Journal of Structural Mechanics and Earthquake Engineering*, 584(12), 19-27.

Toro, G., Abrahamson, N., and Schneider, J. (1997). "Model of strong ground motions from earthquakes in the central and eastern North America: best estimates and uncertainties." *Seismological Research Letters*, 68, 41-57.

Toro, G. R., and Silva, W. J. (2001). "Scenario earthquakes for Saint Louis, MO, and Memphis, TN, and seismic hazard maps for the Central United States Region including the effect of site conditions." *USGS 1434-HQ-97-GR-02981*.

Tuttle, M. P., and Schweig, E. S. (2000). "Earthquake potential of the New Madrid seismic zone." EOS, Trans. Am. Geophys. U., S308-309.

Vahdani, S., and Wikstrom, S. (2002). "Response of the Tarzana strong motion site during the 1994 Northridge earthquake." *Soil Dynamics and Earthquake Engineering*, 22, 837-848.

Van Arsdale, R. B., and TenBrink, R. K. (2000). "Late Cretaceous and Cenezoic Geology of the New Madrid Seismic Zone." *Bulletin of the seismological society of America*, 90(2), 345-356.

Vucetic, M. (1990). "Normalized behavior of clay under irregular cyclic loading." *Canadian Geotechnical Journal*, 27, 29-46.

Vucetic, M., and Dobry, R. (1991). "Effect of soil plasticity on cyclic response." *Journal of Geotechnical Engineering*, 117(1), 87-107.

Wen, Y. K., and Wu, C. L. (2001). "Uniform hazard ground motions for Mid-America Cities." *Earthquake spectra*, 17(2), 359-384.

Whittle, A. J. (1987). "A Constitutive Model for Overconsolidated Clays with Application to the Cyclic Loading of Friction Piles," ScD Thesis, MIT, Cambridge, MA.

Youngs, R. R., and Coppersmith, K. J. (1985). "Implications of fault slip rates and earthquake recurrence models to probabilistic seismic hazard assessments." *Bulletin of Seismological Society of America*, 75(5), 939-964.